Development and description of a novel inducible model of salivary gland inflammation in C57BL/6 mice characterised by tertiary lymphoid structures, autoimmunity and exocrine dysfunction
Lucchesi, Davide

For additional information about this publication click this link.
http://qmro.qmul.ac.uk/jspui/handle/123456789/8565

Development and description of a novel inducible model of salivary gland inflammation in C57BL/6 mice characterised by tertiary lymphoid structures, autoimmunity and exocrine dysfunction

By

Davide Lucchesi

A thesis submitted for the degree of Doctor of Philosophy in the University of London

Queen Mary University, Barts and the London School of Medicine and Dentistry, William Harvey Research Institute

AKNOWLEDGMENTS

friend, a support in my dark moments and he tolerated my sullen and unsociable self for an incredibly long period of time. On top of this, we learnt to know our "adult" life and this fantastic city together. For all these reason and for sharing with me a passion for Count Negroni he will always have my gratitude. He also introduced me to a bunch of people and among these Agostino and Maria Carmela and Andrea, with whom I spent great weekends and fantastic holidays as we visited London and the United Kingdom.

When I started my PhD in London I was lucky enough to find here (and committed to the same hard task: graduation) an old friend, Federica. In her I found someone who could listen, understand and give (habitually not followed) good advices. The long conversations (or more often arguments) we had are now among my fondest memories of the last years of my life and I hope there will be plenty more to come.

The centre of Experimental Medicine and Rheumatology is a fantastic collection of individuals coming from every corner of the world. Each one of the people that populated the laboratory made the stress and frustration that invariably come with a PhD bearable. Mathieu and Shimobi; Dr Francesco Dell'Accio and his group, Suzanne, Jo and in particular Giovanna; Janice, Vladan, Becki and Rita for their invaluable help and their sympathy; all of Bombardieri's group Cristina, Yvonne, Emanuela, Elisa A, Elisa E, Will, Vidalba, Tazeen and Sofia and in particular Alessandra who became my personal clinician and a good friend. A special mention goes to the people who spent only few months in the laboratory but nevertheless left a strong mark and exceptionally good 0memories: Mattia and Chiara and most importantly Elena with whom I had the pleasure to share bench, ideas, confessions, crackers, holidays and glasses of

wine and who made me the honour to become a priceless friend. In different ways, all of these people accomplished the magic to make long days in the laboratory an enjoyable experience and to them goes my gratitude.

A thank goes also to my friends in Italy and in particular to that peculiar collection of individuals that goes under the name of *Peori* and that represents one of the thing that I miss the most from my country. Among them I want to thank in particular Dr Luca Marmugi, who has become in the years a strange hybrid between a friend and a brother, who has always been an understanding and wise counsellor and a companion through happy and sad times. I hope I have been to him the good friend he has been to me.

I also want to express all my gratitude and love to Bethan: she has been a colleague for the last three years but she really popped into my life few months ago. There are many reasons to thank her, but the most important is that she makes me happy as I have never been before. Whatever the future will bring, I will always be thankful for these moths and all the joy she gave to me.

Needless to say, all this could have not been possible without the continuous help and support of my parents and my brother. They never made me lack their love and care and even if they often did not understand what was going on with my life, they have always been there for me. At the end of this journey, I hope that I made them as proud of me as I am proud of them.

DECLARATION

I declare that this thesis is less than 100,000 words. The experiments presented in this work were performed in the laboratories of the Centre for Experimental Medicine and Rheumatology at the William Harvey Research Institute.

I have written this thesis and the results presented in this manuscript are the product of my investigations with the following exceptions:

Dr Michele Bombardieri actively contributed to the development of the model, to the improvement of the project and to the writing of the papers derived from it; Prof Gordon Proctor (King's College, London) trained me in the salivary gland cannulation techniques and performed some of the preliminary procedures and the salivary flow assessment; Dr Francesca Barone (University of Birmingham) performed some of the cannulations and the CXCL13 and CCL21 staining in the mouse salivary glands and participated to the development of the model; Dr Elisa Astorri performed the bright-field staining for FDC-networks; miss Elena Pontarini helped me in all the experiments involving NK cells and in some of the flow cytometry data collection and analysis.

The candidate	First Supervisor	Second Supervisor
Davide Lucchesi	Dr Michele Bombardieri	Prof Costantino Pitzalis

ABSTRACT

The accumulation of leukocytes in non-lymphoid tissues and their structural organization into tertiary lymphoid structures (TLS), a process known as ectopic lymphoid neogenesis (ELN), is observed in response to chronic inflammation and in the target organ of several autoimmune diseases. TLS strongly resemble secondary lymphoid organs with specialised high-endothelial venules (HEV), segregated B/T cell areas and presence of follicular dendritic cells (FDC) networks promoting *in situ* affinity maturation of the antibody response. TLS have been associated with a growing number of autoimmune conditions and usually their presence is prognostic for undesirable disease progression. In Sjögren's syndrome (SS), an autoimmune disease affecting the salivary and lachrymal glands leading to exocrine dysfunction, TLS develop in the salivary glands (SG) of around one-third of the patients.

The immunobiology of the SG and the pathogenesis of SS have been poorly clarified and to date a robust and reproducible inducible animal model of SS and TLS in the SG is still absent. In my PhD, I developed and validated a novel inducible model of ELN in murine SG that also reproduces several features of SS. The retrograde administration of a replication-deficient adenovirus (AdV) in the SGs of wild-type C57Bl/6 mice was able to induce within three weeks fully formed TLS that displayed B/T cell segregation, FDC networks, HEVs and were positive for markers of germinal centres. Moreover, the AdV-treated mice showed a significant reduction of salivary flow and in 75% of the cases development of anti-nuclear antibodies.

The investigation of the dynamic recruitment of different innate leukocyte subsets infiltrating the SG in response to AdV delivery highlighted the presence of a tightly regulated influx of inflammatory monocytes, granulocytes and natural killer (NK) cells in response to viral infection of the SG preceding the formation of TLS.

In summary, during my PhD I have developed and validated a novel inducible model of ELN and SS-like disease in the SG of wild-type mice. This model, which is amenable to gene targeting, could be invaluable in dissecting the mechanisms leading to TLS formation and SG pathology as well as understanding the interrelations between viral infection, autoimmunity and exocrine dysfunction in SS.

LIST OF ABBREVIATIONS

Ab	Antibody
AchR	Acetylcholine receptor
ACPA	Anti-citrullinated protein antibody
AdV	Adenovirus
Ag	Antigen
AID	Activation-induced cytidine deaminase
ANA	Anti-nuclear antibody
APC	Antigen-presenting cell
BAFF	B-cell activating factor of the TNF family
BALT	Bronchus-associated lymphoid tissue
BCR	B cell receptor
BSA	Bovine serum albumin
CCL	Chemokine C-C motif ligand
CCR	C-C chemokine receptor
CD	Cluster of differentiation
cDNA	Complementary DNA
CMV	Cytomegalovirus
CSR	Class-switch recombination
Ct	Cycle threshold
CXCL	Chemokine C-X-C motif ligand
CXCR	C-X-C chemokine receptor
D-MEM	Dulbecco-modified Eagle's medium
DAPI	4',6-diamidino-2-phenylindole

DC	Dendritic cell
DNA	Deoxyribonucleic acid
dNTP	Deoxyribonucleotide triphosphate
dpc	Days post-cannulation
dsRNA	double-stranded DNA
DSS	Dextran sulfate sodium
EAE	Experimental autoimmune encephalomyelitis
EBER	Epstein–Barr virus-encoded small RNA
EBNA	Epstein–Barr nuclear antigen
EBV	Epstein–Barr virus
EDTA	Ethylenediaminetetraacetic acid
ELISA	Enzyme-linked immunosorbent assay
ELN	Ectopic lymphoid neogenesis
FACS	Fluorescence-activated cell sorting
FBS	Foetal bovine serum
Fc	Fragment crystallizable region
FDC	Follicular dendritic cell
FMO	Fluorescence minus one
FSC	Forward scatter
GALT	Gut-associated lymphoid tissue
GC	Germinal centre
GCDC	Germinal centre dendritic cell
GWAS	Genome-wide association study
HCV	Hepatitis C virus
HEV	High-endotherlial

HLA	Human leukocyte antigen
HRP	Horseradish peroxidase
HT	Hashimoto's thyroiditis
HTLV-1	Human T-cell lymphotropic virus type 1
ICAM	Intercellular Adhesion Molecule
ICR	Imprinting Control Region
Idd	Insulin dependent diabetes
IFN	Interferon
Ig	Immunoglobulin
IL	Interleukin
ILC	Innate lymphoid cell
IRF	Interferon regulatory factor
LacZAdV	β-galactosidase reporter AdV
LFA1	Lymphocyte function-associated antigen 1
LMP	Latent membrane protein
Lpr	lymphoproliferation strain
LPS	lipopolysaccharide
LT	lymphotoxin
LTi	Lymphoid tissue inducer cell
LTo	Lymphoid tissue organiser cell
LucAdV	Luciferase reporter AdV
M3R	Muscarinic receptor 3
MADCAM1	Mucosal vascular addressin cell adhesion molecule 1
MALT	Mucosa-associated lymphoid tissue
MC	Mixed cryoglobulinemia

MG	Myasthenia gravis
MHC	Major histocompatibility complex
MRL	Murphy Roths Large strain
mRNA	Messanger RNA
MS	Multiple sclerosis
NCR	Natural cytotoxicity receptors
NK	natural killer cell
NO	Nitric oxide
NOD	Non-obese diabetic strain
PAGE	Polyacrylamide gel electrophoresis
PBMC	Peripheral blood mononuclear cell
PBS	Phosphate buffered saline
PCR	Polymerase chain reaction
pDC	Plasmacytoid dendritic cell
PFU	Plaque-forming unit
PNAd	Peripheral lymph node addressin
PP	Peyer's patches
RA	Rheumatoid arthritis
RANK	Receptor Activator of Nuclear Factor κ B
RBC	Red blood cell
RF	Rheumatoid factor
RIPA	Radioimmunoprecipitation assay buffer
RNA	Ribonucleic acid
RNP	Ribonucleoprotein
RORγt	Retinoid acid receptor-related orphan receptor gamma thymic

RPMI	Roswell Park Memorial Institute medium
rRNA	ribosomal-RNA
RT	Reverse transcriptase
SEM	Standard error of the mean
SG	Salivary gland
SHM	Somatic hypermutation
SLE	Systemic lupus erythematous
SLO	Secondary lymphoid organ
SNP	Single-nucleotide polumorphism
(p/s)SS	(primary/secondary) Sjögren's syndrome
SSA/SSB	Sjögren's syndrome antigen A/B
SSC	Side-scatter
STAT	Signal Transducer and Activator of Transcription
T1D	Type-I diabetes
TBS(T)	Tris buffered saline (Tween-20)
Tfh	T follicular helper cell
TGF	Tumour growth factor
Th	T helper cell
TLR	Toll-like receptor
TLS	Tertiary lymphoid structure
TNF	Tumour necrosis factor
Tris	tris(hydroxymethyl)aminomethane
TUNEL	Terminal deoxynucleotidyl transferase dUTP nick end labeling
VCAM	Vascular cell adhesion protein

LIST OF FIGURES

LIST OF TABLES

TABLE OF CONTENTS

Chapter 1 | Introduction

1 Introduction

1.1 Ectopic lymphoid neogenesis in host defence and pathology

The immune system, in contrast with other compartmentalised systems within organs in animals, is a diffuse system whereby its fundamental components, the immune cells, are not only present in specialised tissues, but most of them constantly recirculate the whole organism to perform their functions.

Nevertheless, for the immune system to work correctly and protect the organism, specialised tissues are necessary where the various types of immune cells either develop, mature, or both. These structures are termed primary and secondary lymphoid organs. A third type of lymphoid structure has been described, that shares many features with secondary lymphoid organs but in contrast to those it is inducible in adult individuals and not formed during embryogenesis or early life. These structures, termed tertiary or ectopic lymphoid structures, are involved in a plethora of different phenomena, from host-defence to graft-rejection and autoimmunity, and understanding them can shed more light on the immune system plasticity and adaptability and on the processes that lead to pathology and disease.

1.1.1 Secondary and tertiary lymphoid organs

The structures where leukocytes preferentially interact with each other and enter in contact with antigens collected in the periphery are called secondary lymphoid organs (SLO). Among those there are: the spleen, pivotal against blood-borne pathogens; lymph nodes that collect leukocytes that patrol the periphery; Peyer's patches in the intestine and tonsils in the oropharyngeal tract. Moreover, mucosa-associated lymphoid tissue (MALT), consisting of the

sparse lymphoid follicles present in the body mucosae, is considered a SLO. SLO are characterised by a highly organised microarchitecture where B and T lymphocytes localise in the so-called B and T cell areas respectively. This architecture allows antigen-presenting cells (APC) to localise in the T cell area where they can present the antigen to and activate T lymphocytes. Primed T cells then can migrate at the boundaries and into the B cell area where in turn activate their cognate B cell counterparts: this process in turn leads to the germinal centre (GC) formation where activated B cells undergo the proliferation and affinity maturation processes that eventually leads to the production of high affinity antibodies (**Figure 1.1**).
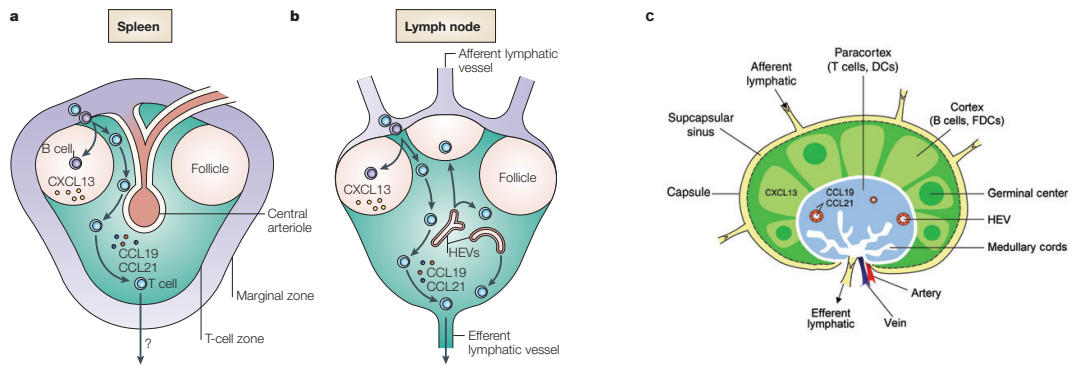
Figure 1.1: The spleen and lymph nodes. (A) Lymphocytes enter the white pulp of the spleen from the marginal zone and entry is mediated by signaling through chemokine receptors: B cells are attracted to the B-cell follicles by CXCL13, whereas T cells are directed to the T-cell zone by responding to CCL19 and CCL21. **(B)** Most lymphocytes enter a lymph node through specialized blood vessels that are known as high endothelial venules (HEVs) and then migrate to the B-cell follicles or the T-cell zone, following CXCL13, and CCL19/CCL21 gradients respectively. Lymphocytes leave the lymph nodes via efferent lymphatic vessels, and eventually return to the bloodstream from the lymph. **(C)** A fibrous capsule and an underlying subcapsular sinus surround the three distinct regions of a lymph node: cortex, paracortex and medulla. The cortex contains primary B cell follicles composed of B cells and FDCs. Antigen stimulation triggers a strong B cells proliferation that culminates with the formation of secondary follicles called germinal centers. The paracortex is composed of T cells and DCs while the deeper medulla entails the medullary cords, which are separated by lymph filled spaces called medullary sinuses. HEVs and lymphatic vessels form the lymph node vasculature. While lymphocytes enter the lymph nodes via HEVs and exit via efferent lymphatic vessels, DCs enter via afferent lymphatic vessels. Activated DCs from the

periphery enter the lymph node in lymph, which also contains soluble antigen, at several points through afferent lymphatic vessels and deposits antigens in the subcapsular sinus. Adapted by permission from Macmillan Publishers Ltd: [1] and [2].

Tertiary lymphoid Structures (TLS) can be defined as aggregates of lymphoid cells forming ectopically in non-lymphoid locations in response to chronic antigenic stimuli. As it will be discussed in more details below, TLS are often characterized by phenotypic features normally present in SLO such as B/T cell compartmentalization, the presence of specialized vessels in the T cell-rich area with the appearance of high-endothelial venules (HEV) and the differentiation of networks of stromal follicular dendritic cells (FDC) [3]. TLS formation has been observed in organ-specific autoimmune diseases [2],[3] but also during the course of microbial infections [4]-[6], solid tumours [7]-[10] and graft rejection [11]-[13]. Thus, it appears that TLS development is a stereotyped process in response to chronic antigenic stimulation, either towards allo- or self-antigens [14].

1.1.2 Characteristics of tertiary lymphoid structures

As anticipated above, TLS present many of the characteristic features of SLO, namely the presence of segregated B and T cell areas, a network of follicular dendritic cells (FDC) in the B cell area and specialised HEV for leukocyte trafficking (Figure 1.2).

FDC present in the B cell areas of SLO and TLS form networks that are essential for maturation of B cells inside the follicles. In fact, FDC produce a plethora of pro-survival signals and expose on their surface unprocessed antigens (Ag) in the form of antigen-antibody complexes (immune complexes) creating a static network of Ag-bearing cells among which B cells can move. Engagement of the B cell receptor (BCR) by one of these antigens is essential for B cell survival and proliferation and all the mechanisms taking place during the GC reaction (discussed later in section 1.1.2.1), in particular

immunoglobulin class switch recombination (CSR) and somatic hypermutation (SHM), production of B memory cells, selection of somatically mutated B-cells with high affinity receptors and antibody affinity maturation [15]. Moreover, as will be discussed shortly, FDCs also provide the main chemotactic signal for B cell localisation in the B cell area. Another important feature of SLO that is present in TLS is the presence of a specialised vasculature, the so-called HEV. HEVs are composed by a layer of endothelial cells surrounded by a basal lamina that are both thicker in comparison to normal venules. Most leukocytes enter lymph nodes across HEVs following the initial interaction between L-selectin on their surface with peripheral-node addressin (PNAd), which is expressed on the luminal surface of HEVs. Conversely, leukocyte migration in the gut lymphoid tissue, such as Peyer's patches (PP), requires the interaction of $\alpha 4\beta 7$-integrin with mucosal vascular addressin cell-adhesion molecule 1 (MADCAM1) expressed on the HEVs of PP and the intestinal lamina propria [16].The interaction between PNAd and L-selectin allows the rolling of the leukocytes on the endothelial surface. At this stage the interaction between $\beta 2$ integrin/LFA1 complex expressed on the leukocyte membrane and the adhesion molecule ICAM1 present on the endothelium, causes the stabilisation of the cell-venule contact. Leukocyte can then gain access to the tissue through transmigration between adjacent endothelium cells following by their positioning in response to chemotactic stimuli. Critically, HEVs allows the preferential recruitment of lymphocytes to SLO, thus excluding most of the remaining leukocytes: this phenomenon cannot be attributed solely to the specific expression of the adhesion molecules on the lumen of HEVs and selectins on

the surface of lymphocytes, as the same set of molecules is expressed on other

leukocytes that do not gain access to the tissue
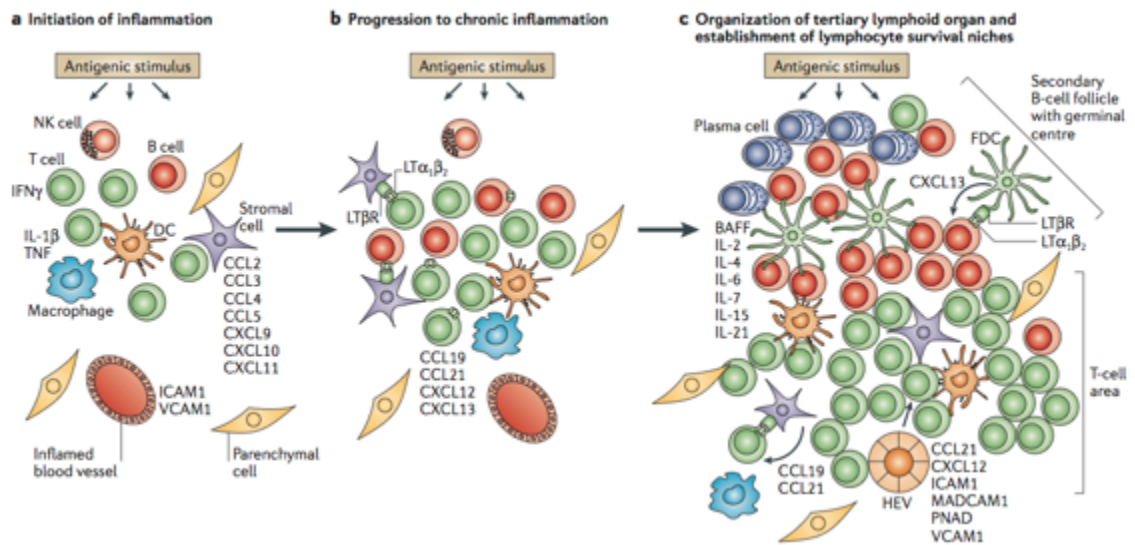
Figure 1.2: Schematic model of the hypothesised cellular and cytokine–chemokine mechanisms in the development of ELN. **(A)** The innate branch of the immune system initiates the inflammatory response that in turn attracts lymphocytes from the periphery into the target tissue. This first inflammatory phase is regulated by inflammatory cytokines, such as interferon-γ (IFNγ), interleukin-1β (IL-1β) and tumour-necrosis factor (TNF), that promote the synthesis of adhesion molecules and chemokines. **(B)** Persistent activation of innate and adaptive immune cells due to chronic antigenic stimulation in the inflamed tissue lead to increased expression of lymphotoxin-α1β2 (Ltβ) by activated B and T cells, and of lymphoid chemokines by resident stromal cells and other parenchymal cells, but also DCs and macrophages. **(C)** Activated endothelial cells acquire a HEV phenotype that helps the recruitment of lymphocytes and DCs to TLS. CCL19 and CCL21 potentially produced by stromal cells are responsible for the formation of T cell areas. It is also speculated that stromal cells would acquire the phenotypic and functional properties of follicular dendritic cells (FDCs), and among those CXCL13 production that would promote B cell area and GC organization. Other

cytokines that mediate lymphocyte survival and/or proliferation contribute to the formation of an optimal milieu for continuous lymphocyte growth and differentiation. Reprinted by permission from Macmillan Publishers Ltd: [3] copyright 2006.

It is now clear that the specific set of surface molecules expressed by HEVs facilitates the rolling and stabilisation of the lymphocytes, but the activation of the extravasation program depends on other signals. In particular, the presence on the luminal surface of the HEVs of specific chemoattractant molecules is essential for an effective and specific extravasation of leukocytes [16] [17].

Early studies on transgenic animals demonstrated that the lymphotoxin-β/lymphoid chemokines axis, which is required for SLO development, is also critically involved in TLS formation in adult life [18]-[20]. Specifically, lymphoid chemokines CCL19 and CCL21, which are mainly produced within the T-cell rich area by stromal reticular cells in association with HEVs expressing PNAd, allow the recruitment and positioning of L-selectin+/CCR7+ naïve and memory T cells within SLO where T cells receive a strong survival signal from stromal cells mediated by IL-7 [21],[22]. On the other hand, another lymphoid chemokine, CXCL13, mainly produced by FDC and germinal centre dendritic cells (GCDC) within the B cell area, drives the migration and localization within B cell follicles of CXCR5-positive B cells together with a subset of CXCR5+/PD1+/ICOS+ T helper cells which act as strong costimulators for B cells, mainly via IL-21 release, and are defined as T-follicular helper cells (Tfh) [23]-[26]. Expression of these chemokines is in turn critically regulated by the binding of the lymphotoxin-β receptor (LTβR) by the membrane-bound heterotrimeric member of the TNF family lymphotoxin-$\alpha_1\beta_2$ (LTβ) which is produced by several cell types at different stages of the lymphoneogenetic process, including lymphoid inducer cells and B cells [27],[28]. It has now been conclusively demonstrated that the lymphotoxin-β/lymphoid chemokines axis is ectopically expressed in the context of TLS developing in several autoimmune

conditions including the rheumatoid synovial tissue [29], SS salivary glands [30]-[32], the meninges of multiple sclerosis patients [33] and Hashimoto's thyroiditis [34],[35], among others. The involvement of ELN in autoimmunity will be discussed in sections 1.1.4 and 1.2.3.
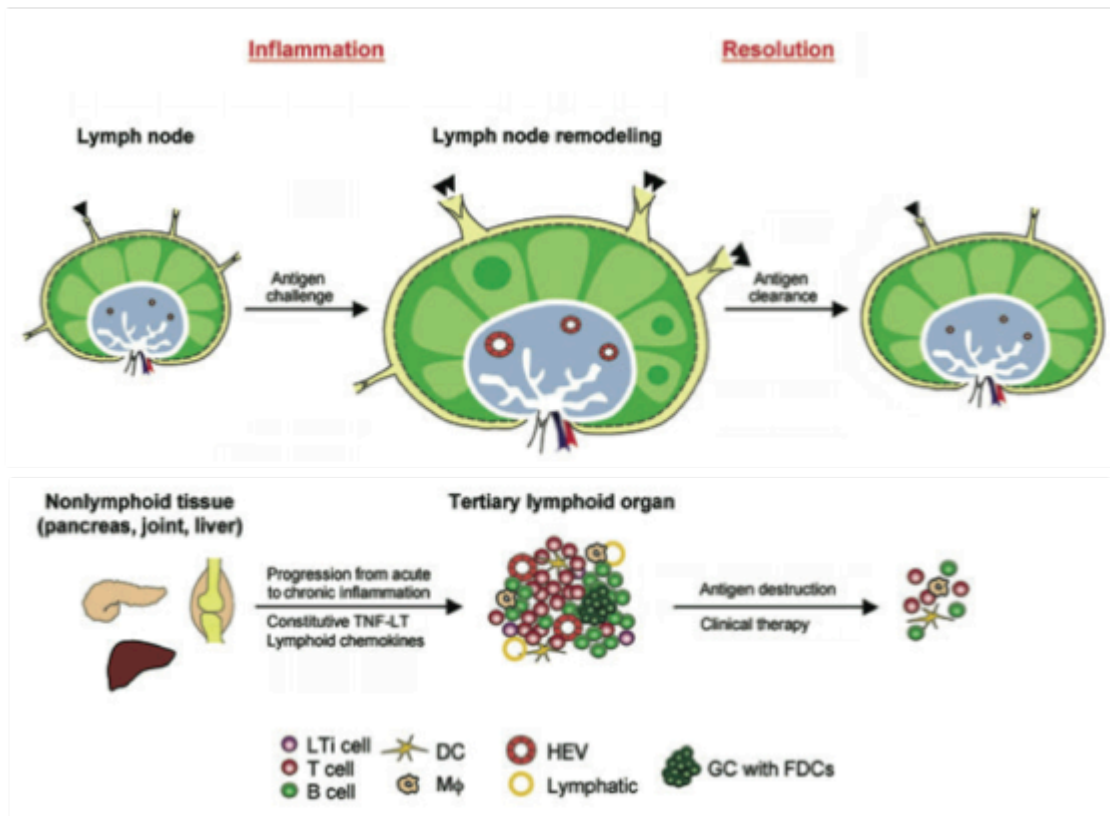
Figure 1.3: Comparison between secondary and tertiary lymphoid organ development. Once established during embryogenesis, lymph nodes cannot be ablated. Nevertheless inflammation can lead to drastic changes in LN, such as increased cell number, blood and lymph flow and neo-lymphoangiogenesis, which correspond to an increase in size. TLS, on the other hand, that can arise at anytime and at nearly any anatomical location in the adult in nonlymphoid tissues. When unresolved inflammation becomes chronic, cytokine and/or chemokine production by stromal and hematopoietic cells can induce ELN. In general, TLS can be reversed once the inflammation-inducing antigen is removed or with therapeutic treatment. Figure amended from [2].

1.1.2.1 Germinal centres in TLS

Two fundamental questions regarding ectopic lymphoid tissues in autoimmune diseases are whether they have the capacity to elicit a humoral response *in situ* and whether they contribute to autoimmunity over and above SLO. In SLO, the antigen-driven activation of the follicle culminates with the formation of GC, which is sustained by the presence of FDC networks and support B cell survival, affinity maturation and antigen selection, eventually leading to the generation of plasma cells and memory B cells (Figure 1.4) [36]. Within the GC, activated B cells selectively express the enzyme activation-induced cytidine-deaminase (AID) which is a critical regulator of the two fundamental processes taking place within the GC: SHM and CSR of the Ig genes [37].

TLS are not only reminiscent of SLO phenotypically but also functionally as they support *in situ* AID expression leading to the production of class-switched antibodies, as demonstrated by the detection of circular transcripts, [38],[39] and diversification of the antibody repertoire [5]. Moreover, in graft-rejection and cancer where ELN is observed (discussed later in section 1.1.5), specific anti-graft and anti-tumour antibodies are detected [11],[40]. Importantly, in autoimmunity TLS support the local production of disease-specific autoantibodies such as citrullinated antigens in rheumatoid arthritis [39], ribonucleoproteins Ro and La in SS [32], anti-thyroglobulin and anti-thyroperoxidase in Hashimoto's thyroiditis [35] and anti-acetylcholine receptor (AchR) antibodies in myasthenia gravis patients' thymuses [41]. Finally, in animal models of infection with pathogens capable of driving ELN, the hallmarks of GC activation and an *in situ* humoral immunity directed against the pathogen are observed [42],[43]. Thus, although the formation of TLS is a

stereotyped process common to several inflammatory environments, the antigenic force driving the development of functional ectopic GC is specific for each condition and leads to the *in situ* generation of specific antibodies (or auto-antibodies).
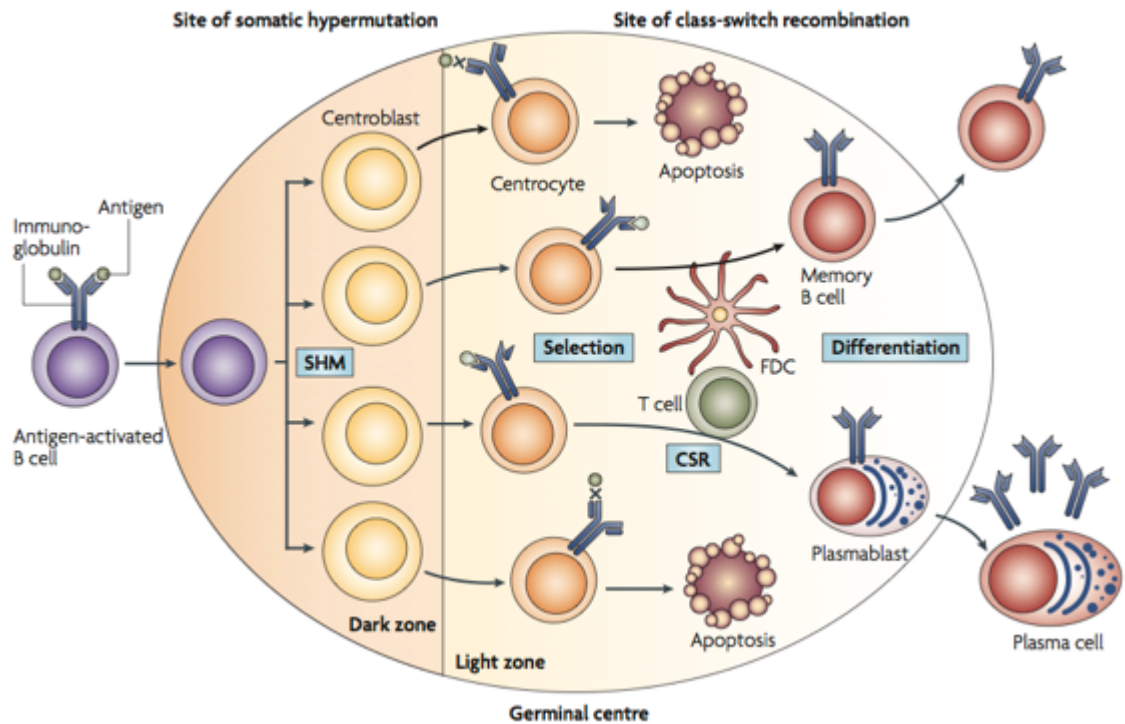
Figure 1.4: The germinal centre microenvironment. Antigen-activated B cells differentiate into centroblasts that undergo clonal expansion in the dark zone of the germinal centre and then differentiate into centrocytes and move to the light zone. During this progression the B cell receptor undergoes the process of somatic hypermutation (SHM) in the dark zone that introduces base-pair changes into the region of the rearranged genes encoding the immunoglobulin variable region (IgV) of the heavy chain and light chain. Some of the mutations introduced during SHM lead to a change in the amino-acid sequence. The modified antigen receptor, thanks to the presence of specialized T cells (T-follicular helper cells) and FDCs in the light zone, is selected for improved binding to the antigen. Mutated B cells that produce an unfavourable antibody undergo apoptosis. Moreover, subsets of B cells also undergo immunoglobulin class-switch recombination (CSR) that is the change of the immunoglobulin isotype. Also centroblasts and centrocytes can circulate several times between

dark and light zones to increase the antibody specificity for the antigen and this process seems to be mediated by a stromal cells-produced chemokine gradient. Antigen-selected B cells eventually differentiate into memory B cells or plasma cells. Reprinted by permission from Macmillan Publishers Ltd: [36] copyright 2008.

1.1.3 Initiation of the ELN programme

Our knowledge of the ELN process and its role in immunity is rapidly increasing but far from satisfactory. In fact, while we have now a substantial amount of data regarding the chemotactic signals required for TLS formation and what are the molecular switches that trigger chemokines production in ELN target tissues, we know very little about the very early cellular and molecular events that activate the ELN programme in these tissues. In particular, there is emerging evidence that the cell types responsible for the production of the critical factors involved in the ELN process differs compared to the established model of lymphoid organogenesis. Recent studies have focused on three cellular categories: lymphoid-tissue inducer cells, IL-17-producing cells and cells belonging to the myeloid lineage.

During lymphoid organogenesis (**Figure 1.5**), VCAM-1$^+$/ICAM-1$^+$/LTβR$^+$ embryonic mesenchimal "organizer" cells (lymphoid-tissue organiser cells, LTo) pre-natally produce lymphoid chemokines in response to close interaction with CD3$^-$/CD4$^+$/CD45$^+$/IL-7Rα$^+$/RANK$^+$ embryonic hematopoietic "inducer" cells (lymphoid-tissue inducer cells, LTi) that also express CXCR5 [44]. After the anchoring of the LTi cells to the SLO anlagen, IL-7 and the member of TNF-family RANK-ligand (RANKL) produced by LTo promote survival and activation of these inducer cells. In particular, LTi cells upregulate the production of LTβ, which in turn triggers LTβR on LTo cells: this interaction promotes the synthesis and the release of CXCL13 and CCL19/21 and the expression of adhesion molecules and the differentiation of HEV [2],[44]. Mice deficient for the transcription factor RORγt, necessary for the development of LTi, do not develop peripheral SLO [45]. Interestingly, LTβ blockade in pregnant mice also

leads to a progeny deficient of LNs and PP and with disrupted spleen architecture [46]. As it will be discussed in detail later, the LTβ/LTβR interaction that is fundamental in embryogenesis, in the adult is important not only in SLO homeostasis but also in TLS formation [47]. On the other hand, a role of LTi in ELN has often been speculated but the topic has been only recently studied in detail. In mice, adult CD4+CD3- LTi are found into SLO in small numbers but they are functional in their organising role as LTi transfer into adult LTα-/- mice restored the normal splenic architectures that in these animals is otherwise disrupted [48]. Moreover, adult LTi transferred in neonatal CXCR5-/- animals that lack almost completely PPs and isolated lymphoid follicles in the gut, restored the intestinal lymphoid tissues, proving that adult LTi can function as their embryonic counterpart in organising neonatal lymphoid tissues [49]. Despite these evidences, proof of a direct involvement of adult LTi in the induction of TLS either in mice or in humans is still missing.

In the last few years an important role for IL-17 in ELN has been hypothesised. This cytokine has been found to be relevant for TLS formation in the brain of mice in the EAE model of multiple sclerosis [50] and in the lungs of mice challenged with *influenza* virus or bacterial LPS [51] while in chronic graft rejection the level of IL-17-producing cells, co-expressing podoplanin, positively correlates with the speed of graft rejection and the presence of germinal centres in the graft [52]. Despite IL-17-producing T-helper cells (Th17) have been considered the main producers of the cytokine, recently a new cell subset has been found to contribute to IL-17 production at mucosal sites. IL-17-producing innate lymphoid cells (ILC17) belong to a novel family of non-T non-B cells named innate lymphoid cells (ILC), as they derive for the common lymphoid

progenitor but do not express any T or B cell receptor [53]. According to this definition, also LTi and NK cells belong to the ILC family. Interestingly, the differentiation of ILC17, Th17 and LTi cells depends on the expression of the same transcription factor RORγt [54], suggesting that the cells that share the expression of this protein might also share a role in the organisation of lymphoid tissues in embryogenesis and in adulthood.

Other recent studies highlighted the importance of myeloid cells in ELN. In a model of acute colitis (dextran sulphate sodium induced colitis, DSS), TLS formation has been shown to be independent from LTi and Th17 cells, as RORγt-/- animals, that are deficient in both subsets and have an impaired lymphoid tissue in the gut, develop intestine TLS as and above their wild-type counterparts [55]. Formation of intestinal TLS depends on the intestinal microbiota and even in the absence of peripheral lymph nodes, RORγt-/- animals were able to control intestinal flora by developing supernumerary TLS. In a similar work, Furtado and colleagues recently confirmed that TLS form in the intestine of RORγt-/-. Strikingly, the authors also shown that TNFα overexpression in RORγt-/- mice was able to partially restore the presence of peripheral lymph nodes, and that these lymph nodes were structurally and functionally indistinguishable from those present in wild-type animals [56]. Furthermore, the authors found that CD11b+F4/80+ myeloid cells were the main producers of TNFα in the lymph node anlagen and that TNFα-dependent LTβR engagement triggered the maturation of stromal cells and the secretion of lymphoid chemokines by these cells. Overall, these two works showed that LTi cells are dispensable for TLS formation and that TNFα-producing myeloid cells can trigger peripheral lymph node formation in the absence of LTi.

Stromal cells activation, perhaps driven by resident macrophages and dendritic cells (DC) that continuously probe peripheral tissues for stress signals and pathogens, and the consequent lymphoid chemokines production, is probably the main cause for the initial lymphocytic influx that characterises the early ELN programme. Nevertheless, cells from the innate immune system have been shown to be able to produce lymphoid chemokines *in vitro* as well as in some human diseases characterised by TLS formation. For instance, human *in vitro*-differentiated monocyte-derived DCs are capable of producing high amount of CXCL13 when stimulated with IL-10 and LPS [57]. Interestingly, in a mouse model of *influenza virus*, DCs are important for the maintenance of TLS arising in the lungs of infected animals (discussed in detail in section 1.1.7.1) but not for the formation of these structures [58]. It is thus likely that CXCL13 produced by DCs has a more important role in the later phases of ELN than in TLS formation.

In the inflamed synovium of rheumatoid arthritis (RA) patients, other cells belonging to the myeloid lineage have been shown to be potent producers of CXCL13. CD11c+CD68+ dendritic cells found in the ectopic lymphoid follicles of RA patients are positive for CXCL13 production [59] and the same authors reported that blood monocytes and monocyte-derived macrophages differentiated *in vitro* produce CXCL13 in response to LPS stimulation. Interestingly, *in vivo* activated monocytes from RA patients were also able to spontaneously induce differentiation of Th17 cells [60] that, as reported above in this section, might have an important role in TLS formation in autoimmunity, infection and in graft rejection.
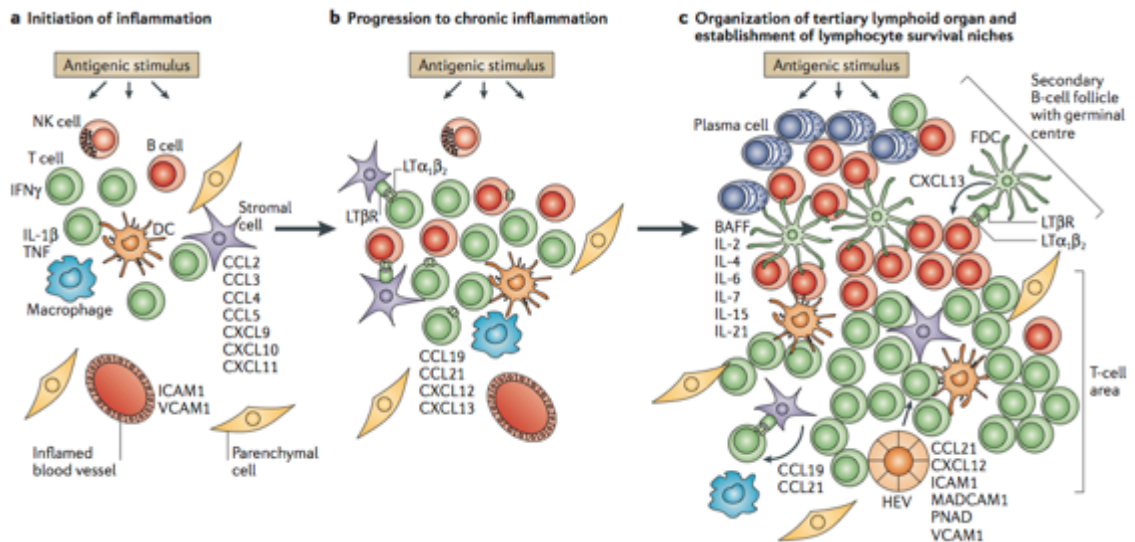
Figure 1.5: A model of SLO development. A) Production of lymphoid chemokines and adhesion molecules by stromal organiser cells is triggered via stimulation of LTβR by LTβ that is expressed by CD3$^-$/CD4$^+$/CD45$^+$ haematopoietic inducer cells (LTi). **B)** Lymphocytes from the blood are recruited thanks to the presence of lymphoid chemokines on the surface of HEV in the SLO anlagen that also express adhesion molecules such as ICAM1, MADCAM1 and PNAd. In particular LTi and lymphocytes express CCR7 and CXCR5 receptor and are attracted by the relative chemotactic stimuli produced by the developing SLO, CCL19 and CCL21 for the former and CXCL13 for the latter. **C)** In the last phases of SLO organisation, T cell area is organized by CCL19 and CCL21 produced by stromal cells and dendritic cells that attracts T CCR7$^+$ T cells and antigen-experienced mature DC from the periphery, whereas FDC and GC DCs produce CXCL13 that attracts CXCR5$^+$ B cells into the follicles. At this stage, B and T cells are the main source of LTβ, which with TNF induces lymphoid chemokines expression by stromal cells and maintains the homeostasis of mature SLO. Lymphoid chemokines, in turn, induce expression of LTβ in lymphocytes establishing a positive feedback loop. Reprinted by permission from Macmillan Publishers Ltd: [3] copyright 2006.

The data reported above are clearly incomplete and insufficient to have a precise idea of the early phases of ELN. Nevertheless, taken together, these evidences suggest that the ELN programme can be initiated by different cell types and through several different mechanisms that all ultimately terminate with the activation of the LTβ/LTβR pathway and consequent lymphoid chemokines production. The B-cell attracting chemokine CXCL13 appears to be pivotal both for the early lymphocytic infiltration and for the late maintenance of TLS. Accordingly, following the initial B cell recruitment, the interaction between LTβ expressed on B cells and LTβR present on activated stromal cells establishes a positive feedback loop promoting lymphoid chemokines production and further cell recruitment [3]. Cells of the innate immune compartment, from lymphoid and/or myeloid lineage, can probably drive this initial lymphocyte influx by inducing CXCL13 secretion in activated stromal cells and/or by direct secretion of the chemokine at the site of inflammation. Moreover, there is growing evidence that the innate immune system might be responsible for the development of an adaptive immune response (e.g. the differentiation of Th17 cells) that possibly favours ELN in infection and chronic inflammation and autoimmunity.

1.1.4 Ectopic lymphoid neogenesis in autoimmunity

Given the pivotal role of chronic antigen stimulation for the generation of TLS, ELN is more often observed in organ-specific autoimmune conditions, where the driving antigen(s) are chronically expressed (whether a self or non-self molecule). ELN has been now confirmed for a vast number of very different autoimmune diseases, in particular the joints in rheumatoid arthritis (RA), the

meninges in multiple sclerosis (MS), the thymus in myasthenia gravis (MG), the thyroid in autoimmune thyroiditis and the salivary glands of SS.

I will first review these conditions in humans and in their animal model counterparts and I will dedicate the next section to a more exhaustive analysis of SS.

1.1.4.1 Rheumatoid arthritis

RA is a chronic, systemic inflammatory disease that affects primarily the joints leading to inflammation of the synovial tissue, followed by destruction of the cartilage and bone erosion [61]. RA affects around 1% of the worldwide population. RA pathology is characterised by the presence of specific autoantibodies, in particular rheumatoid factor (RF) and anti-citrullinated protein antibodies (ACPA) and it is thus considered an autoimmune disease [14],[61].

A sizable portion of RA patients (about 40%) develops TLS in the joint synovium [62],[63]. Studies on the ELN phenomenon in RA confirmed that also in the rheumatoid joints the TLS formation depends on the ectopic expression of the lymphoid chemokines CXCL13 and CCL21 and that upregulation of these chemokines is associated with higher levels of LTβ (reviewed in [64]). Interestingly, the presence of CXCL13 and CCL21 is associated not only with fully organised TLS but also with the small, sparse and poorly organised lymphoid infiltrates [29]. In the last years our laboratory has helped to shed some light on the role of these structures in the pathogenesis and evolution of RA. We and others demonstrated that CXCL13 is not only produced by FDC networks in the ectopic follicles, but also by cells of the monocyte/macrophage lineage [59] and a subset of memory T cells [65]. Additionally, TLS that display FDC networks invariably expressed the AID enzyme, demonstrating that the

molecular machinery to promote Ig class switching and affinity maturation of the antibodies is present within RA synovial TLS. Finally, when transplanting synovial grafts from RA patients into SCID mice (which are devoid of an adaptive immune system), synovial tissue of AID$^+$ patients was capable to produce human ACPA antibodies up to 4 weeks after engraftment. Furthermore, there was a close positive correlation between the level of ACPA antibodies in the blood and the expression level of AID. The same work proved that CSR is occurring *in situ* in the AID$^+$ transplanted synovia and that AID presence correlates with higher levels of CXCL13 and B cell pro-survival factors [39].

Despite TLS-positive RA patients present a more active disease [62] it is still controversial whether TLS identify a distinct clinical phenotype of RA patients. Additionally, it is clear that ACPA and RF autoantibodies can be produced also outside the joints as no association could be made between the presence of ectopic follicles and a specific pattern of autoantibodies production [66].

1.1.4.2 Other autoimmune diseases

In the last decade the presence of TLS in the target organs of several organ-specific autoimmune diseases has been reported and documented at various levels of depth. For example, in autoimmune thyroiditis, the first disease ever defined "autoimmune" (Hashimoto's thyroiditis, HT), lymphoid infiltrates are observed in the thyroid gland. These infiltrates show B/T cell compartmentalisation, often with distinguishable light and dark areas in the B cell area, regions of intense proliferation and apoptosis and in general a striking similarity to SLO [35]. Furthermore, biopsies from patients with autoimmune thyroiditis have high expression levels of LTβ and lymphoid chemokines

(among which CCL21 and CXCL13) in comparison with controls [34]. Finally, specific anti-thyroglobulin and anti-thyroperoxidase antibodies plasma cells are present in the TLS in autoimmune thyroiditis patients [35], strongly supporting the concept that antigen-specific plasma cells undergo *in situ* maturation and differentiation.

The thymus is the organ where ELN is observed in MG: B cells isolated from MG patients' thymuses are positive for activation markers and are capable to produce anti-AchR antibodies [41], one of the diagnostic test for autoimmune MG in the clinical setting, which are also pathogenic and responsible for the typical muscular weakness that characterises this disease. A direct study analysing the gene repertoire of isolated GC-B cells from MG patients showed that these ectopic follicles behave like GCs normally present in SLO, both in terms of immunoglobulins diversification and selection [67]; also in this setting CXCL13 expression has been proven pivotal for the development of TLS within the MG thymus [68].

Type-I diabetes (T1D) has been long considered mainly a T-cell mediated autoimmune disease, characterised by the destruction of pancreatic islets by autoreactive T lymphocytes. Despite the relevance of T cells, one of the hallmarks of T1D is the presence of autoantibodies against islet antigens (e.g. anti-insulin antibodies) [69]. Recent evidences have shed new light on the relevance of B cells in the disease, mainly using a robust autoimmune diabetes murine model, the non-obese diabetic (NOD) mouse. Of relevance, not only B cell infiltration is an important feature of the histology of NOD animals pancreata, but also B cells are necessary for the initiation of insulitis [70]. Indeed, ELN takes place in NOD pancreas, and this phenomenon is dependent

upon the expression of the lymphotoxin/lymphoid chemokines axis. Once again, TLS in this tissue were functional as they expressed activation markers (e.g. AID enzyme activity) and promoted autoimmunity as demonstrated by the perifollicular accumulation of pancreatic CD138$^+$ plasma cells reactive against insulin [71]. Moreover, it has been shown that B cells undergo affinity maturation towards pancreatic antigens *in situ*, suggesting that TLS in the NOD pancreata support the selection of autoreactive B cell clones in this model [72].

MS is a chronic inflammatory disease of the central nervous system with a recognised involvement of T cells. Also in MS a more important involvement of B cells and humoral immunity has been speculated in the last decade. Presence of B cells in the immune infiltrates of MS brains has long been observed together with an oligoclonal expansion of the immunoglobulin repertoire; additionally, some studies have associated higher level of IgG with more aggressive forms of MS. The role of B cells in the pathology has been finally confirmed in MS patients treated with B cell depleting antibodies where a reduction in the brain lesions was observed in comparison with placebo-treated controls [73]. Importantly, the presence of lymphoid follicles in the brain of MS, which has eluded investigators in the field, has finally been observed in the meninges of MS patients. B/T lymphoid follicles expressing lymphoid chemokines and B cell survival factors are observed in human MS brains and also in a mouse model of MS, i.e. EAE [33],[74]. Furthermore, TLS in the MS brain (observed more often in patients with a particular form of disease progression, the so called secondary progressive MS) are adjacent to meningeal lesions, suggesting a pathogenic role of these follicles in some forms of MS [75].

1.1.5 Tertiary Lymphoid in graft rejection and cancer

If ELN is an antigen-driven phenomenon and the formation of TLS occurs in the organ where the antigenic stimulus is present, even if the antigen eliciting the immune response is not always known, it is not surprising that TLS form in allogeneic transplantations, where the graft itself represents a continuous source of non-self antigens. The observation of lymphoid infiltrates in grafts dates back in time, never the less only recently the association between allograft rejection and the presence of TLS in the graft has been highlighted as an important step in graft rejection [12],[13]. Not surprisingly, there is a growing evidence of anti-graft antibodies generation and B cell clonal expansion in the chronically rejected transplant patients [11],[40].

Leukocyte infiltration in solid tumours is a prognostic factor for many different type of cancer. So far, investigations have mainly focused on the cancer-promoting role of the various subsets of infiltrating lymphoid cells, with a particular attention to macrophages that can often promote cancer growth and vascularization. Nevertheless, there is growing evidence of the formation of TLS in the vicinity of colon, lungs, breast and other types of adenocarcinoma, suggesting that the development of TLS represents an attempt to mount an anti-cancer immune response in the vicinity of, and related to, the tumour mass. Recently, it has been shown that different types of cancer-related immune cell infiltration can lead to very different clinical outcomes and prognosis [10]. TLS were also found in the colon mucosa of colorectal cancer patients while in studies on human breast carcinoma, not only cancer-associated ELN was observed, but also an oligoclonal antigen-driven expansion of B cells with *in situ* production of tumour-specific antibodies was demonstrated [8]. Similar findings

were reported for human melanoma where AID activation within B cell follicles was observed in skin metastases [7] as well as lung cancer, where the presence of tumour-induced bronchial-associated lymphoid tissue (Ti-BALT) was associated with a favourable clinical outcome [9].

1.1.6 Tertiary lymphoid structures in chronic bacterial infection

Given the capacity of ELN to mount an efficient adaptive immune response at site of chronic antigen stimulation, it is not surprising that the formation of TLS have also been frequently observed in chronic infections, either caused by bacterial or viral pathogens. I will discuss in more detail the virus-induced TLS formation in section 1.1.7.

When considering chronic bacterial infections, probably the best characterised scenario for ELN formation is the *Helicobacter pylori*-induced gastritis. Bacterial infection of the gastric mucosa leads to the formation of MALT (in this case often called gastric mucosa-associated lymphoid tissue, GALT) and this process is critically dependent on the ectopic expression of CXCL13 and the presence of its receptor CXCR5 [6],[76]. As expected, bacterial infection is also associated with the development of HEV in the mucosa [77] and it has been proven that the appearance of GALT is specifically associated with the presence of *H. pylori*. Accordingly, GALT is normally absent in healthy individuals and in patients affected by non-bacterial gastritis, whilst *H. pylori* eradication following antibiotics results in a significant reduction of the lymphoid infiltrate [78],[79].

Importantly, chronic *H. pylori* infection is also associated with the appearance of primary gastric B cell lymphoma of the MALT, and eradication of bacterial infection results in a regression of the malignancy up to a certain degree of

accumulated genetic abnormalities, after which the survival and proliferation of malignant B cell clones becomes uncoupled from the signals received by the chronic inflammatory milieu [80]. This is of particular relevance to understand the implications of persistent TLS in the development of more severe pathologies, as the appearance of MALT lymphoma in salivary glands positive for TLS is also a feature of SS (discussed in section 1.2.1).

An emerging role for TLS in the control of tuberculosis has emerged from studies conducted both in humans and infected mice. Tuberculosis is an infectious disease caused by the pathogen *Mycobacterium tuberculosis*. The hallmark of the disease is the formation of granulomata in the lungs. A granuloma is an aggregate of multinucleated macrophages forming around a persistent stimulus that cannot be eradicated. Tuberculosis is inextricably linked with granuloma: the name of the disease itself refers to lung granulomata, the tubercles, the first described forms of granuloma. Because of this, research on tuberculosis has mainly focused on understanding the relationship and the interplay between the pathogen and the granuloma, that has always been considered a barrier against bacterial dissemination and thus protective (reviewed in [81]). More recently, not only this protective role of granuloma formation has been questioned but also a new interest has been growing around the other lymphoid structures forming together with the granuloma [81]. TLS showing B/T cells infiltrates and positive for HEV were found in proximity to granulomata (i.e. forming a ring around granulomata) in lung specimens from tuberculosis patients as well as murine models of the disease [82],[83]. Moreover, in the murine model, the relevance of the lymphoid chemokines in the development of TLS in the lungs was demonstrated, as gene and protein

expression of these molecules was present in the samples. Interestingly, CCR7-deficient animals showed disrupted TLS in the lungs and an increased level of pulmonary inflammation but were still capable of controlling the infection [84].

When considering non-mucosal tissues, Lyme's disease is a good example of a pathology caused by a bacterial agent, *Borrelia burgdorferi*, which presents features of ELN. *Borrelia* is transmitted to humans via a tick bite and if left untreated can cause a plethora of symptoms in different organs. One of the most common late-stage manifestations is arthritis: in a subset of patients arthritis symptoms do not disappear even after a course of antibiotics despite an apparent absence of the bacterium [85]. Biopsies from this treatment-resistant subgroup show infiltration of lymphocytes with B/T cells discrete areas but also FDC networks and clusters of plasma cells. The analysis of the immunoglobulin repertoire from plasma cells obtained from patients' biopsies revealed a high number of nucleotide substitutions in comparison to germline, suggesting an antigen-driven process of SHM. The authors speculate that in these patients, since the infection has been supposedly eradicated, the process of antibody affinity maturation is probably driven by self-antigens because of their molecular-mimicry with bacterial components [5].

1.1.7 Tertiary lymphoid structures in viral infection

Viral infections represent one of the major challenges in terms of immune system adaptation to pathogen invasion. Viruses can in fact mount a plethora of different countermeasures against immune surveillance and response, exploiting the host defence mechanisms. In this scenario, many theories regarding autoimmunity development postulate that some of the body responses to persistent viral infections and some of the strategies that viruses

evolved to resist and replicate in the host, might eventually lead to breach of tolerance and self-reactivity as a side effect. Here I will report two cases of virus-induced TLS development: in the first I will discuss the protective role of influenza-induced lung-specific TLS as inductive sites for an efficient adaptive immune response; in the second, I will focus on the *hepatitis C virus*-driven ELN in the liver, and the systemic consequences of an unresolved chronic infection in terms of autoimmunity development.

1.1.7.1 Tertiary lymphoid structures as anti-viral immunity inductive sites

A classic example of TLS formation following infection is *influenza virus*-induced lymphoid neogenesis in the lungs of rodents. In some species, such as pig and rabbit, a lymphoid tissue similar to that found in the gut (gut-associated lymphoid tissue, GALT) is constitutively present in the bronchial tract. This bronchus-associated lymphoid tissue (BALT) is absent in human and rodents in normal conditions but can be induced upon infection and/or chronic inflammation and has been thus termed inducible-BALT (iBALT) [86]. iBALT is characterized by the classic structural hallmarks of SLO and TLS such as B cell follicles surrounded by a more loose T cell area; PNAd$^+$ HEV (in contrast with GALT MadCAM$^+$ HEV), and, in contrast with both GALT and specialized BALT of pigs and rabbits, absence of M cells [87],[88]. In the *Influenza virus* model of lymphoid neogenesis, it is possible to observe the formation of TLS already within 10 days after virus administration. These inducible TLS are characterized, as expected, by densely packed B cell follicles displaying markers of functionality, such as FDC networks and differentiation of GC B cells, as demonstrated by the expression of GL7, an antigen expressed by murine germinal centre B cells undergoing productive immunoglobulin class

switching [89]. These B cell follicles are surrounded by a T cell-rich area populated by proliferating CD4 and CD8 cells in close proximity with PNAd[+] HEV, and develop in association with the expression of high levels of CXCL13, CCL19 and CCL21 transcripts [90]. Recent evidence suggests that TLS maintenance in the lungs of *Influenza virus*-infected mice requires the influx of CD11b^{+}CD11c^{+} dendritic cells, which appear to represent a major source of LTβ, as well as lymphoid chemokines CXCL13, CCL21 and CCL19, particularly at later stages of infection and after viral clearance [58]. Importantly, ectopic GC in the iBALT of *Influenza virus*-infected mice promote the *in situ* differentiation of virus-specific (i.e. anti-nucleoprotein) plasma cells [58]. Even more importantly, bronchial TLS are required for the maintenance of systemic humoral antiviral immunity, as demonstrated by the reduced titres of serum hemagglutinin-inhibiting antibodies and the lower number of nucleoprotein-specific plasma cell numbers in the bone marrow of mice in which the formation of iBALT was ablated [58]. In keeping with a non-redundant role of the iBALT in this model, LTα-deficient mice, which lacks conventional SLO, are still capable of developing functional TLS and express lymphoid chemokines at levels comparable to their wild-type littermates [90],[91]. Additionally, bronchial TLS are sufficient in promoting antiviral immunity, as demonstrated by the generation of protective titres of virus-specific circulating IgM and IgG, and are also capable of producing and maintaining immunological memory upon re-challenge [43]. Overall, the above evidence strongly supports the conclusion that the formation of TLS, particularly at permissive mucosal sites, is required and sufficient to promote protective immunity over and above SLO, thus directly contributing to immune surveillance and viral clearance.

1.1.7.2 Virus-induced tertiary lymphoid structures as a bridge to autoimmunity

Hepatitis C virus (HCV) infection-induced TLS formation is one of the best-characterised examples of ELN following chronic infection. A striking feature of HCV infection and of the subsequent chronic hepatitis that develops in 80% of the cases, is that HCV itself is not a cytolytic virus and that viral replication can be detected in patients where liver damage is absent while tissue damage is largely dependent on the immune reaction towards the pathogen [92]. Moreover, the formation of lymphoid infiltrates in chronic HCV infection, the intraportal lymphoid follicles, has long been known as a hallmark of the disease [93]. Murakami and colleagues showed that B cells in the intrahepatic follicles display markers of a GC response further supporting the hypothesis that these structures represent inductive sites for B cell antigen-driven differentiation [94]. Accordingly, clonally-related intrahepatic CD4+ T cell were found to react specifically with HCV epitopes and significantly more efficient in promoting an IgA antibody response when cultured with B cells in comparison with T cells isolated from peripheral blood of the same patients [95]. Thus, antigen-specific T cell priming is likely to take place within intrahepatic TLS. This is of particular importance as a prompt and potent T cell response from HCV-specific CD4^{+} helper and CD8^{+} cytotoxic T cells, in the context of selective HLA alleles have been linked to viral control and clearance [96] [97]. Conversely, despite the evidence of B cell activation, the humoral response by itself seems unable to fully protect from HCV infection as re-inoculum of the virus in chimpanzees elicits a new viremia in the presence of neutralizing anti-HCV antibodies [98]. The mechanisms leading to lack of viral clearance and the establishment of

chronic HCV infection are still largely undefined despite intensive investigations focusing both on viral mechanisms of escape of immune surveillance as well as defective anti-viral immune responses [99], but it is clear that intrahepatic TLS play a central role in regulating complex viral-host interactions. In fact, lack of viral clearance progressively leads to chronic B cell activation within TLS that, in a subset of HCV[+] patients, contributes to the development of extra-hepatic manifestations and autoimmunity, manifested as mixed cryoglobulinemia (MC). Type II cryoglobulins are monoclonal IgM that precipitates at low temperatures and display rheumatoid factor activity and can give rise to systemic manifestations such as cutaneous vasculitis and glomerulonephritis. Interestingly, despite this deregulated antibody production, HCV[+] patients with MC show a decrease in the total number of B cells. In a recent study, this phenomenon has been attributed to an increased tendency of naïve B cells to die of apoptosis. According to this hypothesis, to maintain B cell homeostasis more immature B cells are produced by the bone marrow [100]. Moreover, and in addition to the monoclonal B cell activation in MC, the IgM memory B cell subset is expanded in a polyclonal fashion in HCV patients with MC and analysis of the Ig genes in these expanded clones showed level of SHM suggestive of Ag-driven selection. Furthermore, some of the clones showed self-reactivity further supporting the idea that HCV chronic infection can influence tolerance mechanisms, allowing the expansion of autoreactive B cell clones [101] [97] .

Finally, two more evidences strongly support a link between HCV infection and a deregulation of the B cell behaviour in the context of TLS. In particular, one of the core proteins encoded by the HCV genome has been shown to interact with

the cytoplasmic tail of LTβ-receptor [102]: the effect of this interaction, far from being completely elucidated, could be a constant activation of the LTβ pathway in the infected cells. To support this hypothesis, there is evidence that cryoglobulinemia in HCV$^+$ patients is closely associated with serum and lesional levels of CXCL13 [103]. This suggests that intrahepatic evolution from a polyclonal to an oligo- and then monoclonal autoreactive B cell activation is a result of chronic antigenic stimulation taking place within TLS.

1.2 Sjögren's syndrome as a model disease of ectopic lymphoid neogenesis in mucosa

The Swedish ophthalmologist Henrik Sjögren in 1932 described a disease characterised by xerostomia (dry mouth), keratoconjunctivitis *sicca* (dry eyes) and RA. That disease became known worldwide as Sjögren's Syndrome.

SS is a chronic autoimmune disease that affects mainly exocrine glands, salivary (SG) and lachrymal, and eventually leads to glandular dysfunction. Falling in the category of autoimmune disease, SS patients produce autoantibodies and might be affected by several extra-glandular systemic features [104].

SS can present alone (primary SS, pSS) or in association with other autoimmune rheumatic diseases (secondary SS, sSS). The prevalence of pSS in the general population is approximately 0.5-1%, while sSS appears in approximately 30% of the patients affected by other autoimmune diseases [104].

Despite the presence of important extra-glandular manifestations, SS is a tissue-specific autoimmune disease. The exocrine glands, in particular the SG, represent a very interesting tissue: "frontier" to the body, not only they are a

natural barrier, but being located in the oral cavity they also are in continuous contact with commensal and pathogenic microorganisms. Furthermore, SG have to fulfil their physiological function of saliva production and systemic regulation of nitric oxide (NO) levels [105],[106].

As we will discuss in depth in the next sections, one of the clinical signs of SS is the presence of lymphocytic infiltration in the salivary and lachrymal glands that often organises in fully formed TLS.

Several pathogens have been regarded as triggers for SS development and although this issue is still controversial, recent evidences point towards a role for chronic infection of the SG mucosa.

Because of their involvement in host-pathogen interaction and as target-organ of autoimmunity, SG represent an ideal tissue where to conduct studies on both these aspects and the potential combined and reciprocal effects of infection and autoimmunity.

1.2.1 Sjögren's syndrome: definition and clinical manifestations

Even if SS can manifest at various ages and in both sexes, the female-to-male ratio is 9:1 and middle-aged women are primarily affected. As indicated above, prevalence of SS is approximately 0.5-1% and thus SS is considered one of the most common autoimmune diseases.

There is little epidemiology for SS outside Europe, North America and some countries of Asia: the highest prevalence of the disease is found in northern Europe, but comparable percentages are observed in North America and mainland Europe while the lowest rates have been observed in Asia [107]

Diagnostic criteria for Sjogren's syndrome

I. Ocular symptoms. A positive response to at least one of the following questions
- Have you had daily, persistent, troublesome dry eyes for > 3 months?
- Do you have recurrent sensation of sand or gravel in the eyes?
- Do you use tear substitutes more than three times a day?

II. Oral symptoms. A positive response to at least one of the following questions
- Have you had a daily feeling of dry mouth for > 3 months?
- Have you had recurrent or persistent swollen salivary glands as an adult?
- Do you frequently drink liquids to aid in swallowing dry food?

III. Ocular signs. Objective evidence of ocular involvement defined as a positive result for at least one of the following tests
- Schrimer's I test, performed without anesthesia (≤ 5 mm in 5 min)
- Rose Bengal score or other ocular dye score (≥ 4 according to van Bijsterveld's scoring system)

IV. Histopathology
- Focal lymphocytic sialoadenitis in minor salivary glands, evaluated by an expert histopathologist, with a focus score ≥ 1, defined as a number of lymphocytic foci (which are adjacent to normal appearing mucous acini and contain more than 50 lymphocytes) per 4 mm^2 of glandular tissue

V. Salivary gland involvement. Objective evidence of salivary gland involvement defined by a positive result for at least of the following diagnostic tests:
- Unstimulated whole salivary flow (≤ 1.5 ml in 15 min)
- Parotid sialography showing the presence of diffuse sialectasis (punctuate, cavitary or destructive pattern), without evidence of obstruction in the major ducts
- Salivary scintigraphy showing delayed uptake, reduced concentration and/or delayed excretion of tracer

VI. Autoantibodies: presence of antibodies to Ro(SSA) or La(SSB) antigens, or both, in the serum
Exclusion criteria
Past head and neck radiation treatment, Hepatitis C infection, Acquired immunodeficiency syndrome
Pre-existing lymphoma or sarcoidosis, Graft versus host disease, Use of anticholinergic drugs

Figure 1.6: Sjögren's syndrome diagnostic criteria. Reprinted from [107], Copyright 2010, with permission from Elsevier.

The ductal epithelium appears to be the main target of the inflammatory autoimmune process. Because epithelia from other exocrine glands, other than the salivary and lachrymal, can be affected during the disease, some authors define SS as an "autoimmune epithelitis" [108].

SS patients complain of dry mouth and dry eyes, the so-called *sicca* syndrome, one of the main hallmarks of disease. Xerostomia causes difficulties in swallowing, taste alterations and often dental caries, mucositis and candidiasis [109]. As a consequence of an insufficient lachrymal flow, patients develop keratoconjunctivitis *sicca*. It is still debated whether these glandular dysfunctions are caused by a disruption of the gland parenchyma or by an interference, supposedly caused by autoantibodies, with the neurological stimuli (i.e. acetylcholine acting on muscarinic receptors) that induce saliva and tear secretion [109].

As reported above, SS also can present extra-glandular features. A high percentage of patients report musculoskeletal manifestations, and articular symptoms develop in 1/3 of the patients before the appearance of the *sicca* syndrome. Myalgia is often present, and frequently associated with fatigue. The articular involvement is symmetric and often polyarticular: mono-oligoarticular features only appear early in the course of disease [109]. Typically, arthritis in pSS is non erosive, while an erosive disease develop in sSS associated with RA.

For a haematological point of view, SS can present a series of abnormalities with different prevalence in various populations, among which anaemia, lymphopenia, gammopathies and lymphoproliferative disorders [110]. Skin

xerosis and, less frequently, vasculitis, urticarial vasculitis and annular lesions can be observed [109],[111].

Peripheral neuropathies and at a less extent central nervous system manifestations are observed [109].

Respiratory system signs, nasal bleeding, hyposimia, xerotrachea and bronchial hyperactivity can affect a vast percentage of SS patients [112].

Dysphagia and oesophageal dysmotility can be observed as a consequence of the broad involvement of the glandular epithelium of the gastrointestinal tract [113]. For similar reasons, SS patients might develop acute pancreatitis, and other pancreas symptoms, as the exocrine component of this organ can also be a target of the disease [114]. Also in terms of mucosal dysfunction, gynaecological symptoms are often reported, again due to dryness and development of infection as a consequence of impaired vaginal exocrine gland secretion [109].

The liver of SS patients is seldom affected by chronic active hepatitis with portal fibrosis and periductal involvement [114],[115]. Interestingly, as insurgence of *sicca* has been associated with liver manifestations during the course of HCV and HCV has a particular tropism for the SG, HCV infection is an exclusion criterion for SS diagnosis [116]. I will discuss in more details the specific role of viral infections and HCV in SS in section 1.2.5.

Renal involvement is also observed but is not one of the most common effects of SS. Reported symptoms are: renal tubular acidosis, glomerulonephritis (rare), mild proteinuria (common) and defects in urine concentration. Kidneys manifestations have been ascribed to the presence of anti-tubular antibodies or to lymphocyte-mediated tissue damage [109].

SS can frequently appear along other autoimmune diseases, the most common being Hashimoto's thyroiditis and coeliac disease [117].

The most important and serious complication of SS is the development of malignancies, in particular MALT-lymphoma of the salivary glands. MALT-lymphomas develop in approximately 5% of pSS, they are mainly non-Hodgkin B cell lymphomas arising usually in the parotid glands and the presence of lymphoma represent the major factor contributing to SS morbidity and increased mortality [118].

1.2.2 Aetiology and immunobiology of Sjögren's syndrome

SS certain aetiology is still not completely understood. As a complex disease, the causes of SS insurgence are multiple: genetic background, immunological abnormalities and pathogens play a major role in aetiology, but gender and other environmental factors are likely also important [104].

Early analysis of the major histocompatibility complex genes reveals a high association of certain histocompatibility antigens (such as HLA DRB1*03 and DQB1*02) with the production of the classic SS antibodies, anti-Ro/SSA and anti-La/SSB [119],[120]. These observations have been confirmed and expanded in more recent genome-wide association studies (GWASs) [121],[122] that have also found strong disease associations in single-nucleotide polymorphisms (SNPs) present in the interferon pathway and certain NK cells receptor genes (discussed in more details in section 1.2.5.1) [123]. Taken together, these observations reveal that susceptibility *loci* can be found in genes regulating both the innate and adaptive arms of immune system.

Several viral infections have been claimed to be relevant for development of SS. To date no clear correlation between a specific pathogen and SS has been

found and the topic is one of the most controversial in the field of SS and in general in the debate about autoimmune diseases. I will discuss old and new piece of information regarding the relative involvement in SS pathogenesis of HCV, Epstein-Barr Virus (EBV), human T-lymphotropic type-I virus (HTLV-I), Coxsackie virus and cytomegalovirus (CMV) in section 1.2.5.

In the diagnosis of SS, together with the presence of circulating autoantibodies directed against the ribonucleoproteins Ro/SSA and La/SSB, one of the hallmarks of the disease, and an essential criterion to be met for classification, is the presence of a positive histopathology in the minor salivary glands. In SS the typical inflammatory infiltrate affecting the SG is the formation of at least one aggregate of more than 50 lymphocytes per 4 mm^2 of glandular tissue, called *focus* [116],[124]. The majority of the data describing these inflammatory *foci* derives from studies on minor and major salivary glands and this is mainly because the disease commonly affects these tissues but also because they can be easily taken with minor surgical procedures (in particular the labial SG biopsies).

Anatomically, SGs are divided in major and minor: parotid, submandibular and sublingual glands belong to the former, labial, buccal and palatine to the latter. Blood and lymphatic vessels, but also nerves, intercalate the parenchyma of the glands, composed of acini and ducts. The acini are the basic secretory components and they can be serous, mucous or mixed. Histologically they are a single layer of cuboidal epithelium secreting the various components of saliva into a central lumen. Intercalated ducts proceed from the acinar units and join in striated ducts: the epithelium of the latters is responsible for the transformation

of the saliva into a hypotonic solution thanks to active and passive ion transporters. In turn striated ducts terminate into interlobular or secretory ducts that collect from the various lobes of the SGs and open in the mouth. Myoepithelial cells surround intercalated ducts and acini and are connected with both the sympathetic and parasympathetic nervous system that regulate saliva secretion [125].

Typically the SS infiltrate is organised around the excretory ducts (mostly at the level of intercalated ducts) and the diagnostic parameter used to classify it in SS is the Chisolm and Mason score. The diagnosis is positive for SS with at least a focus score. A more detailed description of the immune infiltrate is given in the section 1.2.3.

As briefly mentioned above, the epithelium plays a pivotal role in SS, that lead some authors to define the disease as an "autoimmune epithelitis" also because of the involvement of epithelia other than that of SGs in the pathology [108]. SG epithelial cells from SS express mRNA for lymphoid chemokines, suggesting that this cell type might be among the first to produce chemotactic clues for B and T cell recruitment to the gland [126]. Furthermore, SS ductal epithelial cells derived from patients and cultured *in vitro* retain the expression of costimulatory molecules (e.g. CD80/86 [127], CD40 [128] and HLA-DR/DP/DQ [129]). Also, the expression of adhesion molecules has also been demonstrated both in histology and in cultured epithelial cells from SS SGs [130]. Moreover, Th1 cytokines mRNA levels were higher in SS patients and those cytokines, when added to cultured SG epithelial cells from patients, augmented their expression

of HLA and adhesion molecules [130], suggesting that epithelial cells can function as APCs.

Furthermore, elevated expression of Fas and Fas ligand in ductal epithelium suggests an increased apoptosis rate in SS SGs [131]. Interestingly, some of the typical autoantigens of SS, i.e. Ro-SSA and La/SSB, are expressed in apoptotic blebs [132] and thus an amplified presence of apoptotic bodies and self-antigens in an environment prone to favour an adaptive immune response might be partially responsible for breach of self tolerance leading to the initiation and perpetuation of the autoimmune process. Nevertheless, it is important to stress that, given the importance of pathogens in SS, it is still unclear whether SG epithelial cells involvement in the disease has a primary pathogenic role or it is merely a secondary effect to pathogen infection and the subsequent immune response.

1.2.3 Ectopic lymphoid neogenesis in Sjögren's syndrome

The immune infiltrate present in SS SGs is composed mainly of lymphomonocytic cells, in particular B and T lymphocytes. T cells are mainly of the $CD4^+/CD45RO^+$ phenotype. $CD8^+$ T lymphocytes are also present at a lesser extent and preferentially localised around the acinar units where they probably contribute to the glandular damage and the loss of salivary function via the secretion of granzyme/perforins [133]. B cells are also present and their number increases with the development of the inflammatory infiltrate, thus it is more likely to observed higher frequencies later in the disease course [134].

Members of my group and other groups have demonstrated that the expression of lymphoid chemokines CXCL13 and CCL21 is closely associated with the progressive acquisition of lymphoid features in SS SG such as T/B cell

segregation and FDC networks development [31]. However, expression of both CXCL13 and CCL21 in SS did not require the full development of TLS suggesting that lymphoid chemokines act upstream to this process [31]. In the SS SG, CXCL13 and CCL21 retained an expression pattern highly reminiscent of SLO, with CXCL13 confined to the B cell-rich areas and CCL21 expressed in the surrounding T cell area (i.e. mainly produced by perivascular cells in close association with HEV [21],[135]). Of relevance, in SS patients with TLS, both resident cells and infiltrating immune cells produce lymphoid chemokines. Among infiltrating cells, CD68+ macrophages and CD3+ T cells have the capacity to produce CXCL13 within TLS [136] as previously described in the rheumatoid synovium [65],[136]. Conversely, among non-lymphoid cells, ductal epithelial cells can be an important source of CXCL13, CCL19 and CCL21, together with CXCL12, as shown by *in situ* hybridization and immunohistochemistry [32],[126]. Additionally, my laboratory and others showed that stromal reticular-like cells within inflammatory foci and endothelial cells can express CXCL13, although CXCL13 expression in blood vessels is likely the result of transcytosis rather than primary production [30],[135]. Finally, a recent study found an association between genetic variants in the Ltα/Ltβ/TNF family and SS insurgence, again highlighting the role of the whole lymphotoxin/lymphoid chemokines axis in the generation of TLS in SS [137]. Thus, it appears that the interaction between resident (i.e. epithelial and stromal cells) and infiltrating immune cells of both the innate and adaptive immune system contributes to trigger lymphoid neogenesis in the SG, although the exact hierarchical series of cellular and molecular events underlying this process are yet to be elucidated.

More observations coming from others and our group also provided evidence that the TLS arising in SS SG are likely to be functional and support B cell activation and differentiation [38] and are critically implicated in disease-specific autoimmunity. In support to this hypothesis, hypermutation is observed in the immunoglobulin genes of B cells present in highly organised TLS [138]. Furthermore, these B cells can be autoreactive and produce autoantibodies such as anti-Ro/La [32],[139],[140] and in general higher titres of G immunoglobulins, rheumatoid factor and anti-Ro/La are observed in SS patients positive for GC markers in comparison to patients devoid of these structures [141]. A more conclusive evidence of GC functionality in SS SGs comes from the observation that the enzyme AID, necessary for the CSR and SHM processes, is invariably expressed in the *foci* with features of SLO and expression of FDC network markers [38].

Finally, there is now strong evidence that the presence of TLS in the SG of SS patients is an important biomarker of a more severe disease associated with extraglandular manifestation and evolution towards B cell lymphoma of the MALT [38],[136],[142],[143].

1.2.4 Autoantibodies

Antibodies directed towards the ribonucleoparticles Ro and La, two self-antigens, have been historically considered the classic SS autoantibodies, despite being also found in systemic lupus erythematosus (SLE) patients. SS also present in their circulation anti-nuclear antibodies (ANA), RF, type II cryoglobulins and to a lesser extent anti-mitochondrial, anti-centromere and anti-smooth muscle antibodies [144]. Another set of autoantibodies is present in SS and the members, anti-α-fodrin, anti-carbonic anhydrase II and anti-

muscarinic acetylcholine receptor 3 (M3R), have been variously described, albeit not conclusively, as pathogenic and able to affect exocrine function [144],[145].

The ribonuceloparticles (RNP) Ro and La are complexes composed of proteins (Ro 52kDa, Ro 60 kDa and La 48 kDa) and small uridine-rich hY RNAs (human cytoplasmic RNAs) that are 85-112 nucleotides-long RNA polymerase III transcripts [144],[146]. Ro60 protein seems involved in post-transcriptional modification of RNA polymerase III transcripts, while Ro52 is involved in ubiquitination [144],[146]. The phosphoprotein La is a regulator of all RNA polymerase III transcripts and it is also capable to bind to several viral RNAs [144],[146]. Anti-Ro/SSA and anti-La/SSB autoantibodies are unable to recognise the isolated small RNAs without the presence of Ro and La proteins. These autoantibodies are found in approximately 60% (anti-Ro) and 40% (anti-La) of SS patients, most commonly in combination, while anti-La are very rarely found alone [144],[146].

Muscarinic receptors are acetylcholine G-protein-coupled seven-transmembrane domain receptors, they are classified in 5 subtypes (M1-M5) with M3R being involved in particular in endocrine and exocrine glands secretion, smooth muscle contraction and endothelial cells calcium regulation [147]. Acetylcholine stimulation of M3R in the acinar cells of the SGs induces a change in intracellular calcium concentration that in turn leads to activation of membrane channels that secrete sodium and chlorine ions in the lumen of the acini. This in turn osmotically drags water in the lumen for the formation of saliva [147]. Among the autoantibodies characteristic of SS, anti-M3R antibodies have been claimed to be pathogenic and one of the main causes of

sicca syndrome as they can interfere with the influx of calcium in response to acetylcholine, thus impairing saliva production and secretion. In particular, one of the most important observations is that sera from SS patients and from experimental mouse models of SS were able to induce salivary hypofunction when injected in mice devoid of B cells, and a similar effect was obtained when injecting monoclonal antibodies to M3R in immunodeficient mice [147]. Unfortunately, at the moment there is no gold standard for the detection of anti-muscarinic receptor 3 antibodies in the blood of SS patients and up until such an assay is available for clinical use there will be controversies about the real presence and pathological role of such antibodies, making it difficult to correlate epidemiologic data in order to understand whether or not this class of autoantibodies designates a specific subtype of SS patients.

SS patients can also develop autoantibodies against α-fodrin, the main cortical cytoskeleton component of eukaryotic cells. This observation was first made in a mouse model of SS and extended to human patients [145]. Antibodies against α-fodrin [148] can be found in 55-64% of pSS and 40-86% of sSS. α-fodrin has been associated with apoptosis and in particular its abnormal externalisation in apoptotic salivary gland cells has been reported [149]. The granzyme-B enzyme, pivotal in the CD8^{+} T cells cytotoxic process, can also cleave α-fodrin and M3R present in salivary gland epithelial cells, thus producing novel epitopes and potentially boosting the process of breach of tolerance towards common self antigens [150]. To support this hypothesis, another study found a novel cleaved form of α-fodrin which was recognised by autoantibodies present in around 25% of patients enrolled within a sizeable cohort of American SS patients [151]. Finally, EBV reactivation, that has also been recently associated

with SS as discussed in section 1.2.5.2, induces an increase in caspase activity and as a consequence an abnormal production of α-fodrin proteolysis [152].

1.2.5 Chronic viral infection in Sjögren's syndrome

Several groups have investigated whether the SG of SS patients display an aberrant expression of sialotropic viruses capable of triggering autoimmunity as a result of a persistent chronic infection. In this section I shall first review indirect evidence that the type I (and type II) interferon pathways, critically involved in anti-viral immunity, are aberrantly activated in SS patients; I shall then summarize the evidence in support of (or against) the role of viruses in SS over the last 30 years.

1.2.5.1 Evidence of aberrant type I and type II interferon activation in SS patients

If viruses were etiological agents, or at least significant contributors to the pathogenesis of SS, in the presence of persistent viral infections one would expect circumstantial signs in support of the activation in the SS SG of critical immune-defence mechanisms regulating viral infection in physiological conditions. In this regards, type I (IFN-I) and type II (IFN-II) interferons are critically involved in host protection from viral pathogens via their ability to inhibit viral replication, promote DC maturation, enhance NK and CD8$^+$ T cells cytotoxicity, induce phagocytic activity in macrophages and favour B cells survival and antibody production [153]. In keeping with this scenario, IFN-regulated genes have been found differentially expressed in SG biopsies from SS versus controls [154] and in IFN-stimulated SG epithelial cells from SS patients IFN-related gene transcripts were more abundant in comparison with controls [155]. Plasmacytoid dendritic cells (pDC) are the main producer of

type-I interferon in response to microbial stimuli [156] and interestingly pDCs have been found in biopsies from SS SGs but not in control specimens [155]. Moreover, around 50% of SS patients, but not healthy controls, displayed detectable plasma levels of IFN-α and peripheral-blood mononuclear cells (PBMC) from SS patients had a significantly higher expression levels of IFN-α compared to controls [157]. More recently, Brkic and colleagues demonstrated that circulating monocytes from pSS patients with an upregulated expression of IFN-related genes, the so-called type-I IFN signature, had a higher disease index score and higher levels of circulating autoantibodies. Interestingly, the serum from this SS sub-group of patients was capable of inducing in cultured monocytes the expression of BAFF [158], a cytokine member of the TNF family which acts as a pivotal regulator of B cell survival and activation and has been strongly linked with B cell dysregulation in SS [159]. Interestingly, BAFF can also be induced *in vitro* in ductal epithelial cells by the synthetic double-stranded RNA (dsRNA) analogue and by the Toll-like receptor 3 (TLR-3) ligand poly(I:C) as well by viral dsRNA [160].

This excessive activity of type-I interferons in SS, and more in general in autoimmunity, has been ascribed to several causes, such as the activation of pDCs in various autoimmune diseases, the lack of a tight regulation of pDC activation in susceptible individuals and the observation that many autoimmunity-associated risk genes are in the IFN-I signalling pathway [153]. From this perspective, since persistent viral infection of SG does not lead *per se* to autoimmunity in normal individuals, it is conceivable that in SS patients the abnormal IFN-I response may be related to genetic susceptibilities conferred by variability within interferon-related genes. In this regard, single nucleotide

polymorphisms (SNPs) in two genes involved in type-I IFN signalling, IRF-5 and STAT4, have been found associated with a higher risk to develop SS both in case control studies [161],[162] as well as a recently published genome-wide association study (GWAS) [121]. More recently susceptibility for SS development has also been found in the type-II interferon (IFN-γ) pathway whereby a significant association was found between the rs11575837 SNP in the promoter region of the NCR/NKp30 gene and SS [123]. This SNP confers a protective effect in terms of SS development and was associated with a reduced production of IFN-γ in NK cells upon NKp30 stimulation in comparison to individuals who did not carry the rs11575837 SNP.

Overall, the above observations strongly suggest that a genetic background particularly susceptible to IFN-related genes activation upon viral infection might predispose to SS development.

1.2.5.2 Epstein-Barr virus (EBV)

EBV is a B lymphotropic herpesvirus capable of establishing an asymptomatic life-long infection and can cause infectious mononucleosis. EBV infects most of the world population and its characterized by an active lytic cycle during which the virus duplicates and propagates and a latent cycle when the virus remains silent in B cells [163]. EBV latency is maintained by the expression of a limited set of proteins including the main latency proteins LMP1 and LMP2A which mimic the signalling properties of CD40 and the B-cell receptor, respectively, and regulate activation, growth, and survival of the infected B cells in the absence of cognate antigen [164]. Interestingly, while *in vivo* EBV tends to switch to and stay in the latent cycle with temporary activation flares of the lytic program, *in vitro* it induces B cell transformation, leading to activation,

proliferation and expansion [165], the same process that *in vivo* may lead to B cell malignancies such as Hodgkin's and Burkitt's lymphoma [166]. As other viruses, EBV uses mucosal tissue to disseminate from infected individuals. Due to its tropism for the SG and the capacity to preferentially infect B cell, it is not surprising that EBV has attracted significant interest aimed at investigating whether the SG of SS patients display dysregulated EBV infection and persistence. Despite extensive studies, in SS there is significant controversy regarding whether EBV is implicated in disease pathogenesis. There is also conflicting evidence regarding the expression of EBV proteins/nucleic acids in SS-SG compared to *sicca* or healthy controls. Several studies have reported increased EBV expression in SS patients compared to *sicca* controls [167]-[173], while others failed to observe differential expression in SS SG [174]-[176].

Interestingly, B cell lines obtained from SS patients were shown to be more efficient in producing transforming EBV in comparison with non-SS controls, suggesting a more frequent reactivation of EBV lytic cycle in SS patients [169],[170]. When comparing EBV reactivation in SS to other autoimmune diseases with a known B cell involvement, it was shown that B cells from peripheral blood of SS patients were more efficient than the same subset from RA and SLE patients in EBV production [177], suggesting that the polyclonal activation of B cells in SS patients may somehow be correlated with the presence and activation of EBV.

Together with EBV-induced B cell activation, other mechanisms, such as molecular mimicry, have been implicated in support of a role of EBV in contributing to breach of self tolerance and development of autoimmunity in SS.

Molecular mimicry implies that a microbial epitope structurally similar to a self-antigen could be processed via the major histocompatibility complex (MHC) and presented to T cells, thus activating auto-reactive clones that escaped the selection process [178]. In the case of EBV, several examples of possible molecular mimicry between SS auto-antigens and viral proteins have been demonstrated, although the impact of such mechanisms in contributing to autoimmunity and chronic inflammation has not been formally demonstrated. Interestingly, anti-Ro/La autoantibodies can precipitate protein antigens linked with EBV-encoded small RNA (EBERs) [179] while the EBV transcriptional transactivator EBNA1 mimics Ro52 [180]. Additionally, EBV can induce the cleavage of α-fodrin [152], a cytoskeletal molecule that is cleaved during apoptosis into the antigenic 120kDa form which is a target of autoantibodies found in SS sera, as described in more details in section 1.2.4 [145]. Finally, screening of a random peptide library with sera from SS patients allowed the isolation of a specific peptide which is targeted by circulating autoantibodies in SS patients with shared homology between an EBV early antigen, α-fodrin and tear lipocalin, a molecule found in tears and saliva [181]. Thus, EBV may play a role in SS development via different mechanisms: B cell reactivation, persistence and immune evasion in epithelial cells, induction of apoptosis and consequent unmasking of cryptic antigens that could lead to the activation of self-reactive T/B cells through molecular mimicry.

1.2.5.3 Human T-lymphotropic virus Type 1 (HTLV-1)

During the 1980s two different observations lead to the association of the human T-lymhpotropic virus 1 (HTLV-1) and SS. HTLV-1 is a T lymphotropic retrovirus responsible of some forms of T-cell acute leukaemia and tropical

spastic paresis. The first observation was a case report of HTLV-1 patients with tropical spastic paresis, who also showed features of SS [182].The second observation came from a transgenic mouse model expressing a HTLV-1 gene, *tax*, that manifested SG exocrinopathy and lymphocytic infiltration resembling SS [183]. Following these initial discoveries, further investigations focused on the possible link between HTLV-1 retrovirus and SS development, in particular in those regions endemic for HTLV-1, such as Japan and Caribbean Islands. The first studies demonstrated that HTLV-1-infected SS patients were characterised by a stronger peripheral blood mononuclear cell proliferation and increased rated of extraglandular manifestations [184]. In the same period, another group showed that SS biopsies were positive for a protein encoded by the viral gene *gag*, also in individuals seronegative for HTLV-1 antibodies. This allowed to speculate over the presence of an endogenous retrovirus in SG epithelial cells, capable of inducing chronic inflammation in SS [185]. Mariette et al. found, by *in situ* hybridization, a positive signal for *tax* gene in SG biopsies of SS patients without any detectable antibodies to HTLV-1 [186] and similar results were found in Japanese SS patients by Sumida et al. [187]. More recently, Lee et al. replicated the same observations and hypothesised that patients with HTLV-1-associated SS might represent a distinct clinical subgroup from idiopathic SS patients, with different serological features and magnitude of lymphocytic infiltration [188]. Ohyama and colleagues found in the infiltrated SG of HTLV-1-infected SS patients that T cells, but not acinar or ductal cells, were positive for HTLV-1 proviral DNA while viral loads were higher in SG in comparison to PBMCs obtained from the same patients. Thus, HTLV-1 infection in the peripheral compartment and/or in the affected tissue might directly

activate autoreactive T cells while the SG microenvironment might be permissive for the homing, rescuing from apoptosis and proliferation of HTLV-1-infected T cells [189]. Recently, another Japanese group confirmed the association between HTLV-1 infection (by anti-viral serum antibodies) and the presence of SS in a large cohort of Japan patients [190]. Importantly, when considering other geographic areas where HTLV-1 is not endemic, the correlation between the presence of anti-HTLV-1 antibodies in serum (or positive PCR signal for HTLV-1 genome) and presence of SS is lost [191].

1.2.5.4 Coxsackieviruses

Among all the viral infections that have been associated with SS insurgence, a special consideration has to be dedicated to the recently hypothesised role of Coxsackieviruses in the development of this disease, as this class of viruses do not show particular tropism for any immune system cell nor for SG tissue. Coxsackieviruses are enteroviruses belonging to the *picornaviridae* family, capable to infect different tissues and leading to acute manifestations, even if recent evidence shows that establishment of a persistent infection is also possible (reviewed in [192]). In 2004, Triantafyllopoulou et al. noticed, using a differential display technique, that specimens from primary SS patients showed a band that was not present in controls and secondary SS samples and that was identified as P2A, a protein synthesized by Coxsackie virus B4 strain [193]. Triantafyllopoulou and colleagues showed that Coxsackie virus strains B4 and A13 genomes were present in biopsies of primary SS patients but not in controls, and when they stained minor SG with an antibody against the viral capsid particle VP1, they detected a positive signal in the B cell area of the infiltrates and in the ductal epithelial cells [193]. Further analysis on the

peptides encoded by the Coxsackie viral genome lead to the identification of a homology between the protein sequences of viral particle P2B and the Ro60 epitope (one of the epitopes towards which SS patients more often develop autoantibodies). When testing reactivity of sera from SS patients and controls against these peptides, Stathopoulou and colleagues showed that anti-Ra and anti-Ro/La SS sera, but not control sera, reacted with both P2B peptide and Ro60 and the autoantibodies isolated with the Ro60 peptide were capable of reacting with the viral peptide [194], further supporting the hypothesis that molecular mimicry may play a very important role in driving autoimmune reactions specially in the context of persistent infections.

Although significant emphasis was generated by the above data, Gottenberg et al. failed to replicate those observations in a French cohort of SS patients using the same PCR technique [195]. A possible explanation for such discrepancy might be related to different epidemiology of enteroviruses in different geographical regions, as also observed for enteroviral infections and the development of autoimmune diabetes [196], although also different genetic susceptibility in diverse ethical cohorts might account for such discrepancies.

1.2.5.5 Cytomegalovirus (CMV)

Similar considerations to the other viruses can be extended to human CMV infection and SS. As for EBV, controversial issues arise when considering this virus as a possible etiological agent of the disease. Around 70-90% of the world population has encountered CMV and the quest for the detection of CMV genome in the SG of SS patients and non-immune *sicca* patients invariably lead to the detection of the viral genome in both groups [168]. CMV is probably one of the most well-studied viral pathogens and we know that the virus has several

different strategies to evade the immune system surveillance [197] [198]. Moreover, specie-specific CMV viruses exist for rodents and primates, allowing the use of a wide range of animal models.

One of the most striking and conserved CMV evasion mechanism is the production of a viral homologue of interleukin 10 (IL-10) [199]. IL-10 is a pivotal anti-inflammatory cytokine involved in a plethora of immunomodulatory processes, such as the inhibition of inflammatory cytokines production (e.g. IL-2, TNFα, IFN-γ), induction of antibody production by B cells, down-regulation of allergic reactions, etc. [200]. Despite a low sequence homology, cmvIL-10 can compete for IL-10 receptor complex and it is capable to activate the IL-10 signalling pathway. The evolution of an IL-10 homolog has been proven to be important in CMV infection and in the ability of the host to clear the pathogen; accordingly, rhesus macaques infected with specie-specific strains of CMV which where engineered to express or deplete cmvIL-10 showed that the viral version of the cytokine was required to dampen both the innate and adaptive immune response and establish a successful systemic infection [201].

Perhaps the most interesting piece of information about a role of CMV in SS development comes from animal studies. In mice, the *lpr* mutation impairs the Fas mediated apoptotic pathway. The effects of *lpr/lpr* mutation varies greatly from strain to strain and, on a C57Bl/6 background, the mutation induces a mild autoimmunity late in the animals' life, mainly involving kidneys but not SG. Fleck et al. showed that intra-peritoneal injection of murine CMV in C57Bl/6 wild type and *lpr/lpr* mice lead to the development of acute sialoadenitis and SG infiltration in both genotypes, but in the *lpr/lpr* animals it also lead to the development of anti-Ro and anti-La antibodies, the most typical autoantibodies

associated to SS [202]. It is noteworthy the fact that this is the only SS model capable to develop anti-Ro/La antibodies, as in the NOD model, one of the standard SS murine models, only a small percentage of the animals develop anti-Ro antibodies and anti-La antibodies are undetectable [203]. Interestingly, in the rat variant of CMV infection the virus is present and replicates exclusively within a specific class of salivary gland epithelial cells, the striated duct cells, leaving largely uninfected the acinar and other ductal cells [204].

1.2.5.6 Hepatitis C virus (HCV)

HCV is a single stranded RNA virus, member of the family of *Flaviviridae*. HCV is a blood-borne pathogen that can establish a chronic infection in the liver in 80% of HCV-infected individuals. Not only HCV-induced TLS are likely to be involved in hepatotoxicity, but chronic B cell activation within liver TLS can, in a subset of HCV[+] patients, contributes to the development of extra-hepatic manifestations and autoimmunity, manifested as mixed cryoglobulinemia [103]. Although HCV is an exclusion criterion for SS [116], in a sizeable proportion of HCV+ patients the virus can give rise to SG lymphocytic infiltration and *sicca* symptoms often indistinguishable from SS (reviewed in [205]). Interestingly, HCV is present and capable of replicating in SG of SS and non-SS *sicca* patients [206],[207]. Moreover, mice transgenic for HCV envelope genes spontaneously develop sialoadenitis [208]. Additionally, type II cryoglobulinemia is a relatively frequent complication in patients with SS and it is closely associated with TLS formation [143]. Based on the above, it is clear that chronic HCV infection is critically related to TLS formation, both in the liver and SG, and mimic several clinical features and immunological disturbances observed in SS patients (with the notable exception of the lack of anti-Ro/SSA and anti-La/SSB

autoantibodies) whereby some authors proposed to consider patients with SS-like HCV-induced manifestations as a particular subgroup of SS patients [209]. Irrespectively of this debate, HCV is a clear example of a virus with SG tropism capable of inducing SS-like lesions resembling TLS together with clinical features of dryness which could serve as a model pathogen to investigate the mechanisms leading to TLS formation, autoimmunity and exocrine dysfunction.

1.2.6 Animal models of Sjögren's syndrome

Despite an exact model of SS in rodents capable to replicate all the features of the disease is still missing, several murine strains display characteristics of SS and have been helpful to investigate the immunobiology of the pathology.

Here I will briefly review the two main spontaneous models of SS, the NOD and the MRL/*lpr* mice, together with some less-used models that resemble several of the typical features of SS.

The non-obese diabetic (NOD) mouse strain was generated via repetitive brother-sister mating of animals of the ICR strain that spontaneously developed diabetes [210]. NOD strain animals always develop autoimmune insulitis that progresses into overt diabetes in 70% of the females and 3% of the males [211]. The incidence and sex distribution of sialoadenitis in NOD mice is comparable to that of insulitis, while lachrymal glands involvement is more frequently observed in male animals. Moreover, SG infiltration is observed when the animals are 10 weeks old and onwards, significantly later than insulitis that is observed as soon as week 4. A typical feature of NOD mice is that after the initial immune infiltration, by week 16 a reduction in salivary flow is observed, which is absent in other SS models.

The histology of the inflammatory infiltrates in NOD SGs is highly reminiscent of the *foci* observed in SS SGs: aggregates organise around a central duct or a blood vessel and are mainly composed of CD4^{+} and CD8^{+} T cells, with the former more abundant than the latter. Also, B220^{+} B cells are observed. Interestingly, NOD mice infiltrates also show a B/T cell areas formation, as observed in SS and this segregation is more evident in older animals, supporting the hypothesis that in this model the infiltrate organises in time, as observed in human SS SGs [212]. Recent findings from my laboratory helped to elucidate the real nature of the inflammatory infiltrates both in the pancreas and SG of NOD mice, as a full phenotypic and functional characterisation of these aggregates was missing. In particular, we showed that the NOD SG infiltrates display full features of TLS such as FDC networks, GL7^{+} GC B cells, development of HEVs and markers of B cell functionality such as an increased expression of the cytokines involved in the GC B cell survival and proliferation and of the enzyme AID. The data also confirmed the intrinsic Ag-dependent nature of the ELN process: in fact, NOD mice develop autoantibodies against insulin which are produced in pancreatic but not SG TLS and the destruction of the pancreatic islets corresponds to the down regulation of the genes involved in TLS formation and functionality and with the disappearance of these structures ([71] and Astorri et al. unpublished data).

Genetic analysis of NOD animals' genome revealed several susceptibility *loci* associated with development of diabetes versus SG pathology [213],[214]: from this point of view, NOD strain better reproduces the multiple genetic factors involved in autoimmunity development in comparison to other models where self-reactivity is driven by a single genetic defect. Interestingly, it has been also

shown that in NOD mice some *loci* are more strongly associated with the development of diabetes and others with sialoadenitis [215], suggesting that the two autoimmune processes occur differently in their respective target organs. In particular, among the over 20 identified mouse insulin-dependent diabetes mellitus (*Idd*) *loci*, only the *Idd3* and *Idd5* alleles were found to confer genetic susceptibility to develop sialoadenitis, but not insulitis in NOD mice, suggesting that the development of the SG versus pancreatic disease in this strain is regulated by different genetic/epigenetic mechanisms [216].

Another robust and widely used murine model of SS is represented by the MRL/*lpr* strain. The MRL/*lpr* mouse derives from the MRL/*n* strain that is *per se* an autoimmune-prone strain. The *lpr* (lymphoproliferative) mutation, that is the only difference between MRL/*lpr* and MRL/*n*, affects the *Fas* gene that is one of the main players in the regulation/induction of apoptosis [217]. The MRL/*lpr* mouse strain is mainly used as a model of systemic lupus erythematous, but these animals also develop SG infiltrates in the submandibular (but also sublingual and parotid) glands. As I mentioned in section 1.2.5.5, *lpr* animals also develop a plethora of different autoantibodies among which anti-Ro and anti-La antibodies that are observed only in a smaller percentage of NOD animals [217]. On the other hand, *lpr* mice do not show any salivary flow impairment, which is a characteristic of the NOD strain.

Other minor models of SS exist, e.g. NZB/W mice, TGF-β knock-out mice and NFS/*sld* mice thymectomised at 3 days of age [217]. Any one of these models shows some of the features of SS or of a particular clinical SS sub-type.

Collectively, all the minor and major SS murine models develop a spontaneous disease with variable penetrance and severity which is underlined by mono- or

polygenic abnormalities that make the accurate pinpointing of the mechanisms leading to breach of tolerance, autoimmunity, sialoadenitis and exocrine functional impairment a very difficult and laborious enterprise.

Of notice, no model of inducible SS-like disease in rodents (with the exception of an SS-like model induced by Ro immunization that reproduces the disease features only on Balb/c mice [218] which is currently difficult to reproduce due to the long time necessary to induce the symptoms [219]) has been described so far. Such a model would offer significant advantages over existing models in dissecting and clarifying the key pathogenic events leading to sialoadenitis and salivary hyposecretion.

Chapter 2 | Rationale and aims

2 Rationale of the thesis and aims

In the course of gene-delivery experiments aimed at establishing the role of an increased expression of certain molecules in the SG of various mouse strains, but also aimed at therapeutic gene transfer with anti-inflammatory molecules, I and other members of my laboratory observed an unexpected phenomenon. In time course and dose-response experiments using a replication-defective adenoviral vector encoding for a traceable gene (LacZ or Luciferase) injected directly in the submandibular salivary gland of C57/Bl6 mice, we observed that high-doses of the reporter gene-encoding adenovirus induced a strong early inflammatory response which, surprisingly, was followed by the development of a focal lymphocytic infiltration that histologically was very reminiscent of the inflammatory *foci* observed in the SG of patients with SS and of female NOD mice.

My lab has long been interested in the formation of ectopic follicles in SS SGs and in particular in the formation of TLS formation, which, as I reported in the previous chapter, represent a common feature in the background of chronic antigenic stimulation, whether the stimulus is of exogenous (chronic pathogen infection) or endogenous (tumour, graft) origin.

It is also clear that, so far, an elegant and comprehensive model of inducible TLS formation in the salivary glands was missing. The available animal models of SS, although invaluable to understand some of the immunobiology of SS, they all presented flaws difficult to overcome. The key problem of the classic SS models is represented by their genetic background and spontaneous development: a complex genetic susceptibility is necessary for the development of the SS-like syndrome in mice but at the same time the chronic nature of the

process, the variable incidence and the slow and unsynchronised progression of the disease made it difficult to identify neatly the mechanisms involved in the pathogenic process. Additionally, the use of knockout or transgenic mice was only possible after tedious backcrossing, thus impairing the use of genetic modifications.

For these reasons and given the preliminary observations reported above, the main aims of my PhD project were as follows:

1- To develop and validate a robust inducible murine model of sialoadenitis on a wild-type background, using the delivery of reporter gene-encoding replication-deficient adenoviruses. The results of this preliminary work are reported in section 4.1.

2-To investigate whether the SS-like lesions in the SG triggered by AdV delivery represented simple accumulation of lymphocytes or displayed cellular, molecular and functional features of TLS. The results of this work are reported in section 4.2.

3- To clarify whether, together with the histological lesions typical of SS, other hallmarks of SS were reproduced in this putative model of SS, including development of autoimmunity and exocrine dysfunction. The results of this work are reported in section 4.3.

4- To address whether the formation of SS-like lesions were associated with the development of a protective immunity against the pathogen followed by viral clearance or where dependent on the viral escape from the local immune response with the establishment of a persistent infection. The results of this work are reported in section 4.4.

After having addressed the above aims, in the second part of my PhD project I moved to investigate the following aspects according to the aims below:

5- To dissect the recruitment rate and tissue positioning of different innate immune cells subsets following AdV delivery in the SGs with particular focus on the first wave of immune response. The results of this work are reported in section 5.1.

6- To address the role of specific cell type, namely NK cells and myeloid subsets in the formation of SS-like lesions and the development of TLS. The results of this work are reported in section 5.2.

Overall, if successful my PhD work could have the potential to i) generate and validate a novel model of inducible sialoadenitis, ii) to establish a novel platform to study the cellular and molecular events leading to TLS formation, iii) to investigate the mechanisms regulating breach of tolerance and exocrine dysfunction, two hallmarks of SS and iv) dissect critical pathogen-host interactions responsible for viral control and viral persistence in the SG.

Chapter 3 | Materials and Methods

3 Materials and methods

3.1 Reporter-encoding human adenovirus 5 expansion and purification

In preliminary experiments, we discovered that first generation adenoviruses (AdV), which were established as potential vectors for gene transfer experiments directly in the SG, at high doses ($>10^8$ pfu, see below) induced the formation of SS-like lesions in the submandibular glands, with the development of periductal lymphomonocytic aggregates or *foci*. Thus, in order to establish whether such ectopic aggregates displayed cellular, molecular and functional characteristics of TLS, throughout my PhD work I have used first generation E1/E3 deficient human adenovirus 5. These vectors have the advantage of being easy and rapid to produce, and safe to use and yield high-titres, which I then used to deliver at high-doses and in small volumes in the submandibular glands of mice via a retrograde cannulation technique.

I have used two different reporter genes for the aims of this thesis: firefly luciferase or bacterial β-galctosidase. Luciferase-encoding adenovirus (LucAdV) was a kind girft of Dr. Wim Van Der Berg, Radboud University Medical Centre, Nijmegen, The Netherlands. Galactosidase-encoding adenovirus (LacZAdV) was a kind gift of Dr. Luigi Gnudi, King's College London, London, UK.

In this section I will describe the protocols that have been used and perfected to expand, purify and quantify the adenoviruses.

Adenoviral vectors have been used in the past two decades for gene therapy purposes and more generally to transfect tissues or cell lines refractory to other transfection method [220]. The viral strains usually used are human adenovirus type 2 and 5. Adenoviruses are double-strand DNA viruses, 51 human serotypes have been characterised so far. The adenoviral genome is constituted by two sets of genes: the early phase genes (E1-E4) and the late phase genes (L1-L5). Early phase genes are the first to be transcribed and translated and encode for proteins necessary for viral replication and resistance against host defences, in particular E1 is necessary for the expression of the other early genes. Late phase genes encode for structural proteins necessary for the formation of the capsid and viral genome packaging. These viruses have a series of characteristics that favoured their popularity as vectors: i) their genome and biology are well characterised, ii) the viral genome does not integrate into the host genome, which makes AdV safer and particularly suitable for transient expression of transgenes and iii) they can accommodate inserts up to the size of 37kb. During the years three different generations of adenoviral vectors have been developed: first generation AdV are defective in E1 and/or E3 genes; second generation are defective in E1 and various other early genes; third generation AdV are called "gutted" vectors because they lack the entire genome except for the ITR regions and the packaging sequence. All these vectors relies on packaging cell lines for their production: lacking completely or in part of the early genes, the helper cell line must have *in trans* the missing genes for efficient viral production. In the case of first generation AdV, the helper cell line is the human embryonic kidney 293 cell line (Hek293).
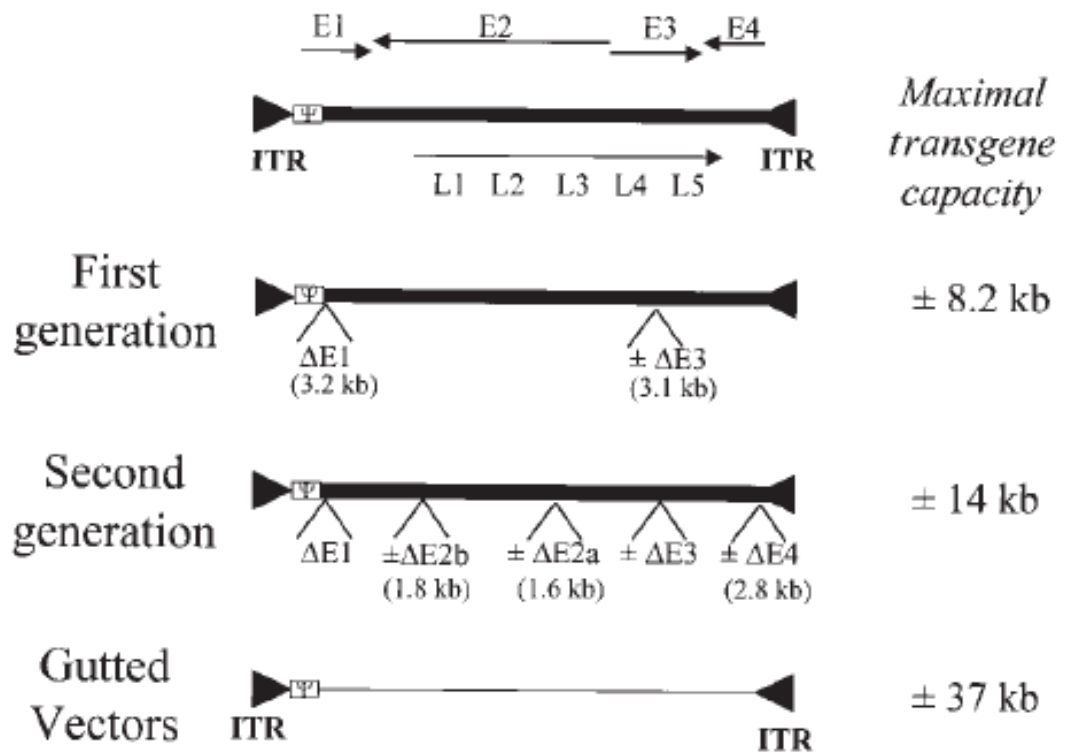
Figure 3.1: Comparison of the first, second and third generation adenoviral vectors. Reprinted by permission from Macmillan Publishers Ltd: [220], copyright 2000.

Despite the larger insert that second and third generation AdV can accommodate, first generation AdV are still the favourite vectors: their construction is relatively easy, the transgene capacity is compatible with most gene transfer applications and they are easy to grow to high titres.

AdV vectors have also downsides that made their use, especially in gene therapy, less popular during the years. This is mainly because i) the transgene does not integrate in the genome, thus its expression is transient; ii) first generation AdV in particular elicit a strong immune response due to the production of viral proteins in the infected cells, therefore a re-challenge *in vivo* for prolonged transfer gene expression is not efficient as the first administration induces a strong inflammatory response in the host.

Various methodologies have been developed to modify and add inserts in the adenoviral genome. These techniques can be broadly divided in two groups: methods requiring DNA recombination in mammalian cells and methods requiring the assembly of the viral genome *before* transfection in mammalian cells. With the former methods, the recombination between a DNA molecule encoding for the leftmost region of the viral genome followed by the gene of interest and the rightmost part of the viral genome is required. The rightmost sequence must slightly overlap the 3' region of the leftmost sequence to allow recombination between the two molecules. The recombination is achieved in the Hek293 helper cell line. These methods have the advantage that the final viral genome is obtained directly in one round of transfection in the host cell line. The main disadvantages are that i) to produce the leftmost fragment restriction enzymes cutting in the E1 region of viral genome are used and the fragment obtained from digestion are similar in size to undigested viral DNA and

therefore is difficult to separate the two DNA species before transfection in 293 cells, increasing the risk of generating replication-competent virions as well as desired replication-defective ones; moreover ii) recombination in mammalian cells is not an efficient process. To overcome these issues various modification to the basic technique have been studied but most of them are tedious and time consuming and thus reduce the advantage of having recombination and virion production all in one step

The methods requiring recombination before transfection into mammalian cells are based on the production of the recombinant genome in bacterial cells, thus reducing the risk of parental viral genome contamination. The main disadvantage is that the lack of selective pressure in bacteria might lead to mutations in the recombinant genome thus impairing the viability of the virus. For this procedure, the cDNA of the reporter gene to be transfected is cloned inside a commercial AdV transfer vector plasmid: these vectors contains short adenoviral sequences from the E1 region of the adenovirus 5 genome, flanking a sequence containing a strong promoter of transcription (usually CMV) the multiple cloning site (where the insertion cassette with the gene of interest is positioned via specific digestions with restriction enzymes followed by ligations to reconstitute the circular plasmid DNA) and a poly-adenylation signal. The gene of interest is first cloned in this transfer vector. The obtained vector, which also bears an antibiotic resistance gene (usually ampicillin) is then transfected into competent bacterial cells, which are selected for antibiotic-resistance allowing amplification of the plasmid for downstream use. Following purification, the plasmid DNA is then co-transfected together with another larger commercial plasmid encoding the AdV5 genome, defective for sections of the E3 and E1

regions. The AdV regions present in the transfer vector facilitate the homologous recombination with the E1 region of the plasmid encoding for the viral genome, allowing the insertion of the gene of interest into the AdV genome. Recombination is then confirmed by restriction digest mapping of the obtained plasmid. The recombined plasmid is then transformed in bacterial cells for large-scale plasmid purification. Finally the obtained plasmid is purified, linearised and used to transfect Hek293 cells for production of bulk amount of viral particles bearing the recombinant genome. Alternatively, homologous recombination can be directly achieved in Hek293 cells following co-precipitation (usually using calcium phosphate) of the shuttle and AdV plasmids with direct formation of complete viral particles harbouring the transferred gene of interest. Because Hek293 cells provide the missing E1-E3 AdV genes for the formation of the full viral capside, this is the only cell type where the virus has full replication and lytic capacity allowing large scale amplification of the viral particles which can be monitored by the formation of cytolytic plaques in the Hek293 cell monolayer. Other plasmid-based kits can be used, where the transgene is first cloned inside a shuttle plasmid with particular restriction sites that after the shuttle plasmid digestion allow its ligation inside another plasmid (bearing the same restriction sites) encoding an E1-E3 defective viral genome (example Figure 3.2 and Figure 3.3).
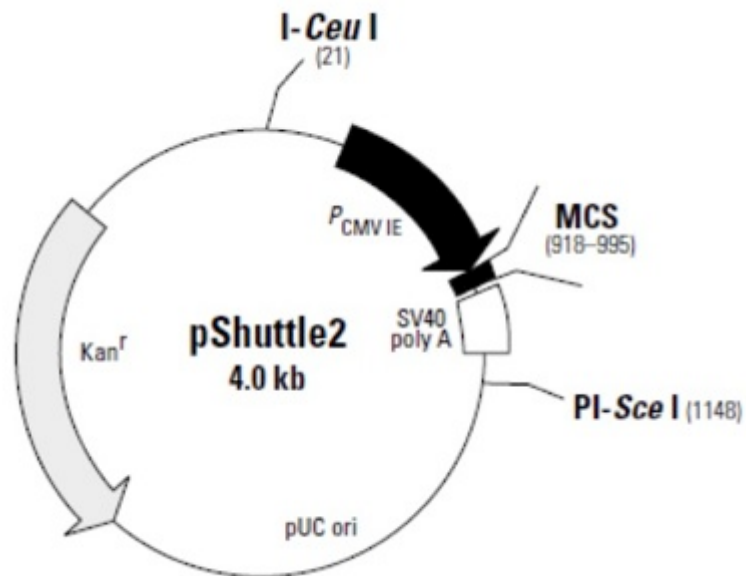
Figure 3.2: Shuttle plasmid bearing a resistance gene for kanamicine and bacterial origin of replication. A multiple cloning site (MCS) is located between CMV promoter and SV40 polyadenilation sites. The gene of interest is cloned in the MCS region and after expansion and selection, the plasmid is digested with I-Cei I and PI-Sce I enzymes. (BD biosciences product).
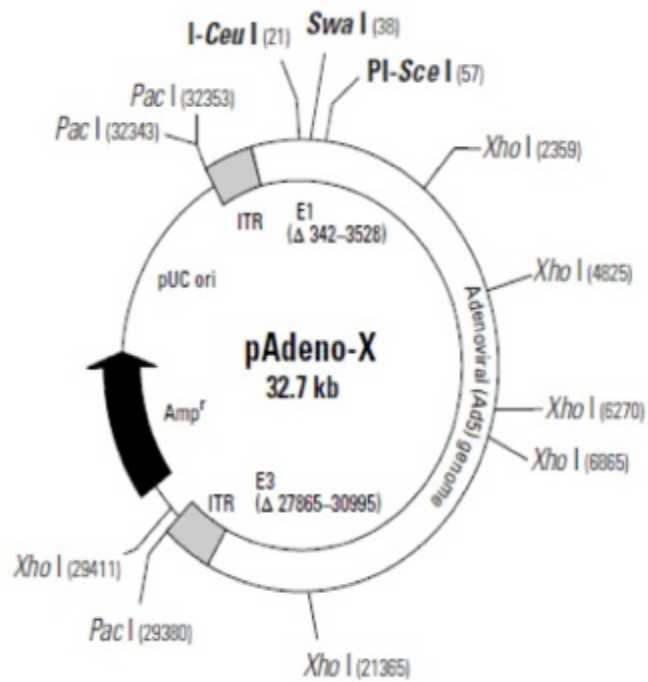
Figure 3.3: A commercial adenoviral vector plasmid map. The plasmid encodes for a viral genome defective of E1 and E3 regions, together with an ampicillin resistance gene for selection and a bacterial origin of replication for expansion. This vector is linearised with I-Ceu I and PI-Sce I enzymes and ligated with the shuttle plasmid bearing the gene of interest (**Figure 3.2**). After ligation the plasmid will encode for the E1-E3 defective adenoviral genome and the transgene under the transcriptional control of the CMV promoter. (BD biosciences product).

3.1.1 Helper cell line preparation and seed stock expansion

Hek293 cells, which are a human embryonic kidney cell line, were cultured in Dulbecco-modified Eagle medium (D-MEM, Gibco) supplemented with 10% foetal bovine serum (Life technology) and penicillin/streptomycin (Life technologies) at 37°C in humidified incubator in 5% carbon dioxide pressure.

The concentrated viral stocks, preserved in a -80°C freezer, were thawed and used to infect one T175 (Corning) flask of 80% confluent Hek293 cells. When cytopathic effect was evident, i.e. when cells started to lose adherence and detach, cells were collected and snap-frozen in liquid nitrogen. Cells underwent three freeze/thaw cycles to allow cell lysis and virus release and then spun for 15 minutes at 800xg. The supernatant was collected and used in the next step.

3.1.2 Bulk virus expansion

AdV seed stock was used to infect twenty 15 cm Petri dishes (Corning) of 80% confluent Hek293 cells. When the cytopathic effect was evident, cells were harvested and spun at 800xg for 15 minutes and supernatant discarded. The cells were resuspended in 26 ml of a buffered solution (100mM Tris pH 8) and underwent 3 cycles of freeze/thaw to allow cell lysis and virus release. The suspension was spun again (3500xg for 15 minutes) and the virus-containing supernatant collected.

3.1.3 Caesium chloride gradient virus purification

The obtained solution is a suspension of viral particles, cellular debris and is contaminated by cell growth medium and bovine serum. Properly packed virions are the more dense elements present in the solution. To obtain a pure suspension of concentrated virions, the solution undergoes ultracentrifugation on a caesium chloride (CsCl) step gradient (Figure 3.4). CsCl is highly soluble

in water and caesium has a very high atomic weight (good to obtain high-density solutions) and low viscosity. CsCl is dissolved in a buffer (TD buffer 137mM NaCl, 5.1mM KCl, 0.704mM Na_2HPO_4, 24.8mM Tris at pH 7.5) to the desired density. A high density CsCl solution (1.4 g/ml) was first layered in transparent ultracentrifuge tubes (Beckman) and a second layer of lower density CsCl solution (1.25 g/ml) was layered above the first. Finally the virus-containing solution was split in half and deposed on top of the CsCl solutions (Figure 3.4A). The tubes were then ultracentrifuged for 2 hours at 15°C at a speed of 25'000RPM (maximum RCF 113'960xg) in a Beckman preparative ultracentrifuge adapted with swinging buckets (L-80 ultracentrifuge, SW32 Ti buckets). The density of the virions lies between the densities of the two CsCl solutions, thus during the ultracentrifuge virions can pass through the top low-density solution but cannot enter the high-density bottom phase. At the end of the centrifugation, virions appear at the interface between the CsCl phases as an opalescent band, while incomplete viral particles, cellular debris and other contaminating materials will remain above or inside the top phase (Figure 3.4B). The viral particles-rich phase was then collected from the interface by mean of puncturing the tube with a sterile needle (BD) adapted to a syringe. The collected solution was mixed with another CsCl solution (1.36 g/ml) in ultracentrifuge tubes and spun at 40'000 RPM (maximum RCF 194'432xg) at 15°C overnight in a Beckman preparative ultracentrifuge (Figure 3.4C) adapted with swinging buckets (L-80 ultracentrifuge, SW55 Ti buckets). The density of this CsCl solution is more similar to the density of the virions and during ultracentrifugation a density gradient is formed. Viral particles move through the solution to the isopycnic point, i.e. the point where the density of the virions is

equal to the density of the solution. This second ultracentrifuge cycle is used to further purify the viral particles from potential carryovers from the previous steps and to increase the concentration of the viral suspension. The viral particles-rich phase was collected again by mean of puncturing the tube with a needle and syringe (Figure 3.4D). The solution was moved in a 50 ml tube (Falcon) where 2 ml of TSG buffer were added (150mM NaCl, 5mM KCl, 1mM Na_2HPO_4, 30mM Tris, 2mM $MgCl_2$, 1.8mM $CaCl_2$, 30% glycerol). This solution was then loaded in a dialysis cassette (Figure 3.4E) as explained in the next section.
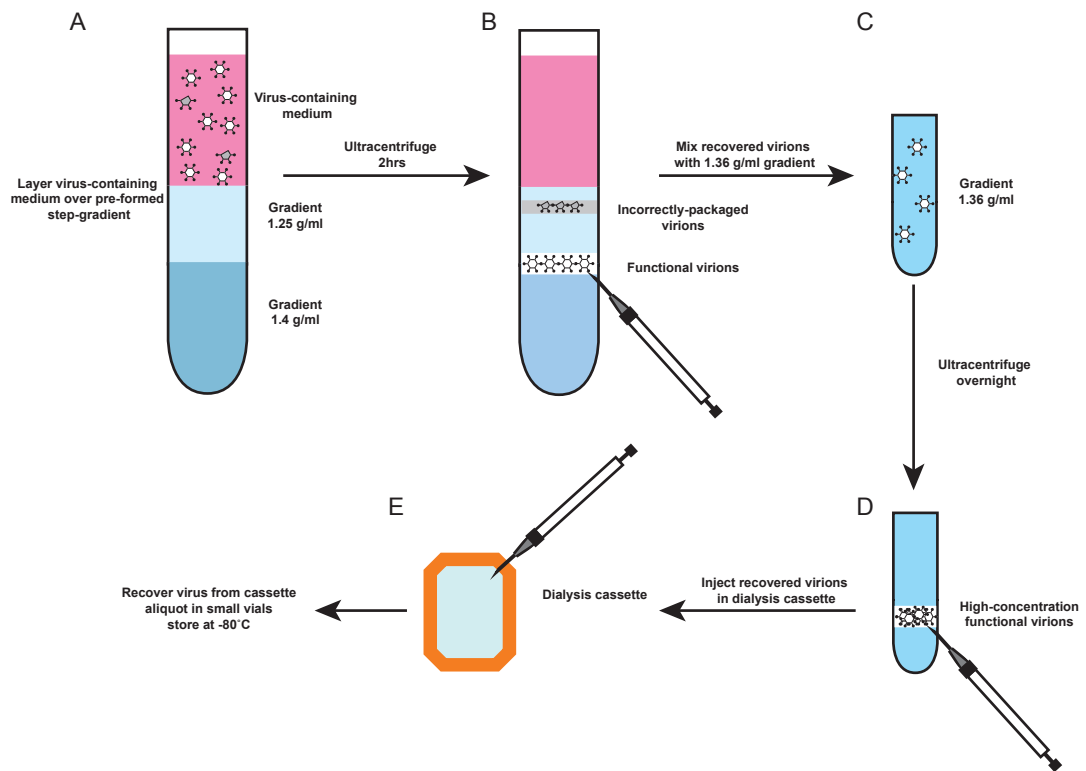
Figure 3.4: Scheme of viral particles isolation and purification. (A) A 1.4 g/ml CsCl solution is deposited on the bottom of the tube followed by a less dense solution (1.25 g/ml) to form the step gradient. Virus-containing supernatant obtained from the lysis of AdV-infected Hek293 cells is layered on top of the step gradient. **(B)** After ultracentrifugation for two hours two bands are observable, a top band containing empty and/or incorrectly packaged virions and a second one at the interface between the two gradients containing the concentrated correctly packaged full virions. **(C)** The tube is punctured and the virus-containing solution is mixed with a 1.36 g/ml CsCl gradient in an ultracentrifuge tube and spun overnight to obtain an isopycnic separation of the viral particles. **(D)** After the second ultracentrifuge a band is formed in the tube that contains concentrated viral particles. Again the tube is punctured to collect the band, which is then injected in a dialysis cassette **(E)** to remove the

impurities and the CsCl contamination. After overnight dialysis the virus-containing solution is aliquoted and stored at -80˚C.

3.1.4 Dialysis

At the end of the second ultracentrifugation the viral particles are evident in the tube as an opalescent band. This band contains now ultrapure suspension of viral particles, contaminated by caesium chloride buffer. To get rid of the contaminants, the solution needs a dialysis step. This was achieved via commercial dialysis cassette (Thermo Scientific): these cassettes have two semi-permeable membranes with specific diameters, which allow the passage of water and salts but not of larger molecules (such as proteins or, in this case, viral particles). The viral suspension obtained as explained above, was loaded inside the cassette with a syringe and needle. The loaded cassette was immerged in 2 litres of dialysis saline buffer (10mM Tris, 1mM $MgCl_2$, 150mM NaCl, 10% glycerol). The cassette was left in the dialysis buffer overnight to allow chemical equilibrium. Since the semi-permeable membrane allows the free movement of salt ions, caesium can freely diffuse across it. The solution tends to reach osmotic equilibrium and since the solution inside the cassette is rich in caesium ions that are completely absent from the dialysis buffer outside, caesium will diffuse from the cassette to the dialysis buffer. Moreover, since the viral solution volume is relatively small (approximately 5-6 ml) and the dialysis buffer volume relatively large (2 litres) after dialysis the amount of caesium remaining in the viral solution is minimal. After the dialysis the virus was divided in 150 µl aliquots and stored at -80°C.

3.1.5 Titration of the viral plaque forming units

There are several methods to quantify the amount of virus produced via the process reported above. The quicker and more straightforward consist in

measuring the absorbance of the virus suspension with the aid of a spectrophotometer: knowing the absorbance associated to the adenovirus is possible to calculate the number of viral particles per volume unit present in the solution. This method, although fast and reliable, does not take into account the viability of the viral particles: in fact the viral suspension also contains viral capsids devoid of viral genome, virus particles with a defective genome and misassembled virions that do not lead to an efficient target cell infection.

Other titration methods allow the quantification of the plaque-forming units (pfu), which is the number of viral particles capable to induce a functional infection that, in the case of adenoviruses, culminates with the target cell lysis and the release of the viral progeny. On a monolayer of Hek293 cells, this corresponds to the formation of plaques: areas of the cellular monolayer where infected cells dye and leave an evident plaque in the cell culture vessel. Infection of confluent Hek293 cells with scalar dilutions of the viral suspension allows the calculation of the pfu per millilitre of solution.

For this thesis, I decided to use a 96-wells plate-based end-point statistical method that reduces variability and handling errors that are typical of the more classic plaques formation assays methods. Briefly, Hek293 cells were plated in a tissue culture-treated 96-wells plate (Corning) at a density of 5×10^5 cells/ml of complete medium, 100 µl per well. Plates were returned to the incubator and left overnight. The next day serial dilutions of the viral stock were prepared in complete medium. The medium was removed and 100 µl of a specific dilution of infective medium (or normal medium) were added to the wells in a row-wise manner (e.g. wells A1 to A10 first dilution, B1 to B10 second dilution etc.). The last two columns were plated with uninfected medium and left as controls. The

dilutions of the stock generally used were from 1:10^7 to 1:10^{14}. For each virus to titrate, at least 4 replicate plates were prepared. Plates were then returned to the incubator and checked daily for cytopathic effect (CPE). At day 7 the plates were observed and scored under an inverted microscope: a well was considered infected when at least a plaque was observed. After the assay a statistical method (in this case Spearman and Karber method [221]) can be used to calculate the 50% Tissue Culture Infective Dose (TCID$_{50}$) of the solution and from the TCID50/ml the pfu/ml can be deducted empirically multiplying the TCID value by 0.69.

$$Titer\ (TCID_{50}/ml) = 10^{1+Z(X-0.5)}$$

Where Z is the Log_{10} of the dilution factor (in this case Z=1 for a 10-fold dilution factor) and X is the sum of the fractions of CPE-positive wells (this sum must take into account also the lower dilutions not plated, i.e. 10^{-1}, 10^{-2} etc. as positive for CPE). For the assay to be considered reliable three conditions must be met: i) the control wells at the end of each row must be devoid of cytopathic effect; ii) the lowest dilution (e.g. 1:10^7 row) wells must all show plaque formation and iii) the highest dilution wells (e.g. 1:10^{14}) must not show any cytopathic effect. After repeating the counting for all the replicate plates, the average was calculated and this value was considered the number of pfu per millilitre.

3.2 Mouse handling and submandibular salivary gland retro-cannulation

For this thesis, I have used C57Bl/6 mice purchased from Charles River (UK) and housed in the biological services unit at the William Harvey Research Institute. Animals were maintained in standard conditions, with food and water

ad libitum. For all the experiments females aged between 11 and 13 weeks were used.

The technique used to deliver AdV in the murine SG was first optimised for rats [20],[222],[223] and then re-adapted for mice. The basic apparatus consists of a 100 µL Hamilton syringe (Sigma, UK) connected to a $30^{1/2}$-gauge syringe needle (BD, UK) in turn connected via fine plastic tubing to the cannula (Figure 3.5). The shaping of the cannula is explained in the next section.

All the experiments were performed delivering either AdV or the viral vehicle alone as control. For some experiments, both glands of the same animal were cannulated with the AdV, for others only one gland was treated with the vector while the other was used as internal control and thus left either untouched or cannulated with the vehicle. Animals were culled at the relevant time-point under sodium pentobarbital terminal anaesthesia, delivered via an intra-peritoneal (i.p.) injection. Blood and tissues were collected as stated in the next sections.

Cannulation apparatus

30 ½ gauge needle

100 µL Hamilton syringe

0.1 mm tubing

Heat-drawn cannula
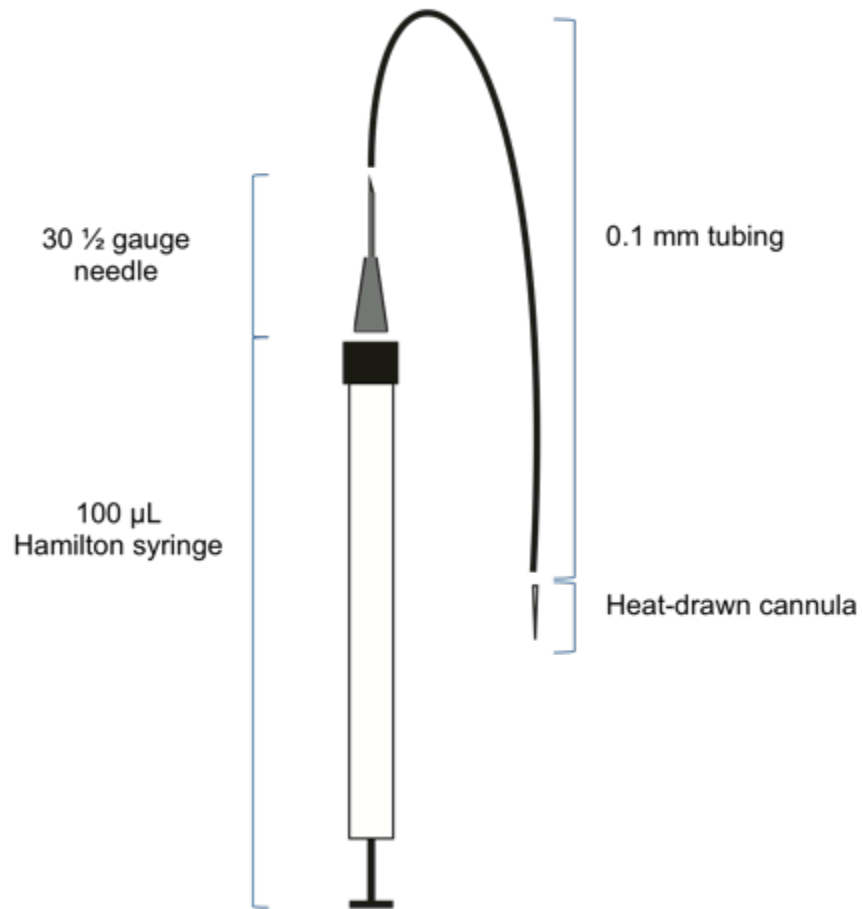
Figure 3.5: Cannulation apparatus, scheme. The 100 µL Hamilton syringe is connected with the needle and AdV-containing solution is loaded in the syringe. The tubing is then connected and the glass cannula added last. After making sure that the cannula is open, liquid is pumped in the apparatus to remove dead volumes.

3.2.1 Glass cannulae shaping

The small cannulae necessary to efficiently enter the SG excretory duct and deliver the AdV solution were obtained stretching sections of silica HPLC tubing (0.1 mm internal diameter, Sigma, UK) over a Bunsen burner flame. From each tubing section (approximately 5 cm long) two cannulae were obtained. This procedure reduces the diameter of the tubing to about 10/20 μm.

3.2.2 Submandibular salivary gland cannulation

For the procedure, mice were initially anaesthetised with a solution of ketamine (60 mg/kg) xylazine (12 mg/kg) in PBS, delivered with an i.p. injection. A homemade device was used to keep the mouth of the animal open and in the correct position (**Figure 1.1**A). All procedures were performed using an operating microscope.

The Hamilton syringe was loaded with the viral solution or control vehicle, the syringe needle was also filled with the relevant solution to avoid dead-volumes. Once the Hamilton and needle were connected to the tubing and cannula, these were also filled with the solution to be transferred, thus applying a positive pressure to the Hamilton syringe plunge (Figure 3.5).

The mouse tongue was lifted, exposing the orifices of the two submandibular excretory ducts (**Figure 1.1**B). The cannula was then carefully inserted in the chosen orifice. Upon successful insertion, a positive pressure was applied to the Hamilton syringe plunge and the solution slowly delivered in the gland. According to the viral titre, a volume between 10 and 50 μl was delivered, so to have the requested virus amount (10^8 pfu) injected in the gland. Any leakage was assessed and recorded.

After the procedure the animals were left to recover and upon successful recovery they were returned to the cages and left undisturbed until the next procedure or relevant culling day in time-course experiments.

3.2.3 Salivary flow assessment

Some of the animals were assessed for salivary flow impairment. This set of animals received AdV in one of the glands and vehicle in the contralateral, as internal control. Secretory function was assessed under terminal anaesthesia (sodium pentobarbital 75 mg/kg i.p.). The animals were anesthetised, placed on a warmed operating table so that the ventral side was exposed and rectal temperature was monitored. After removal of the ventral hair in the neck region, each submandibular duct was exposed by dissection from the ventral surface through the mylohyoid muscle. Individual submandibular ducts were localised, cut, cannulated with 0.1 mm HPLC tubing, and saliva secretion was induced via stimulation with pilocarpine (0.5 mg/kg i.p.), a non-selective muscarinic receptor agonist. Saliva was collected 5 minutes after pilocarpine administration and collected for 10 min. After collection into weighed tubes, the tubes were reweighed and the volume of saliva calculated (1 mg = 1 µl saliva).

3.2.4 Systemic and local antibody-mediated NK cells depletion

In order to deplete NK cells from the circulation, an anti-NK1.1 antibody has been used as previously reported [224]. Briefly, 200 µg of mouse anti-mouse NK1.1, clone PK136 (BioXcell), were administered i.p. on the day before cannulation. Animals were injected with the same dose every 48 hours until day 8 after procedure (i.e. 1, 3, 5, 7 days post cannulation). Control group animals were dosed with control mouse immunoglobulins following the same schedule. To assess the effective depletion of NK cells, digested SG were stained for flow

cytometry using an anti-NK1.1 antibody in combination with an anti-CD49b antibody, another pan-NK cells marker (refer to Section 3.8 for details regarding tissue digestion and cells preparation for flow cytometry). As shown in **Figure 3.6**, PK136 administration induced an almost tenfold depletion of the SG tissue-resident NK cells in comparison to IgG-treated controls. NK cells depletion was observed both in SG and in spleen of PK136-treated animals.
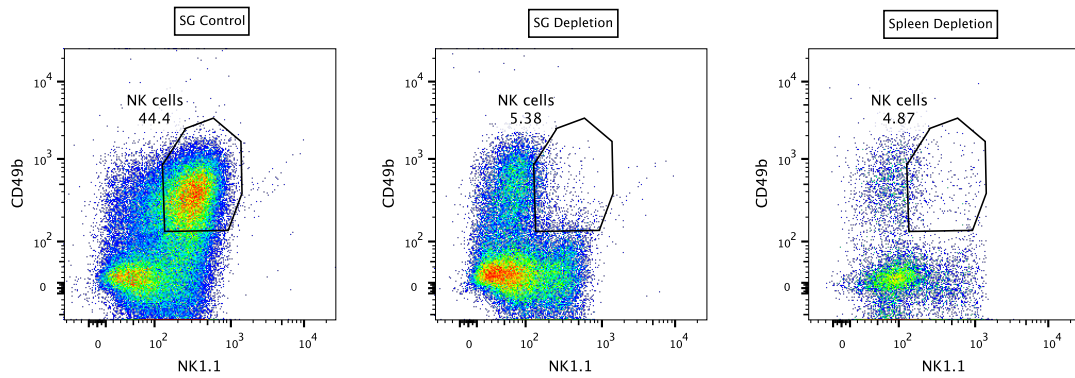
Figure 3.6: Effects of anti-NK1.1 administration on the resident NK cells population. Anti-NK1.1 was injected i.p. from the day before the cannulation and every 48 hours until the culling date or up to day 8 post-cannulation. Depleting antibody injections induced effective NK cells depletion, as showed by the reduction of the NK1.1/CD49b double positive cells in comparison with to the Ig-treated controls (*left* and *center*, respectively). As reported in previous publications, the administration of the antibody induced a systemic depletion of NK cells, as shown by the absence of the NK cells pool in the spleen of PK136-dosed animals (*right*). The plots in this figure show single viable cells gated as non-granulocytic $CD45^+/CD19^-/CD3^-$ cells.

3.3 Tissues and blood collection

3.3.1 Blood collection and storage

For terminal bleeding, after induction of terminal anaesthesia, unconscious animals were positioned on an operating table and blood was collected via intra-cardiac puncture using a fine needle 1 ml insulin syringe. After withdrawal, blood was collected in tubes containing a clotting agent (Startedt, Germany) and left for 2 hours at room temperature to allow clotting. Serum was then separated via centrifugation at 1000xg for 5 minutes, collected in fresh tubes and stored at -20˚C until use.

3.3.2 Salivary glands, loco-regional lymph nodes and spleen dissection and storage

Culled animals were dissected with dedicated tools. Sub-mandibular salivary glands, loco-regional lymph nodes and spleen were collected and stored according to the requested analysis.

For histological studies spleens, lymph nodes and whole SG or part of them were embedded using plastic moulds filled with optimal cutting temperature (OCT) medium (Sakura fineteck, UK) and rapidly snap-frozen in isopentane pre-cooled to optimal temperature in liquid nitrogen. Embedded specimens were stored at -80˚C until use. Tissue destined for RNA extraction and gene expression studies were stored in RNA-later stabilising solution (Life technologies), left overnight at 4˚C and then frozen and stored at -80˚C until use.

Small amounts of tissue from salivary glands treated with LucAdV were collected in test tubes and snap-frozen in liquid nitrogen and then stored at -80˚C for luciferase activity assay.
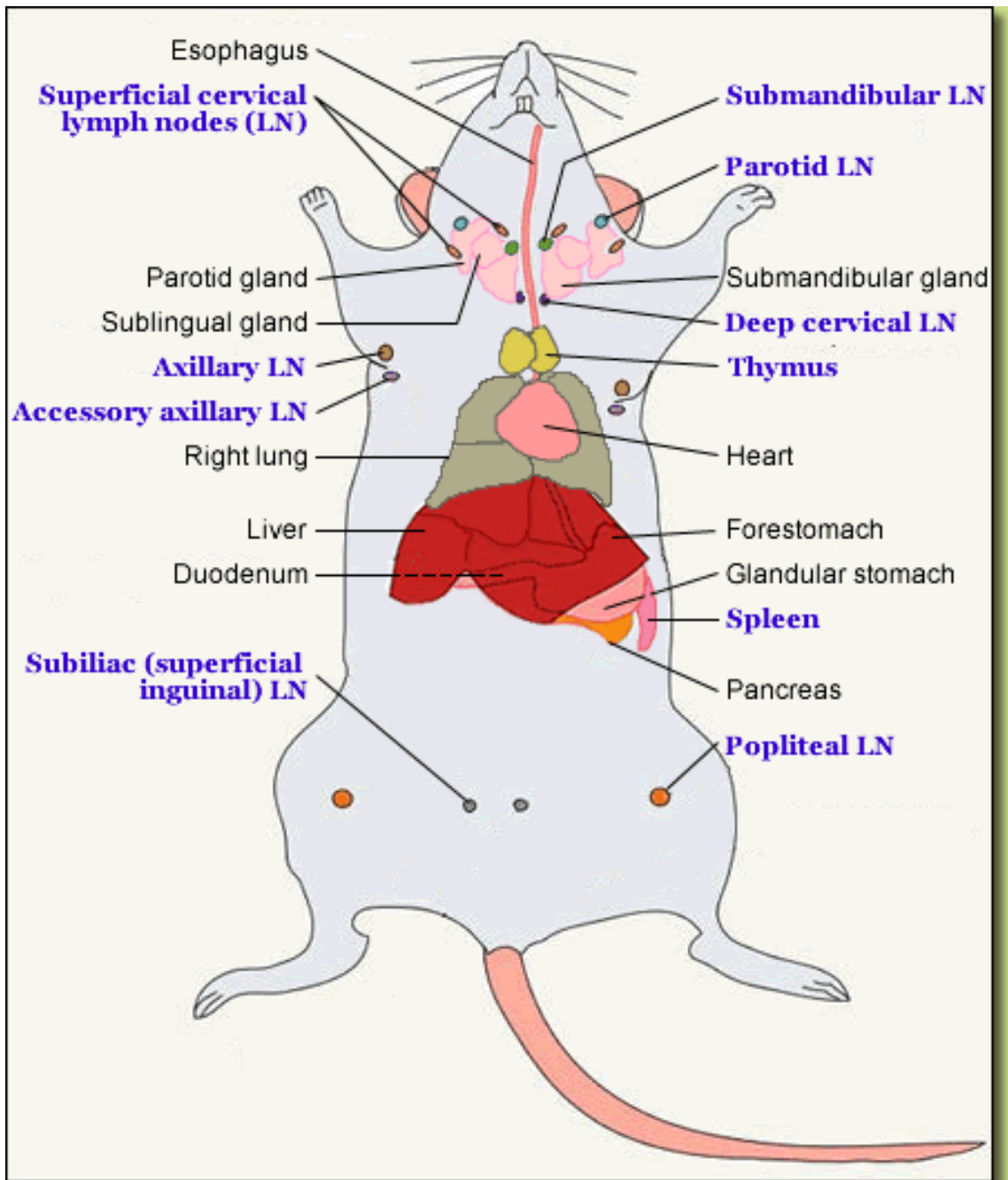
Figure 3.7: Gross ventral anatomy of the mouse, the main lymph nodes are highlighted. From Texas Histopages. http://ctrgenpath.net/static/atlas/mousehistology/Windows/lymphatic/lymphdiagr am.html

3.4 Luciferase assay on LucAdv-treated salivary glands

Bioluminescence, the emission of photons of visible light via a biochemical reaction, is present in several animal species. The enzymes responsible for the production of light go under the common name of "luciferases", and the chemical-energy rich substrates that are catalysed by luciferases are called "luciferins". Luciferases from different species of insects and jellyfishes have been cloned and used as reporter genes in numerous biological applications: in general cells are transfected, or infected with a viral vector coding for a selected luciferase. Once the substrate is provided to the cells, the enzyme starts to catalyse the reaction and produce light that can be measured and recorded. Interestingly, luciferase based technologies can be successfully applied both to *in vivo* and *in vitro* systems. In *in vivo*, luciferase-encoding cells can be injected into animals or the enzyme expression can be restricted to specific tissues in transgenic animals or viral vectors can be used and the enzymatic activity can be efficiently measured by high-sensitivity cameras once the substrate has been administered in live animals. The surrounding tissues will absorb most of the light emitted by the luciferase-positive cells and only few photons will hit the instrument's sensor. Thus, in order to register these events and distinguish the light produced by the specimen form the noise the use of these cameras is necessary. With a different approach, to avoid the use of expensive sensors, *in vitro* cultured cells are first lysed to release the enzyme and the substrate is added directly to the lysate and light emission measured by instruments called luminometers. This latter approach can also be used to measure luciferase activity from tissues collected from luciferase-transfected animals, and this is the technique that I have used in this thesis. In details, tissues from LucAdV-

treated and control animals, prepared and stored as reported above, were thawed on ice. Tissues were then transferred into homogenising micro-beads tubes (Precellys systems, Bertin Technologies, France) filled with 300 μL GloLysis lysis buffer buffer (Promega, USA) and lysed with a shaking micro-beads homogeniser (Precellys systems, Bertin Technologies, France). Tubes were centrifuged to eliminate debris and 50 μL of the tissue lysate were transferred in black luminometer plates (Corning, UK) and 50μL of BrightGlo luciferase substrate (Promega, USA) were added. The mixture was left 5 minutes at room temperature in the dark and then luminescence was quantified in a Microlumat Plus luminometer (EG&G Berthold, Germany) for 10 seconds. Luminescence was normalised for the protein concentration of the sample, calculated with a bicinchoninic acid (BCA) assay (Pierce, USA).

3.4.1 Bicinchoninic acid (BCA) assay

The BCA assay is widely used to calculate protein concentration as is largely unaffected by the presence of detergents, which are often used to lysate tissues and cells. In a BCA assay, a substrate containing cupric sulfate pentahydrate is added to the protein solution to measure. The peptide bonds of the protein reduce the copper and in this reduced form each copper ion chelate two molecules of bicinchoninic acid, also present in the substrate solution. In this form, bicinchoninic acid forms a purple-coloured product that strongly absorbs light at 562 nm. Temperatures above 37°C facilitate the reduction of copper and make the reaction largely independent by the presence of cysteine bonds and tyrosine and tryptophan side chains that can influence the BCA-copper interaction. If this condition is met, the amount of coloured substrate produced by the reaction, dependent from the number of copper ions reduced, is directly

proportional to the amount of protein present in the sample. The colour value is measured in a spectrophotometer and it is compared to the colour value obtained from a standard curve of a known protein, usually bovine serum albumin (BSA).

In this thesis a commercial kit for BCA assay (Pierce, USA) was used. Briefly, the BSA standard provided by the producer (2 mg/ml) was serially diluted with the lysis buffer used for the relevant application (e.g. RIPA buffer or glo-lysis buffer) to the following concentrations 1.5, 1, 0.75, 0.5, 0.25, 0.125, 0.025 mg/ml. Twenty-five microliters of each standard or sample were plated in duplicates in a 96-wells ELISA plate (Corning). The substrate is obtained by mixing two solutions provided by the producer in a 50:1 ratio. Two hundred microliters of the substrate were added to each well and the plate was incubated at 37°C for 30 minutes. Absorbance was read at 562nm and the average optical densities of standard duplicates were plotted against the concentration of the standards. The obtained curve was used to calculate the protein concentration of the samples.

3.5 Immunohistochemistry and immunofluorescence

3.5.1 OCT samples handling and cutting

OCT-embedded tissues were removed from the mould and attached to a small cork. Five microns sequential sections were obtained by cutting the cork-attached specimens in a cryostat (Leica, Germany) and mounted on polarised glass slides (SuperFrost Plus, VWR, USA). Slides were dried overnight at room temperature and the next day slides were stored in plastic boxes at -80°C until use. Prior to use, slides were allowed to adjust to room temperature.

3.5.2 Haematoxylin and eosin staining

All the histological specimens underwent haematoxylin and eosin (H&E) staining in order to assess the microscopic structure of the tissue. H&E staining is based on two different dyes that allow differentiation of cellular nuclei and cytoplasm. In particular, haematoxylin stains nucleic acids with a deep blue/purple colour, while eosin stains the cytoplasm with a red/pink colour that varies intensity according to the pH. Tissue slides prepared as reported above, were fixed in a 4% paraformaldehyde buffered solution for 10 minutes and then washed in distilled water for 5 minutes. Slides were then transferred in a jar containing haematoxylin for 1 minute and then rinsed in tap water to remove the dye excess. Slides were transferred in a jar containing eosin for 2 minutes and then washed in distilled water for 5 minutes. Slides then were dehydrated with two changes two minutes long of absolute ethanol, followed by two changes 2 minutes long of xylene. Slides were blotted on absorbent paper to remove the excess of solvent and immediately fixed using DPX mounting medium (Sigma, UK). Haematoxylin and eosin stained slides were acquired with a bright field motorised microscope (BX61) from Olympus equipped with an Olympus digital camera (DP26) and were analysed with the CellSense software from Olympus.

3.5.3 XGal staining to detect beta-galactosidase activity

For the SG treated with LacZAdV a staining developed to reveal the β-galactosidase activity in transfected cells was used. Infected cells express the bacterial enzyme, which is capable to specific cleave the β-glycosidic bonds. When adding a specific substrate containing a β-glycosidic that changes colour when the bond is hydrolysed, it is possible to identify the infected cells that express the enzyme. Typically, an intense blue nuclear staining identifies the

cells transfected by bacterial β-galactosidase, allowing an easy distinction from rare senescent cells that can give a non-specific pale blue cytoplasmic staining.

Tissue slides prepared as reported above were adjusted to room temperature and then fixed in a 4% paraformaldehyde buffered solution for 10 minutes. Slides were then washed with two changes 5 minutes long in PBS. Slides were then moved in a jar containing a X-gal solution (1mg/ml 5-bromo-4-chloro-3-indolyl-β-D-pyranoside, 5mM $K_4[Fe(CN)_6] \cdot 3H_2O$, 5mM $K_3[Fe(CN)_6]$, 5mM EGTA, 2mM $MgCl_2$, 0.02% NP-40 in PBS) at 37°C in an incubator without addiction of CO_2, overnight or until colour development. Slides were then washed with two changes 5 minutes long in PBS and counter-stained for 30 second in haematoxylin. Slides were washed in tap water and mounted in DPX medium. Images were acquired with a bright field motorised microscope (BX61) from Olympus equipped with an Olympus digital camera (DP26) and were analysed with the CellSense software from Olympus.

3.5.4 Immunofluorescence

Immunofluorescence microscopy allows the usage of one or multiple antibodies to stain the same slide. Where classic bright-field immunohistochemistry permits generally the use of no more than two different antibodies, immunofluorescence staining easily allows detection of three/four epitopes thanks to the different chemistries commercially available.

All the staining protocols used are based on several essential steps: i) slides were thawed and allowed to reach room temperature; ii) slides were fixed either in acetone at -20°C or in a solution of 4% paraformaldehyde in PBS at room temperature for ten minutes; iii) to block the non-specific binding of the antibodies to the sample, slides were incubated with a blocking solution (1%

bovine serum albumin, 10% horse serum in TBS) for 15 minutes at room temperature; iv) the slides were then incubated with the various antibodies according to the detection technique required (explained in the next sections). All the different washes were performed for 5 minutes at room temperature in TBS buffer. At the end of the detection protocol, if required, slides were incubated with 4',6-diamidino-2-phenylindole (DAPI) solution (5 µg/ml in TBS from Life Technologies) for 5 minutes at room temperature to counterstain the nuclei. After the last wash, slides were mounted with a glass coverslip sealed with a solution of poly-vinyl alcohol (Mowiol 4-88, Calbiochem) and left to set in the dark for two hours at room temperature or overnight at 4˚C.

All the antibodies used in this thesis were titrated prior to use. The various antibodies and dyes used for this work, their producing company, catalogue number and dilution are reporter in **Table 3.1**.

Antigen	Raised in	Conjugation	Clone	Producer	Cat. number	Dilution
CD3e	Hamster	Biotin	500A2	BD	553239	1:200
B220	Rat	PE	RA3-6B2	Biolegend	103208	1:200
B220	Rat	Alexa647	RA3-6B2	Biolegend	103229	1:200
FDC	Rat	N/A	FDC-M1	BD	551320	1:100
PNAd	Rat	Biotin	MECA-79	Biolegend	120804	1:100
GL7	Rat	Biotin	GL7	Ebioscience	13-5902	1:50
CD11c	Hamster	Alexa488	N418	Biolegend	117311	1:200
F4/80	Rat	N/A	CI:A3-1	Sertotec	MCA497G	1:100
Lyve-1	Goat	N/A	Poly	R&D	AF2125	1:100
AdV5	Rabbit	N/A	Poly	ABCAM	ab6982	1:100
Pan Cytokeratin	Mouse	N/A	C-11	Biolegend	628601	1:100

Table 3.1: Primary antibodies used for IF staining.

Two different instruments were used to acquire the fluorescence from the slides, a classic motorised epifluorescence microscope (Olympus BX61) equipped with a high-definition digital camera (Hamamatsu, Orca-R2) and a confocal microscope from Leica (DM5500 Q, TCS SPE). Epifluorescence images were analysed with the CellSense software from Olympus, while images

acquired with the confocal microscope were analysed with the LeicaAF software suite from Leica.

Reactivity	Raised in	Conjugation	Producer	Cat. number	Dilution
Rat	Goat	Alexa555	Invitrogen	A21434	1:200
Rat	Chicken	Alexa488	Invitrogen	A21470	1:200
Goat	Rabbit	Alexa488	Invitrogen	A11078	1:200
Rabbit	Goat	Alexa488	Invitrogen	A11034	1:200
Biotin	N/A	Alexa488	Invitrogen	S32354	1:300
Biotin	N/A	Alexa555	Invitrogen	S21381	1:300
Mouse IgG1	Goat	Alexa555	Invitrogen	A21127	1:200
Rat	Goat	Biotin	Serotec	301008	1:200
Rabbit	Goat	Biotin	Dako	E0432	1:200

Table 3.2: Secondary/tertiary antibodies used for IF staining.

3.5.4.1 Staining procedures: two steps detection

For this detection method I first used an un-conjugated purified primary antibody raised against the epitope of interest. After the blocking step described above, the slide was incubated with the primary antibody diluted in blocking solution. The incubation time was either one-hour at room temperature or overnight at 4°C in a humidified chamber. The slide was then washed in buffer and the specimen was incubated with a fluorophore-conjugated secondary antibody raised against the Fc portion of the primary antibody, diluted in blocking solution. Incubation time for the secondary antibodies was one hour at room temperature in the dark. For example, if the primary antibody was raised in rat, the secondary antibody used was a fluorophore-conjugated anti-rat antibody. The list of the secondary anctibodies used in this thesis is reported in **Table 3.2**.

3.5.4.2 Staining procedures: directly conjugated antibodies

In some cases, directly fluorophore-conjugated primary antibodies were available and have been used for the direct detection of the target. In this case, after the blocking step, the sample was simply incubated with the antibody diluted in blocking solution for one hour at room temperature in the dark, the slide was washed in buffer and the sample prepared for imaging.

3.5.4.3 Staining procedures: biotinylated antibodies

This method requires primary antibodies conjugated with biotin. After the incubation with the primary antibody, the specimen is incubated with fluorophore-conjugated biotin binding proteins, such as avidin or streptavidin. This method allows several molecules of fluorophore-conjugated protein to bind the same biotin-conjugated antibody, and thus provides strong signal amplification. When this methodology was used, an additional step of blocking was necessary prior to the protein block step, to neutralise the endogenous biotin that might provide a non-specific signal. Therefore, after sample fixing, slides were washed in buffer and incubated with an avidin solution (Dako) for 5 minutes, washed in buffer and incubated with a biotin solution (Dako) for 5 minutes. After this step, slides were blocked in blocking solution and then incubated with the biotin-conjugated primary antibody diluted in blocking solution. Slides were then washed in buffer and incubated with fluorophore-conjugated streptavidin diluted in blocking solution.

3.5.4.4 Staining procedures: three steps detection

In some cases, to achieve signal amplification when a biotinylated primary antibody was not available, a three steps protocol was used. Briefly, after avidin/biotin block (described above) and incubation in blocking solution, slides

were incubated with a purified primary antibody (as described in the two-steps method) diluted in blocking solution for one hour at room temperature. The slides were then washed in buffer and incubated with a biotin-conjugated secondary antibody diluted in blocking solution for one hour at room temperature. After washing in buffer, slides were then incubated with fluorophore-conjugated streptavidin diluted in blocking solution for one hour in the dark.

3.5.4.5 TUNEL assay for the detection of apoptotic cells

Cells undergoing apoptosis go through a series of consecutive and well-regulated processes that characterise the programmed cell-death mechanism. Among these apoptosis hallmarks, there is the digestion of the nuclear genetic material by endonuclease enzymes. This process produces a vast amount of nicks in the DNA. The terminal deoxynucleotidyl transferase dUTP nick end labelling assay, or TUNEL assay, relies on the capacity of the enzyme terminal deoxynucleotidyl transferase (TdT) to catalyse the addiction of deoxyuridine triphosphate (dUTP) to the DNA nicks. dUPT monomers used in the assay are marked (e.g. they can be radio-labelled or conjugated with a specific chemical moiety) and thus can be detected and measured. In my experiments, the TUNEL assay I used (Trevigen TACS2 TdT Fluo kit) for the detection of apoptotic nuclei is optimised for immunofluorescence detection and relied on biotin-cojugated dUTP monomers. Briefly, slides were fixed in PFA 4% and permeabilised with cytonin solution, a bland permeabilising agent provided by the manufacturer, for 30 minutes at room temperature. The TdT enzyme might require specific ions according to the tissue analysed and the embedding technique used: the best working conditions for the enzyme need to be

determined empirically. For OCT-embedded frozen SG tissue, the labelling mixture was prepared using cobalt cation stock. After incubation with the enzyme, the slides were washed in the suggested buffer and incubated with the provided streptavidin-conjugated fluorophore, counterstained with DAPI and mounted for fluorescence microscopy observation.

3.5.5 Evaluation of the leukocyte infiltration in the salivary glands

From a clinical point of view the lymphocytic infiltrate in the SG of SS patients is graded according to the Chisholm and Mason system [124],[146],[225],[226] that is based on the detection of inflammatory *foci* (a focus being defined as more of 50 periductal lymphocytes in 4 mm^2 of tissue area). For this thesis and the grading of infiltrates forming in murine SG we used a different method proposed from my laboratory in 2005 [31]. According to this system, cellular aggregates with 10–50 periductal lymphocytes are defined as grade 1 aggregates (G1). Grade 2 aggregates display >50 periductal lymphocytes and are divided in non-segregated (NS-G2) and segregated (S-G2) on the basis of the presence of B/T cell compartmentalisation. Grade 3 aggregates (G3) are characterized by >50 periductal lymphocytes and the presence of a GC-like structure, based on the detection of a network of FDCs. The size of the aggregates is easily assessable with a haematoxylin and eosin staining, while to determine the segregation status and the presence of FDC networks I used immunofluorence staining. In particular, for the B/T cell segregation antibodies against CD3ε (T cells) and B220 (B cells) were used on the same slide. To determine the presence of FDC networks an antibody against FDC-M1 (FDC networks) was used either alone or in tandem with B220.
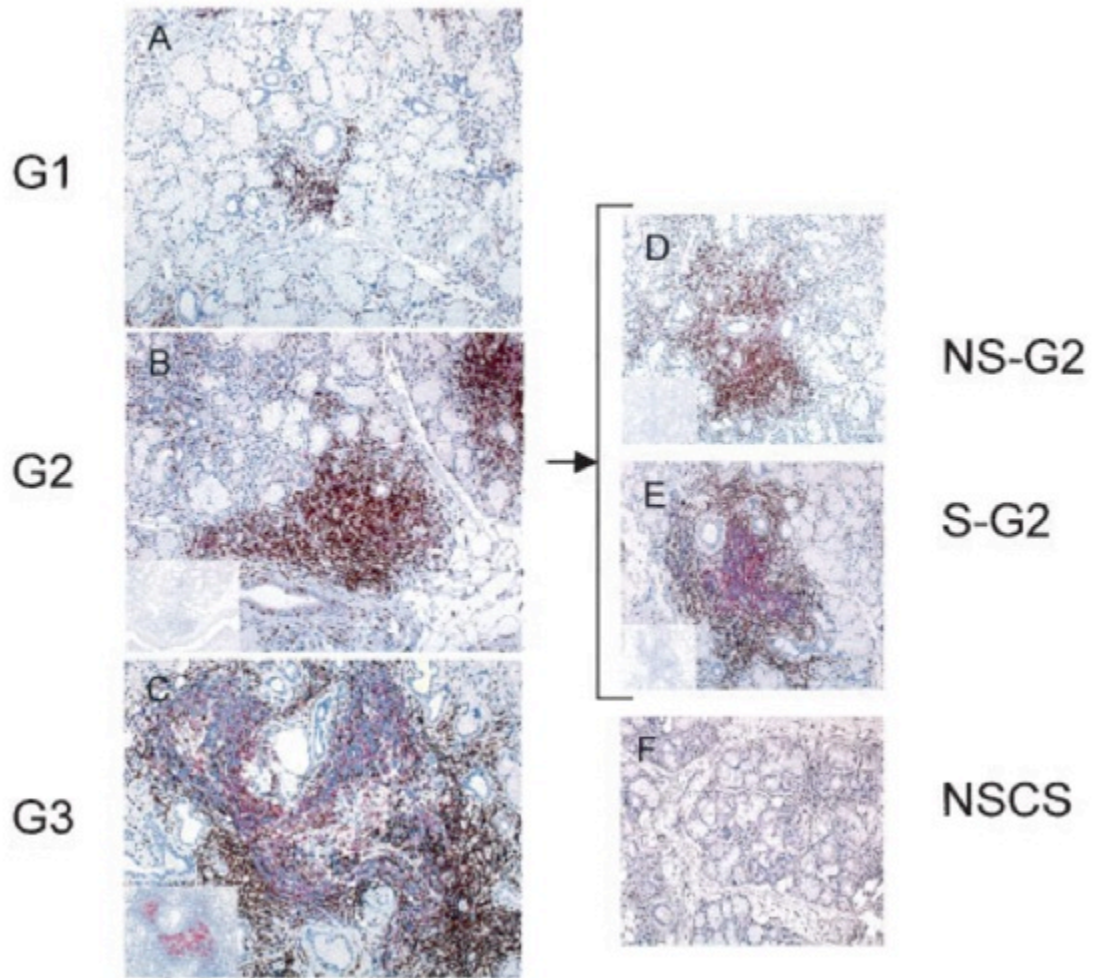
Figure 3.8: Immunostaining of sequential sections of SS salivary glands.
For this thesis the grading system proposed by Barone et al., Arthritis. Rheum.
2005 was used and it is reported in figure. Left, from top to bottom: increasing
grades of aggregation and organization in different patients with SS. **(A)**
Cellular aggregates with 10–50 periductal lymphocytes are defined as grade 1
aggregates (G1). **(B)** Grade 2 aggregates display >50 periductal lymphocytes
and are divided in non-segregated (NS-G2, **D**) and segregated (S-G2, **E**) on the
basis of the presence of B/T cell compartmentalisation (in this picture visualised
via CD3/CD20 staining). **(C)** Grade 3 aggregates are characterized by >50
periductal lymphocytes and the presence of a GC-like structure, based on
histologic features of a GC-like structure and the detection of a network of FDCs

(here visualized via CD21 staining) on sections sequential to those stained for CD3 and CD20. In panel **(F)** a SG from a patient with non-specific chronic sialoadenitis is reported. From [31], copyright 2005.

3.6 PCR and quantitative real-time Taqman PCR

3.6.1 Tissue total RNA extraction

RNA was extracted from tissue using the Qiagen RNeasy mini kit according to manufacturer instructions. Tissues stored in RNA later at -80°C were thawed on ice, weighted and an amount equivalent to approximately 20 mg was put in a sterile RNAse-free test tube with 600 µl of RLT buffer containing with 10 µl/ml of β-mercaptoethanol. Tissues were either homogenised with the aid of a rotor-stator (one cycle of approximately 20 seconds) or with a beads homogeniser. In this last case homogenising micro-beads tubes (Precellys systems, Bertin Technologies, France) were filled with 600 µL of RLT buffer and lysed with a shaking micro-beads homogeniser (Precellys systems, Bertin Technologies, France). After homogenisation, either with rotor-stator or micro-beads, tubes were centrifuged at maximum speed (approximately 10'000xg) for 3 minutes with a bench-top microcentrifuge to eliminate debris and the homogenate transferred in fresh RNAse-free tubes. A volume of 70% ethanol was added to the lysate and the obtained solution readily mixed by pipetting. In the next step the solution was transferred in special silica membrane mini-columns fitted with 2 ml collection tubes and centrifuged for 15 seconds at a speed >8000xg. The ethanol added in the previous step precipitates the nucleic acids that then bind the silica membrane during the centrifugation, while the aqueous solution is eluted in the collection tubes and discarded. After a wash step achieved adding 350 µl of buffer RW1 to the column and centrifuging as above, a solution containing DNAse-I enzyme was added on the silica membrane according to manufacturer's instruction to get rid of the DNA (lyophilised DNAse-I was reconstituted in 550 µl of distilled RNAse-free water and 10 µl of the solution

containing the enzyme were added to 70 µl of buffer RDD and finally the obtained 80 µl were added to the silica membrane and left at room temperature for 15 minutes). To stop the enzymatic cleavage of DNA, 350 µl of buffer RW1 were added to the column and the column centrifuged as described. The flow-through was discarded and 500 µl of buffer RPE were added and the column centrifuged as described previously to wash away remaining contaminants. This step was repeated again this time with a centrifugation time of 2 minutes and the flow-through was discarded. The column was then transferred in a 1.5 ml RNAse-free collection tube and RNA bound to the silica membrane and devoid of protein and DNA contaminants was eluted by the addition of 30 µl of RNAse-free distilled water and centrifugation at a speed >800xg for 1 minute. Elution was immediately transferred on ice, quantified and then stored at -80°C until use.

For FACS sorted cells (see section 3.8.2) RNeasy Micro kit (Qiagen) was used according to the manufacturer instruction. The procedure is essentially identical to that described above, with minor modification to reduce loss of nucleic acids. RNA was eluted in 12 µl of RNAse-free water and elution was immediately transferred on ice, quantified and then stored at -80°C until use.

3.6.2 Total RNA quantification

Total RNA was quantified using a ThermoScientific Nanodrop 2000 device. The Nanodrop is substantially a spectrophotometer adapted to work with small volumes (1-2 µl). The device was first blanked using RNAse-free distilled water and then one microliter of the RNA solution obtained as described above was deposed on the Nanodrop pedestal and the arm closed. Absorbance was then read at 260 nm (nucleic acids absorbance) and 280 nm (protein absorbance)

and the quantity of RNA calculated according to the molar-extinction coefficient for single-stranded RNA. The amount of protein contamination was evaluated via the 260nm/280nm absorbance ratio: for pure RNA this ratio is approximately 2.0 and for my purposes any value ≥1.7 was considered acceptable.

3.6.3 Reverse transcription

The enzyme reverse transcriptase (RT) is capable to convert RNAs into complementary DNA (cDNA). RTs are typical of retroviruses that need the enzyme to propagate into the host. Several commercial RTs are available and are used to convert messenger RNAs into cDNA for downstream applications. To convert mRNA obtained from cells and tissues into cDNA for my thesis I have used the Thermoscript RT-PCR system from Life Technologies. Thermoscript is the name of the RT enzyme is used in this kit and it is obtained via engineering of the enzyme cloned from avian myeloblastosis virus. The mutations introduced into the enzyme sequence make the enzyme less prone to degrade RNA and resistant to temperature up to 70°C. Following the manufactures instructions, 1 μg of RNA obtained and quantified as described above was mixed with 1 μl of a 50 μM solution of Oligo(dT). These are deoxythymidine oligonucleotides that bind to the poly-adenosine monophosphate tail of mRNAs and provide a double-strand necessary for the Thermoscript enzyme to start the reaction. To the same solution 2 μl of a 10 nM solution of deoxyribonucleotides triphosphate (dNTP) were added: dNTPs provide the bases that the enzyme uses to synthesise the cDNA. The solution was then brought to a final volume of 12 μl with nuclease-free distilled water. Samples were then incubated for 5 minutes at 65°C to induce denaturation of the RNA tertiary structures and then quickly placed in ice to induce Oligo(dT)

annealing to the mRNA poly(A) tails. At this point, 8 µl of a master mix containing 15 units of Thermoscript enzyme, 1 µl of 0.1 M dithiothreitol (DTT), 40 units of RNAseOUT, 4 µl of 5x cDNA synthesis buffer and 1 µl of nuclease-free water were added to the previous solution. RNAseOUT is a commercial RNAse inhibitor and DTT serves as its stabiliser in the reaction. The solution was then placed in a thermalcycler (Applied Biosystems 9700) for 1 hour at 50°C to allow the Thermoscript to synthesise cDNA followed by a step at 85°C for 5 minutes to inactivate the enzyme. As a final step, elimination of the mRNA or other contaminating RNAs from the solution was achieved by adding 2 units of RNAse H to the solution that was left for 30 minutes at 37°C. The synthesised cDNA was brought to a final concentration of 10 ng/µl with nuclease-free water and stored at -20°C until use.

RNA extracted from FACS-sorted cells was significantly less abundant than that extracted from tissues. For this reason the maximum volume of RNA allowed by the RT kit was used to produce cDNA from these samples, independently from the starting RNA concentration. Obtained cDNA was not further eluted and was stored to be used directly in the Fluidigm

3.6.4 Quantitative real-time Taqman PCR and Fluidigm Dynamic Array

Polymerase chain-reaction (PCR) is a process that amplifies a specific DNA sequence during sequential amplification cycles. In real-time PCR reactions, the buffer in which the reaction takes place is added with a fluorescent dye that changes its fluorescence emission in function of the level of the amplification achieved for each single cycle, that is in real-time as opposite to the classic end-point PCR where the amplification level is assessed only at the end of the reaction. Several different real-time PCR techniques exist, whit specific up and

down sides. In this thesis, I have used the TaqMan real-time PCR system. In this method in the master mix are present not only two sets of primers that define the sequence of cDNA that will be amplified, but also a probe complementary to a cDNA sequence located in the region defined by the primer pair. The probe is conjugated with a fluorescent dye and a fluorescence quencher. Moreover, the enzyme used in this reaction is a modified version of the Taq polymerase used in classic PCR: the TaqMan enzyme not only polymerases oligonucleotide sequences complementary to the template cDNA, but also has an exonuclease activity that allows the hydrolysis of the probe bound to the cDNA. For each cycle of amplification then, the TaqMan enzyme starts the amplification at the primer-annealing site and during the synthesis of the complementary strand it encounters and digests the probe. The quencher is thus released from the fluorescent dye and fluorescence can be measured.

The real-time PCR was run in duplicates in 384-well plates (Applied Biosystems) with 10 ng/well initial amount of cDNA. The probes used were bought conjugated with the FAM dye from a commercial producer (LifeTechnologies) and used with a commercial master mix (Applied Biosystems). The reaction took place in an ABI Prism 7900HT machine and data were collected and analysed with the SDS software suite (Applied Biosystems). The thermal cycling conditions were as follows: 2 minutes at 50°C, 10 minutes at 95°C, 45 cycles of a denaturation step at 95°C for 15 seconds and an annealing/extension step at 60°C for one minute. A calibrator sample was used for every plate and consisted of either spleen, Peyer's patches or SG from a control animal.

To relative quantification was obtained using the comparative threshold cycle (Ct) method. The Ct cycle of the endogenous control (normally mammalian 18S rRNA) was used to normalise for the initial cDNA amount of each sample by subtracting from the average between Ct duplicates of the gene of interest the average of the endogenous control, obtaining in this way the ΔCt value. To calculate the ΔΔCt value, the ΔCt of each sample was subtracted to the chosen reference sample (usually PP or SG from a control animal). The ΔΔCt value for each sample was then use to calculate the relative quantification (RQ value) using the equation $RQ=2^{-\Delta\Delta Ct}$. The number two in the equation represents the doubling of the amplification product for every cycle of PCR, considering an optimal efficiency of the PCR. For TaqMan PCR, this approximation refers to a high efficiency reaction where the fluorescence doubles for each cycle of amplification. In order to confirm the PCR efficiency, in initial set-up experiments serial 2^5 dilutions (i.e. 1:1, 1:32; 1:1,032) of a control cDNA tissue positive for the gene of interest (i.e. spleen cDNA) were used and the observed CT values reflected the expected difference of 5 cycles of amplification for each sample dilution.

For the real-time PCR analysis of FACS-sorted cells a different technique was used that allowed the relative quantitation of gene expression starting from small amounts of initial mRNA. The sorted cDNA samples, extracted with the RNeasy micro kit and retrotranscribed with the Thermoscript kit as described in the above sections, were loaded on a 48x48 Fluidigm Dynamic Array integrated fluidic circuits (IFCs) chip together with the real-time master-mix (Applied Biosystems) and TaqMan probes (Lifetechnologies) described above. Microfluidic chips allow the use of nano-volumes of cDNA, master mix and

probes in comparison with the micro-volumes necessary for the 384-wells plate method described above. The system can load up to 48 different samples requiring as little as 5 μl of each sample at 5 ng/μl concentration to run as many as 48 different assays (45 genes of interest and 3 housekeeping genes). Any chip can thus run 2'304 single real-time reactions at a time. The Fluidigm chip, loaded with samples and reagents, was then run on a Fluidigm Biomark HD system. As calibrating sample, I used the same Peyer's patches sample used for the 384-wells plate system and the three housekeeping genes used were eukaryotic 18s, β-actin and hypoxanthine-guanine phosphoribosyltransferase (HPRT). The PCR reaction started with a cycle of 10 minutes at 95˚C, followed by 40 cycles formed by a 95˚C for 15 seconds denaturation step followed by a 60˚C for one-minute annealing/elongation step. Relative quantitation was calculated using the $2^{-\Delta\Delta Ct}$ method described above.

A table with the list of all the primers and probes used for this thesis is reported in **Table 3.3**.

Gene Product	mRNA Accession Number	Assay ID	Source
Mouse AID	NM_009645	Mm00507774_m1	Applied Biosystems
Mouse CXCL13	NM_018866	Mm00444533_m1	Applied Biosystems
Mouse CXCR5	NM_007551	Mm00432086_m1	Applied Biosystems
Mouse CCL19	NM_011888	Mm00839967_g1	Applied Biosystems
Mouse CCR7	NM_007719	Mm00432608_m1	Applied Biosystems
Mouse BAFF	NM_033622	Mm00446347_m1	Applied Biosystems
Mouse IL-4	NM_021283	Mm00445259_m1	Applied Biosystems
Mouse IL-21	NM_021782	Mm00517640_m1	Applied Biosystems
Mouse Ltβ	NM_008518	Mm00434774_g1	Applied Biosystems
Mouse LtβR	NM_010736	Mm00440235_m1	Applied Biosystems
Mouse CCL5	NM_013653	Mm01302427_m1	Applied Biosystems
Mouse CCL7	NM_013654	Mm00443113_m1	Applied Biosystems
Mouse CCR1	NM_009912	Mm00438260_s1	Applied Biosystems
Mouse HPRT	NM_013556	Mm00446968_m1	Applied Biosystems
Mouse β-actin	NM_007393	4352341E	Applied Biosystems
Eukaryotic 18S	X03205.1	4319413E	Applied Biosystems

Table 3.3: TaqMan probes used for gene expression analysis.

3.7 Serum antibodies characterization

3.7.1 Western blot analysis using serum antibodies for detection

A Western blot method is commonly used to detect the presence of a determined protein in cell culture or tissues. The technique consists in two main steps: the first is the polyacrylamide gel electrophoresis (PAGE) where the proteins present in a solution are separated on the basis of their molecular weight; the second process, the immunoblot, is the transfer of the separated proteins from the polyacrylamide gel to a membrane that is then incubated with an antibody against the protein of interest and then detected with an enzyme-labelled antibody directed against the primary antibody.

In my thesis I have used the Western blot technique not to detect the presence of a certain protein in a solution, but to assay sera from treated and untreated animals for the presence of antibodies against adenoviral proteins. For this reason, cell lines were infected with luciferase or LacZ-encoding adenoviruses or left uninfected and the cell lysates obtained underwent electrophoresis and immunoblot. At this stage, blotted membranes were incubated with sera from AdV- or control-treated animals culled at different time-points that were used as primary antibodies. As a principle, instead of using a primary antibody with known specificity to detect the presence of the specific target protein on the blotted membrane, membranes containing adenoviral proteins were used to detect the presence of specific antibodies in the sera. Enzyme-conjugated anti-mouse antibodies were used in the last step to detect anti-viral antibodies bound to the viral proteins.

To achieve this, confluent Hek293 cells were infected with LacZAdV, LucAdV or left uninfected. Cells were returned in the incubator at 37°C for 48 hours. At the

end of the incubation period, the medium was discarded and the cells washed in PBS. A lysis buffer (RIPA buffer, 50mM Tris, 150mM NaCl, 0.5% sodium deoxycholate, 1% NP-40, 0.1% sodium dodecyl sulphate, pH=8) containing protease inhibitors (Complete mini EDTA-free, Roche) was then added to the wells to disrupt plasma membranes and free and stabilise the host and viral proteins.

The protein content of the lysates was quantified with a bicinchoninic acid (BCA) assay (Pierce, USA). Cell lysates were diluted in a 5x Laemli solution (10% sodium dodecyl sulphate, 50% glycerol, 25% β-mercaptoethanol, 0.01% bromphenol blue and 0.312 M Tris HCl, pH=6.8) and left on a hotplate at 100°C to denaturise for 5 minutes. β-mercaptoethanol is a reducing agent, which helps breaking the sulphide bonds among peptides. The sodium dodecyl sulphate (SDS) molecules present in the solution and in the lysis buffer help to denaturise the proteins as the non-polar moiety binds to the hydrophobic amino acids of the proteins exposing the negative portion of SDS to the buffer and giving thus a negative charge to the hydrophobic residues of the protein. Moreover, the negatively charged moiety of SDS also binds to the positive residues, neutralising them. Eventually, during the treatment at 100ºC, disulphide bonds are reduced by β-mercaptoethanol and the high temperature allows denaturation of the proteins into their primary structure that is maintained by SDS molecules by neutralising the positive charges and giving to the polypeptide a strongly negative charge. Bromophenol blue is a blue dye that helps monitoring the migration of the proteins in the next steps.

The cells lysates were loaded on a commercial polyacrylamide gel (Nu-PAGE, 4-12% bis-tris, Invitrogen) in an electrophoresis tank (Invitrogen) filled with

running buffer (5mM MOPS, 5mM Tris, 0.1% SDS, 0.1mM EDTA) and a constant electric tension of 100V was applied to the tank for approximately 1.5 hours. The proteins suspended and denatured in the loading buffer have a strong negative charge and when the electric field is applied, they migrate into the polyacrylamide towards the anode. During the migration the proteins separate in bands according to their size and the composition of the gel matrix: smaller peptides migrate faster, while bigger proteins migrate slower. Per every gel lane I loaded the equivalent of 25 µg of protein. At the end of the electrophoresis, the separated bands were transferred to a nitrocellulose membrane with the aid of a commercial semi-dry system (iBlot, Invitrogen) according to manufacturer's instructions. The efficiency of the transfer was assessed incubating for few minutes the membrane with a 0.1% Ponceau red solution in acetic acid: Ponceau red binds proteins in a non-specific manner and thus allows a rapid visual check of a successful and equal transfer. The membrane was then washed from the red dye for 10 minutes in TBST (TBS 0.1% Tween-20) on a rocking shaker. The membrane was then incubated in a solution containing 5% powder milk in TBST for 3 hours at room temperature. Incubation with the milk solution blocks protein non-specific binding.

At this point, membranes were incubated either with a commercial anti-adenovirus antibody (goat anti-adenovirus 5 whole antiserum, AB6982, Abcam, dilution 1:4'000) as a positive control or with sera from the treated mice at a dilution of 1:100 in a 5% milk TBST solution, overnight at 4°C. The membrane was then washed 3 times for 5 minutes in TBST and incubated with a horseradish peroxidase-conjugated detection antibody against the primary (in this case goat anti-mouse IgG from Sigma for the membranes incubated with

mice sera or rabbit anti-goat IgG from Dako for the membranes incubated with the commercial anti-adenovirus antiserum). Secondary antibodies were diluted in blocking solution and the membranes incubated for 1 hour at room temperature.

To detect the binding of the detection antibody to the protein of interest, an enhanced chemiluminescence (ECL) substrate is used. The ECL substrate contains luminol that is oxidised by the peroxidase-linked antibodies present on the membrane. Luminol in its excited state decays to the ground state emitting light at 428 nm. The light emitted from the membrane is used to expose an X-ray film that is then developed. After 3 washes in TBST the membrane was incubate with ECL (Amersham Life Science), wrapped in transparent film and left at room temperature for one minute. The membrane was then used to expose an autoradiography film for various times in a dark room equipped with red-light illumination. After exposure the films were developed in an automated developing machine and studied.

3.7.2 Anti-nuclear antibodies (ANA) detection in serum

Levels of anti-nuclear IgG antibodies (ANA) were assessed using an indirect immunofluorescence method. The human epithelial cell line 2, or HEp-2, is classically used for this assay as HEp-2 cells have a large nucleus and a high rate of mitosis thus being rich of mitosis-associated antigens. The rationale behind this test is that anti-nuclear antibodies present in serum react with the nuclei of the cell line and can thus be detected using an appropriate fluorophore-conjugated secondary antibody (in the case of murine serum, anti-mouse immunogluobulins FITC-conjugated) on a fluorescence microscope. For this thesis twelve-spot slides coated with Hep2 cells were bought from

BioSystems (Spain) and each spot was incubated with 20 µl of diluted serum for 1 hour at room temperature or overnight at 4°C. The dilutions used were 1:80, 1:160 or 1:320 and sera were diluted in a solution of 2% BSA, 0.05% Tween-20 in PBS. These dilutions were used to parallel the dilutions used in clinic to diagnose the presence of ANA in human serum. As a positive control I used pooled sera from autoimmune MRL*lpr/lpr* animals (a murine strain that develops a lupus-like syndrome with a plethora of different anti-nuclear antibodies, a kind gift of Dr. Francesco Carlucci, Imperial College, London) serially diluted to end-point. As negative control, pooled sera from 12 weeks old untreated C57Bl/6 wild-type female mice were used. To detect binding of serum antibodies to the HEp-2 cells, slides were washed twice in PBS for 5 minutes and incubated for 30 minutes at room temperature with a fluorophore-conjugated antibody against the Fc portion of mouse IgGs (Sigma) diluted 1:200 in the dilution buffer used previously. After washing in PBS, coverslips were mounted and images were acquired either with a motorised epifluorescence microscope (Olympus BX61) equipped with a high-definition digital camera (Hamamatsu, Orca-R2) or with a confocal microscope (Leica DM5500 Q, TCS SPE).

3.7.3 Anti-adenovirus antibodies detection in serum

Detection and relative quantitation of the different classes of anti-adenovirus immunoglobulins present in the sera of AdV-treated mice were assessed using indirect enzyme-linked immunosorbent assay (ELISA) methods.

In indirect ELISA an antigen (in this case viral particles) is added to the wells of an ELISA-treated 96-wells plate. The antigen is suspended in a buffer solution that facilitates the binding to the plate wells. After an appropriate incubation, the antigen is removed and the binding sites not coated with the antigen and the

non-specific binding sites are neutralised by adding a blocking solution containing irrelevant proteins. Once the incubation with the blocking solution is finished, the blocking solution is removed and a primary antibody against the antigen of interest is added to the wells. After the incubation with the primary antibody, wells are washed and a solution containing an enzyme-conjugated secondary antibody against the primary antibody is added to the wells. After this incubation, wells are again washed and a substrate for the enzyme conjugated the secondary is added and colour development is observed and measured. Generally, samples are loaded in duplicates and two dilutions for every sample are loaded on the plates. Usually, a standard curve of known concentrations of an antibody against the antigen of interest is added to the plate to allow absolute or relative quantitation. Moreover, one of the wells is normally incubated without the primary antibody to assess the blank, or baseline absorbance, for the assay. For the purpose of this thesis, as sera from cannulated animals and controls were to be tested for the presence of anti-viral antibodies, the ELISA plates were coated with the same amount of AdV particles and the sera were used as primary antibodies (see

Table 3.4 for details of the dilution used). A standard curve was obtained using serial dilutions from a pool of different sera obtained from animals cannulated and culled at different time points. Data were expressed as arbitrary units (AU) with the highest value assigned to the higher concentration.
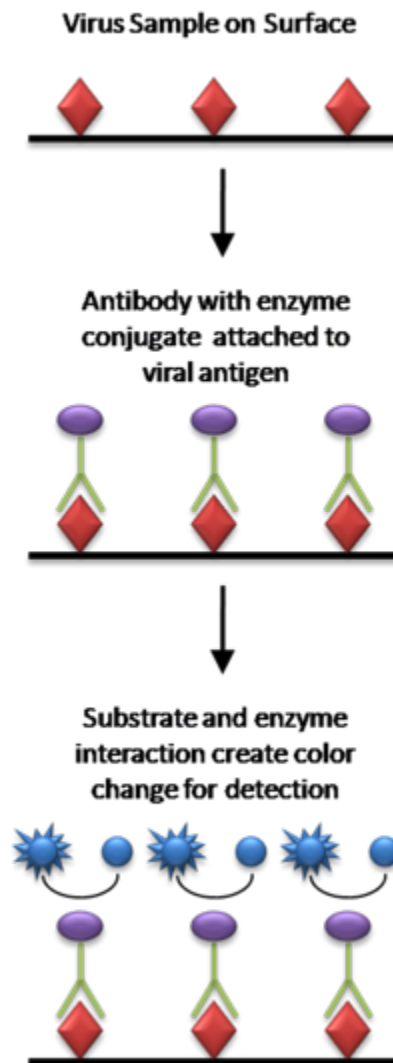
Figure 3.9: General scheme of indirect ELISA. The antigen is used to coat the plate and an enzyme-conjugated primary antibody is used to detect the antigen. In my experiments, sera from treated and control animals were used as primary antibodies and a secondary anti-mouse conjugated-antibody was used to detect the presence of specific anti-virus antibodies in sera. Figure from Wikipedia.

In details, ELISA Maxisorp 96-well plates (Nunc) were coated with 100 µl/well of a 5 µg/ml solution of adenovirus diluted in carbonate/bicarbonate buffer (Sigma). AdV concentration was determined reading the absorbance of the AdV-containing solution at 280 nm with a Nanodrop device, after blanking the instrument with TSG buffer. Plates were incubated overnight at 4°C in a moist chamber (or 2 hours at 37°C). Plates were then washed 3 times with PBS. Non-specific binding was blocked incubating plates for 1 hour at 37°C with 100 µl/well of a solution 1% bovine serum albumin (BSA) in PBS. Plates were washed 3 times in PBS. Plates were incubated with standards, positive and negative controls and samples diluted in PBS containing 1% BSA and 0.05% Tween. Standards were obtained pooling the sera from treated animals at various time-points. The negative control consisted of pooled sera of female 12 weeks old untreated animals. The optimal dilution for standards and samples was determined during preliminary experiments. The dilutions used are reported in Table 3.4. Plates were incubated for 1 hour at 37°C and then washed in PBS 3 times. 100 µl of a HRP-linked or biotinylated anti-mouse immunoglobulin antibodies diluted in PBS containing 1% BSA and 0.05% Tween 20 (Sigma A2554: anti-mouse IgG(H+L)-HRP 1:10'000)

Plates were incubated for 1 hour at 37° and then washed 3 times in PBS. In the case of biotinylated antibodies, a further incubation step with HRP-conjugated streptavidin was necessary (dilution 1:5'000, Biolgend). Binding was detected using 75 µl/well of BD OptEIA TMB substrate reagent set (GE healthcare). Reaction was stopped upon colour development with 30 µl/well of 2M H_2SO_4. Absorbance was read at 450 nm with an ELISA plate reader. Relative

concentrations were calculated from the standard curve and expressed as arbitrary units (AU)/ml.

	Total IgGs
Standard	Highest 1:100 Then 1:2
Samples	1:100/1:200

Table 3.4: Standard and sera dilutions used for immunoglobulin ELISA.

3.8 Flow cytometric analysis and cell sorting

In a flow cytometer, a fluidic stream is created where cells drawn from a solution can pass only one at a time in front of a laser beam. When the laser light hits the cell, photons are scattered in every direction according to the physical parameters of the cell they hit, in particular to its size and complexity (i.e. granularity). Inside the cytometer, photomultipliers measure the photons scattered forward to the laser (forward scatter, FSC) and at an angle of 45° to the light-path (side scatter, SSC): the FSC is in relation to the size of the cell, while the SSC to the complexity and granularity of the cell. Together with these basic physical parameters, flow cytometers can also measure the fluorescence emitted by the cells hit by the laser light. In flow cytometry, before being analysed by the cytometer, cells are incubated with fluorophore-conjugated antibodies directed against specific antigens. When exposed to laser-light of specific wavelength, the fluorophores emit fluorescence that can be recorded by the photomultipliers and analysed. With this technology, size and complexity of a cell can be associated with information about the presence and abundance of specific cellular markers. The data collected are showed in a single dimension (histogram) or plotting two or more parameters against each other (dot plot).

Florescence-activated cell sorting (FACS) systems are based upon the very same principle of flow cytometry and are also able to select and separate a determined population from the analysed cell suspension for downstream applications. Generally, in these flow cytometers the fluidic stream containing the cells is arranged to have a large separation between a cell and the following one. Moreover, the stream is set to break in individual droplets containing only one cell just after the interrogation point. After the interrogation point, a metal ring can give a positive or negative charge to each single droplet passing by, according to the physical parameters and fluorescence readings associated to the cell just analysed. The charged droplets then pass through two charged metal plates that can deflect them towards containers on the basis of the charge of the droplets.
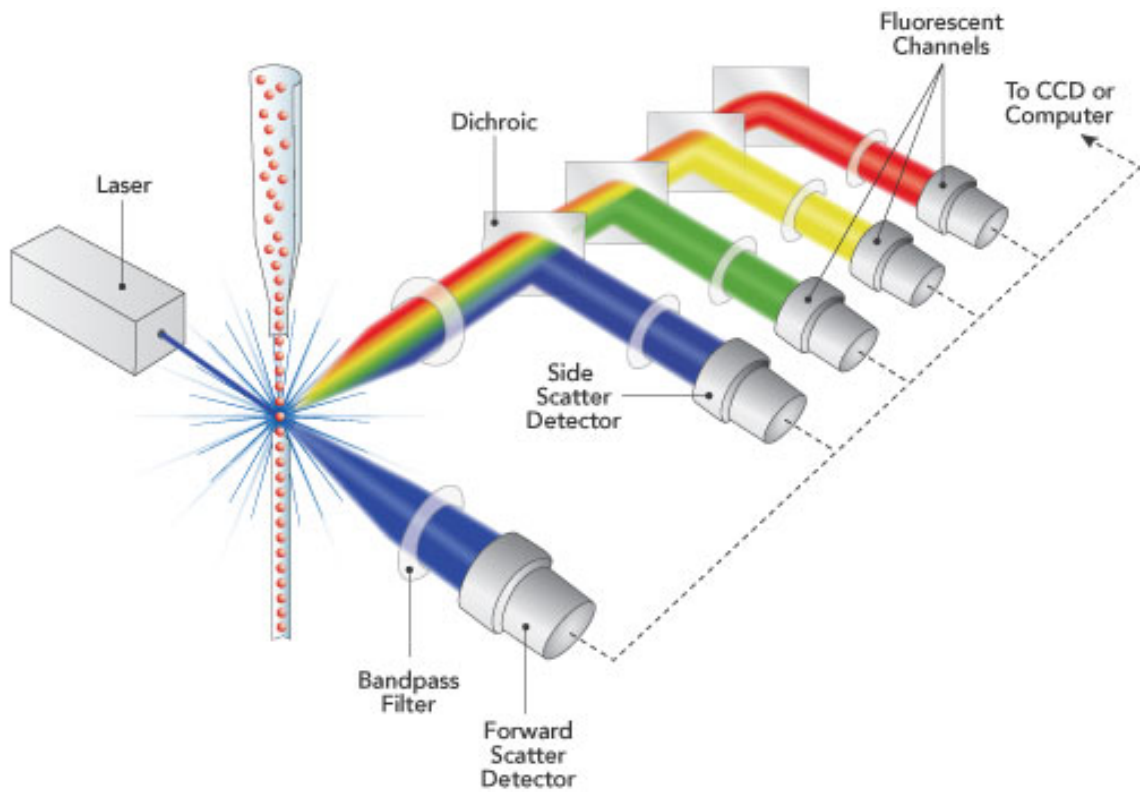
Figure 3.10: basic schematic of a flow cytometer. Laser light is directed against the fluidic stream containing cells passing one at a time in the interrogation point. A forward light scatter detector is placed directly in front of the laser emitter, while an array of detectors is placed at a 45˚ angle to detect side scattered light and fluorescence. A bandpass filter is associated to each detector to separate and discriminate the various wavelengths produced at the interrogation point.

3.8.1 Tissue preparation for flow cytometric analysis/sorting and cell culture

To obtain a homogenous suspension of cells to be analysed via flow cytometry, salivary glands, spleens and lymph nodes were enzymatically digested to dissolve the extracellular matrix and release cells. When needed (e.g. spleen), red blood cells where eliminated from the cell suspension using a lysis buffer. Before surface staining with antibodies, non-specific binding to Ig receptors was blocked with a solution containing anti-Fc receptor specific antibodies and dead cells were marked using either nuclear dyes or new generation viability dyes.

3.8.1.1 Enzymatic tissue digestion

Harvested tissues were rapidly stored in 1.5 ml tubes in 500 µl of RPMI medium (Gibco) supplemented with 2% foetal bovine serum (Life technology). Tissue were then minced in medium using dissecting scissors and transferred in 5 ml FACS tubes (BD) and 1 ml of digestion medium was added. Digestion medium consisted of RPMI 2% FBS, 3.7 mg/ml collagenase-D (Roche), 30 µg/ml DNAse-I (Sigma). Tubes containing minced tissue in digestion medium were then incubated for 30 minutes at 37°C under continuous stirring (2 mm magnetic stirring bars, VWR) at 500 rpm. After this first incubation tissue was vigorously pipetted to favour mechanical dissociation and 15 µl of 0.5 M EDTA (Gibco) were added to stop the enzymatic reaction. The solution was incubated for additional 5 minutes at 37°C under continuous stirring.

The cellular suspension obtained was passed through a 40 µm nylon cell strainer (BD) and the filter was washed with 10 ml RPMI 2% FBS and the flow-through was collected in 50 ml test tubes (BD) and centrifuged for 5 minutes at

400xg. The supernatant was discarded and the cell pellet suspended in the appropriate buffer for downstream applications.

3.8.1.2 Red blood cells lysis

For flow cytometric analysis of spleens, red blood cells (RBC) need to be removed from the solution as they might interfere with staining, data acquisition and analysis. To do so, the suggested volume of a commercial ammonium chloride solution (Biolegend) was added to spleen cell pellets for 5 to 10 minutes to favour RBC lysis. The solution obtained was spun down for 5 minutes at 400xg and suspended in the appropriate buffer for downstream applications.

3.8.1.3 Fc-receptor block and live/dead cells discrimination

Prior to the staining with specific antibodies, the suspension containing the appropriate number of cells was incubated with anti-CD16/32 antibodies cocktail to block the non-specific binding of the staining antibodies to the Fc-receptors present on several hematopoietic cell types. In particular, 1 µl of a commercial Fc-blocking cocktail (TrueStain, Biolegend) was added the cells suspended in 50 µl of 1x PBS. The solution was incubated for 15 minutes at room temperature prior to the next step.

To exclude dead cells from the analysis two strategies are available: the use of a nuclear dye non-permeable to cell membrane or the use of new generation viability dies resistant to fixation and permeabilisation. In the first case, a nuclear dye such as propidium iodide or DAPI is added to the staining cocktail: dead cells lose membrane integrity and are permeable to the dye that irreversibly stains the nuclei. Dead cells will be positive for the dye and will be excluded from the analysis. In the second case, live and dead cells are stained

with new generation dyes that bind amine groups on proteins: live cells with uncompromised plasma membrane will bind the dyes only on their surface, while dead cells will incorporate and bind the dyes also in the intracellular compartment. Eventually, dead cells will incorporate significantly more dye than live cells and will be easily distinguishable. These dyes resist fixation and are suitable for permeabilisation protocols as they are applied to the cells before any kind of staining. In this thesis I have used both methods: in the case of DAPI, a 1:10'000 dilution of the 5 mg/ml stock solution (LifeTechnologies) was used after the surface staining described in the next section; in the case of fixable dyes, a commercial kit from Biolegend was used (Zombie Aqua or Zombie NIR) prior to surface staining according to the manufacturer instructions.

3.8.2 Surface antibody staining, acquisition and sorting

After Fc-receptors block and fixable dye for live/dead discrimination were applied to the cell suspension, cells were spun at 400xg for 5 minutes and suspended in 50 µl of the staining solution containing the relevant conjugated-antibodies in PBS 2% FBS. To determine the antibody concentration to use, titration of each antibody was performed in advance. Cells were incubated in staining cocktail for 30 minutes in the dark. After this step 500 µl of PBS 2% FBS were added to the tubes and cells were spun again at 400xg for 5 minutes. The supernatant was decanted and cells were resuspended in the appropriate volume (300-500 µl) of PBS 2% FBS for flow cytometric analysis.

Samples were acquired on LSR Fortessa flow cytometer or on FACS Aria II (BD) cell sorter with FACSDiva software (BD). Data were analysed using FlowJo 8.7 or FlowJo X (Tree star) for MacOs X systems.

Sorted cells for mRNA extraction and expression analysis were collected in 15 ml Falcon tubes containing PBS, centrifuged for 20' at 400xg. The supernatant was then discarded and the cell pellet dissolved in 350 µl of Qiagen RLT buffer. Lysates were either readily processed for RNA extraction or stored at -80˚C.

3.8.3 Antibodies, antibodies panels and gating strategies

A list of antibodies used in this thesis is reported in **Table 3.5**. Flow cytometry was used on spleen and SG samples. Although different panels have been used to discriminate different populations of cells, a general gating strategy was adopted. A gate based on leukocytes physical parameters was first drawn on a FSC versus SSC dot plot. To exclude doublets and clumps of cells, events gated in the leukocytes gate were then visualised as SSC height versus SSC width and FSC height versus FSC width: the height of the peak generated by an event recorded at the interrogation point of a flow cytometer (i.e. where the cell is hit by the laser light) reflects the intensity of the light that hits the photomultipliers, and this parameter depends on the voltage applied to the photomultiplier; the width reflects the time that the cell takes to pass in front of the interrogation point, thus is directly proportional to the size of the cell and independent from the voltages applied to the photomultipliers. Gating events using the height of the peak versus the width of it excluding those events with a high width allows an efficient exclusion of cellular doublets and clumps.

Dead cells were then excluded gating out events positive for DAPI or live/dead fixable dyes. Live, single cells with the characteristic of leukocytes were then selected for their positivity for the pan-haematopoietic marker CD45. From this general population, the cells unnecessary for the analysis were excluded by

marking them with antibodies carrying the same fluorophore, thus collecting them in the same "dump" channel.

To determine the right position of the various gates, "fluorescence minus one" (FMO) controls were performed for every antibody in order to thoroughly define the negative and positive populations.
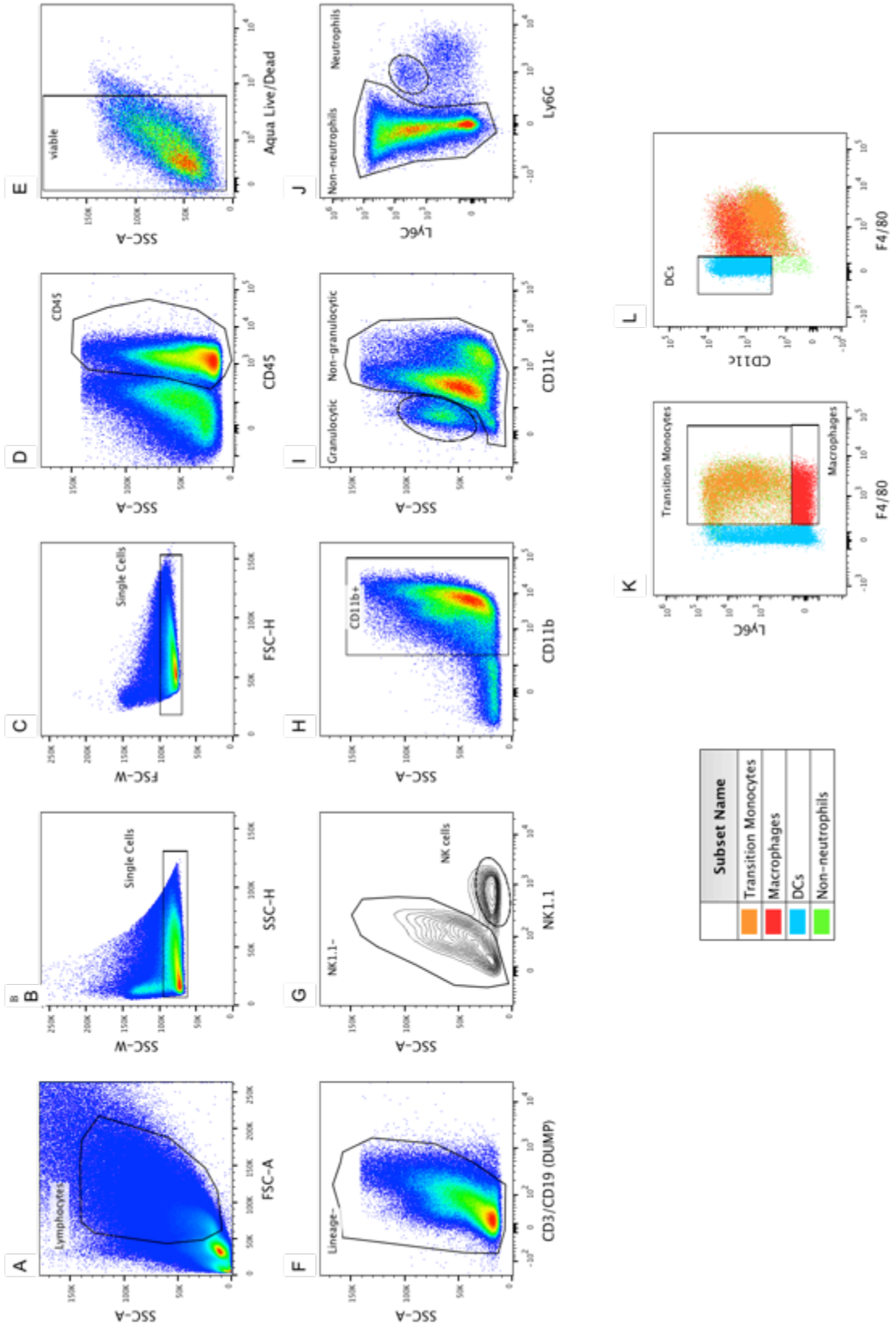
Figure 3.11: General gating strategy for flow cytometry experiments. Stained single cell sample suspensions in the appropriate buffer were acquired by flow cytometer. **A)** The first gate was drawn considering the physical characteristic of size (FSC) and complexity (SSC) of mononuclear cell suspensions. These first gated cells were then selected comparing the height and the width of their FSC and SSC signal, so to exclude cell doublets/agglomerates with a high peak-width (**B** and **C**). Single cells were then selected for the presence of the common hematopoietic marker CD45 (**D**) and from these, those positive for viability dyes were excluded (**E**, here using Zombie Aqua/NIR dye, but with similar results using DAPI). **F)** B and T lymphocytes were removed from the analysis gating out those cells positive for CD3 and CD19 and NK cells were enumerated via their expression of NK1.1 marker (**G,** NKT cells would not be present at this stage because they express CD3 and would be excluded with B and T cells in **F**). Myeloid cells were selected thanks to the expression of CD11b on their surface (**H**) and the SSC-high CD11c-negative granulocytes were gated out at this stage (**I**, this population is also positive for the eosinophil granulocytes Siglec-F as shown in section 5.1.3). Neutrophil granulocytes were gated as Ly6C+Ly6G+ cells (**J**), while the Ly6G- population was gated either according to the expression of F4/80 and Ly6C (**K**) or F4/80 and CD11c (**L**). In **K** monocytes were gated as F4/80-positive and Ly6C-positive to Ly6C-high, while F4/80+/Ly6C- were considered macrophages; in **L**, *bona fide* DCs were gated as F4/80-/CD11c++.

Antigen	Fluorophore	Producer	Catalogue number	Clone	Dilution
CD11b	BV605	BIOLEGEND	101237	M1/70	1:200
CD11c	ALX488	BIOLEGEND	117311	N418	1:200
CD19	APC/H7	BD	560143	1D3	1:200
CD19	PB	BIOLEGEND	115523	6D5	1:200
CD3e	PB	BIOLEGEND	100334	145-2C11	1:50
CD3e	APC/H7	BIOLEGEND	100330	145-2C11	1:100
CD45	PerCP/Cy5 5	BIOLEGEND	103132	30-F11	1:800
F4/80	PC7	BIOLEGEND	123114	BM8	1:200
Ly6C	PE	BIOLEGEND	128007	HK1.4	1:400
Ly6C	ALX647	BIOLEGEND	128010	HK1.4	1:400
Ly6G	APC/H7	BIOLEGEND	127623	1A8	1:400
NK1.1	BV421	BIOLEGEND	108732	PK136	1:200
NK1.1	PE	BIOLEGEND	108708	PK136	1:400
Siglec-F	BV421	BD	562681	E50-2440	1:200
Siglec-H	APC	BIOLEGEND	129611	551	1:400

Table 3.5: List of the antibodies used for flow cytometry experiments.

3.9 Statistical analysis

Differences in quantitative variables were analysed by the Mann–Whitney U test when comparing two groups and by the non-parametric Kruskal-Wallis test followed by Dunn's post-hoc test to compare the differences between each variable among multiple groups. Spearman's rank test was used to assess the presence of correlation between quantitative variables. χ^2 with Yates' correction when required or Fisher's exact test when appropriate was used to evaluate associations of qualitative variables in the different groups. All the statistical analyses were performed using GraphPad Prism version 5.01 for MacOS X (GraphPad, San Diego, CA). A p value <0.05 was considered statistically significant.

Chapter 4 | Results

4 Development and validation of an inducible model of sialoadenitis and breach of self tolerance

4.1 Optimisation of the intra-gland delivery method and replication of preliminary observations

Preliminary observations from our laboratory showed that the administration of high doses of reporter gene-encoding AdV in the SG of wild-type C57Bl/6 animals induced a strong inflammatory response that, over a time of three weeks, lead to periductal infiltrates. These preliminary findings allowed us to speculate that a strong antigenic challenge provided by AdV administration could induce ELN in the SG of the animals.

Thus, during my PhD work I first aimed to replicate these results. In this section I will report the dose-response dynamic of the AdV-mediated genetic transfer and the time-course of expression of the transgene encoded by the AdV.

4.1.1 Optimisation of the intra-gland delivery method and analysis of the dynamic of AdV gene-transfer

Delivery of replication-deficient AdV in murine submandibular SG via retrocannulation of the excretory duct has previously been described as a suitable and efficient tool for transient local gene transfer [227]. With the help of Professor Gordon Proctor (King's College, London, UK) I adapted a retrograde cannulation technique that was previously developed in rats [222] using customized glass cannulae that proved to be a reliable method for specific delivery of small volumes (up to 50 µl) in the sub- mandibular glands. The apparatus used to keep the animals in the correct position, the insertion of the

cannula in the gland orifice and the effect of cannulation of a blue dye in only one of the two submandibular SG are depicted in Figure 4.1 A-C. This preliminary set of experiment proved that the delivery in the SG was restricted to the submandibular SG, leaving the sublingual gland and the contralateral SG unaffected by the procedure. To study the dose-response relationship between the amounts of the viral infective particles delivered and the activity of the reporter gene, I used an E1-E3-deleted replication-defective human adenovirus 5 encoding for firefly luciferase under the control of a CMV promoter (LucAdV). As reported in Figure 4.1 D, increasing luciferase activity was observed using increasing doses of LucAdV within the first week post-cannulation, which then decreased over the next 2 weeks.
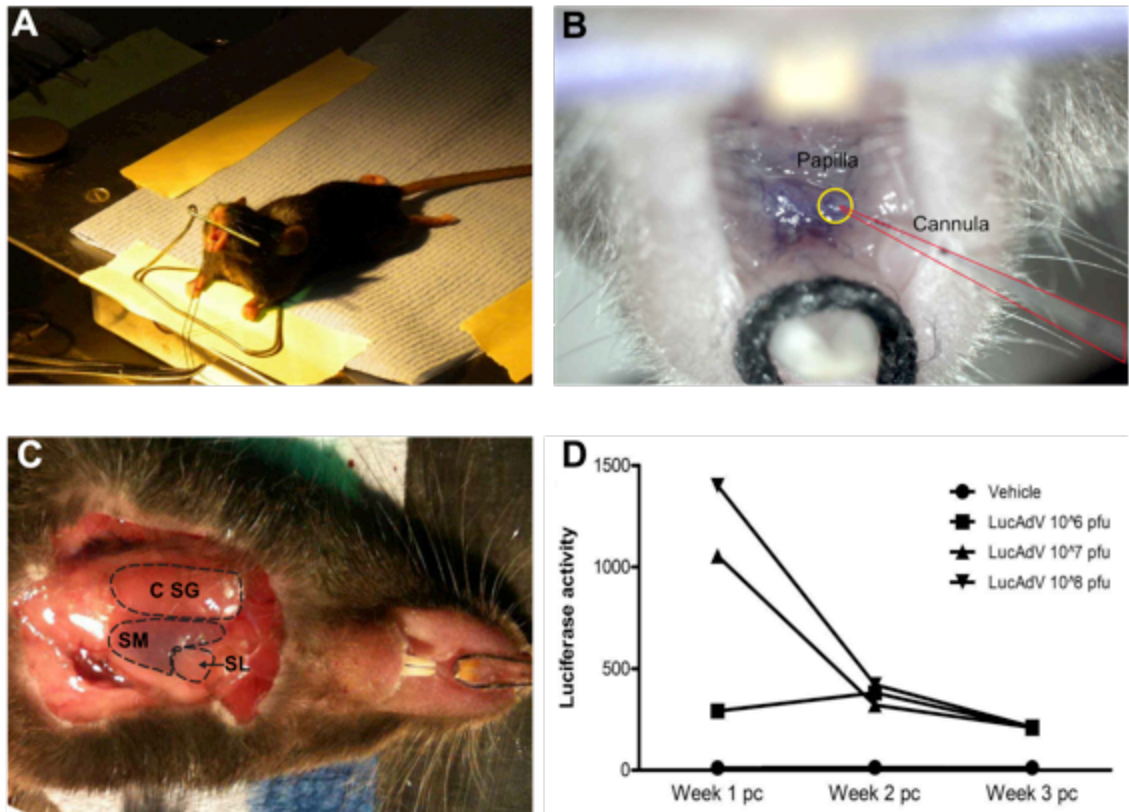
Figure 4.1: Retrocannulation of the submandibulary salivary gland. A) A metal paperclip is shaped to accommodate the animal's upper incisors, while a suture thread passed around the lower incisors is connected to a weight to keep the mouth open. In **(B)** the glass cannula (highlighted in red) is inserted directly in the salivary gland orifice beneath the papilla, highlighted here with a pale blue dye and circled in yellow. **(C)** Delivery of 50 µl of a dye through the left excretory orifice only stains the left submandibular gland (SM) but not the sublingual gland (SL) nor the contralateral gland (C SG). Luciferase activity in the salivary glands of infected animals during the first week post-procedure is dependent on the dose of LucAdV delivered **(D)**, but by week two this dose-dependency is lost. Every symbol represents the mean of the luciferase activity of 3 salivary glands.

4.1.2 AdV delivery to the SG progressively induce SS-like periductal inflammatory foci in wild-type C57BL/6 mice

Histological analysis of the cannulated glands demonstrated that AdV doses of 10^8 PFU/gland, but not vehicle control (or doses $<10^7$ PFU), induced from week 2 post-cannulation the formation of lymphomonocytic infiltrates organized as periductal aggregates, which by week 3 post-cannulation strongly resembled lymphocytic *foci* found in SS patients (Figure 4.2 D–F and Figure 4.10 B-D). The formation of lymphoid aggregates was invariably preceded by a rapidly induced diffuse inflammatory infiltrate, which resolved within the first week post-cannulation to be replaced by typical periductal focal infiltration by week 2 post-cannulation (Figure 4.2 D–F). Importantly, this phenomenon was independent from the reporter gene used, because it was also triggered by same amounts of LacZAdV (Figure 4.10 B–D) with no significant difference in terms of prevalence and size of the periductal foci comparing the two viruses. Delivery of virus-vehicle alone did not induce any significant inflammation and/or lymphomonocytic infiltration (Figure 4.2 A-C). The mean and standard error of the mean (SEM) of the number of periductal foci developing in the salivary glands after delivery of either LucAdV or LacZAdV at the different time points is reported in Figure 4.2 G.
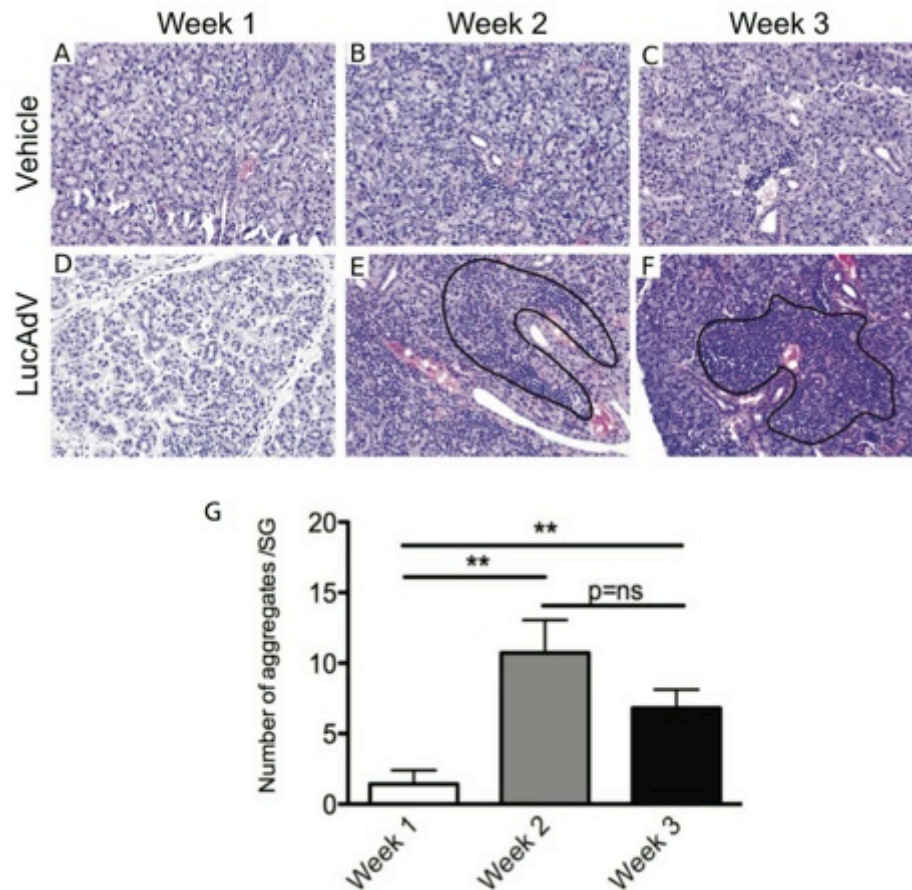
Figure 4.2: AdV delivery to the SG progressively induce SS-like periductal inflammatory foci in wild-type C57BL/6 mice. (A-F) Representative haematoxylin and eosin microphotographs showing inflammatory responses induced by local administration of either vehicle **(A-C)** or LucAdV **(D-F)**. After AdV delivery, diffuse lymphomonocytic infiltration in the first week **(D)** is followed by progressive organization of periductal inflammatory aggregates during week 2 **(E)** and week 3 pc **(F)**, periductal *foci* circled in black. Vehicle delivery induces negligible inflammation **(A-C)**. The mean ± SEM of the number of periductal foci/gland following either LucAdV or LacZAdV delivery at different time points is reported in **(G)**. (**p<0.01 between AdV and vehicle-treated mice at each time point, minimum of 10 mice per time point).

4.2 A novel inducible model of ectopic lymphoid neogenesis

Next, I aimed to investigate whether the periductal inflammatory *foci* triggered by the adenoviral infection displayed features of TLS. To be defined as a model of ELN, several key characteristics need to be present; i) organisation of B and T cell in segregated areas, ii) presence of specialised vasculature such as HEV, iii) expression of lymphoid chemokines, iv) development of FDC networks and v) markers of functional germinal centres.

In this section, I will discuss my findings regarding the above-mentioned criteria.

4.2.1 Progressive development of T/B cell segregation and FDC networks following AdV infection in the submandibular glands

I started evaluating the progressive acquisition of SLO features by the inflammatory *foci*, i.e. T/B cell segregation, presence of specialised HEV and differentiation of FDC networks. Double immunofluorescence sequential section analysis of submandibular gland infiltrates was performed using CD3/B220 and B220/FDC-M1 in order to assess the presence of T/B cell compartmentalization and FDC network formation. Initial infiltrates (within week 1) were mostly diffuse and characterized by a predominance of T cell followed by a progressive influx of B cells and the development of highly organized lymphoid structures with T and B lymphocytes localising in discrete areas (week 2-3) (Figure 4.3 A-C). Thus, upon AdV delivery T and B cells serially enter the glands first with a non-segregated pattern and then gradually develop an organized segregated disposition in up to 70% of the aggregates (Figure 4.3 G). Furthermore, I observed differentiation of FDC networks within the B cell rich areas in the context of segregated infiltrates in over 60% of the mice at week 3 post-cannulation (Figure 4.3 D-F and H). Finally, as shown in Figure 4.3 E-F and I-J,

sequential section analysis demonstrated that T/B-segregated aggregates are characterised by the differentiation of HEV in the T cell-rich area (Figure 4.3 I-J) and FDCs within the B cell follicle (Figure 4.3 E-F).
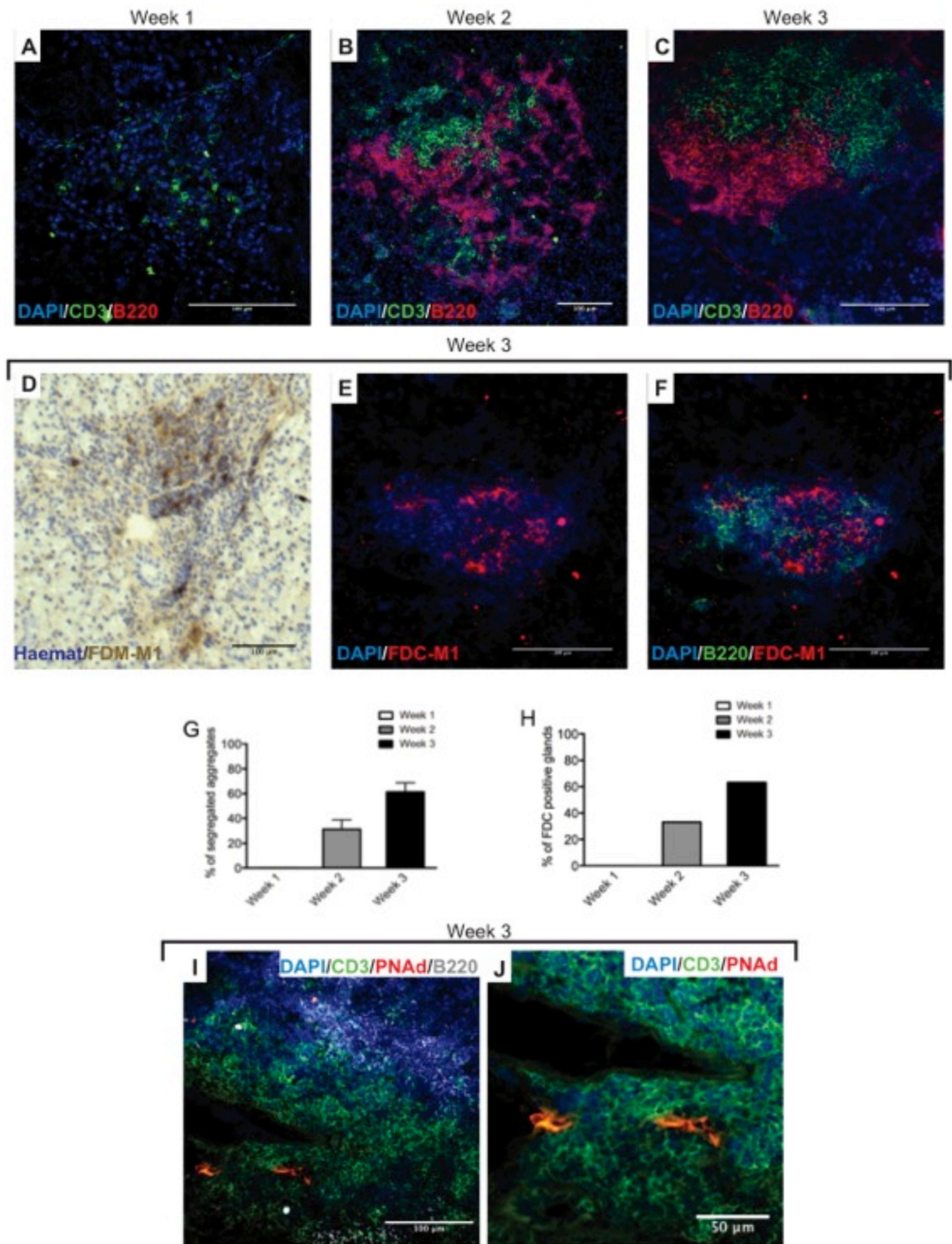
Figure 4.3: Progressive development of T/B cell segregation and FDC networks following AdV infection in the submandibular glands of C57BL/6 mice. **A-C**) Microphotographs showing double immunofluorescent staining for CD3 (T cells, in green) and B220 (B cells, in red) of frozen sections from AdV-treated C57BL/6 SG. Nuclei are counterstained with DAPI (blue). Early diffuse

infiltration is dominated by T cells (**A**) with subsequent recruitment of B cells showing initial T/B cell compartmentalization within the first 2 weeks post-cannulation (**B**). By week 3 post-cannulation over 60% of periductal foci display full segregation of T and B cells in separate areas (**C**, **G**). **(D-F)** Microphotographs of AdV-treated C57BL/6 submandibular glands at week 3 pc showing differentiation of FDC networks as demonstrated by staining for FDC-M1 (**D**, in brown and **E** in red). FDC networks invariably develop in the context of the B cell rich area of the aggregates (**F**) in over 60% of AdV-treated C57BL/6 mice shown in (**H**), where the bars represent the percentage of the glands that have at least one FDC structure against the total number of infiltrated glands). (**I**) Quadruple immunofluorescence staining for T cells (CD3, in green) and HEV (PNAd, in red), B cells (B220, in white) with nuclei counterstained in DAPI (in blue) and (**J**) enlargement from image **I** showing triple staining for T cells (CD3, in green), HEV (PNAd, in red) with blue nuclear counterstain (DAPI) showing that PNAd+ HEV selectively localise in the T cell rich area of segregated aggregates. Bars in pictures represent 100 microns except for **(J)** where the bar is 50 microns long.

4.2.2 ELN in submandibular glands is preceded by ectopic expression of the lymphoid chemokines/Ltβ pathway

Production of lymphoid chemokines CXCL13, CCL21, and CCL19 is of pivotal importance in the development of TLS in chronic autoimmune diseases, including SS [3],[228]. Induction and secretion of lymphoid chemokines has been shown to rely on the expression of the heterotrimeric Ltβ [20],[223],[229]. To verify the involvement of these regulators of TLS in the model, I assessed the ectopic mRNA expression of CXCL13 and CCL19 and their cognate receptors CXCR5 and CCR7, as well as the Ltβ/LtβR axis in the cannulated SG. A list of the TaqMan probes used for expression analysis is presented in **Table 3.3**. As shown in **Figure 4.4** A–F, CXCL13/CXCR5 and CCL19/CCR7 mRNA transcripts were abundantly upregulated in AdV-treated mice, as compared with vehicle-treated mice, and their ectopic expression was consistent with the progressive detection of TLS in the SG, reaching their peak of expression between week 2 and 3 post-cannulation. Of relevance, Ltβ, CXCL13/CXCR5, and CCL19/CCR7 mRNA displayed significant upregulation within the first week post-cannulation, suggesting very early involvement of these factors in the formation of TLS in this inducible model of lymphoid neogenesis. To confirm the presence and expression pattern of lymphoid chemokines at a protein level, multicolour confocal microscopy was used to detect CXCL13 or CCL21 together with B220/CD3. As shown in **Figure 4.4** G-N, in the context of segregated aggregates, CXCL13 and CCL21 retained their expression pattern within the B and T cell-rich areas, respectively, suggesting a prominent role in directing T/B cell segregation.
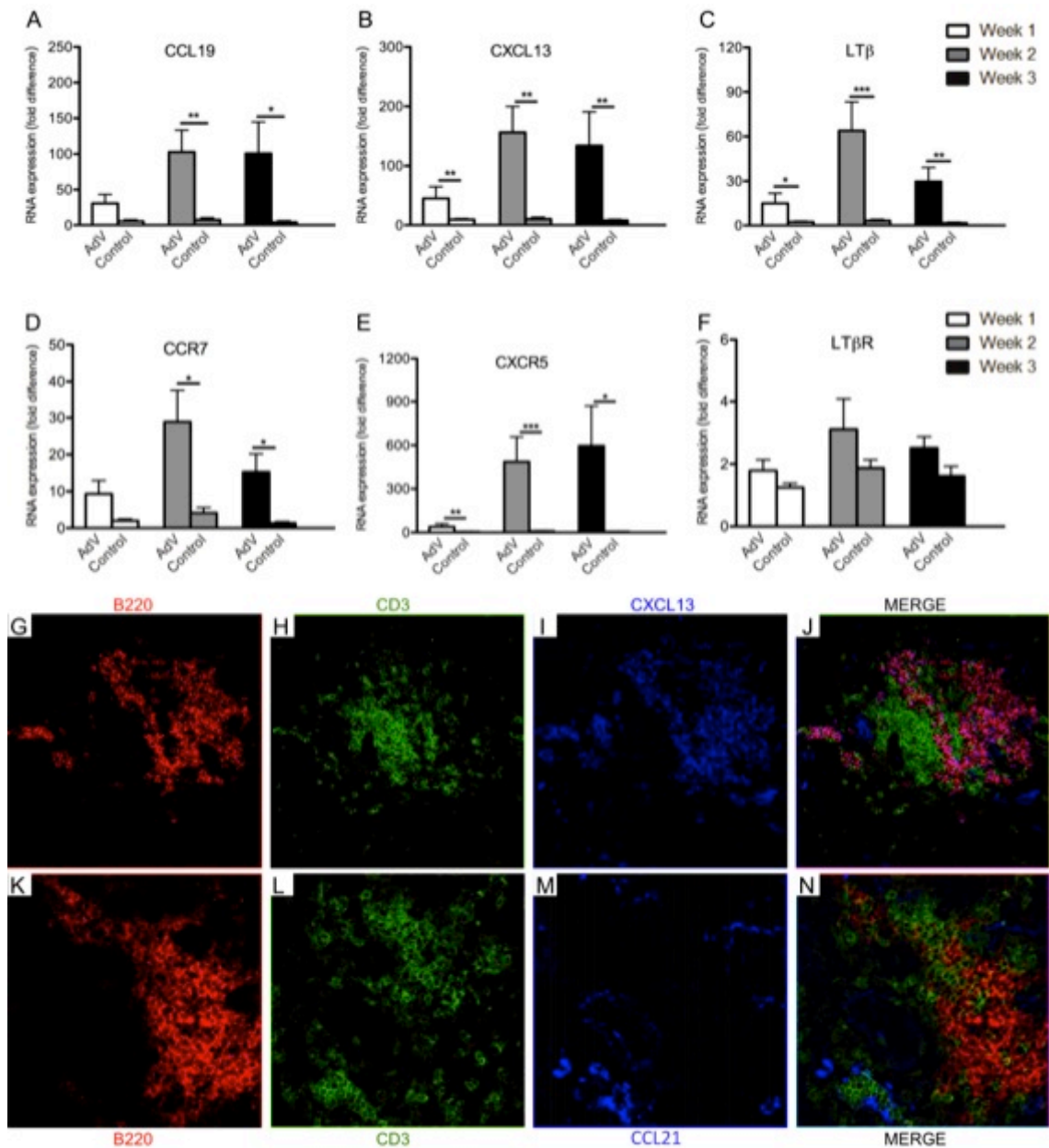
Figure 4.4: Development of TLS in C57BL/6 submandibular glands is preceded by ectopic expression of the lymphoid chemokines/Ltβ pathway. (**A–F**) Quantitative TaqMan real-time PCR time-course analysis of CCL19 (and its receptor CCR7) (**A**, **D**), CXCL13 (and its receptor CXCR5) (**B**, **E**), and Ltβ (and its receptor) (**C**, **F**) mRNA transcripts showing abundant upregulation after AdV delivery in the submandibular glands. Earliest upregulation was observed for CXCL13 and Ltβ mRNA, whereas peak of expression of these factors was detectable in parallel with full histological development of TLS (**A–E**).

Conversely, LtβR expression appears unaffected by AdV treatment (**F**). Data are expressed as mean ± SEM of the fold increase compared with an internal calibrator. *$p < 0.05$, **$p < 0.01$, ***$p < 0.001$ between AdV- and vehicle-treated mice at each time point, minimum of 10 mice/time point. (**G–N**) Microphotographs of multicolour confocal microscopy analysis confirming protein expression of lymphoid chemokines CXCL13 (**I**, in blue) and CCL21 (**M**), and showing colocalisation of CXCL13 within the B cell-rich area (**G–J**) and of CCL21 within the T cell-rich area of the aggregate. (**K–N**). B cells are shown in red (B220) and T cells in green (CD3). Original magnification x200 (**G–N**).

4.2.3 AdV-induced TLS in submandibular glands acquire characteristics of functional ectopic germinal centers

I next assessed the presence of features typically associated with germinal centre function such as differentiation of germinal centre B cells and expression of AID. As shown in Figure 4.5, sequential section analysis (Figure 4.5 A–D) demonstrated that T/B-segregated aggregates characterized by the differentiation of HEV in the T cell-rich area and FDCs within the B cell follicle support the activation of numerous GL7$^+$ germinal centre B cells. The appearance of GL7$^+$ germinal centres was strongly associated with functional B cell activation as demonstrated by the detection of high levels of mRNA transcripts for AID (Figure 4.5 E), the enzyme required for Ig somatic hypermutation (SHM) and class-switch recombination (CSR). Of relevance, ectopic induction of AID was also associated with the expression of several cytokines that are known to cooperate in directly promoting AID expression in B cells, such as IL-4, BAFF, and IL-21 (Figure 4.5 F–H). Overall, these data demonstrate that post-AdV infection TLS support the development of functional niches of B cells that acquire the machinery necessary to undergo SHM and CSR at these ectopic sites.
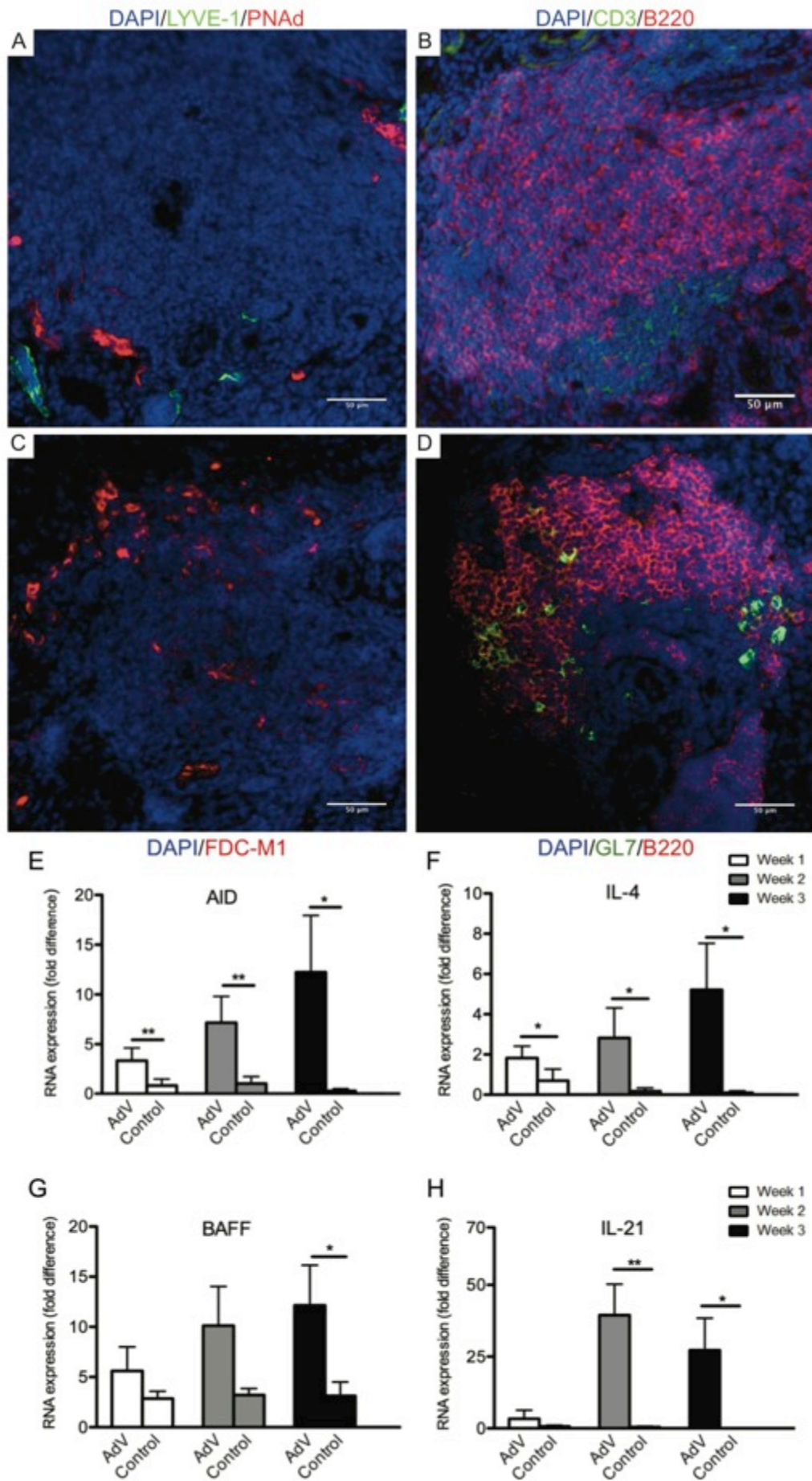
Figure 4.5: AdV-induced TLS in C57BL/6 submandibular glands acquire characteristics of functional ectopic germinal centers. **(A–D)** Sequential immunofluorescence staining of AdV-treated submandibular gland sections of C57BL/6 mice at 3 wk pc showing that highly organized TLS characterized by HEV (**A**, red), T/B cell segregation (**B**, B220 in red and CD3 in green), and FDC networks (**C**) support the differentiation of GL7$^+$ germinal center B cells (**D**, B220 in red and GL7 in green). **(E–H)** Quantitative TaqMan real-time PCR time-course analysis of salivary gland expression of AID mRNA **(E)** and transcripts for cytokine downstream AID activation, such as IL-4, BAFF, and IL-21 (**F–H**). AID expression peaks in parallel with the development of fully formed TLS and is associated with significant upregulation of IL-4, BAFF, and IL-21. Bars in pictures (**A–D**) are 50 μ m long. Data are expressed as mean ± SEM of the fold increase compared with an internal calibrator. *p < 0.05, **p < 0.01 between AdV- and vehicle-treated mice at each time point, minimum of 10 mice/time point.

4.3 Development of exocrine dysfunction and autoimmunity: a model of SS-like disease

The results reported in the previous sections confirmed that upon AdV delivery in the SG of wild-type C57Bl/6 animals, ELN takes place in the mucosa. By three weeks post-treatment, the lymphoid infiltrates formed in the SG fulfilled the main characteristic of SLO: B/T cell infiltration and segregation, expression of lymphoid chemokines, presence of germinal centre markers. These structures are also highly reminiscent of the inflammatory *foci* found in SS SG. The set of experiments reported in the following section aimed to confirm whether the model in our hands was also a model of SS. To confirm this, I searched for two hallmarks of human SS: loss or reduction of salivary flow and presence of humoral self-reactivity.

4.3.1 Sustained reduction in salivary flow post-AdV infection

SS patients are characterized by an excretory dysfunction of the salivary (and lacrimal) glands that leads to mouth (and eye) dryness, also denoted as *sicca* syndrome. To assess whether AdV delivery induced exocrine dysfunction in the affected gland, I cannulated each mouse with 10^8 PFU AdV in one the submandibular glands and with vehicle control in the contralateral gland. At appropriate time points after cannulation, pilocarpine-stimulated salivary flow was measured from each individual gland separately. A significant and acute reduction in salivary flow (Figure 4.6) was observed within week 1 post-cannulation. Surprisingly, albeit less drastic, at weeks 2 and 3 post-cannulation, a significant reduction in saliva production was still evident in AdV-treated mice characterized by the presence of lymphocytic aggregates in SG with an otherwise reconstituted acinar and ductal architecture. This suggests that within

the observed period, immune cell infiltration induces a functional impairment that does not allow the full recovery of the excretory function of the glands.
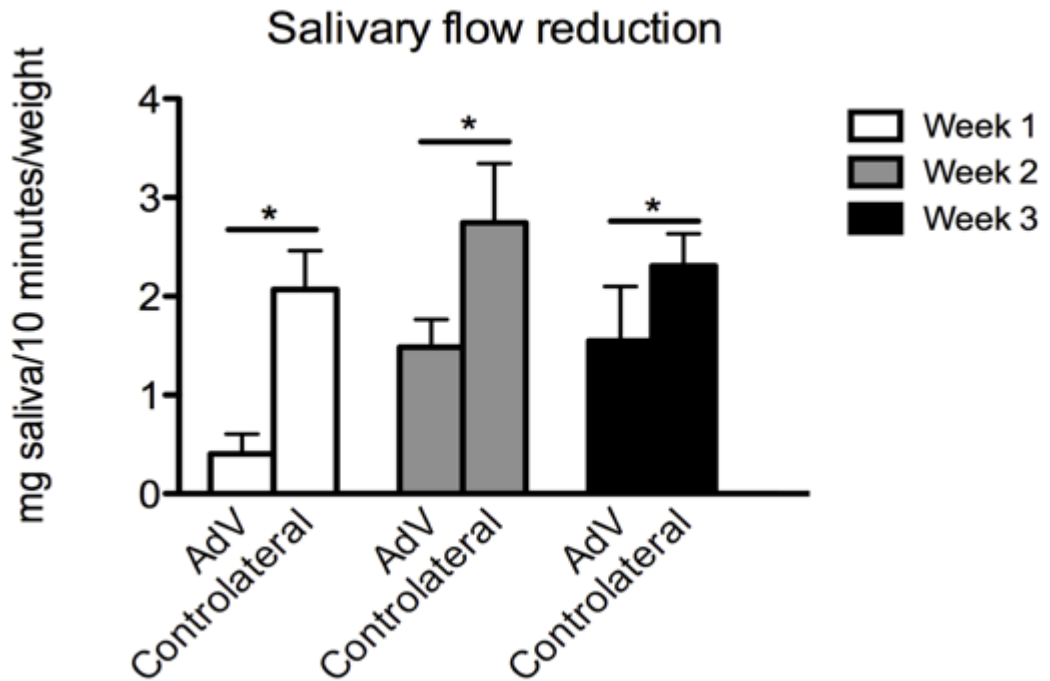
Figure 4.6: Sustained reduction in salivary flow post-AdV infection of C57BL/6 mice submandibular glands. Column graphs comparing salivary flow in the AdV-treated submandibular and the contralateral gland at weeks 1, 2, and 3 pc. Salivary flow is measured as milligram of saliva produced in 10 min/body weight after pilocarpine stimulation. Exocrine dysfunction in the AdV-cannulated glands can be observed up to 3 weeks post-cannulation. Data are expressed as mean ± SEM. *p < 0.05 between AdV- and vehicle-treated mice at each time point, minimum of five mice/time point.

4.3.2 Development of ANA after AdV delivery in the submandibular glands

In patients with SS, the formation of immune cells infiltrates in the SG is associated with the presence of circulating autoantibodies against nuclear antigens and ribonucleoproteins [146],[225],[226]. Thus, I next investigated whether this model of AdV- induced sialoadenitis was associated with breach of self-immunological tolerance and development of anti-nuclear antibodies. The presence and titre of ANAs was determined using Hep2 cells as substrate. An initial serum dilution of 1:80 was chosen because this is considered significant in clinical tests for autoimmunity in patients. As shown in Figure 4.7 B–E, no sera from AdV-cannulated mice within week 1 post-cannulation displayed ANA positivity. Conversely, ANA reactivity was detected in 30.7% of mice by week 2 post-cannulation, and this percentage increased to 75% in animals culled at week 3 post-cannulation. Finally, age/sex-matched vehicle control C57BL/6 mice did not show any reactivity. Taken together, these observations demonstrate that AdV-induced sialoadenitis in non-autoimmune prone mice is associated with the induction of humoral autoimmunity toward nuclear antigens.
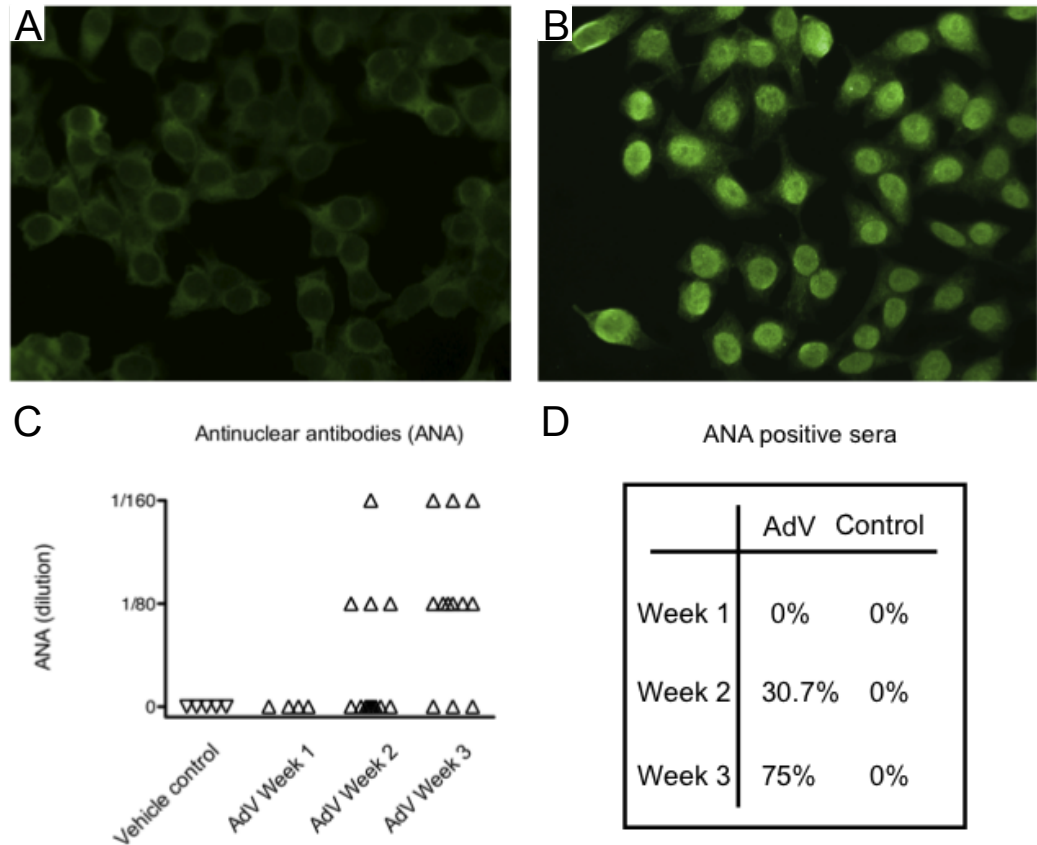
Figure 4.7: Development of ANA after AdV delivery in the submandibular glands of C57BL/6 mice. Representative microphotographs of immunofluorescent detection of ANA using Hep2 cells as substrate (**A, B**) demonstrating strong nuclear reactivity in sera of AdV-treated (**B**), but not in vehicle-cannulated (**A**), C57BL/6 mice 3 weeks post-cannulation (dilution 1:80). ANA reactivity was progressively evident over time in AdV-cannulated C57BL/6 mice (**C**), with 75% of mice displaying ANA positivity by week 3 pc (**D**). In **C** each triangle represents a single animal. Original magnification x400 (**A–B**).

4.3.3 Different patterns of apoptosis can be observed at various time points in AdV-treated submandibular glands

As reported in sections 1.2.2 and 1.2.4, amplified presence of apoptotic bodies and self-antigens in an environment prone to favour an adaptive immune response might be partially responsible for breach of self-tolerance leading to the initiation and perpetuation of the autoimmune process. Moreover, I reported in section 4.1.2 that in AdV-treated SG the acinar structures are almost completely lost in the early phases after virus delivery, but recovery of the parenchyma is observable at week 2 and it appears complete by week 3 post-cannulation. Thus, I assayed the level and extent of apoptosis in cannulated SG at different time points to verify whether programmed cell death was taking place in my model and could be responsible for the loss of acinar structures and the development of self-reactivity against intracellular antigens. To do so, slides from AdV-treated animals at 1, 2 and 3 weeks post-cannulation were thawed at room temperature and stained with a TUNEL assay kit to mark apoptotic cells. During the early phases of inflammation apoptosis was readily detectable and abundant in the treated glands and apoptotic cells could be detected in all the compartments of the SG, including ductal structures and glandular parenchyma (Figure 4.8 A and B). Interestingly, as soon as week 2 post treatment and during week 3, the amount of apoptotic cells declined and they preferentially localised into the periductal aggregates (Figure 4.8 C-F).
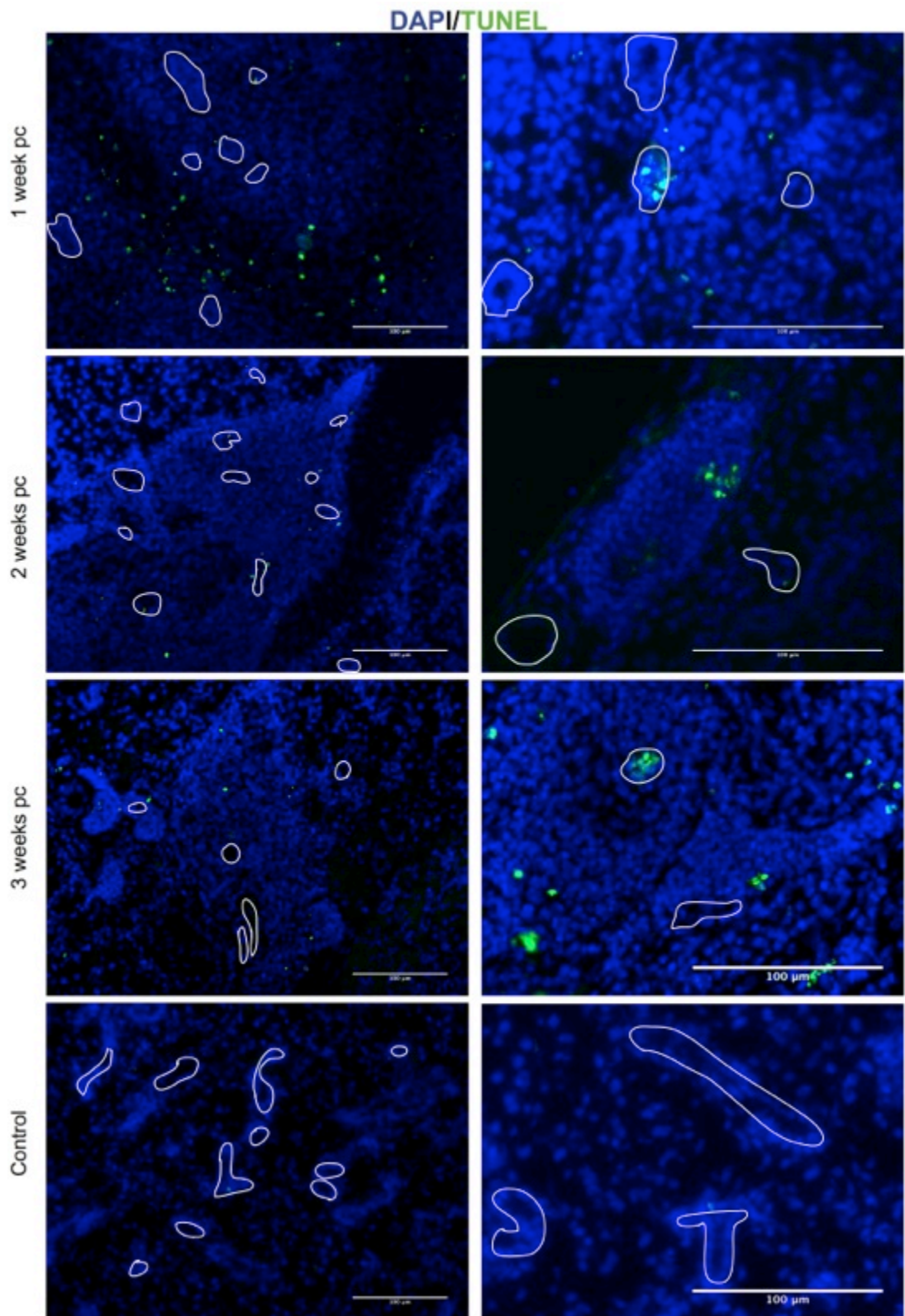
Figure 4.8: Early and late apoptosis following AdV-delivery in the submandibular glands of C57BL/6. TUNEL assay identifying apoptotic cells (in green with DAPI nuclear counterstaining in blue) in the salivary glands of

AdV-treated mice at 1 (**A**, **B**), 2 (**C**, **D**) and 3 (**E**, **F**) weeks post-cannulation. Within the first week apoptotic cells are abundant and diffuse within the parenchyma of the AdV-treated glands (**A**), often within the ductal epithelium, highlighted in white (**B**). By week 2 and 3 post-cannulation the degree of apoptosis is reduced with TUNEL-positive cells almost exclusively localized within periductal *foci* (**C-F**). White bars in pictures are 100 μ m in length.

4.4 Viral persistence and immune system evasion

ELN takes place in response to a chronic antigenic stimulation, whether endogenous or endogenous [3]. As I reported in the introduction of this thesis, there are examples of viral infections where the infection itself is the first driver of TLS formation (i.e. *influenza virus*). I also reported data in support of the hypothesis that a chronic infection, such as HCV, can drive first ELN and then breach of tolerance towards self-antigens thanks to the capacity of the virus to evade the immune system and establish a chronic infection. In this section, I report the results of my investigation regarding the persistence of the adenovirus in the SG of treated animals. I will first describe the anti-viral systemic humoral response and then I will report observations regarding the survival of infected cells as a result of an inefficient immune clearance.

4.4.1 AdV delivery induces the development of IgG humoral response

I first started to assay the presence of anti-virus antibodies in the sera of AdV-treated animals in a qualitative manner using a western blot approach. Probing the sera of treated and control animals against a western blot membrane blotted with AdV-infected cells lysates, I observed that sera from AdV-cannulated mice, but not control C57BL/6, progressively displayed a strongly antiviral activity from day 5 post-cannulation onward (Figure 4.9 A). To have a relative quantitation of this antiviral response, I characterised via ELISA assay the specific IgG response to the virus in sera of treated and control animals. As expected, sera from control animals and collected from AdV-treated mice during the first week after cannulation did not show any specific anti-AdV activity (Figure 4.9 B). By week two, an IgG response against AdV components is observable and the concentration of the immunoglobulins continues to increase

in time. These data show how the cannulation procedure induces a strong humoral activation that leads to the development of a specific antiviral IgG response by week two after treatment. This response increases in time and highlights an adaptive immune activation against the virus.

A

Control Bl6 | Anti-AdV antiserum | AdV 5 dpc | AdV 9 dpc | AdV 12 dpc | AdV 15 dpc | AdV 20 dpc | AdV 23 dpc

293 infection: + − + − + − + − + − + − + − + −

B

Total anti-AdV IgGs
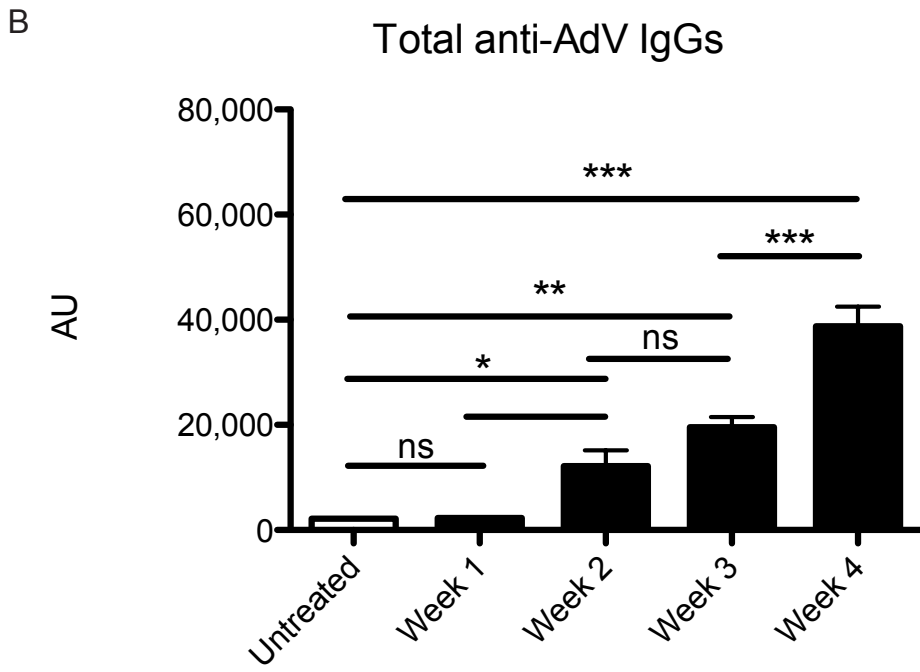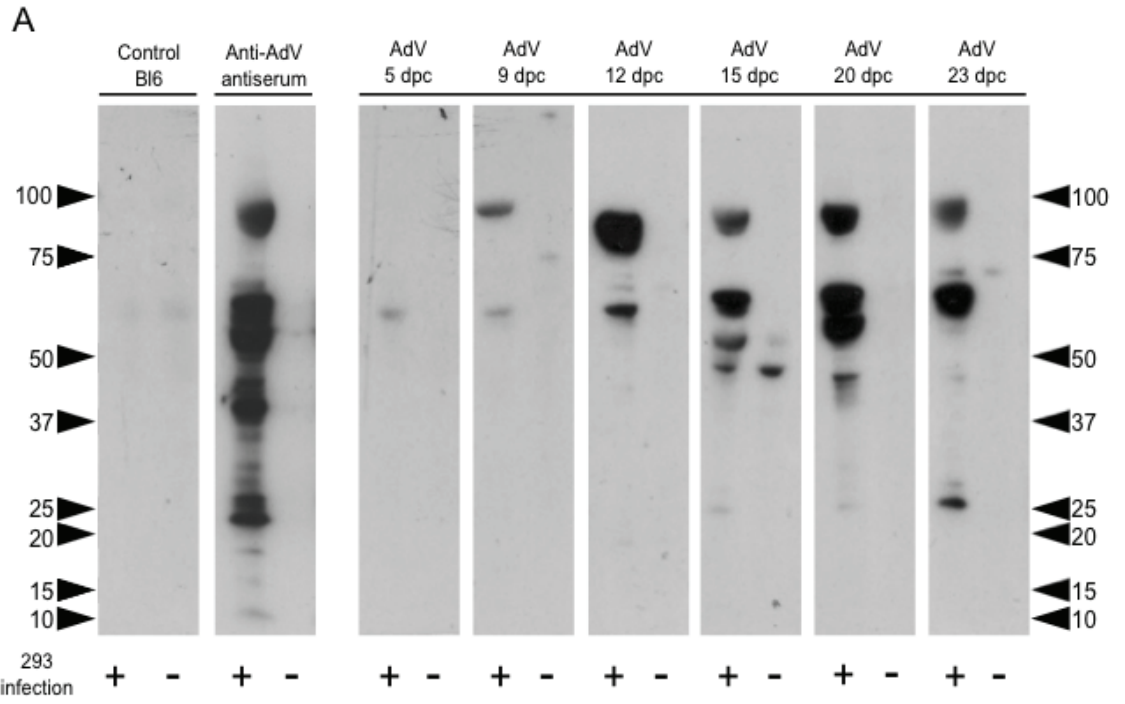
Figure 4.9: AdV delivery induces the development of IgG humoral response. **A)** Western blot showing progressive development of anti-AdV IgG in the serum of AdV-treated, but not vehicle-cannulated mice. Protein extracts from AdV-infected (+) and uninfected (−) Hek293 cells were run in parallel. (*Left to right*) Vehicle-treated C57BL/6 mouse serum at 20 days post-cannulation, commercial anti-AdV antiserum, sera from AdV-cannulated mice at different time points (5, 9, 12, 15, 20, 23 days post-cannulation). Anti-AdV responses are observed as early as day 5 post-treatment and are mainly directed against proteins of the viral core and capside. **B)** Anti-AdV class G immunoglobulins ELISA assay performed on sera from cannulated animals at 1, 2, 3 and 4 weeks after procedure and controls show an increasing titre of anti-AdV IgG starting from week 2 pc. Data are expressed as mean ± SEM. *$p < 0.05$, **$p<0.01$, ***$p<0.001$ between AdV- and vehicle-treated mice at each time point, minimum of five mice/time point.

4.4.2 Infected ductal epithelial cells are not efficiently cleared by the immune system

Given the observation reported above about the development of a strong IgG response against the AdV in treated animals, an efficient clearance of the virus-infected cells by the time the humoral response is developed and anti-AdV IgGs are detectable in blood was expected. To confirm this, I followed the fate on AdV-infected cells using luciferase-encoding AdV for cannulation and monitoring the persistence of luciferase activity in the glands as a read-out of viral persistence. As expected, I detected a significant drop of luciferase activity after the first week post-cannulation (Figure 4.10 A), however luciferase activity was detectable in the glands at all the time-points analysed (i.e. week 4 post-cannulation). This finding suggested that despite a strong and specific humoral response directed against the viral components, AdV-infected cells are not efficiently cleared from the glands.

This observation is extremely important in the context of ELN in general and SS in particular. In fact, as I reported in the introduction, several viruses have a tropism for the SG mucosa and some of them are known to establish a life-long chronic infection. Moreover, some of these sialotropic viruses tend to infect and replicate in the ductal cells of the gland, leaving the acinar cells uninfected [204]. With this in mind, I performed a staining on SG sections to identify the virus-infected cells. To do so, I adopted two different strategies: I either used a β-galactosidase-encoding AdV (LacAdV) to detect the enzymatic activity in the gland, or performed an immunofluorescent staining to detect AdV components in the tissue. As shown in Figure 4.10 B–D, staining for β-galactosidase demonstrated early widespread distribution of the virus within the gland (Figure

4.10 B). By week 2 post-cannulation, the LacZAdV was almost exclusively localised within ductal epithelial cells surrounded by initial inflammatory aggregates (Figure 4.10 C). Confirmation of this came by double immunostaining with an anti-AdV and an anti-cytokeratin antibody (Figure 4.10 E-J) that showed how, at 3 days post-cannulation, AdV particles selectively co-localise within ductal epithelial cells.

These data demonstrate that ductal epithelial cells, particularly in intercalated ducts, are a preferential site for viral persistence, an observation which is highly relevant as intercalated ducts are typically surrounded by periductal lymphomonocytic aggregates not only in this novel model of SS-like sialoadenitis, but also in other spontaneous animal models of SS as well as in patients with SS.
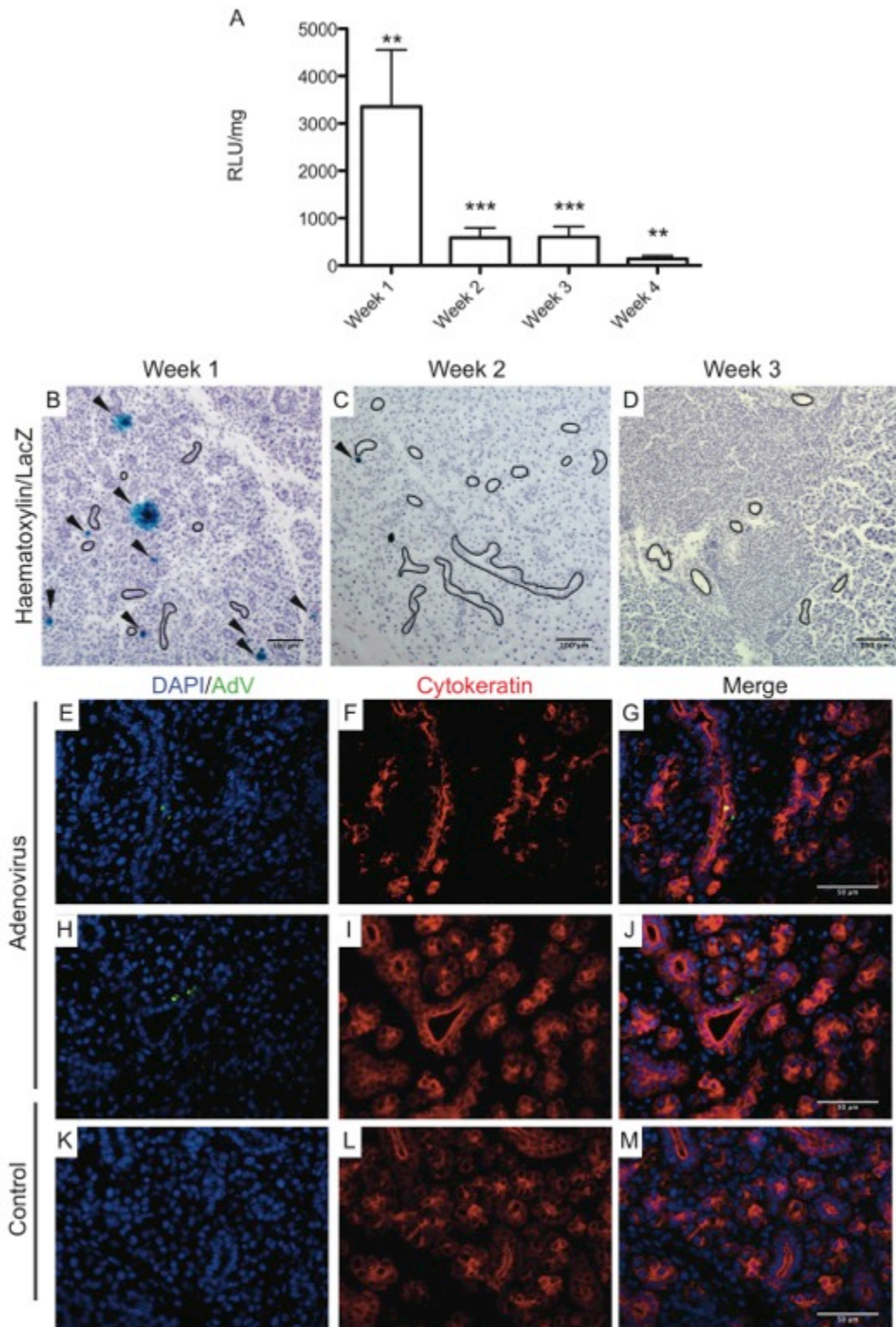
Figure 4.10: Infected cells persist in the gland and are mainly ductal epithelial cells. (A) Luciferase activity assay in LucAdV-infected glands shows persistent signal well above background levels up to 4 weeks pc (mean ± SEM

of luciferase activity, **p < 0.01, ***p < 0.001 between AdV- and vehicle-treated mice at each time point, minimum of 10 mice/time point.). (**B–D**) Representative microphotographs of submandibular glands infected with LacZAdV and stained for β-galactosidase (X-Gal, with nuclear counterstaining with haematoxylin, some ductal structures highlighted in black). Numerous X-Gal⁺ cells are present in the gland within the first week pc (**B**, arrowheads). By week 2 pc, only ductal epithelial cells, often surrounded by periductal inflammatory infiltrates, show enzymatic activity **(C)**. By week 3 pc, no residual X-Gal⁺ cells are detectable **(D).** The scale bars represent a length of 100 μ m **(B–D)**. (**E-M**) Double immunofluorescence staining for AdV (green) and a pan-cytokeratin marker (red) in AdV-treated **(E-J)** and vehicle-treated salivary glands **(K-M)**. Expression of AdV5 proteins from day 3 post-cannulation is exclusively detectable within ductal but not acinar epithelial cells. The scale bars represent a length of 50 µm.

Chapter 5 | Results

5 A tightly organised recruitment and activation of innate immune cells precedes the formation of ELS in response to AdV infection

5.1 Recruitment rate and tissue positioning of different innate immune cells subsets following AdV delivery

As reported in the introduction, several studies previously focused on the cellular events that trigger lymphoid organogenesis, while the mechanisms preceding ELN formation in non-lymphoid tissues are less known (section 1.1.3). Whilst previous investigations primarily employed genetically modified animals to induce TLS via the ectopic expression of lymphoid chemokines/Ltβ, the AdV-induced model of TLS that I described in the previous chapter offers the unique opportunity to tightly dissect the early phases of TLS formation following a more physiological stimulus such as pathogen infection. In this chapter, I will describe the results of experiments aimed at clarifying the dynamics of the immune infiltration developing within the first week post-viral cannulation in order to pinpoint the cell types involved in initiation and maintenance of the salivary immune response preceding TLS formation.

This part of my PhD project relied mostly on the study of single cell suspension obtained at different time points from murine submandibular glands from both AdV-cannulated animals and control mice. In all cases, careful experimental controls were implemented, including the use of FMO analysis for the assessment of flow-cytometric staining specificity as well standard control procedures such as the incubation with Fc-block cocktail and live/dead

discrimination dyes as described in the Methods Chapter (Section 3.8). Additionally, to account for any potential effect of the enzymatic digestion on the expression different immune cells markers, in each flow cytometry experiment at least one spleen from C57Bl/6 mice was digested and stained as a positive control. Importantly, in the flow cytometric data reported in the next sections the abundance of any cell population is always expressed as a percentage of a parent population (e.g. percentage of the total cells, percentage of $CD45^+$ cells, etc), and an absolute quantification of the number of the cells is missing. This depends from the fact that those reported below are still preliminary data. This is clearly an issue that needs to be addressed, in particular considering some of the events that take place in the gland upon AdV infection, such as extensive apoptosis and strong cell infiltration, that might substantially affect the total number of cells present in the gland. Thus further experiments, comprehensive of an absolute quantitation of the cell numbers, will be necessary to support the findings presented here. Despite this caveat, the flow cytometry data presented in this section, together with immunofluorescence images and gene expression data, clearly illustrate the events sequence and the cell dynamic that take place in the SG upon AdV infection.

5.1.1 The early SG immune cell infiltration in response to AdV infection is dominated by both Ly6C^{Hi} inflammatory monocytes and neutrophil granulocytes and is followed by NK cells infiltration and activation.

From the initial haematoxylin and eosin staining performed as described in the previous Chapter (Section 4.1.2), it was immediately evident that the first immune response following viral infection of the salivary gland was characterised by a polymorphic and extensive immune cell infiltration with a

peri-acinar diffuse inflammation, associated with tissue oedema and disruption of the parenchymal structure (Figure 4.2 D and Figure 4.3 A). To better evaluate the extent of this initial inflammation and characterise the nature of the haematopoietic cells present in the gland in the first 5 days after infection compared to the steady state, isolated mononuclear cells were stained for CD45, and the percentage of CD45$^+$ in the whole gland lysate was calculated (Figure 5.1, top). The resident hematopoietic population in the murine submandibular glands accounts, at steady state, for approximately the 5% of the whole gland cellularity. Conversely, as early as 1 day post-cannulation, the percentage of CD45$^+$ cells dramatically increased to reach almost 30% of the cells present in the gland at the peak of acute inflammation. From day 3 post-AdV delivery onward, a constant decrease in the general percentage of CD45$^+$ cells was observed, although the difference in infiltrating leukocytes between control and treated glands was still highly significant at 5 days post-cannulation and onwards.

From the immunofluorescence staining for TLS performed in the previous Chapter of this thesis (Figure 4.3 A) I excluded that the massive infiltration observed during the first days post-infection could be due to B and T lymphocytes recruited from the periphery as in the SG tissue of animals culled within one week post-cannulation B220$^+$ B cells were almost undetectable and the CD3$^+$ T cell could only account for a small minority of the total number of CD45$^+$ leukocytes observed in flow cytometry.

Because NK cells represent one of the major components of the resident leukocyte populations in the salivary glands in homeostatic conditions and they have a well-known role in pathogen clearance upon viral infection [230],[231], I

first sought to investigate whether the increase in CD45$^+$ cells was due to an enlarged presence of these cells. To identify NK cells, in the flow cytometry panel CD3ε$^+$ and CD19$^+$ cells were excluded and NK cells were identified as CD3ε$^-$/NK1.1$^+$. This strategy allowed the identification of *bona fide* NK cells as in C57Bl/6 mice NK1.1 is a pan-NK marker and the exclusion of CD3ε$^+$ cells avoided the contamination of CD3ε$^+$/NK1.1$^+$ NKT cells. At steady state, the percentage of salivary gland CD3ε$^-$/NK1.1$^+$ NK cells among CD45$^+$ leukocytes is almost 20%, but, unexpectedly, relative percentage of NK cells radically dropped to 5% at 1 day post-procedure (Figure 5.1, bottom). From these data, I speculated that the percentage of NK cells decreased due to other cell types responsible for the early growth of the leukocyte population in the salivary glands within the first 24-48h post-cannulation. Conversely, from day 3 to day 5 post-cannulation, NK cells accounted for almost 40% of the total CD45$^+$ cells, suggesting a selective expansion of NK cells in the salivary glands following the early acute immune response. The increase in NK cells was both relative to the CD45$^+$ population and absolute compared to the salivary glands steady state NK.1.1 subsets as the prevalence CD45$^+$ cells was still significantly higher in AdV cannulated mice compared to vehicle control and non-cannulated animals.

CD45+ haematopoietic cells

CD3-NK1.1+ NK cells
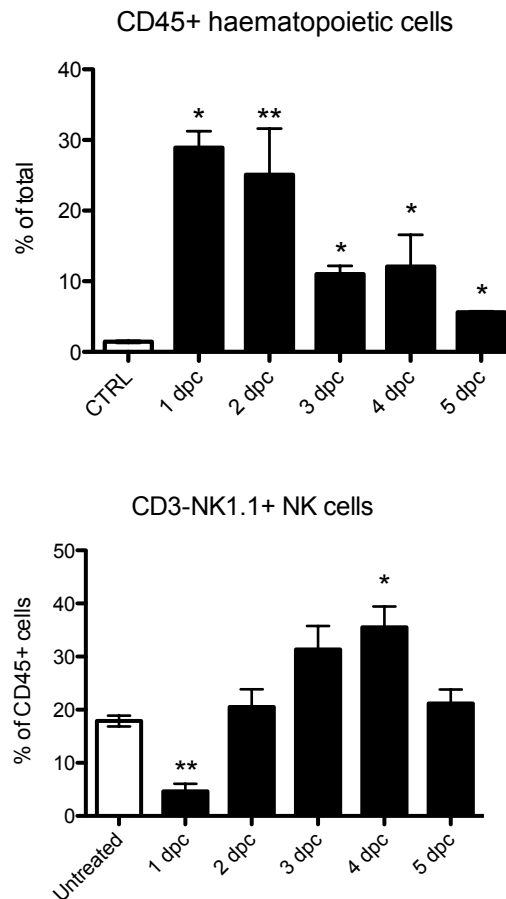
Figure 5.1: AdV treatment triggers a strong increase in leukocyte percentage that is only partially due to NK cells. Top) Leukocytes were gated as viable single cells and their percentage calculated against the total amount of cells obtained from enzymatic digestion of the gland. NK cells (**bottom**), defined as single viable CD45$^+$/CD3$^-$ cells, appear to diminish during the first day post-infection, probably due to a strong increase in other CD45$^+$ cells populations observed in the top panel. By day 2 post-cannulation, the percentage of NK cells among leukocytes is comparable to control glands and by day 4 it is significantly higher, suggesting either an influx of NK cells from periphery or an *in situ* proliferation. Data expressed as mean ± SEM, at least 4 glands per time point, *p < 0.05, **p<0.01 between AdV-treated and control animals.

Since during infection the first cells recruited are generally polymorphonucleate cells and inflammatory monocytes, which extravasate from the circulation and localise to the affected tissue, I next investigated whether infiltrating myeloid cells were responsible for the observed increased in the number of CD45$^+$ cells following AdV infection.

Using the same basic strategy described above, myeloid cells were first identified using an anti-integrin αM (CD11b) antibody that is strongly expressed on cells from the innate immune system. CD11b$^+$ cells were further subdivided based on the presence and expression levels of Ly6G$^+$ and Ly6C as follows: i) Ly6G$^+$/Ly6C^{Int} neutrophils and ii) Ly6G$^-$/Ly6C^{Hi} monocytes. Ly6G is a neutrophil granulocytes specific marker, while Ly6C is widely expressed on the cell membrane of different leukocytes, among which, plasmacytoid DCs [232], T cells [233],[234], neutrophil granulocytes, monocytes and macrophages [235],[236]. Nevertheless, Ly6C can be readily used as a monocyte marker in combination with other antigens. In particular, CD45$^+$/CD3$^-$/CD19$^-$/NK1.1$^-$ /CD11b$^+$/Ly6G$^-$ cells with a high expression of Ly6C were considered of monocyte origin and are commonly described as inflammatory monocytes.

As shown in Figure 5.2, Ly6C bright monocytes and Ly6G$^+$ polymorphonucleate cells represented over 40% of the leukocytes present in the gland 1 day after infection. Interestingly, while neutrophils were retained in the infected glands for less than 48 hours (Figure 5.2 B), Ly6C^{Hi} monocytes persisted for a longer time (Figure 5.2 A), before differentiating in resident macrophages (as discussed in Section 5.2.1).
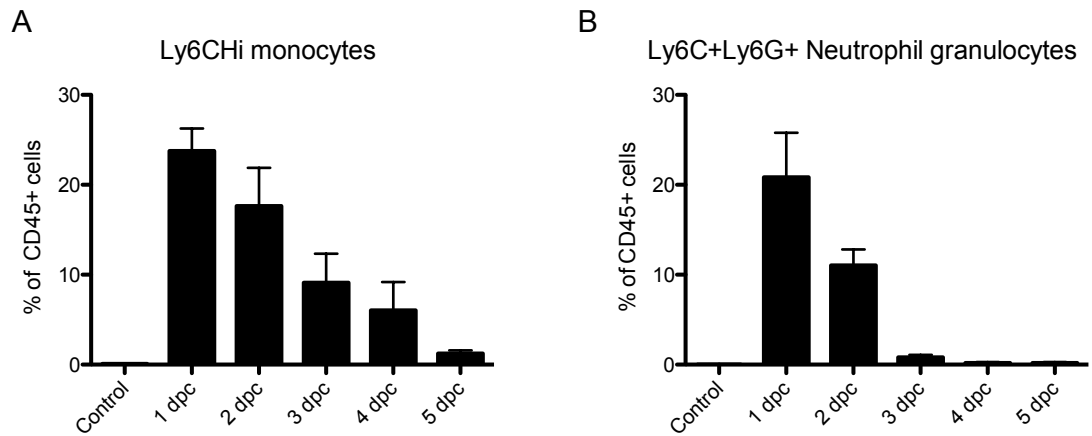
Figure 5.2: Inflammatory monocytes and neutrophil granulocytes represent more than half of the inflammatory infiltrate populating the glands 1 day post-cannulation. Single viable $CD45^+/CD3^-/CD19^-/NK1.1^-/CD11b^+/Ly6G^-$ cells with high expression of Ly6C marker were considered inflammatory monocytes (**A**) while $CD45^+/CD3^-/CD19^-/NK1.1^-/CD11b^+/Ly6C^{Int}/Ly6G^+$ were classified as neutrophil granulocytes (**B**). Together at 1 day post-cannulation these two populations represented more than half of the initial infiltrate, but as monocytes number remained elevated during the course of 5 days after cannulation, neutrophils rapidly decreased and were almost undetectable by 4 days post-AdV delivery. Data expressed as mean ± SEM, at least 4 glands per time-point.

5.1.2 Plasmacytoid dendritic cells are present in the untreated salivary gland and their number increases upon infection

Plasmacytoid dendritic cells (pDC) are professional type-I interferon producers both in human and mouse [237]. Belonging to the innate immune system, this cell subset is specially equipped to respond to viral infections as they constitutively express TLR7 and TLR9. In response to viral ligand pDC produce large amounts of IFN-α and IFN-β [238]. Plasmacytoid DCs can also respond to bacterial stimuli and can produce other inflammatory cytokines such as TNF-α and IL-12 [238]. Moreover, pDC express both inflammatory and homeostatic chemokines receptor and thus can migrate both to inflamed tissues and to SLO [232],[237]. As I reported in Section 1.2.5.1, plasmacytoid DC and type-I interferons are also associated with several autoimmune diseases. For these reasons, I investigated whether also pDC were infiltrating the salivary glands upon viral challenge compared to steady state. To characterise pDCs, single cells with the physical characteristic of leukocytes were selected for their expression of CD45 and from these cells, CD11c$^+$ cells were gated and from this subset B220$^+$/Siglec-H$^+$ cells were considered pDCs (Figure 5.3 A) [239].

As it appears from the preliminary experiments reported in Figure 5.3 B, pDCs were barely detectable in the resting salivary glands, representing a very small percentage of resident leukocytes. Upon infection, the number of Siglec-H$^+$ pDCs increased in parallel with the inflation of CD45$^+$ cells, particularly from day 3 post-cannulation onward.
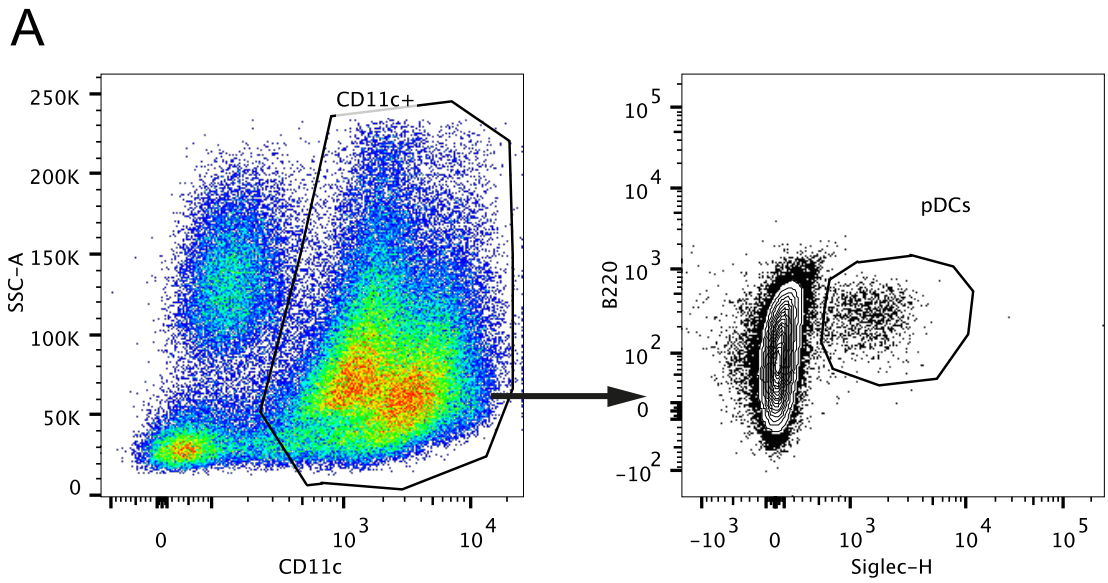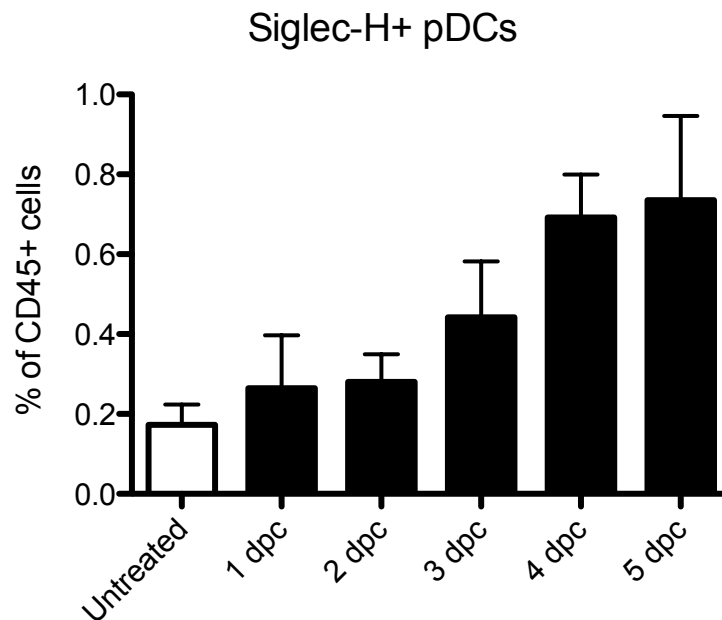
Figure 5.3: B220⁺/CD11c⁺/Siglec-H⁺ pDC percentage increases during the early phases of infection. **A)** Representative plot from a 4 days post-cannulation AdV-treated gland. CD11c⁺ cells were plotted for their expression of B220 and Siglec-H, pDCs are gated as double-positive cells. **B)** Histogram representing the Siglec-H⁺ pDCs percentage of the total CD45⁺ hematopoietic cells infiltrating the SG upon AdV-challenge. Data represent mean ± SEM, at least 3 glands per time-point.

5.1.3 The CD11b$^+$/SSCHi cells present in the SG and increasing upon infection resemble eosinophil granulocytes

While analysing the plots for cannulated animals between 1 and 5 days post-procedure, an unexpected population showing high SSC was detected. As this population showed physical characteristics (i.e. high SSC) and expression markers (in particular CD11c) different from the other CD11b$^+$ cells, it was excluded from the monocyte-macrophage analysis presented in the next sections. My first idea was that these cells might have been neutrophil granulocytes, but they were not positive for the neutrophil marker Ly6G. A more detailed analysis of these cells revealed that they were also F4/80$^+$ and had a variable expression of Ly6C (from high to negative) while they were consistently CD11c negative. When I gated this population as CD11b$^+$/CD11c$^-$/SSC^{Hi} I observed a constant increase in their percentage among the leukocytes during the course of infection (Figure 5.4 A). Given the complexity of this subset indicating probably a high presence of granules in the cytoplasm, I sought to investigate whether these cells were eosinophil or basophil granulocytes or mast cells. Basophils and mast cells constitutively express the high affinity receptor for IgE immunoglobulins FcεRI, while eosinophil granulocytes can be identified using the sialic acid-binding immunoglobulin-type lectins F (Siglec-F) [240]. Indeed, CD11c$^+$/SSC^{Hi} cells were strongly positive for Siglec-F but only a small percentage was FcεRI positive (Figure 5.4 B).
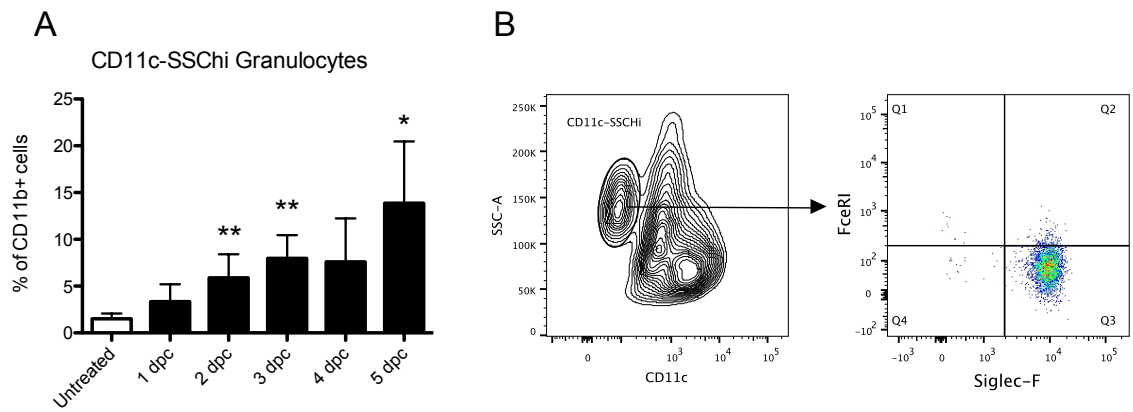
Figure 5.4: A high-complexity population with phenotype corresponding to eosinophil granulocytes is present in the gland in the early phases of inflammation. A) Histogram representing $CD11b^+/CD11c^-/F480^+/Siglec\text{-}F^+$ granulocytes characterised by high side-scatter. This population shows a trend to increase as soon as day 1 post-cannulation and its percentage against $CD11b^+$ myeloid cells infiltrating the gland results significantly higher than controls for most of the observed time-points. The representative plot in **B** shows that when staining the $CD11c^-/SSC^{Hi}$ population for Siglec-F and FcεRI, the cells resulted positive for the eosinophil marker (Siglec-F) but only a small percentage stained for FcεRI, excluding the possibility that the cells were mast cells or basophil granulocytes. Data in **A** represent mean ± SEM, at least 4 glands per time point, *p < 0.05, **p<0.01 between AdV-treated and control animals.

5.2 The role of NK cells and myeloid cells in the formation of SS-like lesions and the development of TLS

5.2.1 Recently extravasated monocytes progressively acquire the macrophage marker F4/80 and concomitantly downregulate Ly6C

On a careful analysis of the data reported above, I noticed that Ly6C bright cells did not seem to disappear from the infected salivary gland over time, but rather appeared to downregulate the expression of Ly6 (Figure 5.5 A). Previous studies reported that recently extravasated monocytes can lose expression of Ly6C and acquire the F4/80 macrophage marker [236] during their differentiation into monocyte-derived macrophages. Thus, I investigated whether this phenomenon was also taking place in the virus-infected salivary glands. The differentiation of monocytes into macrophages was followed studying CD11b$^+$ cells according to their expression of Ly6C versus F4/80.

The analysis was conducted on viable CD19$^-$/CD3$^-$/NK1.1$^-$/Ly6G$^-$/ CD11b$^+$ deprived of the CD11c$^-$/SSC^{Hi} population and the results reported in Figure 5.5 B are expressed as percentages of this population. F480$^+$/Ly6C$^+$ cells were considered blood-recruited monocytes and F480$^+$/Ly6C$^-$ cells were considered macrophages. Monocytes, that represent approximately 5% of the myeloid cells in the resting salivary gland, increased to over 80% as soon as day 1 post-cannulation and this percentage remained stable for the first 3 days after procedure (in Figure 5.5 B). This strong increase in monocytes compressed the relative amount of macrophages that represent more than 80% of the resident CD11b$^+$ cells in the non-stimulated gland. However, by day 4 post-cannulation, the percentage of Ly6C$^+$ cells significantly decreased in parallel with the increased relative amount of F4/80$^+$ macrophages in keeping with the

progressive entering of inflammatory macrophages within the pool of salivary gland macrophages.
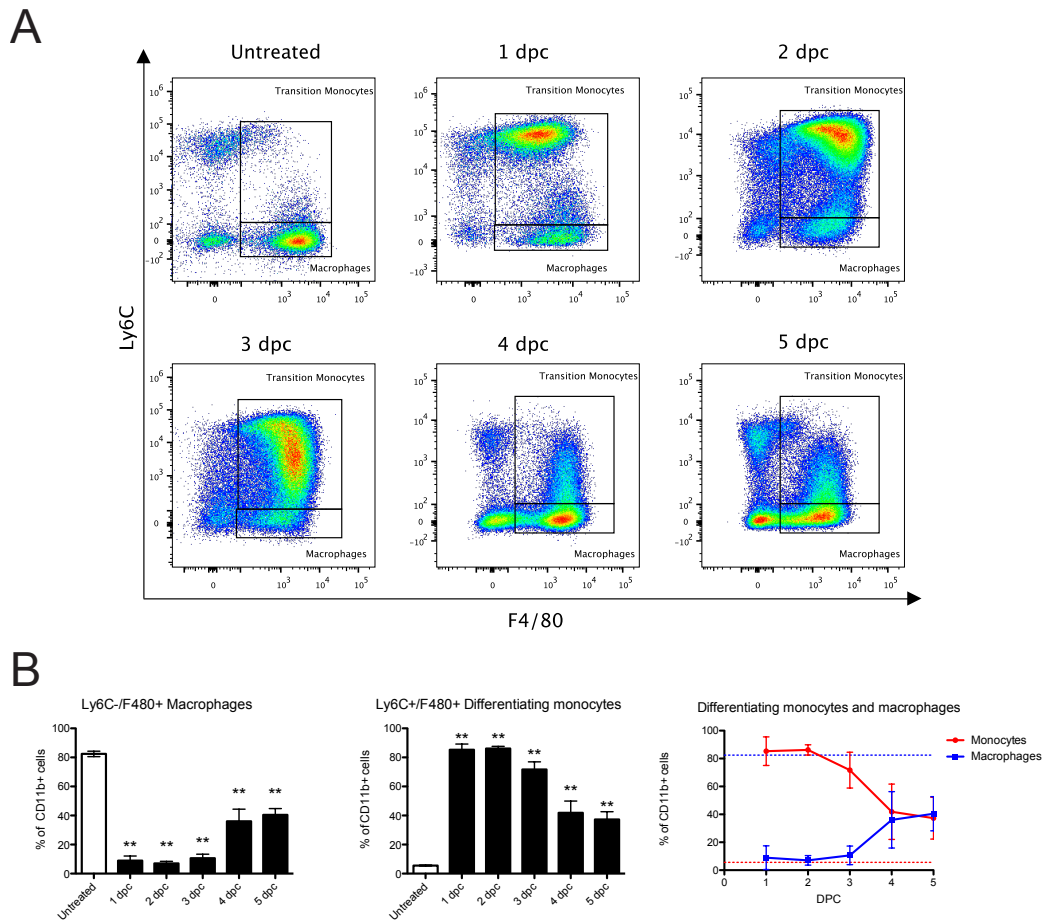
Figure 5.5: Infiltrating monocytes lose expression of Ly6C as they differentiate into macrophages. CD11b$^+$/Ly6G$^-$/F4/80$^+$/Ly6C^{Hi} monocytes downregulate Ly6C expression as soon as day 2 post-cannulation (**A**) while they retain the expression of F4/80. Upon the strong inflammation that develops after infection the percentage of Ly6G$^-$/Ly6C$^-$/F480$^+$ macrophages among the CD11b$^+$ myeloid cells suddenly decreases in favour of a strong increase of the inflammatory monocytes (**B**). Both the flow cytometry plots and the statistic view of this shift suggest that infiltrating monocytes differentiates into macrophages soon after their access to the gland. Data represent means ± SEM, Untreated =

4 glands; 1 dpc = 7 glands, 2 dpc = 6 glands, 3 dpc = 6 glands, 4 dpc = 6 glands, 5 dpc 8 glands, **p<0.01 between AdV-treated and control animals.

5.2.2 A distinct subset of non-resident CD11c+ dendritic cells infiltrates the salivary gland upon viral infection and precedes TLS development.

Dendritic cells, as professional antigen presenting cells, continuously probe tissues for antigen and once activated at site if inflammation upregulate CCR7 expression and migrate to secondary lymphoid organs where they present the antigen to T cells. DCs are also important for TLS maintenance in mice, as selective ablation of CD11c$^+$ DCs resulted in disruption of iBALT forming in murine lungs after *influenza virus* infection, probably due to their capacity to activate the Ltβ pathway [58]. To test the role of DCs in my model, myeloid cells were analysed in function of their expression of CD11c (integrin αX). This integrin can be also expressed on monocytes and macrophages at lower levels, thus only F4/80$^-$/CD11c^{Hi} cells were considered true myeloid DCs. At steady state, Ly6C$^-$/F4/80$^+$ resident macrophages are positive for CD11c and F480$^-$/CD11c^{Hi} DCs represent only 5% of CD11b$^+$ cells (**Error! Reference source not found.** A and B)

When inflammation begins at days 1 and 2 post-procedure, the relative percentage of DCs decreased only slightly despite the strong influx of Ly6C$^+$/F480$^+$ monocytes, suggesting that a parallel increase in the number of DCs was taking place (**Error! Reference source not found.** B). In support to this hypothesis, at day 4 post-cannulation, when the number of CD45$^+$ cells had more than halved compared to day 1 post-cannulation but was still significantly higher than in control glands (Figure 5.1, top), the relative percentage of CD11c^{Hi}/F480$^-$ DCs was still significantly higher than in control glands (**Error!**

A

| Untreated | 1 dpc | 2 dpc |
| 3 dpc | 4 dpc | 5 dpc |

CD11c

F4/80

B

CD11c+ F480- Dendritic Cells

% of CD11b+ cells
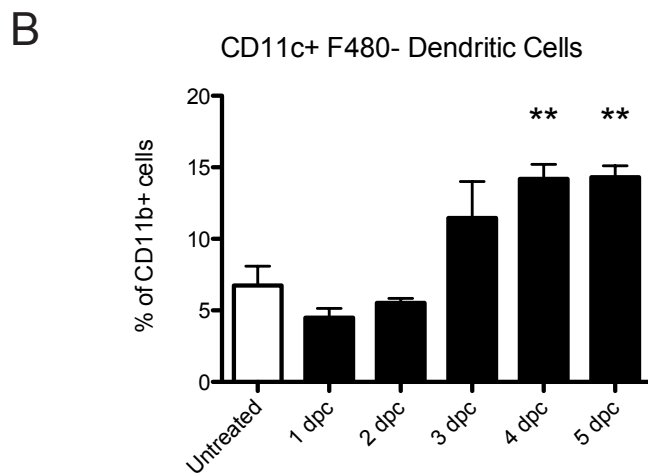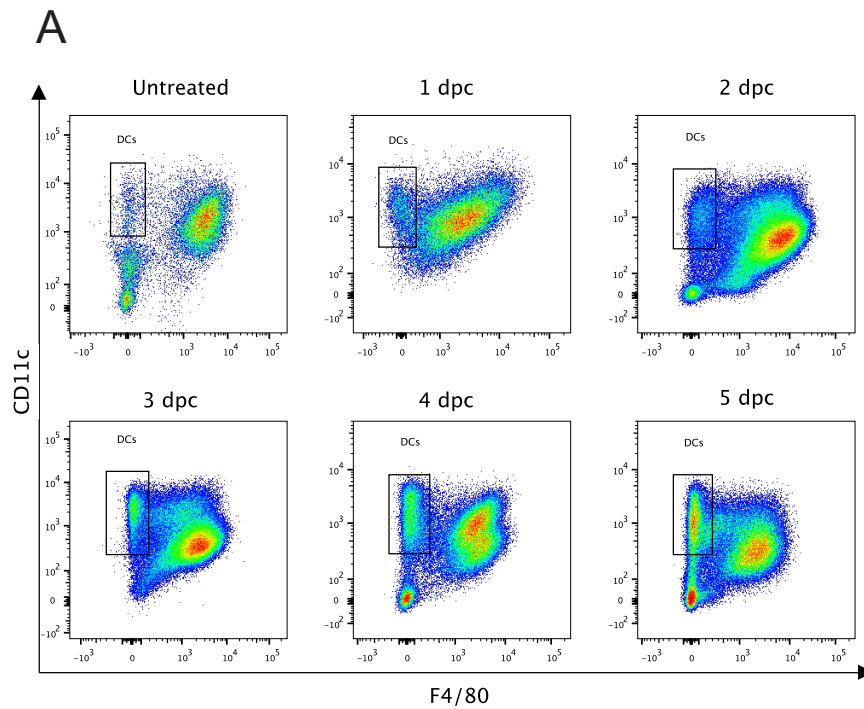
Reference source not found. B), indicating an inflammation-induced increase of this population.

Figure 5.6: The percentage of CD11c^{Hi}/F480^{-} DCs present in the gland increases with the progression of the infection. **A-B**) CD11b^{+}/F480^{-}/CD11c^{Hi} DCs percentage increases during the first 5 days after viral infection and is significantly higher than controls by 4 days post-cannulation. Data represent

means ± SEM, at least 4 glands per time-point, **p<0.01 between AdV-treated and control animals.

5.2.3 NK depletion does not affect inflammatory monocytes infiltration, macrophages differentiation and DCs accumulation in the cannulated SG

The anti-tumour and anti-viral function of NK cells has been known since the first description of this cell type [241]. Surprisingly, despite the wide interest regarding AdV-mediated gene therapy, few studies focused on the effect of the adenoviral vectors themselves on the immune system in general and on NK cells in particular. Ruzek et al. studied specifically the NK cells reaction to adenoviral vectors in mice and concluded that NK cells are activated by replication-defective AdV even if the vector does not encode for any transgene. Moreover, they also proved that UV-treated but not heat-denatured AdV vectors can induce a NK response, suggesting that the structural integrity of virions is more important than the viral genome in the stimulation of anti-viral activity [242]. In another scenario involving a non-viral pathogen, i.e. a murine model of intestinal inflammation triggered by *T. gondii*, a NK cells subset resident in the gut was shown to be responsible for the recruitment of inflammatory monocytes that eventually contributed to the tissue damage [243]. Furthermore, the cross-talk between NK cells and monocytes, macrophages and DCs has been recently reported both in human and mouse disease models [244],[245]. For these reasons, I hypothesised that the intra-gland AdV delivery triggered a NK cells response that in turn lead to the considerable monocyte infiltration described in the previous sections.

To test this hypothesis, I performed a selective depletion of NK cells using a mouse anti-mouse NK1.1 antibody that proved to be a quick and highly efficient system for NK ablation from the circulation and within the SG, as reported in

Section 3.2.4). Mice treated with the NK-depleting antibody and Ig control were cannulated and culled at 1, 3, 5 and 7 days post-AdV delivery. SGs were digested and analysed by flow cytometry using the same gating strategy described above for the monocyte/macrophage populations.

Contrarily to what expected, the absence of NK cells modified the relative percentages of DCs and monocytes only at 1 and 3 days post-cannulation, respectively (**Figure 5.7**). By day 5 after AdV delivery, and at all the observed time-points for the F480+/Ly6C- macrophages, no statistical difference was observed between anti-NK1.1-treated and control mice, suggesting that resident NK cells were not responsible for the chemotactic signals driving myeloid cells accumulation in the SG upon AdV delivery.
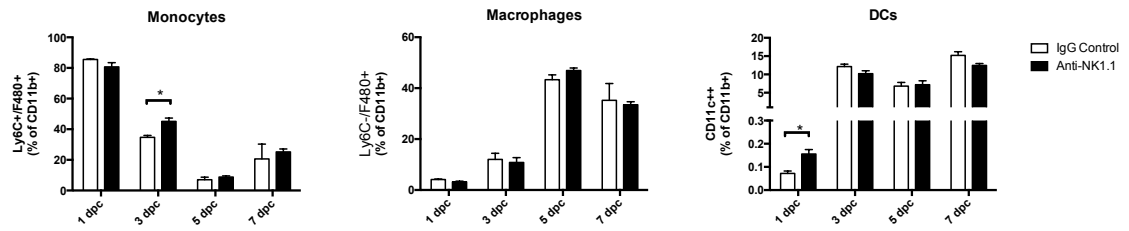
Figure 5.7: NK depletion only temporarily affects relative abundance of myeloid populations. Flow cytometry analysis of SG myeloid populations in presence or absence of NK cells. The ablation form the SG of the NK cells population only affected the relative amount of $F480^-$/$Ly6C^-$/$CD11c^{Hi}$ DCs and $Ly6C^+$/$F480^+$ infiltrating monocytes at 1 and 3 days post-cannulation. Data represent means ± SEM. For the Ig control group observations number is 1 dpc = 4, 3 dpc = 4, 5 dpc = 8, 7 dpc = 4; for anti-NK1.1 group observations number is 1 dpc = 5, 3 dpc = 5, 5 dpc = 9, 7 dpc = 4; $*p < 0.05$ between NK-depleted and Ig control-treated animals.

5.2.4 NK cells selective depletion does not affect SG TLS formation, number and organisation upon AdV infection

After the analysis of the flow cytometric data reported above and the unexpected results, I decided to use the same depletion scheme inside the AdV-triggered ELN model to test whether the absence of NK cells would affect the development of TLS in the cannulated glands.

Animals were treated with the depletion antibody and Ig control and AdV-cannulated as described in Section 3.2.4 and animals were culled at 3, 7 and 17 days post-cannulation. SG were used for mRNA expression analysis (3, 7 and 17 days post-cannulation time-points) and histological analysis (17 days post-cannulation).

Surprisingly, when analysing histological specimens collected during the third week post-AdV delivery (17 days after procedure) from NK-depleted and control animals, I observed no difference in TLS formation and organisation between the two groups. In particular, as shown in **Figure 5.8** A, peri-ductal lymphocytic aggregates formed and appeared similar in size and segregation between control and NK-depleted mice. The histological evaluation of the number of G2 aggregates and the level of segregation also confirmed that NK cells were dispensable for the ELN process (**Figure 5.8** B). To confirm these observations, I assessed the expression of the genes involved in the ELN process on AdV-cannulated NK-depleted and control-treated animals. In accordance with the histological evidence, at 2 and 3 weeks post-treatment there was no significant difference in the expression of lymphoid chemokines and their receptors between depleted animals and controls (**Figure 5.8** C). Also, the absence of NK cells did not affect the functionality of TLS forming in the SG upon AdV delivery,

as the expression of AID did not change between the two groups. Although the final formation and functionality of TLS were unaltered by the lack of NK cells, at 3 days post cannulation I observed a significant increase in the expression of CCL19, CXCR5 and Ltβ in treated animals in comparison to controls. Albeit preliminary, this observation suggests that the ablation of NK cells might influence the Ltβ/lymphoid chemokines in the very early inflammatory response, but this effect is rapidly compensated as soon as day 7 after treatment and does not affect the final TLS formation and organisation in the SG.
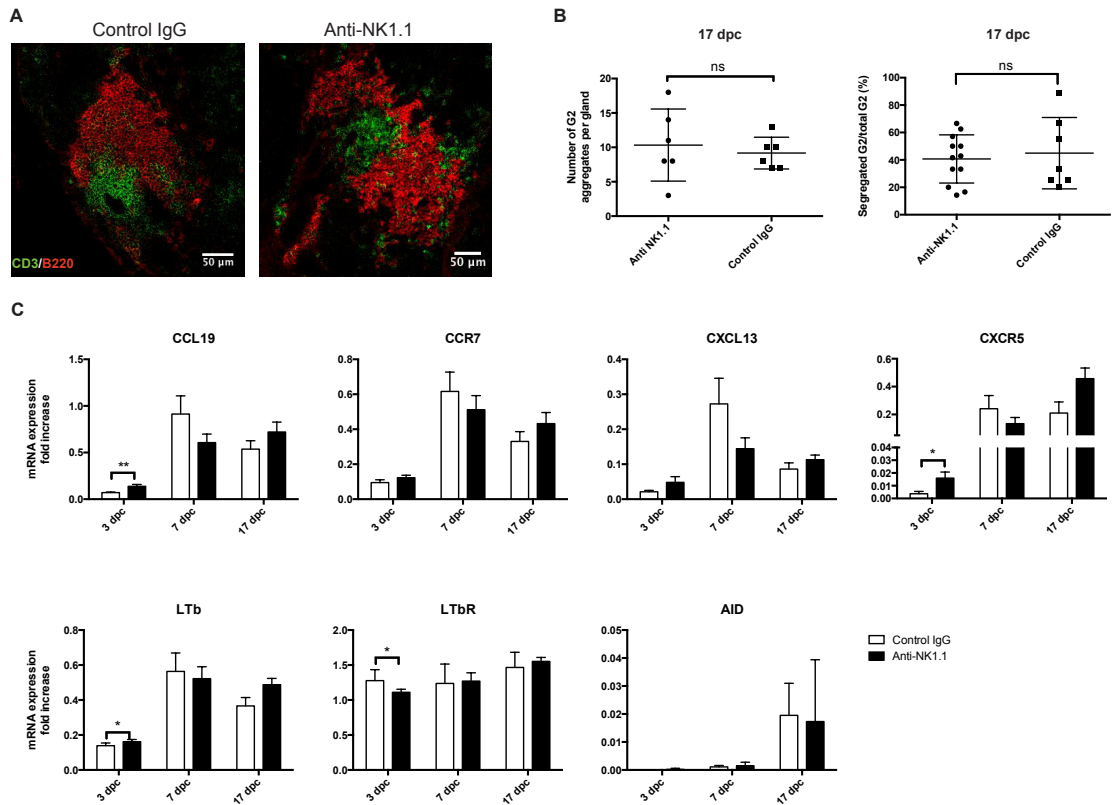
Figure 5.8: NK depletion does not affect TLS formation, organisation and functionality. (A) Microphotograph showing no difference in infiltration and segregation of B (B220, red) and T (CD3, green) lymphocytes in AdV-treated SG in NK-depleted mice (*right*) and controls (*left*). Scale bar represent 50 μm. (**B**) Comparison of the number of G2 aggregates (*left*) and ratio between segregated and non-segregated G2 aggregates (*right*) in AdV-treated SG from anti-NK1.1-treated and control mice. (**C**) Real-time analysis of the expression of lymphoid chemokines and receptors, Ltβ/LtβR and AID in SG at 3, 7 and 17 days post-cannulation. Data represent means ± SEM, at least 4 glands per time-point, *p<0.05, **p<0.01 between NK-depleted and control animals.

5.2.5 Developing TLS display structural segregation of different myeloid cells: DCs infiltrate newly formed B/T cell aggregates while macrophages are excluded from ectopic follicles

To further characterise the dynamic positioning of macrophages and myeloid DCs in the virus-infected SG during the course of TLS development, I performed immunofluorescence staining for F4/80 and CD11c in tissue sections from animals infected with AdV and culled at 3, 10 and 18 days post-cannulation.

To test whether resident macrophages, that co-express F4/80 and CD11c in flow cytometry, were also double positive in immunofluorescence, I first performed a double staining for the two antigens on tissue sections. As shown in Figure 5.9, in resting conditions F4/80$^+$ macrophages were interspersed in the gland and localised preferentially around the acinar and ductal structures of the gland. CD11c$^+$ DCs also localised proximal to ductal structures. The staining for F4/80 and CD11c did not show any overlap.

Three days post-cannulation numerous CD11c$^+$ DCs were interspersed in the gland parenchyma, more often associated with ductal structures (Figure 5.10 B). In comparison with the control gland, their number appeared increased in accordance with the flow cytometry data (Figure 5.10 A and **Figure 5.6** B). At later time-points the close association with salivary ducts was even more evident (Figure 5.10 C) and at 10 days post-cannulation most CD11c$^+$ DCs were intimately associated with inflammatory *foci* forming in the proximity of ductal structures. Interestingly, during the third week after infection, when TLS assumed their more complex and segregated form (Figure 4.3 C), DCs were strongly associated with the ectopic follicles (Figure 5.10 D).

Although, as expected by the flow cytometry data, the presence of F4/80$^+$ macrophages strongly increased in the inflamed gland at 3 days post-cannulation in comparison to controls (Figure 5.10 E and F), these cells were surprisingly excluded from TLS and typically organised as cuffs of highly dense F4/80$^+$ cells surrounding T/B cell follicles. This phenomenon was already present at week 2 post-cannulation but became immediately evident 3 weeks after AdV delivery when TLS were fully formed and sustained a GC response (Figure 4.5). To my knowledge, this is the first demonstration that different myeloid subsets segregate in discrete areas during TLS development, suggesting that different chemotactic gradients drive on one side the positioning of DCs within TLS and on the other a follicular exclusion of F4/80 macrophages. (Figure 5.10 G and H).
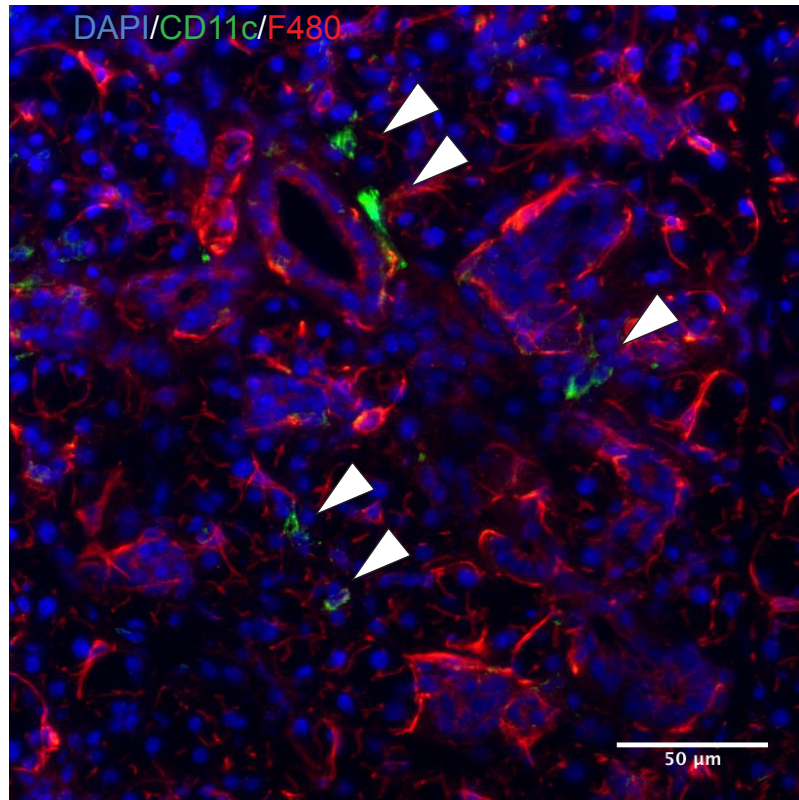
Figure 5.9: F4/80 macrophage marker and CD11c DC marker expression do not overlap in double IF-stained SG tissue. This control salivary gland section has been stained for F4/80 (red) and CD11c (green, arrowheads) and nuclei were counterstained with DAPI (blue). Macrophages are present around the ductal structures and interspersed in the gland parenchyma. DCs also share a diverse distribution in the gland and often associate with ductal epithelium but their number at steady state is lower than macrophages. Scale bar is 50 μ m long.
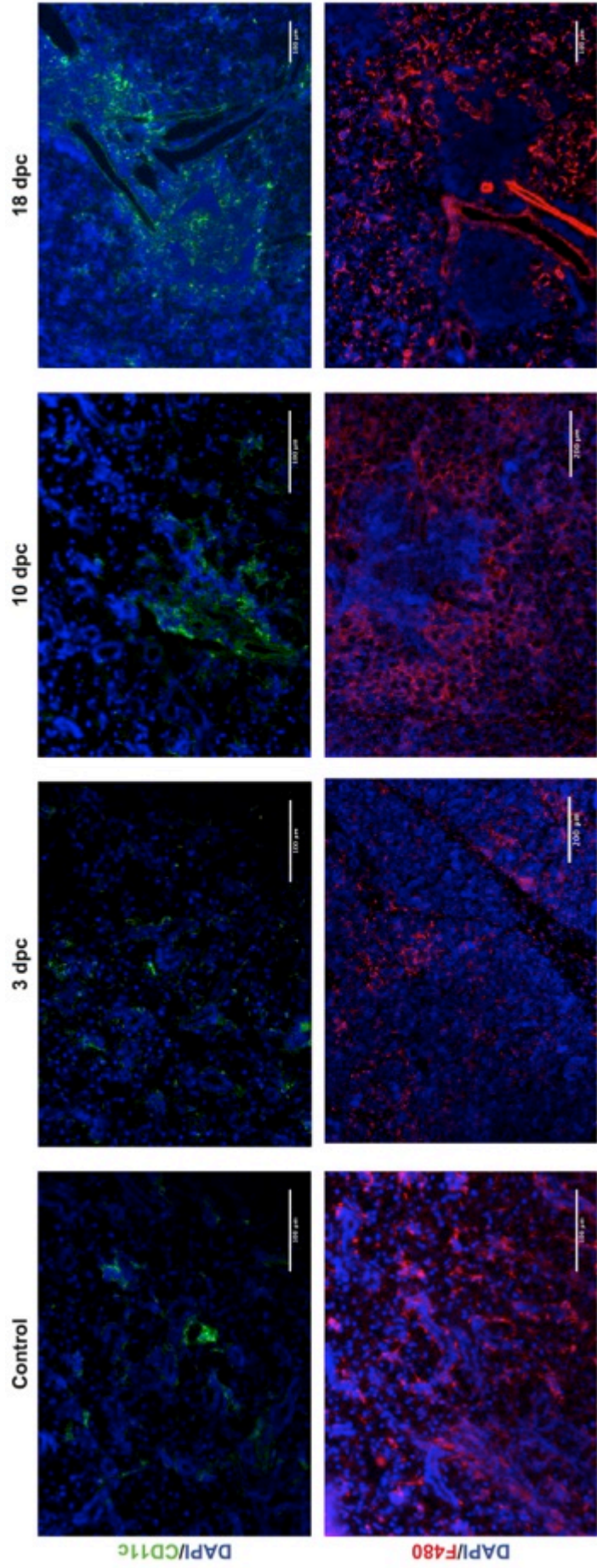
Figure 5.10: CD11c$^+$ DCs increase in number after infection and co-localise in the inflammatory foci while F4/80$^+$ macrophages are excluded from the infiltrates. Top row microphotographs showing CD11c$^+$ DCs (in green, nuclei counterstained in blue) at steady state associate preferentially with ductal structures (**control**) but upon infection their number increases and they present a sparse distribution (**3 dpc**). As the ELN process progresses, DCs associate with the nascent inflammatory *foci* (**10 dpc**) and by three weeks post-cannulation they localise preferentially within the infiltrates (**18 dpc**). Bottom row F4/80$^+$ macrophages (in red, nuclei counterstained in blue) are more abundant than DCs at steady state. Upon infection (**control**) macrophage distribution is diffuse, but during the organisation of the TLS there is an evident association of these cells with the forming infiltrates (**3 dpc**) but opposite to DCs, macrophages are systematically excluded from the *foci* (**10 and 18 dpc**) and tend to form a cap along the edge of the infiltrates..

5.2.6 CD11c$^+$ dendritic cells associate with B220$^+$ B and CD3$^+$ T cells in the early phases of ELN and preferentially with CD3$^+$ T cells in the late stages.

Given the presence of CD11c$^+$ DCs inside the inflammatory foci during the development of TLS, I sought to identify whether DCs associated preferentially with the B cell rich or T cell rich areas. To do so, I performed a triple IF confocal staining for CD11c$^+$ DCs, CD3$^+$ T cells and B220$^+$ B cells in SG of animals culled at 1, 2 and 3 weeks after cannulation. As shown in Figure 5.11 (top panels), in the early phases of the AdV-induced inflammation prior to the migration of B and T cells, DCs were abundantly present in close association with ductal structures. Conversely, by week 2 post-cannulation, when significant numbers of B and T were present in the infected gland, DCs strongly migrated towards the forming ectopic follicle with CD11c$^+$ cells closely intertwined with both B and T cells (Figure 5.11, middle panels). Finally, at the peak of TLS formation at week 3 post-cannulation, DCs were strongly associated with ductal structures but also in intimate contact with CD3$^+$ cells, but not B220 B cells, in the T cell-rich areas of the periductal infiltrates, suggesting active antigen presentation to T cells and a possible direct role in TLS formation (Figure 5.11, bottom panels).
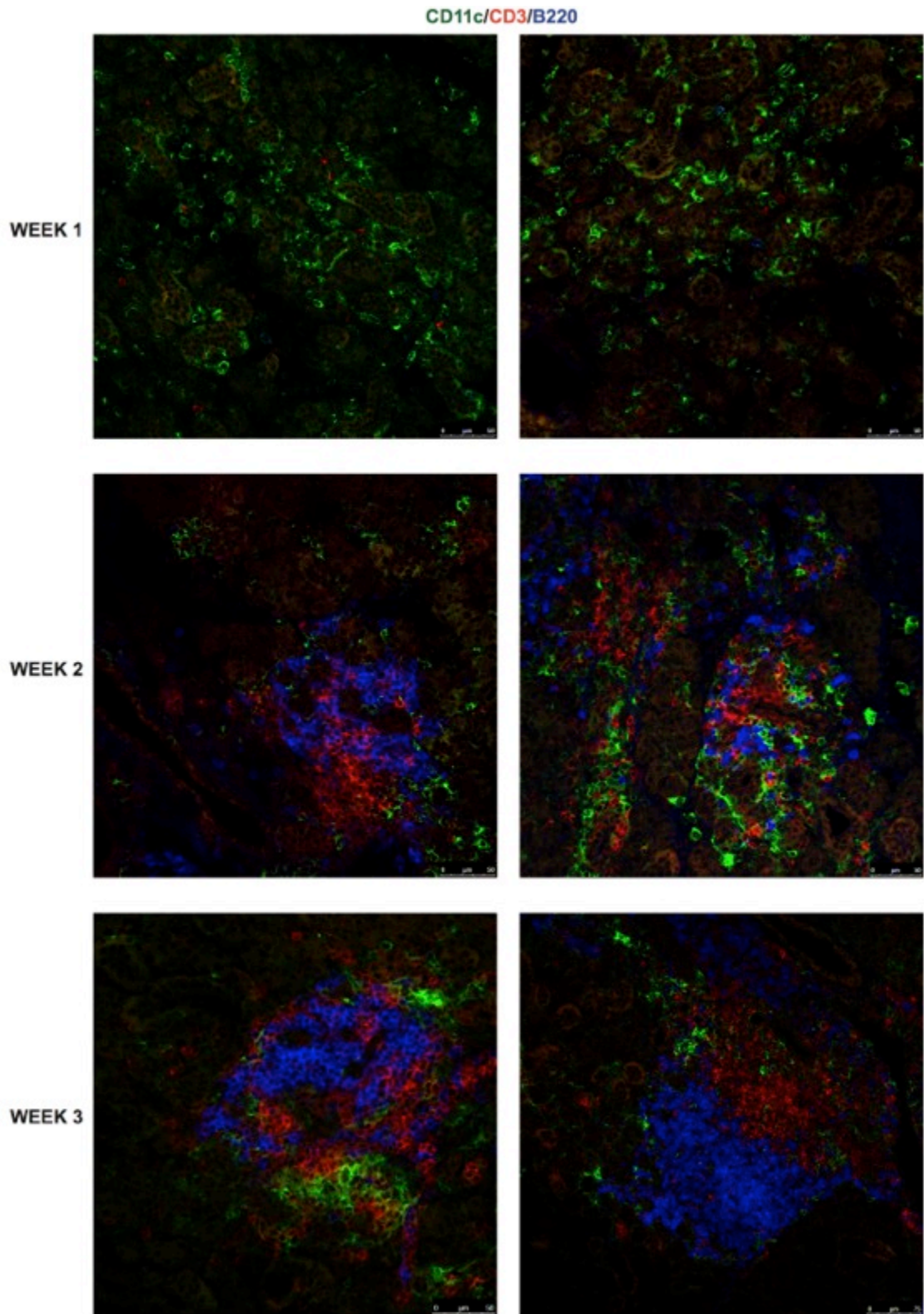
Figure 5.11: CD11c⁺ DCs are present during all stages of ELN in the SG and when TLS are fully formed their presence is enriched inside the T cell areas. Microphotographs showing CD11c⁺ DCs in green, CD3⁺ T cells in red

and B220$^+$ B cells in blue. Upon infection DCs number increase and they exhibit a sparse distribution with some cells showing an uncharacteristic round shape (**top**). During the second week after infection as the ELN process advances, DCs associate with the forming inflammatory infiltrates in contact with both B and T cells (**middle**). By 3 weeks post-cannulation DCs are present within the infiltrates only in correspondence of the T cell area while they surround, but are excluded from, the B cell areas (**bottom**).

5.2.7 During the first week after AdV infection myeloid cells express inflammatory and lymphoid chemokines in a bimodal fashion

Given the novel observations that I reported in the above sections, I decided to perform a preliminary set of experiments to investigate whether the number increase and the specific positioning of F4/80$^+$ and CD11c$^+$ myeloid cells was associated with a ELN-related expression profile. Essentially I hypothesised that the myeloid cells observed in the gland upon AdV-infection actively contributed to the formation of TLS thank to the production of lymphoid chemokines and activation of the LTβ pathway.

In order to test this hypothesis, I cannulated wild-type mice and collected the SG between 2 and 7 days after the procedure. The glands were digested and the cell suspension was stained with fluorescent antibodies for FACS. In this first set of experiments I only sorted viable non-eosinophil-like CD45$^+$/CD3$^-$/CD19$^-$/NK1.1$^-$/CD11b$^+$/F480$^+$/CD11c$^+$ cells, corresponding to a mixed population of monocytes/macrophages and DCs. The same population sorted from untreated animals was used as control. As the number of sorted cells from each gland was very small, SG from different mice that underwent the same treatment were pooled and the extracted and retrotranscribed RNA was analysed with the Fluidigm technology, a new TaqMan real-time PCR techniques that allows efficient gene expression analysis using small amounts of starting RNA material (see 3.6.4 for details). The results of the expression analysis are reported in **Figure 5.12**. Albeit not significant as only preliminary data were collected, interestingly the expression analysis showed that myeloid cells infiltrating in the gland upon AdV-infection indeed upregulate CCL19, CXCL13 and LTβ mRNA expression, in particular towards the end of the first

week after cannulation. On the contrary, the expression levels of the inflammatory chemokines CCL5, CCL7 and the CC-chemokines receptor CCR1 were strongly increased between day 2-4 after cannulation but progressively decreased in from day 5-7. CCL5 is an inflammatory chemoattractant for eosinophils and basophils but also T cells; CCL7 is a monocyte specific inflammatory chemokine while CCR1 is the receptor for a plethora of inflammatory chemokines, among which CCL2, CCL7 but also CCL5 and is expressed mainly in monocyte/macrophages and NK cells [246]. If confirmed in larger experiments (currently on-going), these data would support the idea of a bimodal chemokine production by the myeloid cells present in the gland: an initial production of inflammatory chemokines that induces the infiltration of the gland by inflammatory cells from the periphery is followed by a second phase of lymphoid chemokines synthesis able to attract B and T cells and modulate TLS formation.
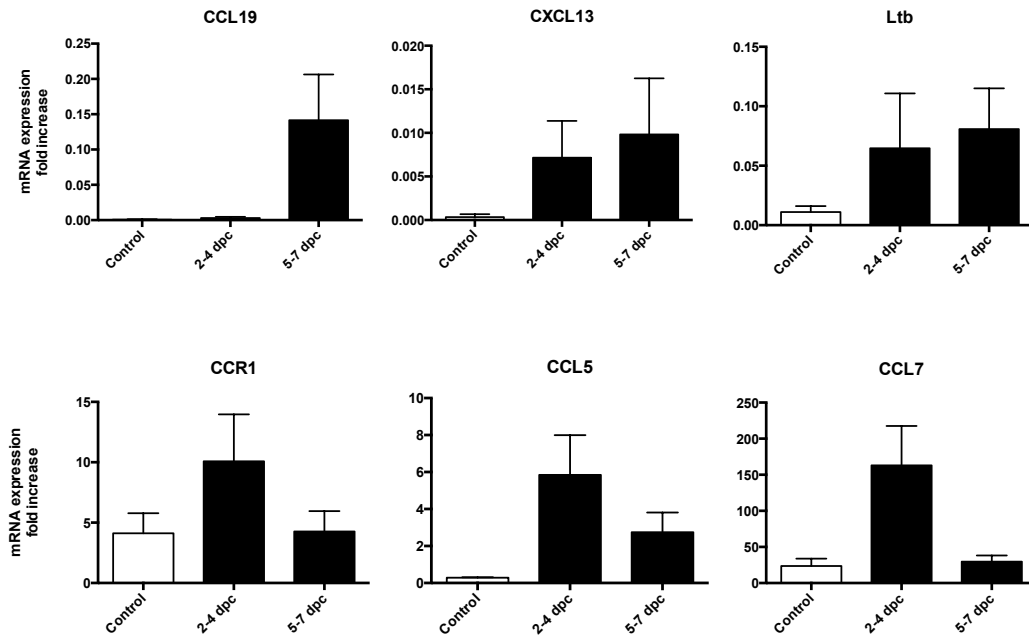
Figure 5.12: Inflammatory and lymphoid chemokines expression by myeloid cells in the first week after AdV-delivery follows opposite trends. Sorted non-esonophil-like CD45$^+$/CD3$^-$/CD19$^-$/NK1.1$^-$/CD11b$^+$/F480$^+$/CD11c$^+$ cells were analysed for the expression of inflammatory chemokines CCL5 and CCL7 and receptor CCR1 and lymphoid chemokines CCL19, CXCL13 and LTβ. The preliminary data for the first 6 days after treatment show a time-dependent increment of expression for lymphoid chemokines that is paralleled by an opposite trend for inflammatory chemokines that are higher in expression soon after infection than toward the end of the first week post-cannulation. Data represent mean ± SEM from at least 3 experiments on cells pooled from at least 4 SG. The statistical test failed to reach a p value ≤ 0.05 between control and treated groups for every gene tested, probably due to the small number of observations, in particular for the control group where n=3 (2-4 dpc group and 5-7 dpc group have both n=9).

Chapter 6 | Discussion

6 Discussion

The formation of TLS in the target organ of several chronic inflammatory conditions, including SS, has long been recognized [2],[3],[14],[47],[138],[247]. TLS formation is highly relevant to SS as germinal centre-like structures in the labial salivary glands are independent predictors of increased disease severity and evolution towards B cell lymphomas [141],[143].

The lack of reliable inducible animal models of ectopic lymphoid neogenesis has limited our understanding of the mechanisms leading to the formation of TLS in the salivary glands. Murine models of inducible sialoadenitis with some features of SS in response to systemic or local viral infection have been reported. However, in order to induce sialoadenitis previous work relied either on the use of fully infectious and replicating sialotropic viruses in autoimmune prone mice such as *lpr/lpr* mice [202],[248], or replication-deficient AdV vectors harbouring genes encoding for pro-inflammatory mediators such as IL-17 [249]. In addition, no comprehensive demonstration that viral-induced sialoadenitis can progress towards the formation of functional TLS and resembles the main physiopathological characteristics of SS (i.e. the formation of autoantibodies and the development of exocrine dysfunction) has been provided as yet.

As reported in this thesis, during my PhD I developed and validated a novel model of inducible lymphoid neogenesis that rapidly develops in the submandibular glands of wild-type C57Bl/6 mice in response to local delivery of replication-deficient adenoviral vectors. In this model of sialoadenitis, immune cell infiltration rapidly progresses from a diffuse inflammatory process towards the formation of periductal lymphocytic aggregates that further evolve into highly organised TLS within 3 weeks from viral infection. This process is

reproducible and synchronous with lymphocytic *foci* developing in 100% of the mice by week 2 post-cannulation and evolving by week 3 post-cannulation into fully formed TLS characterised in approximately 70% of the mice by T/B cell segregation and formation of FDC networks with germinal centre-like structures sharing high similarity to the human counterpart [31].

The formation of TLS has been suggested to be the result of a tightly regulated series of immunological and molecular processes with recapitulation of the main pathways involved in lymphoid organogenesis in prenatal life [250]. Embryonic lymphoid organ development is critically dependent on lymphoid chemokines CXCL13, CCL19 and CCL21 which are produced by VCAM-1$^+$ICAM-1$^+$LTβR$^+$ mesenchymal "organizer" cells in response to close interaction with CD3$^-$ CD4$^+$CD45$^+$IL-7Rα^+RANK$^+$ lymphoid "inducer" cells (Lti) expressing the membrane-bound heterotrimeric (α1β2) member of TNF family LTβ [2],[44],[250]. The establishment of a positive feedback loop between lymphoid chemokines and LTβ is critical in promoting the development of the stromal and vascular architecture of SLO, including the differentiation of HEVs [229].

Although a role for adult LTi cells in ELN has been often speculated, to date we have only proof that these cells can take the place of neonatal LTi in transgenic mice that lack them [48],[49]. Conversely, evidence from transgenic models of TLS has questioned the relevance of Lti in ectopic lymphoid neogenesis in adult life [251]. Similarly, lymphoid chemokine expression in patients with TLS developing during chronic inflammatory diseases, including SS [30]-[32],[126],[136], suggests that the lymphoid chemokines/LTβ pathway in inducible TLS formation is regulated by cellular and molecular mechanisms

which are different from the conventional interactions observed during embryonic development.

In this thesis I showed that, following AdV delivery, early up-regulation of lymphoid chemokines CXCL13, CCL19 and CCL21 mRNA preceded the development of TLS and peaked in concomitance with fully functional TLS. Of interests, lymphoid chemokines retained their discrete expression pattern observed in SLOs, with CXCL13 confined to the B cell-rich areas of the periductal aggregates and CCL21 in the surrounding T cell area. This suggests that the progressive recruitment and positioning of T and B cells subsets following AdV infection in the salivary glands are not random events but follow tightly regulated chemoattractive gradients. Additionally, this evidence establishes this inducible model of TLS as a suitable platform to dissect the dynamic expression, source of production and hierarchical importance of the critical factors regulating ectopic lymphoid neogenesis.

Importantly, in my PhD work I have also demonstrated that AdV-induced TLS not only recapitulate the cellular and molecular organization of SLO but also support functional B cell activation with expression of AID, the enzyme which initiates somatic hypermutation (SHM) and class switch recombination (CSR) of the Ig genes [252], leading to affinity maturation and differentiation of memory B and plasma cells [253],[254]. Expression of AID in the salivary glands required the formation of TLS acquiring markers of germinal centres such as FDC networks and GL7, similarly to SS patients [38]. AID expression and subsequent CSR in naïve B cells can be directly induced by a combination of cytokines among which BAFF, IL-4, IL-10 and IL-21, even in the absence of B-cell receptor cross-linking [255]-[259]. Accordingly, in this model AID transcript

levels were strictly associated with the expression of BAFF, IL-4 and IL-21 mRNA suggesting a functional role for these factors in downstream B cell activation.

Because the architectural, cellular and molecular features of TLS in this model were highly reminiscent of those observed in SS, I also investigated whether typical features of the human disease were also present in this model. The two hallmarks of SS are i) the breach of self-immunological tolerance towards nuclear antigens resulting in the detection of circulating autoantibodies and ii) a progressive exocrine dysfunction, which results in the classical signs and symptoms of mouth/eye dryness (*sicca* syndrome). Interestingly, at week 3 post-cannulation 75% of the AdV-cannulated mice developed positivity for IgG ANA, in comparison none of the vehicle controls displayed evidence of autoimmunity. Interestingly, onset of ANA was preceded by the rapid and abundant induction of epithelial cells apoptosis following AdV infection, as demonstrated by the presence of pyknotic nuclei and positive TUNEL staining. In SS autoimmunity, the involvement of the TLR on epithelial cells and B cells is likely to play a major role. In particular, it has been shown that ductal epithelial cells release a high level of the B cell survival/BAFF upon sensing viral dsDNA via the TLR3 and the type I IFN pathways [160]. Similarly, B cells express TLR7, which recognizes ssRNA (including viral RNAs, usually released within phagosomes), and TLR9, which recognizes unmethylated CpG DNA motifs (including dsDNA viruses, such as herpes viruses) [260]. In keeping with an important role of TLRs in direct viral recognition by B cells, TLR9 ligation on B cells has strongly been implicated in the enhancement of antiviral immune responses within GC [261]. In the context of viral-induced autoimmunity, the

release of nuclear material from apoptotic/necrotic cells as a direct result of viral replication or the resulting cytotoxic immune response likely represents a continuous source of potential autoantigens, and the rapid release of apoptotic material might be the leading cause of ANA generation in my model. In this regard, it will be interesting to dissect whether TLS forming in the SG are directly involved in the generation of autoantibodies over and above draining lymph nodes, as previously demonstrated for TLS in patients with SS [32],[140] and proposed in a mouse model of the disease [42].

In addition to the breach of self-tolerance, I also showed that the development of sialoadenitis and TLS following AdV infection was also accompanied by prolonged exocrine dysfunction. This is extremely interesting because while hyposalivation would be expected in the early stage post-viral infection given the high degree of diffuse inflammation and acinar loss, it was surprising to observe a lack of secretory recover up to 3 weeks post-cannulation when the glandular parenchyma returned to a normal appearance, with the exception of the formation of focalised periductal lymphoid aggregates. Although I did not elucidate the pathophysiologic mechanisms responsible for such hyposecretion in this model, which might be due to viral and/or immune mediated mechanisms, these observations would be in keeping with indications in patients with SS that exocrinopathy in the context of focal sialoadenitis is primarily due to a functional rather than anatomical impairment [262] as also in patients with SS, particularly at early stages of disease, the loss of salivary flow is not paralleled by a synchronized loss of secretory units in the diseased tissue. These observations have also been confirmed in another mouse model of virus-triggered sialoadenitis, where murine cytomegalovirus administered i.p.

induces salivary impairment well before the appearance of immune infiltration and viral colonisation of the SG [263].

Interestingly, I also found that in this model formation of TLS was invariably associated with the persistence of the transgene product within the salivary glands at least up to 4 weeks after AdV delivery, despite the viral inability to replicate, the presence of cytotoxic cells (e.g. NK cells) and production of AdV-specific IgG response as soon as the second week after infection. Strikingly, I observed prolonged viral and transgene protein expression only within ductal epithelial cells, an observation in keeping with the well-known tropism for the ductal cells in the SG shown by several viruses (such as CMV in rodents and humans and EBV and HCV in humans, that can establish a lifelong infection [168],[264]) and the inability of ductal cells to clear viral pathogens described both in rodent and human salivary glands [197],[204]. The reason why SG represent such a permissive site for persistent viral infection is only partially understood, but it is possible to speculate that viral persistence might depend on the ability of viruses to adapt to and evade immune recognition, but also on the fact that mucosal sites are naturally skewed toward a Th2 humoral immunity and recent reports regarding the specific environment-driven SG NK cells functional phenotype seem to confirm this hypothesis [265].

In the second part of my thesis, which was focused on the dissection of the series of very early events happening in response to viral infection in the submandibular glands prior to TLS formation, I clarified the dynamic rate and degree of immune cell infiltrations from the peripheral compartment. Of

relevance, I discovered that, similar to the formation of TLS, also the recruitment and positioning of innate immune cells within the virus-infected salivary glands seems to follow tightly regulated mechanisms.

First, I showed that neutrophil granulocytes are abundantly recruited to the salivary gland within the first 24-48 hours after infection. The presence of neutrophils in response to a viral infection is somewhat surprising but potentially not irrelevant in the context of the development of an adaptive immune response and autoimmunity. In fact, several unexpected functions have been recently associated to this subset of polymorphonuclear leukocytes and among those the capacity to promote B cell immunoglobulin production in the spleen marginal zone via the secretion of B cell survival factors such as BAFF, APRIL and IL-21 [266],[267]. Interestingly, the formation of neutrophil extracellular traps (NET), which is another important and unique feature of these granulocytes, has been recently recognized as a potential mechanism for the development of autoantibodies to citrullinated proteins, one of the key mechanism in the development of RA [268].

Plasmacytoid DCs, natural type-I interferon producing cells [237] involved in viral control, were present within the SG during the first 5 days post AdV infection and showed a trend towards increment in their number. This evidence is also relevant for the human disease as SS salivary glands are characterized by a strong type-I interferon signature [269],[270] which is associated with the presence of activated pDC in the SG infiltrate. pDCs have been shown not only to respond to classic viral stimuli but also by autoantibodies and antimicrobial peptides secreted by activated neutrophils [153]. In turn, activated pDCs promotes an increased inflammatory activity in several target immune cells and

also B cell survival and antibody production. [271]. Thus, the recruitment of pDCs in the gland upon AdV delivery observed in my model might boost immune activation in the early phases of infection but it could also promote B cell *in situ* activation, potentially rescuing autoreactive clones and supporting breach of self-tolerance. This series of events has been proposed to take place in the SG of virus-infected SS patients during the development of the disease [272] and my model could be the perfect tool to test the relevance of this hypothesis.

Eosinophil granulocytes-resembling cells were also observed to gradually appear in the gland after infection. The presence of eosinophils in a mucosal tissue is not surprising, but whether or not these cells have a role either in viral control, TLS formation and/or induction of adaptive immunity and breach of tolerance is difficult to ascertain at this stage. Recently eosinophils have been found important not only in defence against parasitic infection and in allergic reactions but also in anti-viral protection [273], thus the only speculation regarding the presence of these cells in my model that is probably safe to make with the little evidence in my hands, is that the Th2-skewed mucosal milieu might be encouraging the recruitment of a type-2 associated cell type, i.e. eosinophil granulocytes, together with classic type-1 immune cells such as NK cells and inflammatory monocytes.

Together with neutrophils, inflammatory monocytes are the most abundant infiltrating cell type in the first 72 hours post-infection of the SG. From previous data and the preliminary flow cytometry data that I presented in this thesis, it is very likely that most of the infiltrating monocytes differentiate into macrophages

and monocyte-derived DCs [236],[274]. Monocytes and monocyte-derived macrophages and DCs can execute a plethora of different functions from pathogen control to tissue remodelling and re-establishment of homeostatic conditions going through modulation of the innate and adaptive immune system. Moreover, resident macrophages are essential for the steady state condition of the tissue and patrolling DCs continuously enter and leave the peripheral tissues probing for pathogens and alarm signals. For this reasons it is very difficult to speculate regarding a specific role of these cells in my model, as I expect them to be involved at different levels in the host-pathogen interaction, TLS formation and tissue repair. Nevertheless, previous data supports several interesting observations that I made during my thesis which are worth discussing. In terms of TLS development in the context of autoimmunity, it has been shown that cells from the monocyte-macrophage lineage can produce the B cell-attracting chemokine CXCL13 in RA patients' synovium [59]. Resident and/or monocyte-derived macrophages could contribute to ELN also via the induction of lymphoid chemokines production by stromal cells. In fact, TNF overexpression by F4/80$^+$ macrophages in the intestine of LTi-deficient mice was sufficient to induce the acquisition by stromal cells of an "organiser" phenotype that eventually led to the formation of mesenteric lymph nodes in animals normally devoid of these structures [56].

In my model I also observed an increase of the DC population in the SG after AdV-delivery. The increase in CD11c$^+$ DCs might be important both in organisation and maintenance of TLS in the infected SGs. In fact, in a transgenic mouse model of ELN in the thyroid, interaction between CD3$^+$CD4$^+$ T cells and CD11c$^+$ DCs is essential for TLS formation [251], while in an

influenza virus-induced TLS formation murine model, CD11c$^+$ DCs were necessary for TLS maintenance in the lungs but not for the initiation of ELN [58].

In support for a role of the above-mentioned cellular subsets in the formation of TLS, in a set of preliminary experiments I showed that inflammatory chemokines are more strongly expressed by F4/80$^+$/CD11c$^+$ cells present in the gland between days 2 and 4 after AdV delivery than between days 5 and 7. Conversely, in the same time frame, lymphoid chemokines expression, initially low or absent, increases. With these data in hand, it is tempting to speculate that resident macrophages and myeloid cells that infiltrate the gland rapidly after infection produce an initial set of chemotactic signals that promote further accumulation of inflammatory cells in the gland. The observed differentiation of inflammatory myeloid cells into macrophages and DCs that follows this initial phase, characterised by the downregulation of Ly6C expression and upregulation of F4/80 and CD11c markers, corresponds to a dampening of the inflammatory chemokines genes expression and an increase of the lymphocytes attracting signals, namely Ltβ, CCL19 and CXCL13. The positioning of CD11c$^+$ DCs relative to the lymphoid aggregates forming in the infected glands observed in IF also supports the idea that this subset in particular might actively participate to the secretion of chemotactic signals that first attract and then organise and maintain B and T cells infiltrates during the ELN process. This last point certainly deserves more studies (more detailed future plans are reported in Chapter 7), as the specific pattern of localisation for DCs and macrophages in relation to B and T cells that I described here for the first time might be extremely important for the formation and maintenance of

TLS structures in the SG mucosa and consequently for the development and progression of SS.

The possible high relevance of the myeloid compartment for the development of TLS in the SG is also indirectly supported by another set of experiment where I dissected the role of NK cells, a cellular type strongly involved in viral control and clearance, in the formation of these structures. When systemically and locally deprived of NK cells, wild-type mice still developed TLS with the same dynamic and magnitude of the control-treated animals. Interestingly, in contrast with other model of mucosal infection and inflammation [243], NK depletion also did not affect the number of infiltrating monocytes and the development of the macrophage and DC subsets in the AdV-treated SG compared to controls. Thus, not only the augmented presence of NK cells in the gland observed in the first week after infection is not paralleled by an efficient viral clearance as shown by the persistence of infected cells up to 4 weeks after cannulation, but NK cells are also dispensable for the monocytes infiltration and differentiation and TLS formation in this model. This, again, supports the idea that the SG mucosa differs from other tissues and other types of mucosa in terms of anti-viral defence and cross-talk with the peripheral and local myeloid compartment. Whether NK depletion affects viral persistence, salivary flow reduction and production of ANA upon SG infection is still to be tested, but given the observations reported above I expect that lack of NK cells might not influence viral clearance and thus the general progression of ELN in my model as it has been described in this thesis.

Thus, in this model induction of TLS likely derives from lack of viral clearance resulting in prolonged antigenic exposure which is a potent trigger for TLS

formation, as previously suggested in other models of ectopic lymphoid neogenesis such as chronic graft rejection {Thaunat:2010ec} and autoimmune insulitis in NOD mice [71]. Therefore, this model has the potential to unravel the intimate physiopathological viral-host interactions leading to the formation of TLS in SS.

In conclusion, I developed a novel model of AdV-induced lymphoid neogenesis which has the potential to shed light on the critical interactions between viral infection, formation of TLS, breach of immunological tolerance and exocrine dysfunction in the salivary glands, providing a suitable platform to investigate the mechanisms regulating TLS formation in response to viral infection and their role in the development of features typical of SS.

As a final remark, I would like to collate the observations that this model has already provided, and I have presented in this thesis, with previous literature to provide a hypothesis that links persistent viral infections, ELN in the salivary glands and development of breach of tolerance and autoimmunity.

From my preliminary data it is possible to speculate that resident and infiltrating myeloid cells, probably with the help of stromal cells, can activate the lymphoid chemokines pathway and trigger the initiation of the ELN program in response to pathogen infection of the salivary gland mucosa. In predisposed individuals, for example those with an aberrant activation of the type-I interferon pathway, viral infection might furthermore lead to an abnormal activation of NK and CD8^{+} T cells but also promote B cells survival and antibody production [153]. Ectopic lymphoid follicles forming in the SG, not only are favourable niches for lymphocytic activation and proliferation, but in response to infection they are

rich in autoantigens released by apoptotic and necrotic cells. Moreover, TLS could attract from the periphery autoreactive lymphocytes rescued from apoptosis by a persistent latent viral infection (e.g. EBV in B cells and HTLV-1 in T cells) [275] and promote their survival and differentiation toward disease-specific autoreactive cells [276],[277] eventually leading to the symptoms and manifestations of SS. This hypothesis is summarised in **Figure 6.1**.
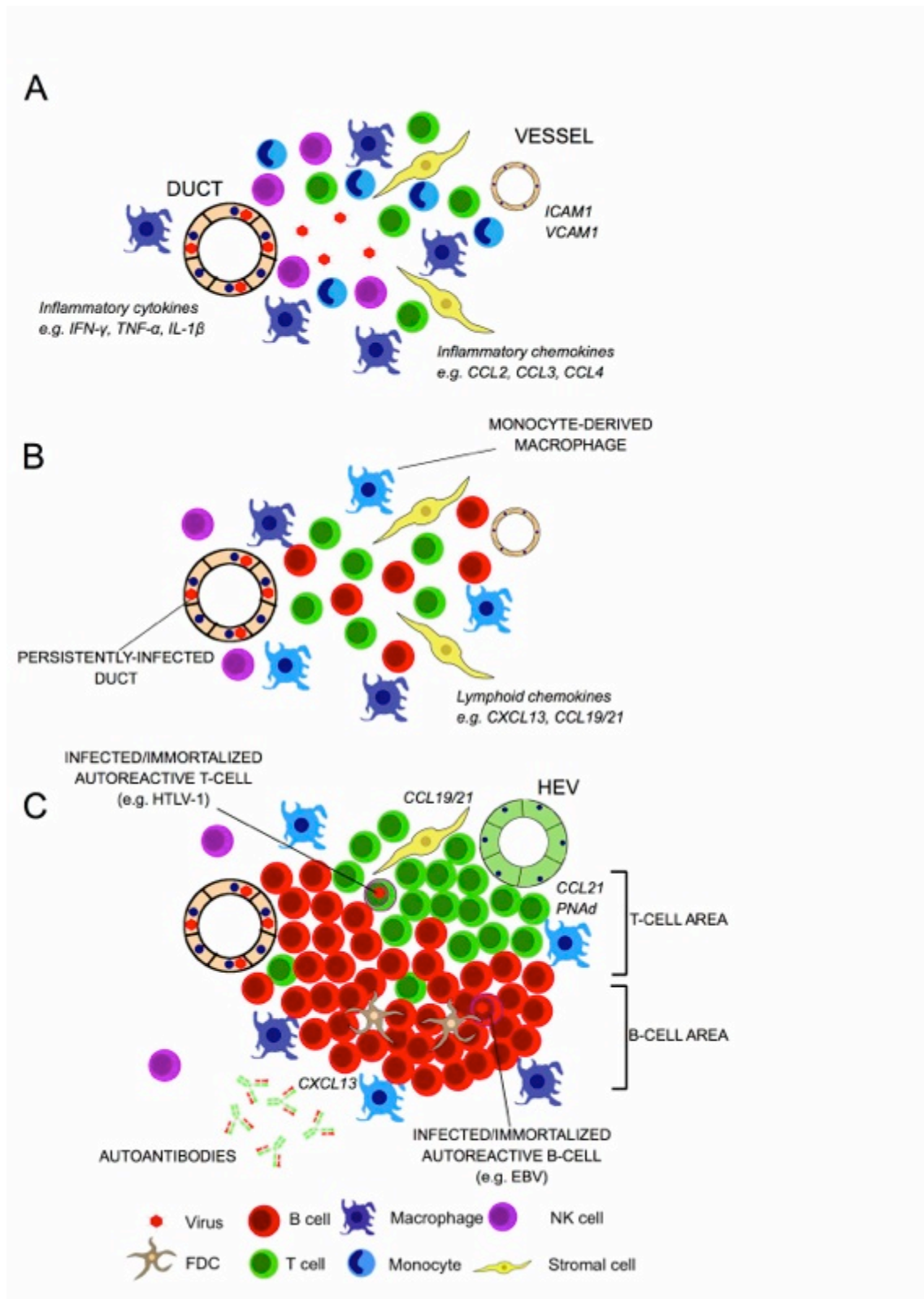
Figure 6.1: Evolution of TLS in response to viral infection in the SGs and development of autoimmunity. (**A**) Viral infection of the SG mucosa induces activation of epithelial and stromal cells and resident macrophages, triggering

the production of inflammatory chemokines and the expression of adhesion molecules on blood vessels, leading to the recruitment of innate immune cells from the peripheral compartment to the SG. Inflammatory chemokines attract inflammatory monocytes and within the first week from infection, T cells leading to the secretion of inflammatory cytokines (e.g., IFN-γ, TNF-α, IL-1β) that in turn, activate resident NK cells and drive macrophage polarization and a Th1-mediated antiviral response. (**B**) Despite potent antiviral immune responses, several viruses (e.g., CMV, EBV, and Coxsackie) can escape immune surveillance, leading to lack of viral clearance and persistent infection, preferentially within ductal epithelial cells. Chronic antigen stimulation promotes the ELN program. This triggers the activation of the LTβ pathway and the production of lymphoid chemokines CXCL13, CCL19, and CCL21 by stromal cells and monocyte-derived cells with the accumulation of B and T cells in the gland. (**C**) In the context of persistent chronic stimulation, the LTβ condition vessels to acquire a HEV phenotype with expression of PNAd, whereas CCL19 and CCL21 facilitate T lymphocyte influx and organize the T cell area of the ectopic follicle. Similarly, stromal cells via CXCL13 production promote the organization of the ectopic B cell follicle. Further differentiation of FDCs leads to the GC response, which is sustained by the production of B cell-activating cytokines, such as BAFF and IL-21, leading to in situ activation and proliferation of B cells. TLS fail to exclude autoreactive B cells from entering the ectopic GC, leading to breach of self-tolerance and development of autoimmunity. In this context, immune-modulating viruses, such as HTLV-1 in T cells and EBV in B cells, further promote autoreactive T and B cell survival in the periphery and their preferential recruitment in the ectopic B cell follicles, whereby autoreactive

EBV-infected B cells undergo plasma cell differentiation and autoantibody production. Republished with permission of Society of leukocytes biology, from [277], 2013; permission conveyed through Copyright Clearance Center, Inc.

Chapter 7 | Future plans

7 Future plans

The model that I have developed during my PhD and presented in this thesis has the main characteristic of being extremely flexible and apt to the study of several immunological pathways, spanning from host-pathogen interaction to the role of TLS formation in physiological conditions but also involving breach of self-tolerance and the onset of autoimmunity.

Despite the wide spectrum of extremely interesting questions that my model could potentially answer, there are several topics that I would like to tackle in the short and middle term. Specifically, in the short term I plan to i) complete the studies on the NK compartment and ii) strengthen the initial observations on the lymphoid chemokines expression by DCs and macrophages. In the medium term and according to the results produced by the short term experiments I plan to: iii) block the infiltration of and/or deplete the inflammatory monocytes to functionally prove the relevance of these cells in ELN formation; iv) track the inflammatory monocytes infiltration in the SG upon AdV delivery and prove their differentiation into resident macrophages and/or DCs.

I will now describe in some more details these goals.

i) Completion of the analysis of the NK cells role in the AdV-infected SG. Reports on the role of NK cells in the murine CMV-driven model of salivary gland infiltration are controversial [263],[265],[278]. I already showed in this thesis that NK cells depletion does not affect TLS formation and myeloid cells infiltration. In the discussion, I hypothesised that NK depletion would not affect the breach of tolerance observed in this model nor the viral clearance. If development of ANA is dependent on the formation of functional GC in the infected salivary glands and since NK depletion in my hands does not affect

ELN formation and functionality, I expect that NK cells absence will not modify the observed prevalence of anti-nuclear antibody generation. For the same reason, as viral presence and persistence seems to be essential for the formation and maintenance of TLS in the gland and absence of NK cells did not modify these processes, I expect that NK depleted mice will not have significant differences in the level of viral control.

To prove these hypotheses I plan to use the same experimental approach described above, i.e. cannulation of the salivary glands of depleted and control-treated mice, culling of the mice the third week post-procedure and collect serum for ANA test. Salivary gland collected at this time-point will be digested and prepared for luciferase assay. As a parallel approach to measure viral persistence, part of the gland tissue could be prepared for expression analysis using the reporter gene transcript as a target to prove whether NK cells absence changes the amount of virus-infected cells in the gland. Contextually, I plan to take advantage of an *in vivo* imaging system to monitor the luciferase activity in the gland of NK-depleted animals and control. The system has the advantage to allow continuous monitoring of the transgene activity and for this reason I plan to acquire reporter activity measures at several time points after cannulation, to test if there is a difference in the early versus late response to viral infection in NK-depleted mice in comparison to controls.

ii) Test the hypothesis that macrophages and DCs in the gland are producer of lymphoid chemokines and thus contribute to ELN formation and maintenance. In this thesis I showed that infiltrating monocytes potentially differentiate into macrophages and dendritic cells. I also presented preliminary

observations suggesting that these infiltrating myeloid cells, in line with previous literature in mouse lung infection [58],[279] and human SS SG [59], might contribute to the ELN program by expressing lymphoid chemokines toward the end of the first week after infection, thus favouring the influx of lymphocytes. Hence, as a further short-term goal, I plan to reinforce these observation with more targeted experiments. Namely a) FACS sorting of CD11c^{Hi} DCs and F4/80^{+} macrophages from AdV-treated mice glands collected at various time-points in the first three weeks after procedure and real time expression analysis on this population for the chemokines genes; b) double IF staining for lymphoid chemokines and CD11c or F4/80 on samples collected at various time-points. These two relatively simple experiments, if confirming the preliminary observations, would rapidly provide support to the hypothesised role of DCs and macrophages in TLS formation and maintenance. Moreover, this approach would also allow for discriminating the role of each specific population.

iii) Blockade/depletion of the SG infiltrating monocytes. According to the results of the plans reported in i) and ii), I envisage a more functional approach to assay the role of monocyte/macrophages/DC populations in ELN formation. Similarly to what I have done for NK cells, I plan to deplete circulating monocytes or to block their access to the AdV-treated gland. To do so, several strategies are available and I am already conducing preliminary experiments to identify the more suitable to my purposes. Clodronate-containing liposomes delivered intra-venously have proved to provide an efficient depletion of the circulating monocytes in several models [280]-[282]. The depletion is reported to be only temporary, as monocytes start to repopulate the blood as soon as 24

hours after depletion [280] and this could represent an issue for my model, as new a wave of recently bone-marrow emerged monocytes could infiltrate the gland even if the circulating counterpart has been efficiently depleted. Nevertheless, this seems a sound approach and a widely validated one, which deserves further investigation.

A different approach to the complete ablation of the monocyte population from blood would be to block the access of these cells to the infected salivary gland. To do so, I will need to understand the exact nature of the chemotactic gradient that drives the inflammatory influx. If I manage to achieve this, I can then try to block the inflammatory infiltration using chemokine-binding drugs or chemokine-receptors antagonists. The cells isolated from the gland via FACS sorting as described above would be my starting point in this project, as I plan to assay the expression levels of inflammatory chemokines and receptors in these populations at very early time-points after AdV-delivery (e.g. 1, 2, 4, 8, 12 hours post-cannulation). In parallel, I plan to collect SG from untreated wild-type mice and either digest the tissue and plate the cells and/or directly plate pieces of undigested tissue. I will then infect the wells with doses of AdV comparable to those used in the cannulation. Tissue and cells will be collected and analysed for inflammatory chemokines gene expression and supernatants will be assayed for chemokines presence. There are many monocyte-attracting chemokines and monocytes express several different chemokine receptors in an often redundant and overlapping fashion [246], thus isolating a sole chemokine responsible for inflammatory cells infiltration might prove difficult, but I am confident that I will be able to isolate at least some of the inflammatory chemokines pathways activated by AdV infection. As an alternative to this *ex*

vivo approach or in parallel to it, I could use an *in vitro* system: a murine salivary gland epithelial cell line is already present in this laboratory that I could culture and infect with the virus and analyse at various time-points to study the epithelial contribution to the chemotactic gradient.

iv) Monocyte infiltration and differentiation tracking *in vivo*. Another medium-term goal in the study of the relevance of the monocyte/macrophage family in the formation of TLS would be the tracking of the monocytes from the blood to the SG and the analysis of their final fate to demonstrate whether these cells can effectively differentiate in tissue macrophages and/or DC in the SG. To do so, in the context of my model I plan the passive transfer of blood or bone marrow monocytes from a wild-type untouched donor to a recipient animal, in the presence or absence of AdV-cannulation. Several approaches exist to track transferred cells: the labelling of monocytes from donor animals (e.g. CFSE labelling); the use of congenic strain to differentiate donor and recipient cells (e.g. CD45.1 versus CD45.2 animals); the use of the widely validated CX3CR1$^{gfp/gfp}$ transgenic mouse that also allows the identification of the different blood monocyte populations [283],[284] or a combination of these approaches. I have already started experiment with CFSE labelling and collected preliminary experiments in CX3CR1$^{gfp/gfp}$ transgenic mice, which support the hypothesis that inflammatory monocytes recruited following AdV infection enter the local myeloid pool.

All these experiments could hopefully provide some novel cellular target and molecular pathways in the context of ELN formation and breach of self-tolerance in response to viral infection that not only might shed new light on

these processes but could also be of relevance for the human counterpart. Specifically this model and the data that it could provide might help in dissecting the host-pathogen interactions in the SG mucosa and the role of TLS in the generation of protective immunity, but the findings could also pinpoint new targets useful to better understand the pathogenesis and evolution of SS disease.

List of publications related to this work

The work presented in this thesis lead to several publications.

Published papers in peer-reviewed international journals:

- Bombardieri M., F. Barone, D. Lucchesi, S. Nayar, W. B. van den Berg, G. Proctor, C. D. Buckley, C. Pitzalis "Inducible tertiary lymphoid structures, autoimmunity, and exocrine dysfunction in a novel model of salivary gland inflammation in C57BL/6 mice." Journal of Immunology, Volume 189, Issue 7, pp. 3767-3776, 2012.

- Lucchesi D., M. Bombardieri. "The role of viruses in autoreactive B cell activation within tertiary lymphoid structures in autoimmune diseases." Journal of leukocyte biology, Volume 94, Issue 6, pp. 1191-1199, 2013.

- Lucchesi D., C. Pitzalis, M. Bombardieri. "EBV and other viruses as triggers of tertiary lymphoid structures in primary Sjögren's syndrome." Expert review of clinical immunology, Volume 10, Issue 4, pp. 445-455, 2014.

Papers in preparation:

- Pontarini E. and Lucchesi D., Bombardieri M., D. Mavilio. "Recruitment and activation of NK cells in murine salivary glands regulate early immune response to viral infection but are dispensable for inducible lymphoneogenesis and autoimmunity"

- Murray-Brown W., Lucchesi D., Pontarini E., De Courcey J., Pitzalis C., M. Bombardieri. "Lesional expression of IL-21 correlates with ELS formation in Sjögren's syndrome patients salivary glands "

Appendix

Solution and buffers used for this work:

- **Complete culture medium for Hek293 cells**: Dulbecco-modified Eagle's medium (D-MEM) supplemented with 10% heat-inactivated FBS (Gibco), 100 µg/ml streptomycin and 100 U/ml penicillin G (Life technologies).

- **Infected cells collection buffer (100mM Tris pH 8):** 12.141 gr Trizma (Sigma) dissolved in 1 litre of distilled water, brought to pH with HCl

- **TD buffer:** NaCl 137 mM, KCl 5.1 mM, Na_2HPO_4 0.704 mM, Tris 24.8 mM brought to pH 7.5 with HCl

  - **CsCl gradient ρ=1.25:** 36.16 gr CsCl (Sigma) in 100 ml TD buffer

  - **CsCl gradient ρ=1.4:** 62 gr CsCl (Sigma) in 100 ml TD buffer

  - **CsCl gradient ρ=1.35:** 51.2 gr CsCl (Sigma) in 100 ml TD buffer

- **TSG buffer:** 90 ml solution A + 450 µl solution B + 38.4 ml glycerol

  - **Solution A:** NaCl 150 mM, KCl 5 mM, Na_2HPO_4 1 mM, Tris 30 mM (all from Sigma) brought to a final pH of 7.4

  - **Solution B:** $MgCl_2$ 200 mM, $CaCl_2$ 180 mM

- **Dialysis buffer:** Tris 10 mM, $MgCl_2$ 1 mM, NaCl 150 mM, 10% glycerol. Final pH 7.4.

- **1x PBS:** 144 mg/L KH_2PO_4, 9 gr/L NaCl, 796 mg/L Na_2HPO_4 without calcium and magnesium, pH 7.3-7.5 (Lonza)

- **XGal (β-galactosidase detection solution):** 1 mg/ml 5-bromo-4-chloro-3-indolyl-β-D-pyranoside, 5 mM $K_4[Fe(CN)_6]\cdot 3$ H2O, 5 mM $K_3[Fe(CN)_6]$, 5 mM EGTA, 2 mM $MgCl_2$, 0.02% NP-40 (all from Sigma) in PBS

- **TBS:** Tris 50 mM, NaCl 150 mM, pH 7.6

- **IF blocking/dilution buffer:** 1% bovine serum albumin (Sigma), 10% horse serum (Gibco) in TBS

- **RIPA biffer:** Tris 50 mM, NaCl 150 mM, sodium deoxycholate 0.5%, NP-40 1%, sodium dodecyl sulphate 0.1%, pH 8

- **5x Laemli solution:** sodium dodecyl sulphate 10%, glycerol 50%, β-mercaptoethanol 25%, bromphenol blue 0.01% and Tris 0.312 M, pH 6.8

- **PAGE running buffer:** MOPS 5 mM, Tris 5 mM, sodium dodecyl sulphate 0.1%, EDTA 0.1 mM

- **ANA dilution/blocking buffer:** BSA 2%, Tween-20 0.05% in PBS

- **Carbonate/bicarbonate buffer:** carbonate/bicarbonate 0.5 M, pH 9.6 at 25°C (capsules from Sigma reconstituted in distilled water)

- **Tissue digestion buffer:** 2% foetal bovine serum (Life Technologies), 3.7 mg/ml collagenase-D (Roche), 30 µg/ml DNAse-I (Sigma) in RPMI-1640 (Gibco)

- **FACS buffer:** 2% foetal bovine serum (Life Technologies) in PBS

References

1. **Mebius RE**, **Kraal G**. Structure and function of the spleen. *Nature Publishing Group*. 2005; **5**:606–616.DOI: 10.1038/nri1669.

2. **Drayton DL**, **Liao S**, **Mounzer RH**, **Ruddle NH**. Lymphoid organ development: from ontogeny to neogenesis. *Nat Immunol*. 2006; **7**:344–353.DOI: 10.1038/ni1330.

3. **Aloisi F**, **Pujol-Borrell R**. Lymphoid neogenesis in chronic inflammatory diseases. *Nature Publishing Group*. 2006; **6**:205–217.DOI: 10.1038/nri1786.

4. **Sansonno D**, **Lauletta G**, **De Re V**, **Tucci FA**, **Gatti P**, **Racanelli V**, **Boiocchi M**, *et al.* Intrahepatic B cell clonal expansions and extrahepatic manifestations of chronic HCV infection. *Eur. J. Immunol.* 2004; **34**:126–136.DOI: 10.1002/eji.200324328.

5. **Ghosh S**, **Steere AC**, **Stollar BD**, **Huber BT**. In situ diversification of the antibody repertoire in chronic Lyme arthritis synovium. *J. Immunol.* 2005; **174**:2860–2869.

6. **Winter S**, **Loddenkemper C**, **Aebischer A**, **Räbel K**, **Hoffmann K**, **Meyer TF**, **Lipp M**, *et al.* The chemokine receptor CXCR5 is pivotal for ectopic mucosa-associated lymphoid tissue neogenesis in chronic Helicobacter pylori-induced inflammation. *J Mol Med*. 2010; **88**:1169–1180.DOI: 10.1007/s00109-010-0658-6.

7. **Cipponi A**, **Mercier M**, **Seremet T**, **Baurain J-F**, **Théate I**, **van den Oord J**, **Stas M**, *et al.* Neogenesis of lymphoid structures and antibody responses occur in human melanoma metastases. *Cancer Research*. 2012; **72**:3997–4007.DOI: 10.1158/0008-5472.CAN-12-1377.

8. **Coronella JA**, **Spier C**, **Welch M**, **Trevor KT**, **Stopeck AT**, **Villar H**, **Hersh EM**. Antigen-driven oligoclonal expansion of tumor-infiltrating B cells in infiltrating ductal carcinoma of the breast. *J. Immunol.* 2002; **169**:1829–1836.

9. **Dieu-Nosjean MC**, **Antoine M**, **Danel C**, **Heudes D**, **Wislez M**, **Poulot V**, **Rabbe N**, *et al.* Long-Term Survival for Patients With Non-Small-Cell Lung Cancer With Intratumoral Lymphoid Structures. *Journal of Clinical Oncology*. 2008; **26**:4410–4417.DOI: 10.1200/JCO.2007.15.0284.

10. **Pagès F**, **Galon J**, **Dieu-Nosjean MC**, **Tartour E**, **Sautès-Fridman C**, **Fridman WH**. Immune infiltration in human tumors: a prognostic factor that should not be ignored. *Oncogene*. 2009; **29**:1093–1102.DOI: 10.1038/onc.2009.416.

11. **Cheng J**, **Torkamani A**, **Grover RK**, **Jones TM**, **Ruiz DI**, **Schork NJ**, **Quigley MM**, *et al.* Ectopic B-cell clusters that infiltrate transplanted human kidneys are clonal. *Proc. Natl. Acad. Sci. U.S.A.* 2011; **108**:5560–5565.DOI:

10.1073/pnas.1101148108.

12. **Kerjaschki D**, **Regele HM**, **Moosberger I**, **Nagy-Bojarski K**, **Watschinger B**, **Soleiman A**, **Birner P**, *et al.* Lymphatic neoangiogenesis in human kidney transplants is associated with immunologically active lymphocytic infiltrates. *J. Am. Soc. Nephrol.* 2004; **15**:603–612.

13. **Thaunat O**, **Nicoletti A**. Lymphoid neogenesis in chronic rejection. *Current Opinion in Organ Transplantation*. 2008; **13**:16–19.DOI: 10.1097/MOT.0b013e3282f3df15.

14. **Manzo A**, **Bombardieri M**, **Humby F**, **Pitzalis C**. Secondary and ectopic lymphoid tissue responses in rheumatoid arthritis: from inflammation to autoimmunity and tissue damage/remodeling. *Immunol. Rev.* 2010; **233**:267–285.DOI: 10.1111/j.0105-2896.2009.00861.x.

15. **Shikh El MEM**, **Pitzalis C**. Follicular dendritic cells in health and disease. *Front Immunol*. 2012; **3**:292.DOI: 10.3389/fimmu.2012.00292.

16. **Miyasaka M**, **Tanaka T**. Lymphocyte trafficking across high endothelial venules: dogmas and enigmas. *Nat Rev Immunol*. 2004; **4**:360–370.DOI: 10.1038/nri1354.

17. **Andrian von UH**, **Mempel TR**. Homing and cellular traffic in lymph nodes. *Nat Rev Immunol*. 2003; **3**:867–878.DOI: 10.1038/nri1222.

18. **Chen S-C**, **Vassileva G**, **Kinsley D**, **Holzmann S**, **Manfra D**, **Wiekowski MT**, **Romani N**, *et al.* Ectopic expression of the murine chemokines CCL21a and CCL21b induces the formation of lymph node-like structures in pancreas, but not skin, of transgenic mice. *J. Immunol.* 2002; **168**:1001–1008.

19. **Luther SA**, **Bidgol A**, **Hargreaves DC**, **Schmidt A**, **Xu Y**, **Paniyadi J**, **Matloubian M**, *et al.* Differing activities of homeostatic chemokines CCL19, CCL21, and CXCL12 in lymphocyte and dendritic cell recruitment and lymphoid neogenesis. *J. Immunol.* 2002; **169**:424–433.

20. **Luther SA**, **Lopez T**, **Bai W**, **Hanahan D**, **Cyster JG**. BLC expression in pancreatic islets causes B cell recruitment and lymphotoxin-dependent lymphoid neogenesis. *Immunity*. 2000; **12**:471–481.

21. **Carlsen HS**. Disparate lymphoid chemokine expression in mice and men: no evidence of CCL21 synthesis by human high endothelial venules. *Blood*. 2005; **106**:444–446.DOI: 10.1182/blood-2004-11-4353.

22. **Link A**, **Vogt TK**, **Favre S**, **Britschgi MR**, **Acha-Orbea H**, **Hinz B**, **Cyster JG**, *et al.* Fibroblastic reticular cells in lymph nodes regulate the homeostasis of naive T cells. *Nat Immunol*. 2007; **8**:1255–1265.DOI: 10.1038/ni1513.

23. **Gunn MD**, **Ngo VN**, **Ansel KM**, **Ekland EH**, **Cyster JG**, **Williams LT**. A B-cell-homing chemokine made in lymphoid follicles activates Burkitt's lymphoma receptor-1. *Nature*. 1998; **391**:799–803.DOI: 10.1038/35876.

24. **King C**, **Tangye SG**, **Mackay CR**. T Follicular Helper (T FH) Cells in Normal and Dysregulated Immune Responses. *Annu. Rev. Immunol.* 2008; **26**:741–766.DOI: 10.1146/annurev.immunol.26.021607.090344.

25. **Linterman MA**, **Beaton L**, **Yu D**, **Ramiscal RR**, **Srivastava M**, **Hogan JJ**, **Verma NK**, *et al.* IL-21 acts directly on B cells to regulate Bcl-6 expression and germinal center responses. *Journal of Experimental Medicine.* 2010; **207**:353–363.DOI: 10.1084/jem.20091738.

26. **Vissers JL**, **Hartgers FC**, **Lindhout E**, **Figdor CG**, **Adema GJ**. BLC (CXCL13) is expressed by different dendritic cell subsets in vitro and in vivo. *Eur. J. Immunol.* 2001; **31**:1544–1549.

27. **Lane PJL**, **McConnell FM**, **Withers D**, **Gaspal F**, **Saini M**, **Anderson G**. Lymphoid tissue inducer cells: bridges between the ancient innate and the modern adaptive immune systems. *Mucosal Immunol.* 2009; **2**:472–477.DOI: 10.1038/mi.2009.111.

28. **León B**, **Ballesteros-Tato A**, **Browning JL**, **Dunn R**, **Randall TD**, **Lund FE**. Regulation of T(H)2 development by CXCR5+ dendritic cells and lymphotoxin-expressing B cells. *Nature Publishing Group.* 2012; **13**:681–690.DOI: 10.1038/ni.2309.

29. **Manzo A**, **Paoletti S**, **Carulli M**, **Blades MC**, **Barone F**, **Yanni G**, **Fitzgerald O**, *et al.* Systematic microanatomical analysis of CXCL13 and CCL21 in situ production and progressive lymphoid organization in rheumatoid synovitis. *Eur. J. Immunol.* 2005; **35**:1347–1359.DOI: 10.1002/eji.200425830.

30. **Amft N**, **Curnow SJ**, **Scheel-Toellner D**, **Devadas A**, **Oates J**, **Crocker J**, **Hamburger J**, *et al.* Ectopic expression of the B cell-attracting chemokine BCA-1 (CXCL13) on endothelial cells and within lymphoid follicles contributes to the establishment of germinal center-like structures in Sjögren's syndrome. *Arthritis Rheum.* 2001; **44**:2633–2641.

31. **Barone F**, **Bombardieri M**, **Manzo A**, **Blades MC**, **Morgan PR**, **Challacombe SJ**, **Valesini G**, *et al.* Association of CXCL13 and CCL21 expression with the progressive organization of lymphoid-like structures in Sjögren's syndrome. *Arthritis Rheum.* 2005; **52**:1773–1784.DOI: 10.1002/art.21062.

32. **Salomonsson S**, **Jonsson MV**, **Skarstein K**, **Brokstad KA**, **Hjelmström P**, **Wahren-Herlenius M**, **Jonsson R**. Cellular basis of ectopic germinal center formation and autoantibody production in the target organ of patients with Sjögren's syndrome. *Arthritis Rheum.* 2003; **48**:3187–3201.DOI: 10.1002/art.11311.

33. **Serafini B**, **Rosicarelli B**, **Magliozzi R**, **Stigliano E**, **Aloisi F**. Detection of ectopic B-cell follicles with germinal centers in the meninges of patients with secondary progressive multiple sclerosis. *Brain Pathol.* 2004; **14**:164–174.

34. **Armengol M-P**, **Cardoso-Schmidt CB**, **Fernández M**, **Ferrer X**, **Pujol-**

Borrell R, **Juan M**. Chemokines determine local lymphoneogenesis and a reduction of circulating CXCR4+ T and CCR7 B and T lymphocytes in thyroid autoimmune diseases. *J. Immunol.* 2003; **170**:6320–6328.

35. **Armengol MP**, **Juan M**, **Lucas-Martín A**, **Fernández-Figueras MT**, **Jaraquemada D**, **Gallart T**, **Pujol-Borrell R**. Thyroid autoimmune disease: demonstration of thyroid antigen-specific B cells and recombination-activating gene expression in chemokine-containing active intrathyroidal germinal centers. *Am. J. Pathol.* 2001; **159**:861–873.DOI: 10.1016/S0002-9440(10)61762-2.

36. **Klein U**, **Dalla-Favera R**. Germinal centres: role in B-cell physiology and malignancy. *Nature Publishing Group*. 2008; **8**:22–33.DOI: 10.1038/nri2217.

37. **Muramatsu M**, **Kinoshita K**, **Fagarasan S**, **Yamada S**, **Shinkai Y**, **Honjo T**. Class switch recombination and hypermutation require activation-induced cytidine deaminase (AID), a potential RNA editing enzyme. *Cell*. 2000; **102**:553–563.

38. **Bombardieri M**, **Barone F**, **Humby F**, **Kelly S**, **McGurk M**, **Morgan P**, **Challacombe S**, *et al.* Activation-induced cytidine deaminase expression in follicular dendritic cell networks and interfollicular large B cells supports functionality of ectopic lymphoid neogenesis in autoimmune sialoadenitis and MALT lymphoma in Sjögren's syndrome. *J. Immunol.* 2007; **179**:4929–4938.

39. **Humby F**, **Bombardieri M**, **Manzo A**, **Kelly S**, **Blades MC**, **Kirkham B**, **Spencer J**, *et al.* Ectopic lymphoid structures support ongoing production of class-switched autoantibodies in rheumatoid synovium. Humby F, Bombardieri M, Manzo A, Kelly S, Blades MC, Kirkham B, Spencer J, et al., eds. *Plos Med*. 2009; **6**:e1. Available at: http://www.plosmedicine.org/article/fetchSingleRepresentation.action?uri=info:doi/10.1371/journal.pmed.0060001.sd003.DOI: 10.1371/journal.pmed.0060001.sd003.

40. **Thaunat O**, **Field A-C**, **Dai J**, **Louedec L**, **Patey N**, **Bloch M-F**, **Mandet C**, *et al.* Lymphoid neogenesis in chronic rejection: evidence for a local humoral alloimmune response. *Proc. Natl. Acad. Sci. U.S.A.* 2005; **102**:14723–14728.DOI: 10.1073/pnas.0507223102.

41. **Leprince C**, **Cohen-Kaminsky S**, **Berrih-Aknin S**, **Vernet-Der Garabedian B**, **Treton D**, **Galanaud P**, **Richard Y**. Thymic B cells from myasthenia gravis patients are activated B cells. Phenotypic and functional analysis. *J. Immunol.* 1990; **145**:2115–2122.

42. **Grewal JS**, **Pilgrim MJ**, **Grewal S**, **Kasman L**, **Werner P**, **Bruorton ME**, **London SD**, *et al.* Salivary glands act as mucosal inductive sites via the formation of ectopic germinal centers after site-restricted MCMV infection. *The FASEB Journal*. 2011; **25**:1680–1696.DOI: 10.1096/fj.10-174656.

43. **Moyron-Quiroz JE**, **Rangel-Moreno J**, **Hartson L**, **Kusser K**, **Tighe MP**, **Klonowski KD**, **Lefrançois L**, *et al.* Persistence and responsiveness of immunologic memory in the absence of secondary lymphoid organs. *Immunity*.

2006; **25**:643–654.DOI: 10.1016/j.immuni.2006.08.022.

44. **Mebius RE**. Organogenesis of lymphoid tissues. *Nat Rev Immunol*. 2003; **3**:292–303.DOI: 10.1038/nri1054.

45. **Sun Z**, **Unutmaz D**, **Zou YR**, **Sunshine MJ**, **Pierani A**, **Brenner-Morton S**, **Mebius RE**, *et al.* Requirement for RORgamma in thymocyte survival and lymphoid organ development. *Science*. 2000; **288**:2369–2373.

46. **Rennert PD**, **Browning JL**, **Mebius R**, **Mackay F**, **Hochman PS**. Surface lymphotoxin alpha/beta complex is required for the development of peripheral lymphoid organs. *J. Exp. Med.* 1996; **184**:1999–2006.

47. **Pitzalis C**, **Jones GW**, **Bombardieri M**, **Jones SA**. Ectopic lymphoid-like structures in infection, cancer and autoimmunity. *Nat Rev Immunol*. 2014; **14**:447–462.DOI: 10.1038/nri3700.

48. **Kim M-Y**, **McConnell FM**, **Gaspal FMC**, **White A**, **Glanville SH**, **Bekiaris V**, **Walker LSK**, *et al.* Function of CD4+CD3- cells in relation to B- and T-zone stroma in spleen. *Blood*. 2007; **109**:1602–1610.DOI: 10.1182/blood-2006-04-018465.

49. **Schmutz S**, **Bosco N**, **Chappaz S**, **Boyman O**, **Acha-Orbea H**, **Ceredig R**, **Rolink AG**, *et al.* Cutting Edge: IL-7 Regulates the Peripheral Pool of Adult ROR + Lymphoid Tissue Inducer Cells. *The Journal of Immunology*. 2009; **183**:2217–2221.DOI: 10.4049/jimmunol.0802911.

50. **Peters A**, **Pitcher LA**, **Sullivan JM**, **Mitsdoerffer M**. Th17 Cells Induce Ectopic Lymphoid Follicles in Central Nervous System Tissue Inflammation. *Immunity*. 2011.

51. **Rangel-Moreno J**, **Hartson L**, **Navarro C**, **Gaxiola M**, **Selman M**, **Randall TD**. Inducible bronchus-associated lymphoid tissue (iBALT) in patients with pulmonary complications of rheumatoid arthritis. *Journal of Clinical Investigation*. 2006; **116**:3183–3194.DOI: 10.1172/JCI28756.

52. **Deteix C**, **Attuil-Audenis V**, **Duthey A**, **Patey N**, **McGregor B**, **Dubois V**, **Caligiuri G**, *et al.* Intragraft Th17 Infiltrate Promotes Lymphoid Neogenesis and Hastens Clinical Chronic Rejection. *The Journal of Immunology*. 2010; **184**:5344–5351.DOI: 10.4049/jimmunol.0902999.

53. **Spits H**, **Di Santo JP**. The expanding family of innate lymphoid cells: regulators and effectors of immunity and tissue remodeling. *Nature Publishing Group*. 2010; **12**:21–27. Available at: http://www.nature.com/doifinder/10.1038/ni.1962.DOI: doi:10.1038/ni.1962.

54. **Sawa S**, **Cherrier M**, **Lochner M**, **Satoh-Takayama N**, **Fehling HJ**, **Langa F**, **Di Santo JP**, *et al.* Lineage relationship analysis of RORgammat+ innate lymphoid cells. *Science*. 2010; **330**:665–669.DOI: 10.1126/science.1194597.

55. **Lochner M**, **Ohnmacht C**, **Presley L**, **Bruhns P**, **Si-Tahar M**, **Sawa S**, **Eberl G**. Microbiota-induced tertiary lymphoid tissues aggravate inflammatory

disease in the absence of RORgamma t and LTi cells. *Journal of Experimental Medicine*. 2011; **208**:125–134.DOI: 10.1084/jem.20100052.

56. **Furtado GC**, **Pacer ME**, **Bongers G**, **Bénézech C**, **He Z**, **Chen L**, **Berin MC**, *et al.* TNFα-dependent development of lymphoid tissue in the absence of RORγt⁺ lymphoid tissue inducer cells. *Mucosal Immunol*. 2014; **7**:602–614.DOI: 10.1038/mi.2013.79.

57. **Perrier P**, **Martinez FO**, **LOCATI M**, **Bianchi G**, **Nebuloni M**, **Vago G**, **Bazzoni F**, *et al.* Distinct Transcriptional Programs Activated by Interleukin-10 with or without Lipopolysaccharide in Dendritic Cells: Induction of the B Cell-Activating Chemokine, CXC Chemokine Ligand 13. *The Journal of Immunology*. 2004; **172**:7031–7042.DOI: 10.4049/jimmunol.172.11.7031.

58. **GeurtsvanKessel CH**, **Willart MAM**, **Bergen IM**, **van Rijt LS**, **Muskens F**, **Elewaut D**, **Osterhaus ADME**, *et al.* Dendritic cells are crucial for maintenance of tertiary lymphoid structures in the lung of influenza virus-infected mice. *Journal of Experimental Medicine*. 2009; **206**:2339–2349.DOI: 10.1084/jem.20090410.

59. **Carlsen HS**, **Baekkevold ES**, **Morton HC**, **Haraldsen G**, **Brandtzaeg P**. Monocyte-like and mature macrophages produce CXCL13 (B cell-attracting chemokine 1) in inflammatory lesions with lymphoid neogenesis. *Blood*. 2004; **104**:3021–3027.DOI: 10.1182/blood-2004-02-0701.

60. **Evans HG**, **Gullick NJ**, **Kelly S**, **Pitzalis C**, **Lord GM**, **Kirkham BW**, **Taams LS**. In vivo activated monocytes from the site of inflammation in humans specifically promote Th17 responses. *Proc. Natl. Acad. Sci. U.S.A.* 2009; **106**:6232–6237.DOI: 10.1073/pnas.0808144106.

61. **Firestein GS**. Evolving concepts of rheumatoid arthritis. *Nature*. 2003; **423**:356–361.DOI: 10.1038/nature01661.

62. **Thurlings RM**, **Wijbrandts CA**, **Mebius RE**, **Cantaert T**, **Dinant HJ**, **van der Pouw-Kraan TCTM**, **Verweij CL**, *et al.* Synovial lymphoid neogenesis does not define a specific clinical rheumatoid arthritis phenotype. *Arthritis Rheum*. 2008; **58**:1582–1589.DOI: 10.1002/art.23505.

63. **Cañete JD**, **Celis R**, **Moll C**, **Izquierdo E**, **Marsal S**, **Sanmartí R**, **Palacín A**, *et al.* Clinical significance of synovial lymphoid neogenesis and its reversal after anti-tumour necrosis factor alpha therapy in rheumatoid arthritis. *Annals of the Rheumatic Diseases*. 2009; **68**:751–756.DOI: 10.1136/ard.2008.089284.

64. **Corsiero E**, **Bombardieri M**, **Manzo A**, **Bugatti S**, **Uguccioni M**, **Pitzalis C**. Role of lymphoid chemokines in the development of functional ectopic lymphoid structures in rheumatic autoimmune diseases. *Immunol. Lett.* 2012; **145**:62–67.DOI: 10.1016/j.imlet.2012.04.013.

65. **Manzo A**, **Vitolo B**, **Humby F**, **Caporali R**, **Jarrossay D**, **Dell'accio F**, **Ciardelli L**, *et al.* Mature antigen-experienced T helper cells synthesize and secrete the B cell chemoattractant CXCL13 in the inflammatory environment of

the rheumatoid joint. *Arthritis Rheum.* 2008; **58**:3377–3387.DOI: 10.1002/art.23966.

66. **Cantaert T**, **Kolln J**, **Timmer T**, **van der Pouw Kraan TC**, **Vandooren B**, **Thurlings RM**, **Cañete JD**, *et al.* B lymphocyte autoimmunity in rheumatoid synovitis is independent of ectopic lymphoid neogenesis. *J. Immunol.* 2008; **181**:785–794.

67. **Zuckerman NS**, **Howard WA**, **Bismuth J**, **Gibson K**, **Edelman H**, **Berrih-Aknin S**, **Dunn-Walters D**, *et al.* Ectopic GC in the thymus of myasthenia gravis patients show characteristics of normal GC. *Eur. J. Immunol.* 2010; **40**:1150–1161.DOI: 10.1002/eji.200939914.

68. **Meraouna A**, **Cizeron-Clairac G**, **Panse RL**, **Bismuth J**, **Truffault F**, **Tallaksen C**, **Berrih-Aknin S**. The chemokine CXCL13 is a key molecule in autoimmune myasthenia gravis. *Blood.* 2006; **108**:432–440.DOI: 10.1182/blood-2005-06-2383.

69. **Silveira PA**, **Grey ST**. B cells in the spotlight: innocent bystanders or major players in the pathogenesis of type 1 diabetes. *Trends in Endocrinology & Metabolism.* 2006; **17**:128–135.DOI: 10.1016/j.tem.2006.03.006.

70. **Noorchashm H**, **Noorchashm N**, **Kern J**, **Rostami SY**, **Barker CF**, **Naji A**. B-cells are required for the initiation of insulitis and sialitis in nonobese diabetic mice. *Diabetes.* 1997; **46**:941–946.

71. **Astorri E**, **Bombardieri M**, **Gabba S**, **Peakman M**, **Pozzilli P**, **Pitzalis C**. Evolution of Ectopic Lymphoid Neogenesis and In Situ Autoantibody Production in Autoimmune Nonobese Diabetic Mice: Cellular and Molecular Characterization of Tertiary Lymphoid Structures in Pancreatic Islets. *The Journal of Immunology.* 2010; **185**:3359–3368.DOI: 10.4049/jimmunol.1001836.

72. **Kendall PL**, **Yu G**, **Woodward EJ**, **Thomas JW**. Tertiary Lymphoid Structures in the Pancreas Promote Selection of B Lymphocytes in Autoimmune Diabetes. *The Journal of ….* 2007.

73. **Cross AH**, **Waubant E**. MS and the B cell controversy. *Biochim. Biophys. Acta.* 2011; **1812**:231–238.DOI: 10.1016/j.bbadis.2010.07.020.

74. **Magliozzi R**, **Columba-Cabezas S**, **Serafini B**, **Aloisi F**. Intracerebral expression of CXCL13 and BAFF is accompanied by formation of lymphoid follicle-like structures in the meninges of mice with relapsing experimental autoimmune encephalomyelitis. *J. Neuroimmunol.* 2004; **148**:11–23.DOI: 10.1016/j.jneuroim.2003.10.056.

75. **Magliozzi R**, **Howell O**, **Vora A**, **Serafini B**, **Nicholas R**, **Puopolo M**, **Reynolds R**, *et al.* Meningeal B-cell follicles in secondary progressive multiple sclerosis associate with early onset of disease and severe cortical pathology. *Brain.* 2006; **130**:1089–1104.DOI: 10.1093/brain/awm038.

76. **Mazzucchelli L**, **Blaser A**, **Kappeler A**, **Schärli P**, **Laissue JA**, **Baggiolini M**, **Uguccioni M**. BCA-1 is highly expressed in Helicobacter pylori-induced

mucosa-associated lymphoid tissue and gastric lymphoma. *Journal of Clinical Investigation*. 1999; **104**:R49–54.DOI: 10.1172/JCI7830.

77. **Kobayashi M**, **Mitoma J**, **Nakamura N**, **Katsuyama T**, **Nakayama J**, **Fukuda M**. Induction of peripheral lymph node addressin in human gastric mucosa infected by Helicobacter pylori. *Proc. Natl. Acad. Sci. U.S.A.* 2004; **101**:17807–17812.DOI: 10.1073/pnas.0407503101.

78. **Genta RM**, **Lew GM**, **Graham DY**. Changes in the gastric mucosa following eradication of Helicobacter pylori. *Mod. Pathol.* 1993; **6**:281–289.

79. **Genta RM**, **Hamner HW**, **Graham DY**. Gastric lymphoid follicles in Helicobacter pylori infection: frequency, distribution, and response to triple therapy. *Hum. Pathol.* 1993; **24**:577–583.

80. **Bayerdörffer E**, **Neubauer A**, **Rudolph B**, **Thiede C**, **Lehn N**, **Eidt S**, **Stolte M**. Regression of primary gastric lymphoma of mucosa-associated lymphoid tissue type after cure of Helicobacter pylori infection. MALT Lymphoma Study Group. *Lancet*. 1995; **345**:1591–1594.

81. **Ramakrishnan L**. Revisiting the role of the granuloma intuberculosis. *Nat Rev Immunol*. 2012; **12**:352–366.DOI: 10.1038/nri3211.

82. **Ulrichs T**, **Kosmiadi GA**, **Trusov V**, **Jörg S**, **Pradl L**, **Titukhina M**, **Mishenko V**, *et al.* Human tuberculous granulomas induce peripheral lymphoid follicle-like structures to orchestrate local host defence in the lung. *J. Pathol.* 2004; **204**:217–228.DOI: 10.1002/path.1628.

83. **Khader SA**, **Rangel-Moreno J**, **Fountain JJ**, **Martino CA**, **Reiley WW**, **Pearl JE**, **Winslow GM**, *et al.* In a murine tuberculosis model, the absence of homeostatic chemokines delays granuloma formation and protective immunity. *The Journal of Immunology*. 2009; **183**:8004–8014.DOI: 10.4049/jimmunol.0901937.

84. **Kahnert A**, **Höpken UE**, **Stein M**, **Bandermann S**, **Lipp M**, **Kaufmann SHE**. Mycobacterium tuberculosis triggers formation of lymphoid structure in murine lungs. *J Infect Dis*. 2007; **195**:46–54.DOI: 10.1086/508894.

85. **Steere AC**, **Duray PH**, **Butcher EC**. Spirochetal antigens and lymphoid cell surface markers in Lyme synovitis. Comparison with rheumatoid synovium and tonsillar lymphoid tissue. *Arthritis Rheum*. 1988; **31**:487–495.

86. **Rangel-Moreno J**, **Carragher D**, **Randall TD**. Role of lymphotoxin and homeostatic chemokines in the development and function of local lymphoid tissues in the respiratory tract. *Inmunologia*. 2007; **26**:13–28.

87. **Xu B**, **Wagner N**, **Pham LN**, **Magno V**, **Shan Z**, **Butcher EC**, **Michie SA**. Lymphocyte homing to bronchus-associated lymphoid tissue (BALT) is mediated by L-selectin/PNAd, alpha4beta1 integrin/VCAM-1, and LFA-1 adhesion pathways. *J. Exp. Med.* 2003; **197**:1255–1267.DOI: 10.1084/jem.20010685.

88. **Rangel-Moreno J**, **Moyron-Quiroz JE**, **Hartson L**, **Kusser K**, **Randall TD**. Pulmonary expression of CXC chemokine ligand 13, CC chemokine ligand 19, and CC chemokine ligand 21 is essential for local immunity to influenza. *Proc. Natl. Acad. Sci. U.S.A.* 2007; **104**:10577–10582.DOI: 10.1073/pnas.0700591104.

89. **Cervenak L**, **Magyar A**, **Boja R**, **László G**. Differential expression of GL7 activation antigen on bone marrow B cell subpopulations and peripheral B cells. *Immunol. Lett.* 2001; **78**:89–96.

90. **Moyron-Quiroz JE**, **Rangel-Moreno J**, **Kusser K**, **Hartson L**, **Sprague F**, **Goodrich S**, **Woodland DL**, *et al.* Role of inducible bronchus associated lymphoid tissue (iBALT) in respiratory immunity. *Nature Medicine*. 2004; **10**:927–934.DOI: 10.1038/nm1091.

91. **Lund FE**, **Partida-Sánchez S**, **Lee BO**, **Kusser KL**, **Hartson L**, **Hogan RJ**, **Woodland DL**, *et al.* Lymphotoxin-alpha-deficient mice make delayed, but effective, T and B cell responses to influenza. *J. Immunol.* 2002; **169**:5236–5243.

92. **Cerny A**, **Chisari FV**. Pathogenesis of chronic hepatitis C: immunological features of hepatic injury and viral persistence. *Hepatology*. 1999; **30**:595–601.DOI: 10.1002/hep.510300312.

93. **Mosnier JF**, **Degott C**, **Marcellin P**, **Hénin D**, **Erlinger S**, **Benhamou JP**. The intraportal lymphoid nodule and its environment in chronic active hepatitis C: an immunohistochemical study. *Hepatology*. 1993; **17**:366–371.

94. **Murakami J**, **Shimizu Y**, **Kashii Y**, **Kato T**, **Minemura M**, **Okada K**, **Nambu S**, *et al.* Functional B-cell response in intrahepatic lymphoid follicles in chronic hepatitis C. *Hepatology*. 1999; **30**:143–150.DOI: 10.1002/hep.510300107.

95. **Minutello MA**, **Pileri P**, **Unutmaz D**, **Censini S**, **Kuo G**, **Houghton M**, **Brunetto MR**, *et al.* Compartmentalization of T lymphocytes to the site of disease: intrahepatic CD4+ T cells specific for the protein NS4 of hepatitis C virus in patients with chronic hepatitis C. *J. Exp. Med.* 1993; **178**:17–25.

96. **Thimme R**, **Oldach D**, **Chang KM**, **Steiger C**, **Ray SC**, **Chisari FV**. Determinants of viral clearance and persistence during acute hepatitis C virus infection. *J. Exp. Med.* 2001; **194**:1395–1406.

97. **Terilli RR**, **Cox AL**. Immunity and hepatitis C: a review. *Curr HIV/AIDS Rep*. 2013; **10**:51–58.DOI: 10.1007/s11904-012-0146-4.

98. **Farci P**, **Alter HJ**, **Govindarajan S**, **Wong DC**, **Engle R**, **Lesniewski RR**, **Mushahwar IK**, *et al.* Lack of protective immunity against reinfection with hepatitis C virus. *Science*. 1992; **258**:135–140.

99. **Horner SM**, **Gale M**. Regulation of hepatic innate immunity by hepatitis C virus. *Nature Medicine*. 2013; **19**:879–888.DOI: 10.1038/nm.3253.

100. **Holz LE**, **Yoon JC**, **Raghuraman S**, **Moir S**, **Sneller MC**, **Rehermann B**. B cell homeostasis in chronic hepatitis C virus-related mixed cryoglobulinemia is maintained through naïve B cell apoptosis. *Hepatology*. 2012; **56**:1602–1610.DOI: 10.1002/hep.25821.

101. **Roughan JE**, **Reardon KM**, **Cogburn KE**, **Quendler H**, **Pockros PJ**, **Law M**. Chronic hepatitis C virus infection breaks tolerance and drives polyclonal expansion of autoreactive B cells. *Clin. Vaccine Immunol.* 2012; **19**:1027–1037.DOI: 10.1128/CVI.00194-12.

102. **Matsumoto M**, **Hsieh TY**, **Zhu N**, **VanArsdale T**, **Hwang SB**, **Jeng KS**, **Gorbalenya AE**, *et al.* Hepatitis C virus core protein interacts with the cytoplasmic tail of lymphotoxin-beta receptor. *Journal of Virology*. 1997; **71**:1301–1309.

103. **Sansonno D**, **Tucci FA**, **Troiani L**, **Lauletta G**, **Montrone M**, **Conteduca V**, **Sansonno L**, *et al.* Increased serum levels of the chemokine CXCL13 and up-regulation of its gene expression are distinctive features of HCV-related cryoglobulinemia and correlate with active cutaneous vasculitis. *Blood*. 2008; **112**:1620–1627.DOI: 10.1182/blood-2008-02-137455.

104. **Yamamoto K**. Pathogenesis of Sjögren's syndrome. *Autoimmunity Reviews*. 2003; **2**:13–18.

105. **Qin L**, **Liu X**, **Sun Q**, **Fan Z**, **Xia D**, **Ding G**, **Ong HL**, *et al.* Sialin (SLC17A5) functions as a nitrate transporter in the plasma membrane. *Proceedings of the National Academy of Sciences*. 2012; **109**:13434–13439.DOI: 10.1073/pnas.1116633109.

106. **Lundberg JO**. Nitrate transport in salivary glands with implications for NO homeostasis. *Proceedings of the National Academy of Sciences*. 2012; **109**:13144–13145.DOI: 10.1073/pnas.1210412109.

107. **Mavragani CP**, **Moutsopoulos HM**. The geoepidemiology of Sjögren's syndrome. *Autoimmunity Reviews*. 2010; **9**:A305–10.DOI: 10.1016/j.autrev.2009.11.004.

108. **Mitsias DI**, **Kapsogeorgou EK**, **Moutsopoulos HM**. Sjögren's syndrome: why autoimmune epithelitis? *Oral Dis*. 2006; **12**:523–532.DOI: 10.1111/j.1601-0825.2006.01292.x.

109. **Fox RI**. Sjögren's syndrome. *Lancet*. 2005; **366**:321–331.DOI: 10.1016/S0140-6736(05)66990-5.

110. **Manganelli P**, **Fietta P**, **Quaini F**. Hematologic manifestations of primary Sjögren's syndrome. *Clin. Exp. Rheumatol.* 2006; **24**:438–448.

111. **Sais G**, **Admella C**, **Fantova MJ**, **Montero JC**. Lymphocytic autoimmune hidradenitis, cutaneous leucocytoclastic vasculitis and primary Sjögren's syndrome. *Br. J. Dermatol.* 1998; **139**:1073–1076.

112. **Constantopoulos SH**, **Papadimitriou CS**, **Moutsopoulos HM**.

Respiratory manifestations in primary Sjögren's syndrome. A clinical, functional, and histologic study. *Chest*. 1985; **88**:226–229.

113. **Grande L**, **Lacima G**, **Ros E**, **Font J**, **Pera C**. Esophageal motor function in primary Sjögren's syndrome. *Am. J. Gastroenterol.* 1993; **88**:378–381.

114. **Ebert EC**. Gastrointestinal and hepatic manifestations of Sjogren syndrome. *J. Clin. Gastroenterol.* 2012; **46**:25–30.DOI: 10.1097/MCG.0b013e3182329d9c.

115. **Skopouli FN**, **Barbatis C**, **Moutsopoulos HM**. Liver involvement in primary Sjögren's syndrome. *Br. J. Rheumatol.* 1994; **33**:745–748.

116. **Vitali C**, **Bombardieri S**, **Jonsson R**, **Moutsopoulos HM**, **Alexander EL**, **Carsons SE**, **Daniels TE**, *et al.* Classification criteria for Sjögren's syndrome: a revised version of the European criteria proposed by the American-European Consensus Group. In: Vol 61. 2002:554–558.

117. **D'Arbonneau F**, **Ansart S**, **Le Berre R**, **Dueymes M**, **Youinou P**, **Pennec Y-L**. Thyroid dysfunction in primary Sjögren's syndrome: a long-term followup study. *Arthritis Rheum*. 2003; **49**:804–809.DOI: 10.1002/art.11460.

118. **Royer B**, **Cazals-Hatem D**, **Sibilia J**, **Agbalika F**, **Cayuela JM**, **Soussi T**, **Maloisel F**, *et al.* Lymphomas in patients with Sjogren's syndrome are marginal zone B-cell neoplasms, arise in diverse extranodal and nodal sites, and are not associated with viruses. *Blood*. 1997; **90**:766–775.

119. **Rischmueller M**, **Lester S**, **Chen Z**, **Champion G**, **Van Den Berg R**, **Beer R**, **Coates T**, *et al.* HLA class II phenotype controls diversification of the autoantibody response in primary Sjögren's syndrome (pSS). *Clinical & Experimental Immunology*. 1998; **111**:365–371.

120. **Harley JB**, **Reichlin M**, **Arnett FC**, **Alexander EL**, **Bias WB**, **Provost TT**. Gene interaction at HLA-DQ enhances autoantibody production in primary Sjögren's syndrome. *Science*. 1986; **232**:1145–1147.

121. **Lessard CJ**, **Li H**, **Adrianto I**, **Ice JA**, **Rasmussen A**, **Grundahl KM**, **Kelly JA**, *et al.* Variants at multiple loci implicated in both innate and adaptive immune responses are associated with Sjögren's syndrome. *Nat. Genet.* 2013; **45**:1284–1292.DOI: 10.1038/ng.2792.

122. **Li Y**, **Zhang K**, **Chen H**, **Sun F**, **Xu J**, **Wu Z**, **Li P**, *et al.* A genome-wide association study in Han Chinese identifies a susceptibility locus for primary Sjögren's syndrome at 7q11.23. *Nat. Genet.* 2013.DOI: 10.1038/ng.2779.

123. **Rusakiewicz S**, **Nocturne G**, **Lazure T**, **Semeraro M**, **Flament C**, **Caillat-Zucman S**, **Sene D**, *et al.* NCR3/NKp30 Contributes to Pathogenesis in Primary Sjögren's Syndrome. *Science Translational Medicine*. 2013; **5**:195ra96–195ra96.DOI: 10.1126/scitranslmed.3005727.

124. **Chisholm DM**, **Mason DK**. Labial salivary gland biopsy in Sjögren's disease. *J. Clin. Pathol.* 1968; **21**:656–660.

125. **Kerr JB**. *Atlas of Functional Histology*. Elsevier Health Sciences; 1999.

126. **Xanthou G**, **Polihronis M**, **Tzioufas AG**, **Paikos S**, **Sideras P**, **Moutsopoulos HM**. 'Lymphoid' chemokine messenger RNA expression by epithelial cells in the chronic inflammatory lesion of the salivary glands of Sjögren's syndrome patients: possible participation in lymphoid structure formation. *Arthritis Rheum*. 2001; **44**:408–418.DOI: 10.1002/1529-0131(200102)44:2<408::AID-ANR60>3.0.CO;2-0.

127. **Manoussakis MN**, **Dimitriou ID**, **Kapsogeorgou EK**, **Xanthou G**, **Paikos S**, **Polihronis M**, **Moutsopoulos HM**. Expression of B7 costimulatory molecules by salivary gland epithelial cells in patients with Sj gren's syndrome. *Arthritis Rheum*. 1999; **42**:229–239. Available at: http://onlinelibrary.wiley.com/doi/10.1002/1529-0131(199902)42:2%3C229::AID-ANR4%3E3.0.CO;2-X/abstract.DOI: 10.1002/1529-0131(199902)42:2<229::AID-ANR4>3.0.CO;2-X.

128. **Ohlsson M**, **Szodoray P**, **Loro LL**, **Johannessen AC**, **Jonsson R**. CD40, CD154, Bax and Bcl-2 expression in Sjögren's syndrome salivary glands: a putative anti-apoptotic role during its effector phases. *Scand. J. Immunol.* 2002; **56**:561–571.

129. **Moutsopoulos HM**, **Hooks JJ**, **Chan CC**, **Dalavanga YA**, **Skopouli FN**, **Detrick B**. HLA-DR expression by labial minor salivary gland tissues in Sjögren's syndrome. *Annals of the …*. 1986.

130. **Tsunawaki S**, **Nakamura S**, **Ohyama Y**, **Sasaki M**, **Ikebe-Hiroki A**, **Hiraki A**, **Kadena T**, *et al.* Possible function of salivary gland epithelial cells as nonprofessional antigen-presenting cells in the development of Sjögren's syndrome. *The Journal of …*. 2002.

131. **Polihronis**, **Tapinos**, **Theocharis**, **Economou**, **Kittas**, **Moutsopoulos**. Modes of epithelial cell death and repair in Sjogren's syndrome (SS). *Clinical & Experimental Immunology*. 1998; **114**:485–490.DOI: 10.1046/j.1365-2249.1998.00705.x.

132. **Casciola-Rosen LA**, **Anhalt G**, **Rosen A**. Autoantigens targeted in systemic lupus erythematosus are clustered in two populations of surface structures on apoptotic keratinocytes. *J. Exp. Med.* 1994; **179**:1317–1330.

133. **Fujihara T**, **Fujita H**, **Tsubota K**, **Saito K**, **Tsuzaka K**, **Abe T**, **Takeuchi T**. Preferential localization of CD8+ alpha E beta 7+ T cells around acinar epithelial cells with apoptosis in patients with Sjögren's syndrome. *J. Immunol.* 1999; **163**:2226–2235.

134. **Çelenligil H**, **Kansu E**, **Ruacan Ş**, **Eratalay K**, **Irkeç M**. Characterization of peripheral blood and salivary gland lymphocytes in Sjögren's syndrome. *Oral Surgery, Oral Medicine, Oral Pathology*. 1990; **69**:572–577.DOI: 10.1016/0030-4220(90)90238-N.

135. **Baekkevold ES**, **Yamanaka T**, **Palframan RT**, **Carlsen HS**, **Reinholt FP**,

Andrian von UH, Brandtzaeg P, *et al.* The CCR7 ligand elc (CCL19) is transcytosed in high endothelial venules and mediates T cell recruitment. *J. Exp. Med.* 2001; **193**:1105–1112.

136. Barone F, Bombardieri M, Rosado MM, Morgan PR, Challacombe SJ, De Vita S, Carsetti R, *et al.* CXCL13, CCL21, and CXCL12 expression in salivary glands of patients with Sjogren's syndrome and MALT lymphoma: association with reactive and malignant areas of lymphoid organization. *J. Immunol.* 2008; **180**:5130–5140.

137. Bolstad AI, Le Hellard S, Kristjansdottir G, Vasaitis L, Kvarnström M, Sjöwall C, Johnsen SJA, *et al.* Association between genetic variants in the tumour necrosis factor/lymphotoxin α/lymphotoxin β locus and primary Sjogren's syndrome in Scandinavian samples. *Annals of the Rheumatic Diseases.* 2012; **71**:981–988.DOI: 10.1136/annrheumdis-2011-200446.

138. Stott DI, Hiepe F, Hummel M, Steinhauser G, Berek C. Antigen-driven clonal proliferation of B cells within the target tissue of an autoimmune disease. The salivary glands of patients with Sjögren's syndrome. *Journal of Clinical Investigation.* 1998; **102**:938–946.DOI: 10.1172/JCI3234.

139. Tengnér P, Halse AK, Haga HJ, Jonsson R. Detection of anti-Ro/SSA and anti-La/SSB autoantibody-producing cells in salivary glands from patients with Sjögren's syndrome - Tengnér - 2004 - Arthritis & Rheumatism - Wiley Online Library. *Arthritis & ….* 1998.

140. Le Pottier L, Devauchelle V, Fautrel A, Daridon C, Saraux A, Youinou P, Pers JO. Ectopic Germinal Centers Are Rare in Sjogren's Syndrome Salivary Glands and Do Not Exclude Autoreactive B Cells. *The Journal of Immunology.* 2009; **182**:3540–3547.DOI: 10.4049/jimmunol.0803588.

141. Jonsson MV, Skarstein K, Jonsson R, Brun JG. Serological implications of germinal center-like structures in primary Sjögren's syndrome. *J. Rheumatol.* 2007; **34**:2044–2049.

142. Mavragani CP, Moutsopoulos HM. Sjögren's Syndrome. *Annu. Rev. Pathol. Mech. Dis.* 2013; **9**:130919210859006.DOI: 10.1146/annurev-pathol-012513-104728.

143. Theander E, Vasaitis L, Baecklund E, Nordmark G, Warfvinge G, Liedholm R, Brokstad K, *et al.* Lymphoid organisation in labial salivary gland biopsies is a possible predictor for the development of malignant lymphoma in primary Sjogren's syndrome. *Annals of the Rheumatic Diseases.* 2011; **70**:1363–1368.DOI: 10.1136/ard.2010.144782.

144. Bournia V-K, Vlachoyiannopoulos PG. Subgroups of Sjögren syndrome patients according to serological profiles. *J. Autoimmun.* 2012; **39**:15–26.DOI: 10.1016/j.jaut.2012.03.001.

145. Haneji N, Nakamura T, Takio K, Yanagi K, Higashiyama H, Saito I, Noji S, *et al.* Identification of alpha-fodrin as a candidate autoantigen in primary

Sjögren's syndrome. *Science*. 1997; **276**:604–607.

146. **Routsias JG**, **Tzioufas AG**. Sjögren's syndrome--study of autoantigens and autoantibodies. *Clinic Rev Allerg Immunol*. 2007; **32**:238–251.DOI: 10.1007/s12016-007-8003-8.

147. **Dawson L**, **Tobin A**, **Smith P**, **Gordon T**. Antimuscarinic antibodies in Sjögren's syndrome: where are we, and where are we going? *Arthritis Rheum*. 2005; **52**:2984–2995.DOI: 10.1002/art.21347.

148. **Witte T**, **Matthias T**, **Arnett FC**, **Peter HH**, **Hartung K**, **Sachse C**, **Wigand R**, *et al.* IgA and IgG autoantibodies against alpha-fodrin as markers for Sjögren's syndrome. Systemic lupus erythematosus. *J. Rheumatol.* 2000; **27**:2617–2620.

149. **McArthur C**, **Wang Y**, **Veno P**, **Zhang J**, **Fiorella R**. Intracellular trafficking and surface expression of SS-A (Ro), SS-B (La), poly(ADP-ribose) polymerase and α-fodrin autoantigens during apoptosis in human salivary gland cells induced by tumour necrosis factor-α. *Archives of Oral Biology*. 2002; **47**:443–448.DOI: 10.1016/S0003-9969(02)00025-0.

150. **Nagaraju K**, **Cox A**, **Casciola-Rosen L**, **Rosen A**. Novel fragments of the Sjögren's syndrome autoantigens alpha-fodrin and type 3 muscarinic acetylcholine receptor generated during cytotoxic lymphocyte granule-induced cell death. *Arthritis Rheum*. 2001; **44**:2376–2386.DOI: 10.1002/1529-0131(200110)44:10<2376::AID-ART402>3.0.CO;2-E.

151. **Maruyama T**, **Saito I**, **Hayashi Y**, **Kompfner E**, **Fox RI**, **Burton DR**, **Ditzel HJ**. Molecular Analysis of the Human Autoantibody Response to α-Fodrin in Sjögren's Syndrome Reveals Novel Apoptosis-Induced Specificity. *Am. J. Pathol.* 2004; **165**:53–61.DOI: 10.1016/S0002-9440(10)63274-9.

152. **Inoue H**, **Tsubota K**, **Ono M**, **Kizu Y**, **Mizuno F**, **Takada K**, **Yamada K**, *et al.* Possible involvement of EBV-mediated alpha-fodrin cleavage for organ-specific autoantigen in Sjogren's syndrome. *J. Immunol.* 2001; **166**:5801–5809.

153. **Rönnblom L**, **Eloranta M-L**. The interferon signature in autoimmune diseases. *Curr Opin Rheumatol*. 2013; **25**:248–253.DOI: 10.1097/BOR.0b013e32835c7e32.

154. **Hjelmervik TOR**, **Petersen K**, **Jonassen I**, **Jonsson R**, **Bolstad AI**. Gene expression profiling of minor salivary glands clearly distinguishes primary Sjögren's syndrome patients from healthy control subjects. *Arthritis Rheum*. 2005; **52**:1534–1544.DOI: 10.1002/art.21006.

155. **Gottenberg J-E**, **Cagnard N**, **Lucchesi C**, **Letourneur F**, **Mistou S**, **Lazure T**, **Jacques S**, *et al.* Activation of IFN pathways and plasmacytoid dendritic cell recruitment in target organs of primary Sjögren's syndrome. *Proc. Natl. Acad. Sci. U.S.A.* 2006; **103**:2770–2775.DOI: 10.1073/pnas.0510837103.

156. **Siegal FP**, **Kadowaki N**, **Shodell M**, **Fitzgerald-Bocarsly PA**, **Shah K**, **Ho S**, **Antonenko S**, *et al.* The nature of the principal type 1 interferon-

producing cells in human blood. *Science*. 1999; **284**:1835–1837.

157. **Zheng L**, **Zhang Z**, **Yu C**, **Tu L**, **Zhong L**, **Yang C**. Association between IFN-alpha and primary Sjogren's syndrome. *Oral Surg Oral Med Oral Pathol Oral Radiol Endod*. 2009; **107**:e12–8.DOI: 10.1016/j.tripleo.2008.09.015.

158. **Brkic Z**, **Maria NI**, **van Helden Meeuwsen CG**, **van de Merwe JP**, **van Daele PL**, **Dalm VA**, **Wildenberg ME**, *et al.* Prevalence of interferon type I signature in CD14 monocytes of patients with Sjögren's syndrome and association with disease activity and BAFF gene expression. *Annals of the Rheumatic Diseases*. 2013; **72**:728–735.DOI: 10.1136/annrheumdis-2012.

159. **Mariette X**, **Roux S**, **Zhang J**, **Bengoufa D**, **Lavie F**, **Zhou T**, **Kimberly R**. The level of BLyS (BAFF) correlates with the titre of autoantibodies in human Sjögren's syndrome. *Annals of the Rheumatic Diseases*. 2003; **62**:168–171.

160. **Ittah M**, **Miceli-Richard C**, **Gottenberg J-E**, **Sellam J**, **Lepajolec C**, **Mariette X**. B-cell-activating factor expressions in salivary epithelial cells after dsRNA virus infection depends on RNA-activated protein kinase activation. *Eur. J. Immunol.* 2009; **39**:1271–1279.DOI: 10.1002/eji.200839086.

161. **Miceli-Richard C**, **Comets E**, **Loiseau P**, **Puechal X**, **Hachulla E**, **Mariette X**. Association of an IRF5gene functional polymorphism with Sjögren's syndrome. *Arthritis Rheum*. 2007; **56**:3989–3994.DOI: 10.1002/art.23142.

162. **Gestermann N**, **Mekinian A**, **Comets E**, **Loiseau P**, **Puechal X**, **Hachulla E**, **Gottenberg JE**, *et al.* STAT4 is a confirmed genetic risk factor for Sjögren's syndrome and could be involved in type 1 interferon pathway signaling. *Genes Immun.* 2010; **11**:432–438.DOI: 10.1038/gene.2010.29.

163. **Young LS**, **Rickinson AB**. Epstein-Barr virus: 40 years on. *Nat. Rev. Cancer*. 2004; **4**:757–768.DOI: 10.1038/nrc1452.

164. **Küppers R**. B cells under influence: transformation of B cells by Epstein-Barr virus. *Nat Rev Immunol*. 2003; **3**:801–812.DOI: 10.1038/nri1201.

165. **Thorley-Lawson DA**. Epstein-Barr virus: exploiting the immune system. *Nat Rev Immunol*. 2001; **1**:75–82.DOI: 10.1038/35095584.

166. **Maeda E**, **Akahane M**, **Kiryu S**, **Kato N**, **Yoshikawa T**, **Hayashi N**, **Aoki S**, *et al.* Spectrum of Epstein-Barr virus-related diseases: a pictorial review. *Jpn J Radiol*. 2009; **27**:4–19.DOI: 10.1007/s11604-008-0291-2.

167. **Fox RI**, **Pearson G**, **Vaughan JH**. Detection of Epstein-Barr virus-associated antigens and DNA in salivary gland biopsies from patients with Sjogren's syndrome. *J. Immunol.* 1986; **137**:3162–3168.

168. **Maitland N**, **Flint S**, **Scully C**, **Crean SJ**. Detection of cytomegalovirus and Epstein-Barr virus in labial salivary glands in Sjogren's syndrome and non-specific sialadenitis. *J. Oral Pathol. Med.* 1995; **24**:293–298.DOI: 10.1111/j.1600-0714.1995.tb01187.x.

169. **Yamaoka K**, **Miyasaka N**, **Yamamoto K**. Possible involvement of Epstein-Barr virus in polyclonal B cell activation in Sjögren's syndrome. *Arthritis Rheum.* 1988; **31**:1014–1021.

170. **Saito I**, **Servenius B**, **Compton T**, **Fox RI**. Detection of Epstein-Barr virus DNA by polymerase chain reaction in blood and tissue biopsies from patients with Sjogren's syndrome. *J. Exp. Med.* 1989; **169**:2191–2198.

171. **S Wen NSHYYMFSKT**. Association of Epstein-Barr virus (EBV) with Sjögren's syndrome: differential EBV expression between epithelial cells and lymphocytes in salivary glands. *Am. J. Pathol.* 1996; **149**:1511.

172. **Pflugfelder SC**, **Crouse CA**, **Atherton SS**. Epstein-Barr virus and the lacrimal gland pathology of Sjögren's syndrome. *Adv. Exp. Med. Biol.* 1994; **350**:641–646.

173. **Mariette X**, **Gozlan J**, **Clerc D**, **Bisson M**, **Morinet F**. Detection of Epstein-Barr virus DNA by in situ hybridization and polymerase chain reaction in salivary gland biopsy specimens from patients with Sjögren's syndrome. *Am. J. Med.* 1991; **90**:286–294.

174. **DiGiuseppe JA**, **Wu TC**, **Corio RL**. Analysis of Epstein-Barr virus-encoded small RNA 1 expression in benign lymphoepithelial salivary gland lesions. *Mod. Pathol.* 1994; **7**:555–559.

175. **Venables PJ**, **Teo CG**, **Baboonian C**, **Griffin BE**, **Hughes RA**. Persistence of Epstein-Barr virus in salivary gland biopsies from healthy individuals and patients with Sjögren's syndrome. *Clinical & Experimental Immunology*. 1989; **75**:359–364.

176. **Deacon LM**, **Shattles WG**, **Mathews JB**, **Young LS**, **Venables PJ**. Frequency of EBV DNA detection in Sjögren's syndrome. *Am. J. Med.* 1992; **92**:453–454.

177. **Tateishi M**, **Saito I**, **Yamamoto K**, **Miyasaka N**. Spontaneous production of Epstein-Barr virus by B lymphoblastoid cell lines obtained from patients with Sjögren's syndrome. Possible involvement of a novel strain of Epstein-Barr virus in disease pathogenesis. *Arthritis Rheum.* 1993; **36**:827–835.

178. **Kohm AP**, **Fuller KG**, **Miller SD**. Mimicking the way to autoimmunity: an evolving theory of sequence and structural homology. *Trends in Microbiology*. 2003; **11**:101–105.

179. **Lerner MR**, **Andrews NC**, **Miller G**, **Steitz JA**. Two small RNAs encoded by Epstein-Barr virus and complexed with protein are precipitated by antibodies from patients with systemic lupus erythematosus. *Proc. Natl. Acad. Sci. U.S.A.* 1981; **78**:805–809.

180. **Poole BD**, **Scofield RH**, **Harley JB**, **James JA**. Epstein-Barr virus and molecular mimicry in systemic lupus erythematosus. *Autoimmunity*. 2006; **39**:63–70.DOI: 10.1080/08916930500484849.

181. **Navone R**, **Lunardi C**, **Gerli R**, **Tinazzi E**, **Peterlana D**, **Bason C**, **Corrocher R**, *et al.* Identification of tear lipocalin as a novel autoantigen target in Sjögren's syndrome. *J. Autoimmun.* 2005; **25**:229–234.DOI: 10.1016/j.jaut.2005.09.021.

182. **Vernant JC**, **Buisson G**, **Magdeleine J**, **De Thore J**, **Jouannelle A**, **Neisson-Vernant C**, **Monplaisir N**. T-lymphocyte alveolitis, tropical spastic paresis, and Sjögren syndrome. *Lancet.* 1988; **1**:177.

183. **Green JE**, **Hinrichs SH**, **Vogel J**, **Jay G**. Exocrinopathy resembling Sjögren's syndrome in HTLV-1 tax transgenic mice. *Nature.* 1989; **341**:72–74.DOI: 10.1038/341072a0.

184. **Eguchi K**, **Matsuoka N**, **Ida H**, **Nakashima M**, **Sakai M**, **Sakito S**, **Kawakami A**, *et al.* Primary Sjögren's syndrome with antibodies to HTLV-I: clinical and laboratory features. *Annals of the Rheumatic Diseases.* 1992; **51**:769–776.

185. **Shattles WG**, **Brookes SM**, **Venables PJ**, **Clark DA**, **Maini RN**. Expression of antigen reactive with a monoclonal antibody to HTLV-1 P19 in salivary glands in Sjögren's syndrome. *Clinical & Experimental Immunology.* 1992; **89**:46–51.

186. **Mariette X**, **Agbalika F**, **Daniel MT**, **Bisson M**, **Lagrange P**, **Brouet JC**, **Morinet F**. Detection of human T lymphotropic virus type I tax gene in salivary gland epithelium from two patients with Sjögren's syndrome. *Arthritis Rheum.* 1993; **36**:1423–1428.

187. **Sumida T**, **Yonaha F**, **Maeda T**, **Kita Y**, **Iwamoto I**, **Koike T**, **Yoshida S**. Expression of sequences homologous to HTLV-I tax gene in the labial salivary glands of Japanese patients with Sjögren's syndrome. *Arthritis Rheum.* 1994; **37**:545–550.

188. **Lee SJ**, **Lee JS**, **Shin MG**, **Tanaka Y**, **Park DJ**, **KIM TJ**, **PARK YW**, *et al.* Detection of HTLV-1 in the Labial Salivary Glands of Patients with Sjogren's Syndrome: A Distinct Clinical Subgroup? *J. Rheumatol.* 2012; **39**:809–815.DOI: 10.3899/jrheum.111075.

189. **Ohyama Y**, **Nakamura S**, **Hara H**, **Shinohara M**, **Sasaki M**, **Ikebe-Hiroki A**, **Mouri T**, *et al.* Accumulation of human T lymphotropic virus type I-infected T cells in the salivary glands of patients with human T lymphotropic virus type I-associated Sjögren's syndrome. *Arthritis Rheum.* 1998; **41**:1972–1978.DOI: 10.1002/1529-0131(199811)41:11<1972::AID-ART12>3.0.CO;2-M.

190. **Hida A**, **Imaizumi M**, **Sera N**, **Akahoshi M**, **Soda M**, **Maeda R**, **Nakashima E**, *et al.* Association of human T lymphotropic virus type I with Sjogren syndrome. *Annals of the Rheumatic Diseases.* 2010; **69**:2056–2057.DOI: 10.1136/ard.2010.128736.

191. **Nelson PN**, **Lever AM**, **Bruckner FE**, **Isenberg DA**, **Kessaris N**, **Hay FC**. Polymerase chain reaction fails to incriminate exogenous retroviruses HTLV-I

and HIV-1 in rheumatological diseases although a minority of sera cross react with retroviral antigens. *Annals of the Rheumatic Diseases*. 1994; **53**:749–754.

192. **Triantafyllopoulou A**, **Moutsopoulos HM**. Autoimmunity and coxsackievirus infection in primary Sjogren's syndrome. *Ann. N. Y. Acad. Sci.* 2005; **1050**:389–396.DOI: 10.1196/annals.1313.090.

193. **Triantafyllopoulou A**, **Tapinos N**, **Moutsopoulos HM**. Evidence for coxsackievirus infection in primary Sjögren's syndrome. *Arthritis Rheum*. 2004; **50**:2897–2902.DOI: 10.1002/art.20463.

194. **Stathopoulou EA**, **Routsias JG**, **Stea EA**, **Moutsopoulos HM**, **Tzioufas AG**. Cross-reaction between antibodies to the major epitope of Ro60 kD autoantigen and a homologous peptide of Coxsackie virus 2B protein. *Clinical & Experimental Immunology*. 2005; **141**:148–154.DOI: 10.1111/j.1365-2249.2005.02812.x.

195. **Gottenberg J-E**, **Pallier C**, **Ittah M**, **Lavie F**, **Miceli-Richard C**, **Sellam J**, **Nordmann P**, *et al.* Failure to confirm coxsackievirus infection in primary Sjögren's syndrome. *Arthritis Rheum*. 2006; **54**:2026–2028.DOI: 10.1002/art.21906.

196. **Viskari H**, **Ludvigsson J**, **Uibo R**, **Salur L**, **Marciulionyte D**, **Hermann R**, **Soltesz G**, *et al.* Relationship between the incidence of type 1 diabetes and enterovirus infections in different European populations: results from the EPIVIR project. *J. Med. Virol.* 2004; **72**:610–617.DOI: 10.1002/jmv.20033.

197. **Campbell AE**, **Cavanaugh VJ**, **Slater JS**. The salivary glands as a privileged site of cytomegalovirus immune evasion and persistence. *Med Microbiol Immunol*. 2008; **197**:205–213.DOI: 10.1007/s00430-008-0077-2.

198. **Amsler L**, **Verweij MC**, **DeFilippis VR**. The tiers and dimensions of evasion of the type I interferon response by human cytomegalovirus. *Journal of Molecular Biology*. 2013; **425**:4857–4871.DOI: 10.1016/j.jmb.2013.08.023.

199. **Kotenko SV**, **Saccani S**, **Izotova LS**, **Mirochnitchenko OV**, **Pestka S**. Human cytomegalovirus harbors its own unique IL-10 homolog (cmvIL-10). *Proc. Natl. Acad. Sci. U.S.A.* 2000; **97**:1695–1700.

200. **Moore KW**, **de Waal Malefyt R**, **Coffman RL**, **O'Garra A**. Interleukin-10 and the interleukin-10 receptor. *Annu. Rev. Immunol.* 2001; **19**:683–765.DOI: 10.1146/annurev.immunol.19.1.683.

201. **Chang WLW**, **Barry PA**. Attenuation of innate immunity by cytomegalovirus IL-10 establishes a long-term deficit of adaptive antiviral immunity. *Proceedings of the National Academy of Sciences*. 2010; **107**:22647–22652.DOI: 10.1073/pnas.1013794108.

202. **Fleck M**, **Kern ER**, **Zhou T**, **Lang B**, **Mountz JD**. Murine cytomegalovirus induces a Sjögren's syndrome-like disease in C57Bl/6-lpr/lpr mice. *Arthritis Rheum*. 1998; **41**:2175–2184.DOI: 10.1002/1529-0131(199812)41:12<2175::AID-ART12>3.0.CO;2-I.

203. **Skarstein K**, **Wahren M**, **Zaura E**, **Hattori M**, **Jonsson R**. Characterization of T Cell Receptor Repertoire and Anti-Ro/SSA Autoantibodies in Relation to Sialadenitis of NOD Mice. …. 1995.

204. **Kloover JS**, **Hillebrands JL**, **de Wit G**, **Grauls G**, **Rozing J**, **Bruggeman CA**, **Nieuwenhuis P**. Rat cytomegalovirus replication in the salivary glands is exclusively confined to striated duct cells. *Virchows Arch.* 2000; **437**:413–421.

205. **Ramos-Casals M**, **García-Carrasco M**, **Cervera R**, **Rosas J**, **Trejo O**, **la Red de G**, **Sánchez-Tapias JM**, *et al.* Hepatitis C virus infection mimicking primary Sjögren syndrome. A clinical and immunologic description of 35 cases. *Medicine (Baltimore)*. 2001; **80**:1–8.

206. **Arrieta JJ**, **Rodríguez-Iñigo E**, **Ortiz-Movilla N**, **Bartolomé J**, **Pardo M**, **Manzarbeitia F**, **Oliva H**, *et al.* In situ detection of hepatitis C virus RNA in salivary glands. *Am. J. Pathol.* 2001; **158**:259–264.DOI: 10.1016/S0002-9440(10)63964-8.

207. **Toussirot E**, **Le Huédé G**, **Mougin C**, **Balblanc J-C**, **Bettinger D**, **Wendling D**. Presence of hepatitis C virus RNA in the salivary glands of patients with Sjögren's syndrome and hepatitis C virus infection. *J. Rheumatol.* 2002; **29**:2382–2385. Available at: http://eutils.ncbi.nlm.nih.gov/entrez/eutils/elink.fcgi?dbfrom=pubmed&id=12415596&retmode=ref&cmd=prlinks.

208. **Koike K**, **Moriya K**, **Ishibashi K**, **Matsuura Y**, **Suzuki T**, **Saito I**, **Iino S**, *et al.* Expression of hepatitis C virus envelope proteins in transgenic mice. *J. Gen. Virol.* 1995; **76 (Pt 12)**:3031–3038.

209. **Ramos-Casals M**, **Loustaud-Ratti V**, **De Vita S**, **Zeher M**, **Bosch J-A**, **Toussirot E**, **Medina F**, *et al.* Sjögren syndrome associated with hepatitis C virus: a multicenter analysis of 137 cases. *Medicine (Baltimore)*. 2005; **84**:81–89.

210. **Makino S**, **Kunimoto K**, **Muraoka Y**, **Mizushima Y**, **Katagiri K**, **Tochino Y**. Breeding of a non-obese, diabetic strain of mice. *Jikken Dobutsu*. 1980; **29**:1–13.

211. **Kikutani H**, **Makino S**. The murine autoimmune diabetes model: NOD and related strains. *Adv. Immunol.* 1992; **51**:285–322.

212. **van Blokland SC**, **van Helden-Meeuwsen CG**, **Wierenga-Wolf AF**, **Drexhage HA**, **Hooijkaas H**, **van de Merwe JP**, **Versnel MA**. Two different types of sialoadenitis in the NOD- and MRL/lpr mouse models for Sjögren's syndrome: a differential role for dendritic cells in the initiation of sialoadenitis? *Lab. Invest.* 2000; **80**:575–585.

213. **Wicker LS**, **Todd JA**, **Peterson LB**. Genetic control of autoimmune diabetes in the NOD mouse. *Annu. Rev. Immunol.* 1995; **13**:179–200.DOI: 10.1146/annurev.iy.13.040195.001143.

214. **Anderson MS**, **Bluestone JA**. The NOD mouse: a model of immune

dysregulation. *Annu. Rev. Immunol.* 2005; **23**:447–485.DOI: 10.1146/annurev.immunol.23.021704.115643.

215. **Brayer J**, **Lowry J**, **Cha S**, **Robinson CP**, **Yamachika S**, **Peck AB**, **Humphreys-Beher MG**. Alleles from chromosomes 1 and 3 of NOD mice combine to influence Sjögren's syndrome-like autoimmune exocrinopathy. *J. Rheumatol.* 2000; **27**:1896–1904.

216. **Cha S**, **Nagashima H**, **Brown VB**, **Peck AB**, **Humphreys-Beher MG**. Two NOD Idd-associated intervals contribute synergistically to the development of autoimmune exocrinopathy (Sjögren's syndrome) on a healthy murine background. *Arthritis Rheum.* 2002; **46**:1390–1398.DOI: 10.1002/art.10258.

217. **van Blokland SCA**, **Versnel MA**. Pathogenesis of Sjögren's syndrome: characteristics of different mouse models for autoimmune exocrinopathy. *Clin. Immunol.* 2002; **103**:111–124.DOI: 10.1006/clim.2002.5189.

218. **Kurien BT**, **Dsouza A**, **Igoe A**, **Lee YJ**, **Maier-Moore JS**, **Gordon T**, **Jackson M**, *et al.* Immunization with 60 kD Ro peptide produces different stages of preclinical autoimmunity in a Sjögren's syndrome model among multiple strains of inbred mice. *Clinical & Experimental Immunology*. 2013; **173**:67–75.DOI: 10.1111/cei.12094.

219. **Scofield RH**, **Asfa S**, **Obeso D**, **Jonsson R**, **Kurien BT**. Immunization with short peptides from the 60-kDa Ro antigen recapitulates the serological and pathological findings as well as the salivary gland dysfunction of Sjogren's syndrome. *J. Immunol.* 2005; **175**:8409–8414.

220. **Danthinne X**, **Imperiale MJ**. Production of first generation adenovirus vectors: a review. *Gene Ther.* 2000; **7**:1707–1714.DOI: 10.1038/sj.gt.3301301.

221. **Hierholzer JC**, **Killington RA**. *Virology Methods Manual*. Virology methods manual; 1996.

222. **Correia PN**, **Carpenter GH**, **Paterson KL**, **Proctor GB**. Inducible nitric oxide synthase increases secretion from inflamed salivary glands. *Rheumatology (Oxford)*. 2010; **49**:48–56.DOI: 10.1093/rheumatology/kep313.

223. **Ngo VN**, **Korner H**, **Gunn MD**, **Schmidt KN**, **Riminton DS**, **Cooper MD**, **Browning JL**, *et al.* Lymphotoxin alpha/beta and tumor necrosis factor are required for stromal cell expression of homing chemokines in B and T cell areas of the spleen. *J. Exp. Med.* 1999; **189**:403–412.

224. **Seaman WE**, **Sleisenger M**, **Eriksson E**, **Koo GC**. Depletion of natural killer cells in mice by monoclonal antibody to NK-1.1. Reduction in host defense against malignancy without loss of cellular or humoral immunity. *J. Immunol.* 1987; **138**:4539–4544.

225. **Dawson LJ**, **Stanbury J**, **Venn N**, **Hasdimir B**, **Rogers SN**, **Smith PM**. Antimuscarinic antibodies in primary Sjögren's syndrome reversibly inhibit the mechanism of fluid secretion by human submandibular salivary acinar cells. *Arthritis Rheum.* 2006; **54**:1165–1173.DOI: 10.1002/art.21764.

226. **Humphreys-Beher MG**, **Brayer J**, **Yamachika S**, **Peck AB**, **Jonsson R**. An alternative perspective to the immune response in autoimmune exocrinopathy: induction of functional quiescence rather than destructive autoaggression. *Scand. J. Immunol.* 1999; **49**:7–10.

227. **Samuni Y**, **Baum BJ**. Gene delivery in salivary glands: from the bench to the clinic. *Biochim. Biophys. Acta*. 2011; **1812**:1515–1521.DOI: 10.1016/j.bbadis.2011.06.014.

228. **Bombardieri M**, **Pitzalis C**. Ectopic lymphoid neogenesis and lymphoid chemokines in Sjogren's syndrome: at the interplay between chronic inflammation, autoimmunity and lymphomagenesis. *Curr Pharm Biotechnol*. 2012; **13**:1989–1996.

229. **Browning JL**, **Allaire N**, **Ngam-ek A**, **Notidis E**, **Hunt J**, **Perrin S**, **Fava RA**. Lymphotoxin-β Receptor Signaling Is Required for the Homeostatic Control of HEV Differentiation and Function. *Immunity*. 2005; **23**:539–550.DOI: 10.1016/j.immuni.2005.10.002.

230. **Horowitz A**, **Stegmann KA**, **Riley EM**. Activation of natural killer cells during microbial infections. *Front Immunol*. 2011; **2**:88.DOI: 10.3389/fimmu.2011.00088.

231. **Shi F-D**, **Ljunggren H-G**, **La Cava A**, **Van Kaer L**. Organ-specific features of natural killer cells. *Nat Rev Immunol*. 2011; **11**:658–671.DOI: 10.1038/nri3065.

232. **Wendland M**, **Czeloth N**, **Mach N**, **Malissen B**, **Kremmer E**, **Pabst O**, **Forster R**. CCR9 is a homing receptor for plasmacytoid dendritic cells to the small intestine. *Proc. Natl. Acad. Sci. U.S.A.* 2007; **104**:6347–6352.DOI: 10.1073/pnas.0609180104.

233. **Hänninen A**, **Maksimow M**, **Alam C**, **Morgan DJ**, **Jalkanen S**. Ly6C supports preferential homing of central memory CD8+ T cells into lymph nodes. *Eur. J. Immunol.* 2011; **41**:634–644.DOI: 10.1002/eji.201040760.

234. **Marshall HD**, **Chandele A**, **Jung YW**, **Meng H**, **Poholek AC**, **Parish IA**, **Rutishauser R**, *et al.* Differential Expression of Ly6C and T-bet Distinguish Effector and Memory Th1 CD4+ Cell Properties during Viral Infection. *Immunity*. 2011; **35**:633–646.DOI: 10.1016/j.immuni.2011.08.016.

235. **Rose S**, **Misharin A**, **Perlman H**. A novel Ly6C/Ly6G-based strategy to analyze the mouse splenic myeloid compartment. *Cytometry A*. 2011; **81A**:343–350.DOI: 10.1002/cyto.a.22012.

236. **Yona S**, **Jung S**. Monocytes: subsets, origins, fates and functions. *Curr. Opin. Hematol.* 2010; **17**:53–59.DOI: 10.1097/MOH.0b013e3283324f80.

237. **Liu Y-J**. IPC: professional type 1 interferon-producing cells and plasmacytoid dendritic cell precursors. *Annu. Rev. Immunol.* 2005; **23**:275–306.DOI: 10.1146/annurev.immunol.23.021704.115633.

238. **Hochrein H**, **O'Keeffe M**, **Wagner H**. Human and mouse plasmacytoid dendritic cells. *Hum. Immunol.* 2002; **63**:1103–1110.

239. **Zhang J**, **Raper A**, **Sugita N**, **Hingorani R**, **Salio M**, **Palmowski MJ**, **Cerundolo V**, *et al.* Characterization of Siglec-H as a novel endocytic receptor expressed on murine plasmacytoid dendritic cell precursors. *Blood.* 2006; **107**:3600–3608.DOI: 10.1182/blood-2005-09-3842.

240. **Zhang JQ**, **Biedermann B**, **Nitschke L**, **Crocker PR**. The murine inhibitory receptor mSiglec-E is expressed broadly on cells of the innate immune system whereas mSiglec-F is restricted to eosinophils. *Eur. J. Immunol.* 2004; **34**:1175–1184.DOI: 10.1002/eji.200324723.

241. **Vivier E**, **Tomasello E**, **Baratin M**, **Walzer T**, **Ugolini S**. Functions of natural killer cells. *Nature Publishing Group.* 2008; **9**:503–510.DOI: 10.1038/ni1582.

242. **Ruzek MC**, **Kavanagh BF**, **Scaria A**, **Richards SM**, **Garman RD**. Adenoviral vectors stimulate murine natural killer cell responses and demonstrate antitumor activities in the absence of transgene expression. *Mol. Ther.* 2002; **5**:115–124.DOI: 10.1006/mthe.2002.0529.

243. **Cerf-Bensussan JSBMER-PNMSDBBFRCCJDDB-GN**, **Meresse B**, **Ramiro-Puig E**, **Montcuquet N**, **Darche S**, **Bègue B**, **Ruemmele F**, *et al.* Interleukin-15-Dependent NKp46+ Innate Lymphoid Cells Control Intestinal Inflammation by Recruiting Inflammatory Monocytes. *Immunity.* 2012; **37**:108–121.DOI: 10.1016/j.immuni.2012.05.013.

244. **Bellora F**, **Castriconi R**, **Dondero A**, **Reggiardo G**, **Moretta L**, **Mantovani A**, **Moretta A**, *et al.* The interaction of human natural killer cells with either unpolarized or polarized macrophages results in different functional outcomes. *Proc. Natl. Acad. Sci. U.S.A.* 2010; **107**:21659–21664.DOI: 10.1073/pnas.1007654108.

245. **Ferlazzo G**, **Münz C**. Dendritic cell interactions with NK cells from different tissues. *J. Clin. Immunol.* 2009; **29**:265–273.DOI: 10.1007/s10875-009-9283-y.

246. **Mantovani A**, **SICA A**, **SOZZANI S**, **ALLAVENA P**, **VECCHI A**, **LOCATI M**. The chemokine system in diverse forms of macrophage activation and polarization. *Trends in Immunology.* 2004; **25**:677–686.DOI: 10.1016/j.it.2004.09.015.

247. **Bombardieri M**, **Barone F**, **Pittoni V**, **Alessandri C**, **Conigliaro P**, **Blades MC**, **Priori R**, *et al.* Increased circulating levels and salivary gland expression of interleukin-18 in patients with Sjögren's syndrome: relationship with autoantibody production and lymphoid organization of the periductal inflammatory infiltrate. *Arthritis Research & Therapy.* 2004; **6**:R447–56.DOI: 10.1186/ar1209.

248. **Fleck M**, **Zhang HG**, **Kern ER**, **Hsu HC**, **Müller-Ladner U**, **Mountz JD**. Treatment of chronic sialadenitis in a murine model of Sjögren's syndrome by

local fasL gene transfer. *Arthritis Rheum*. 2001; **44**:964–973.DOI: 10.1002/1529-0131(200104)44:4<964::AID-ANR154>3.0.CO;2-5.

249. **Nguyen CQ**, **Yin H**, **Lee BH**, **Carcamo WC**, **Chiorini JA**, **Peck AB**. Pathogenic effect of interleukin-17A in induction of Sjögren's syndrome-like disease using adenovirus-mediated gene transfer. *Arthritis Research & Therapy*. 2010; **12**:R220.DOI: 10.1186/ar3207.

250. **van de Pavert SA**, **Mebius RE**. New insights into the development of lymphoid tissues. *Nature Publishing Group*. 2010; **10**:664–674.DOI: 10.1038/nri2832.

251. **Marinkovic T**, **Garin A**, **Yokota Y**, **Fu Y-X**, **Ruddle NH**, **Furtado GC**, **Lira SA**. Interaction of mature CD3+CD4+ T cells with dendritic cells triggers the development of tertiary lymphoid structures in the thyroid. *Journal of Clinical Investigation*. 2006; **116**:2622–2632.DOI: 10.1172/JCI28993.

252. **Muramatsu M**, **Sankaranand VS**, **Anant S**, **Sugai M**, **Kinoshita K**, **Davidson NO**, **Honjo T**. Specific expression of activation-induced cytidine deaminase (AID), a novel member of the RNA-editing deaminase family in germinal center B cells. *J. Biol. Chem.* 1999; **274**:18470–18476. Available at: http://eutils.ncbi.nlm.nih.gov/entrez/eutils/elink.fcgi?dbfrom=pubmed&id=10373455&retmode=ref&cmd=prlinks.

253. **Dörner T**, **Radbruch A**. Selecting B cells and plasma cells to memory. *J. Exp. Med.* 2005; **201**:497–499. Available at: http://jem.rupress.org/content/201/4/497.full.DOI: 10.1084/jem.20050218.

254. **Manser T**. Textbook germinal centers? *J. Immunol.* 2004; **172**:3369–3375.

255. **Recher M**, **Berglund LJ**, **Avery DT**. Blood Journal | IL-21 is the primary common γ chain-binding cytokine required for human B-cell differentiation in vivo. *….* 2011. Available at: http://bloodjournal.hematologylibrary.org/content/118/26/6824.short.

256. **Schneider P**, **Mackay F**, **Steiner V**, **Hofmann K**, **Bodmer JL**, **Holler N**, **Ambrose C**, *et al.* BAFF, a novel ligand of the tumor necrosis factor family, stimulates B cell growth. *J. Exp. Med.* 1999; **189**:1747–1756. Available at: http://eutils.ncbi.nlm.nih.gov/entrez/eutils/elink.fcgi?dbfrom=pubmed&id=10359578&retmode=ref&cmd=prlinks.

257. **Castigli E**, **Wilson SA**, **Scott S**, **Dedeoglu F**, **Xu S**, **Lam K-P**, **Bram RJ**, *et al.* TACI and BAFF-R mediate isotype switching in B cells. *J. Exp. Med.* 2005; **201**:35–39. Available at: http://jem.rupress.org/content/201/1/35.full.DOI: 10.1084/jem.20032000.

258. **Xu W**, **He B**, **Chiu A**, **Chadburn A**, **Shan M**, **Buldys M**, **Ding A**, *et al.* Epithelial cells trigger frontline immunoglobulin class switching through a pathway regulated by the inhibitor SLPI. *Nat Immunol*. 2007; **8**:294–303. Available at: http://www.nature.com/doifinder/10.1038/ni1434.DOI: 10.1038/ni1434.

259. **Bombardieri M**, **Kam N-W**, **Brentano F**, **Choi K**, **Filer A**, **Kyburz D**, **McInnes IB**, *et al.* A BAFF/APRIL-dependent TLR3-stimulated pathway enhances the capacity of rheumatoid synovial fibroblasts to induce AID expression and Ig class-switching in B cells. *Annals of the Rheumatic Diseases*. 2011; **70**:1857–1865.DOI: 10.1136/ard.2011.150219.

260. **Arpaia N**, **Barton GM**. Toll-like receptors: key players in antiviral immunity. *Curr Opin Virol*. 2011; **1**:447–454.DOI: 10.1016/j.coviro.2011.10.006.

261. **Hou B**, **Saudan P**, **Ott G**, **Wheeler ML**, **Ji M**, **Kuzmich L**, **Lee LM**, *et al.* Selective utilization of Toll-like receptor and MyD88 signaling in B cells for enhancement of the antiviral germinal center response. *Immunity*. 2011; **34**:375–384.DOI: 10.1016/j.immuni.2011.01.011.

262. **Jonsson R**, **Vogelsang P**, **Volchenkov R**, **Espinosa A**, **Wahren-Herlenius M**, **Appel S**. The complexity of Sjögren's syndrome: Novel aspects on pathogenesis. *Immunol. Lett.* 2011; **141**:1–9. Available at: http://linkinghub.elsevier.com/retrieve/pii/S0165247811001799.DOI: 10.1016/j.imlet.2011.06.007.

263. **Carroll VA**, **Lundgren A**, **Wei H**, **Sainz S**, **Tung KS**, **Brown MG**. Natural Killer Cells Regulate Murine Cytomegalovirus-Induced Sialadenitis and Salivary Gland Disease. *Journal of Virology*. 2012; **86**:2132–2142.DOI: 10.1128/JVI.06898-11.

264. **Caldeira PC**, **Oliveira e Silva KR**, **Silva TA**, **de Mattos Camargo Grossmann S**, **Teixeira R**, **Carmo MAVD**. Correlation between salivary anti-HCV antibodies and HCV RNA in saliva and salivary glands of patients with chronic hepatitis C. *Journal of Oral Pathology & Medicine*. 2013; **42**:222–228.DOI: 10.1111/j.1600-0714.2012.01201.x.

265. **Tessmer MS**, **Reilly EC**, **Brossay L**. Salivary gland NK cells are phenotypically and functionally unique. *PLoS Pathog*. 2011; **7**:e1001254.DOI: 10.1371/journal.ppat.1001254.

266. **Puga I**, **Cols M**, **Barra CM**, **He B**, **Cassis L**, **Gentile M**, **Comerma L**, *et al.* B cell–helper neutrophils stimulate the diversification and production of immunoglobulin in the marginal zone of the spleen. *Nat Immunol*. 2011; **13**:170–180.DOI: 10.1038/ni.2194.

267. **Mantovani A**, **Cassatella MA**, **Costantini C**, **Jaillon S**. Neutrophils in the activation and regulation of innate and adaptive immunity. *Nat Rev Immunol*. 2011; **11**:519–531.DOI: 10.1038/nri3024.

268. **Khandpur R**, **Carmona-Rivera C**, **Vivekanandan-Giri A**, **Gizinski A**, **Yalavarthi S**, **Knight JS**, **Friday S**, *et al.* NETs Are a Source of Citrullinated Autoantigens and Stimulate Inflammatory Responses in Rheumatoid Arthritis. *Science Translational Medicine*. 2013; **5**:178ra40–178ra40.DOI: 10.1126/scitranslmed.3005580.

269. **Mariette X**, **Gottenberg J-E**. Pathogenesis of Sjögren's syndrome and

therapeutic consequences. *Curr Opin Rheumatol*. 2010; **22**:471–477.DOI: 10.1097/BOR.0b013e32833c36c5.

270. **He Li JAICJLKLS**. Interferons in Sjögren's Syndrome: Genes, Mechanisms, and Effects. *Front Immunol*. 2013; **4**:1–7. Available at: http://www.frontiersin.org/Journal/10.3389/fimmu.2013.00290/abstract.DOI: 10.3389/fimmu.2013.00290/abstract.

271. **Le Bon A**, **Thompson C**, **Kamphuis E**, **Durand V**, **Rossmann C**, **Kalinke U**, **Tough DF**. Cutting edge: enhancement of antibody responses through direct stimulation of B and T cells by type I IFN. *J. Immunol.* 2006; **176**:2074–2078. Available at: http://www.jimmunol.org/content/176/4/2074.full.DOI: 10.4049/jimmunol.176.4.2074.

272. **Triantafyllopoulou A**, **Moutsopoulos H**. Persistent Viral Infection in Primary Sjogren's Syndrome: Review and Perspectives. *Clinic Rev Allerg Immunol*. 2007; **32**:210–214.DOI: 10.1007/s12016-007-8004-7.

273. **Rothenberg ME**, **Hogan SP**. THE EOSINOPHIL. *Annu. Rev. Immunol.* 2006; **24**:147–174. Available at: http://www.annualreviews.org/doi/abs/10.1146/annurev.immunol.24.021605.090720.DOI: 10.1146/annurev.immunol.24.021605.090720.

274. **Tamoutounour S**, **Henri S**, **Lelouard H**, **de Bovis B**, **de Haar C**, **van der Woude CJ**, **Woltman AM**, *et al.* CD64 distinguishes macrophages from dendritic cells in the gut and reveals the Th1-inducing role of mesenteric lymph node macrophages during colitis. *Eur. J. Immunol.* 2012; **42**:3150–3166.DOI: 10.1002/eji.201242847.

275. **Pender MP**. Infection of autoreactive B lymphocytes with EBV, causing chronic autoimmune diseases. *Trends in Immunology*. 2003; **24**:584–588.

276. **Lucchesi D**, **Pitzalis C**, **Bombardieri M**. EBV and other viruses as triggers of tertiary lymphoid structures in primary Sjögren's syndrome. *Expert Review of Clinical Immunology*. 2014:1–11.DOI: 10.1586/1744666X.2014.892417.

277. **Lucchesi D**, **Bombardieri M**. The role of viruses in autoreactive B cell activation within tertiary lymphoid structures in autoimmune diseases. *Journal of Leukocyte Biology*. 2013; **94**:1191–1199.DOI: 10.1189/jlb.0413240.

278. **Walton SM**, **Mandaric S**, **Torti N**, **Zimmermann A**, **Hengel H**, **Oxenius A**. Absence of cross-presenting cells in the salivary gland and viral immune evasion confine cytomegalovirus immune control to effector CD4 T cells. *PLoS Pathog*. 2011; **7**:e1002214.DOI: 10.1371/journal.ppat.1002214.

279. **Muniz LR**, **Pacer ME**, **Lira SA**, **Furtado GC**. A critical role for dendritic cells in the formation of lymphatic vessels within tertiary lymphoid structures. *The Journal of Immunology*. 2011; **187**:828–834.DOI: 10.4049/jimmunol.1004233.

280. **Sunderkötter C**, **Nikolic T**, **Dillon MJ**, **Van Rooijen N**, **Stehling M**,

Drevets DA, **Leenen PJM**. Subpopulations of mouse blood monocytes differ in maturation stage and inflammatory response. *Multiple values selected*. 2004; **172**:4410–4417.

281. **Arnold L**, **Henry A**, **Poron F**, **Baba-Amer Y**, **Van Rooijen N**, **Plonquet A**, **Gherardi RK**, *et al.* Inflammatory monocytes recruited after skeletal muscle injury switch into antiinflammatory macrophages to support myogenesis. *J. Exp. Med.* 2007; **204**:1057–1069.DOI: 10.1084/jem.20070075.

282. **Ferenbach DA**, **Sheldrake TA**, **Dhaliwal K**. Kidney International - Abstract of article: Macrophage/monocyte depletion by clodronate, but not diphtheria toxin, improves renal ischemia/reperfusion injury in mice. *Kidney ….* 2012.

283. **Yona S**, **Kim K-W**, **Wolf Y**, **Mildner A**, **Varol D**, **Breker M**, **Strauss-Ayali D**, *et al.* Fate mapping reveals origins and dynamics of monocytes and tissue macrophages under homeostasis. *Immunity*. 2013; **38**:79–91.DOI: 10.1016/j.immuni.2012.12.001.

284. **Geissmann F**, **Jung S**, **Littman DR**. Blood Monocytes Consist of Two Principal Subsets with Distinct Migratory Properties. *Immunity*. 2003.